The American Mineralogist

Journal of the Mineralogical Society of America

VOL. 46 JULY–AUGUST, 1961 Nos. 7 and 8

Contents

(*Continued on Cover 2*)

Published bi-monthly by the Society

(*Contents continued*)

Mineralogical Society of America

ASSOCIATED WITH THE GEOLOGICAL SOCIETY OF AMERICA

The enlarged issues of this journal for 1961 are made possible by a grant from the Penrose Fund of the Geological Society of America.

The American Mineralogist—Journal of the Mineralogical Society of America

The journal, containing articles on mineralogy, crystallography, and allied sciences, is issued every two months. Contributions are invited.

The general conduct of the journal is in the hands of the editor, Lewis S. Ramsdell, Department of Mineralogy, University of Michigan, to whom all manuscripts should be submitted.

Second class postage paid at Menasha, Wis., under Act of March 3, 1879. Acceptance for mailing at the special rate of postage provided for in section 1103, Act of Oct 3, 1917, paragraph 4 section 429 P. L. & R. authorized March 13, 1922.

Notice of change of address, orders, and remittances should be sent to Marjorie Hooker, c/o U. S. Geological Survey, Washington 25, D. C.

Printed by George Banta Company, Inc., Menasha, Wisconsin
Printed in the United States of America

SCOTT WILLIAMS Mineral Company, INC.

BULLETIN

MINERAL SPECIMENS · BOOKS · MICROSCOPES · COLLECTING EQUIPMENT · SUPPLIES

440 N. SCOTTSDALE ROAD • SCOTTSDALE, ARIZONA • WHitney 5-0805

NATIVE ELEMENTS

NATIVE ANTIMONY

Arechuybo, Chihuahua, Mexico

Brilliant tin-white metallic crystalline aggregates. These specimens occur in small to large nodule imbedded in a white clay bank close to the surface. All of the specimens are nearly-pure nativ antimony with a white to yellow oxide rind. Some of the oxide minerals in association ar stibiconite, valentinite and kermesite. ½" to 1", 25c and 50c. 1x1 to 1x1½, 75c, $1.00 and $1.25 1½x1½ to 1x2½, $1.50 and $2.00. 2x2 to 2x2½, $2.50, $3.00 and $3.50. 2x3 to 3x3, $4.50 $5.00 and $6.50. 3x4 to 4x4, $7.50, $8.50, $9.50 and $10.00. 4x5 to 4x6, $12.50 and $15.00

DIAMOND CRYSTAL

Premier Mine, Kimberly, Union of South Africa

Beautiful, sparkling transparent colorless to tinted single crystals. The average size of th crystals is 1/16". Superb for **micromounters.** Many crystals have interesting inclusions o other minerals. The crystals occur in octahedrons, dodecahedrons and various combinations an modifying forms. 1/16" crystal for $1.00. **Fluorescent** green, blue or yellow diamonds at $2.00 ea

NATIVE SELENIUM

Homestake Mine, Sec. 23, Ambrosia Lakes District
Near Grants, Valencia Co., New Mexico

Very rare native element previously reported from but three localities. The mineral occurs o bluish to deep reddish-black prismatic microscopic crystals coating sandstone. All of our spec mens exhibit enough selenium to be visible to the eye. Every specimen will produce fir **micromount** material. 1" to 1x1, $1.00, $1.50 and $2.50. 1x1½ to 1½x2, $2.00, $2.50, $3.5 and $5.00. 2x2 to 2x3, $3.50, $4.00, $5.00, $6.50 and $7.50. 3x3 to 3x5, $7.50, $8.50, $9.5 $12.50 and $15.00. 4x5 to 4x6, $17.50 and $25.00.

TERRESTRIAL NATIVE IRON

Uifak, Disko Island, Greenland

Veinlets and masses of a bronze metallic color disseminated in basalt. The native iron has bee found in large masses up to 20 tons in the basalt off the shore islands of Greenland. It was use by the inhabitants of Greenland for knives and utensils and was known as early as 1819. It wa at first thought to be of meteoric origin, but its terrestrial nature has been proven. The action the intruded basalt upon the carbonaceous shales has reduced the silicates in the basalt to nati iron. ½" to 1", 50c and $1.00. 1x1 to 1½x2, $1.50, $2.00 and $2.50. 2x2 to 2x3, $3.50, $4.5 $5.00 and $7.50. 2½x3½ to 4x4, $8.50, $9.50, $10.00 and $12.50. 4x5 to 4x6, $15.00, $17. and $25.00.

NATIVE ARSENIC

Burraton Combe Quarry, St. Stephens-By-Saltash, Cornwall, England

Pure gray crystalline semi-botryoidal mass, tin-white metallic on fresh surface. This is a most u usual occurrence since the native element was not found in association with other materic 1" to 1x1, 50c and $1.00. 1x1½ to 1½x2½, $1.50, $2.00, $2.50, $3.50, $4.50 and $5.(2x2 to 2x2½, $6.50 and $7.50.

ADD TO YOUR NATIVE ELEMENT COLLECTION BY ORDERING TODAY
SATISFACTION GUARANTEED

BIG SAVINGS NOW

33% off

Terrific Values on JEWELRY CRAFT and ROCKHOUNDING Supplies!

ROCKHOUNDER'S KNAPSACK

The buy of the year

Tremendous value — this is army surplus material at a low, low price. Made of a sturdy, waterproof khaki canvas, very well stitched—well made. Perfect to carry rocks, equipment, books, maps, everything you might tote on a Rockhounding trip. Sportsmen, fishermen, hunters—everybody likes them. They sling easily over your shoulder to carry any kind of load. 7½" x 5" wide x 12" deep—with shoulder strap.

H115-1 J . . . . . *each only* $1.50

NEW epoxy ADHESIVE

So good it's replacing rivets

MIRACLE ADHESIVE — you've seen it on T-V and in LIFE — *it bonds materials* stronger than anything else. Aircraft industry using it instead of Rivets—replaces nails and screws. Perfect for jewelry making — *Unconditionally guaranteed!* Kit of 2 jars with complete instructions.

Order as: Z1- J .....only $1.50

This "15X Ruper" Magnifier with ½" diameter corrected lens! Full any magnifier you now use! Full plated metal folding frame. Equivalent to other $6 magnifiers.

Order as: T130-25J $1.00

WE DARE YOU TO COMPARE

FLASHLIGHT MAGNIFIER

Enlarges Objects 7X

e "Flash Magnifier" ON object r scrutiny — snap on flashlight d get 7 times magnification ex- where you need it. Gem stones minerals look more beautiful... kings, flaws, defects are easily ed. 7" long. Metal and plastic Colossal value.

Z-179 J only $1.95

plete including 2 batteries ...

Z-180 J . only $2.15

49er GOLD PANNING OUTFIT

GOLD PANNING KIT

. . . exciting fun for the entire family

Everything you need to pan for gold — including directions, 12" gold pan, sample of placer gold ore — ready to pan, leather pouch of ore and an alnico magnet. Shows you how to go about it . . . just like the old 49'ers did. It's a real thrill . . . and many streams in all parts of the country have gold in them. Get a kit and head for the open country. Excellent gift item too. Start panning for gold now. Order —

Z-72 J - 49'er Gold Panning Outfit . . 1 for $2.95

YOU JUST CAN'T GO ROCK HUNTING WITHOUT IT!

ESTWING PROSPECTOR PICK

Forged all-steel one-piece head-handle prospecting pick with the new blue everlasting nylon cushion handle grip — non slip. 13 inches long with 7" head which weighs 22 oz. Guaranteed unbreakable.

Order as Z-60- J . . . . . now only $4.75

TERRIFIC VALUES IN READER MAGNIFIERS

Imported quality — 2x magnification — optical lens. Ideal for jewelry making, rockhounding, stamp collecting, etc. Fits easily in pocket. Black Ebonite handle — polished chrome frame.

Z-181 J 2" Magnifier . each $1.00

Z-182 J 3" Magnifier . each 1.95

SPARKLING — SUPERB SPECIMEN CARDS!

erent specimens on card — nbled and polished — many n quality!

-ful cards for everyone inter- rockhounding. Educational — ive — good for class work — "absolute must" for the begin- llector.

e . . . terrific buy — order one now — you must see them to ate . . . we guarantee you'll be d!

Mexico and the Southwest" . . . . . *only* $1.00
Brazilian Agates" . . . . . *only* $1.00
Mother of Pearl" . . . . . *only* $1.00
Brazilian Gem Materials" . . *only* $1.00
Gem Materials of the West' . *only* $1.00
World Wide Gem Materials" *only* $1.00
International Gem Stones" . *only* $1.00
Colorful Gem Stones" . . . . *only* $1.00
California Gem Materials" . *only* $1.00

YOU DO BETTER WORK WHEN YOU SEE BETTER WITH MAGNI-FOCUSER

Binocular Magnifier

Leaves both hands free to work

MAGNI-FOCUSER

Designed for All Professions and Trades

Make all precision work easier work

T121-3 J	MAGNI-FOCUSER, magnifies 1¾ times at 14" . . .	$10.50
T121-5 J	MAGNI-FOCUSER, magnifies 2¼ times at 10" . . .	$10.50
T121-7 J	MAGNI-FOCUSER, magnifies 2¾ times at 8" . . .	$10.50
T121-10 J	MAGNI-FOCUSER, magnifies 3½ times at 4" . . .	$12.50
T121-15 J	MAGNI-FOCUSER, magnifies 4¾ times at 3" . . .	$15.00
T121-17 J	MAGNI-FOCUSER, magnifies 5¼ times at 2½" . . .	$15.00

2 lbs.
2 lbs.
2 lbs.
2 lbs.
2 lbs.
2 lbs.

Any work that requires **precision** can be done easier, faster and more accurately with a Magni-Focuser — the **binocular** magnifier.

Magni-Focuser shows an object in **third dimension** and greatly magnified—with the depth and clarity of normal vision. It **reduces eye-strain** and **prevents squinting**—thereby **saving time,** increasing accuracy, and minimizing the chance of errors and accidents.

RELIEVE "EYE STRAIN" WITH A MAGNI-FOCUSER

All items sold on Money Back Guarantee!

GRIEGER'S

1633 E. WALNUT
PASADENA, CALIF.

Prices include Taxes and Postage!

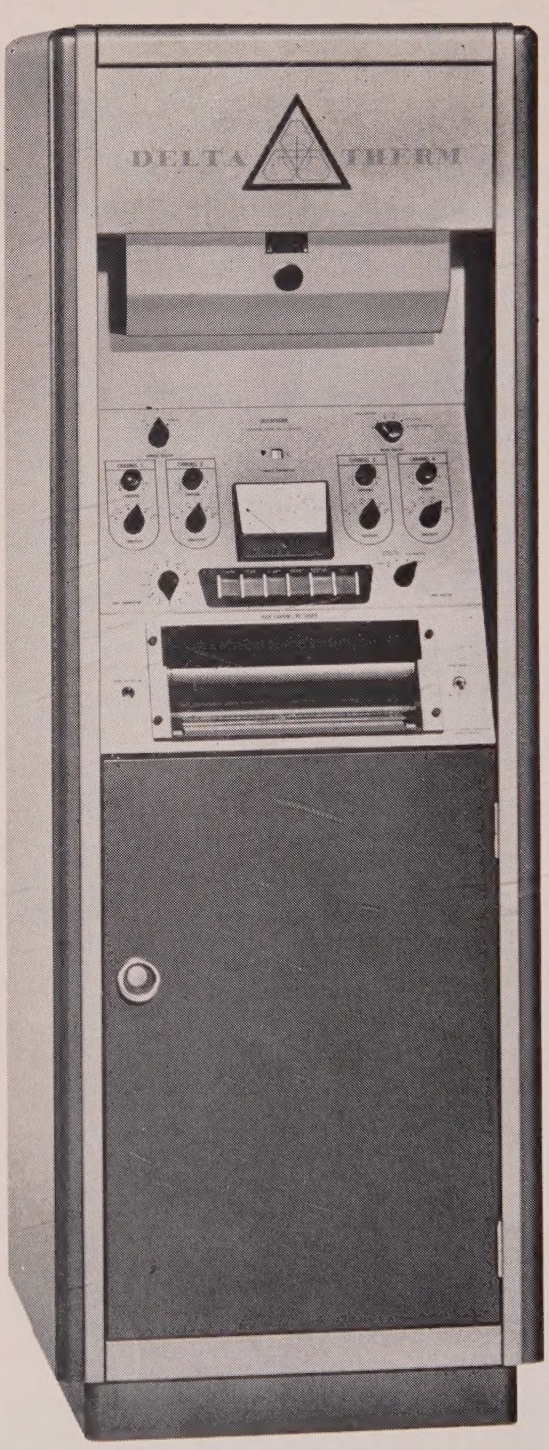

A complete system for differential thermal analysis

SYMBOL OF DEPENDABILI
AND ACCURACY

THE AMERICAN MINERALOGIST
JOURNAL OF THE MINERALOGICAL SOCIETY OF AMERICA

Vol. 46 JULY–AUGUST, 1961 Nos. 7 and 8

THE REACTION SERIES, GIBBSITE→CHI ALUMINA →KAPPA ALUMINA→CORUNDUM*

G. W. BRINDLEY AND J. O. CHOE, *Department of Ceramic Technology, The Pennsylvania State University, University Park, Pennsylvania.*

ABSTRACT

The reactions of micron-sized powders of gibbsite heated in air progressively to 1350° C. were followed by single crystal electron diffraction patterns, *x*-ray powder patterns, thermogravimetric measurements, infra-red absorption spectrometry and differential thermal analysis. The reaction series gibbsite→χ-Al_2O_3→K-Al_2O_3→corundum is confirmed, with χ-Al_2O_3 in the range 270°–870° C. At about 270° C., the product still retains 25% 'water' which is lost progressively up to about 800° C. From about 970–1180° C., K-Al_2O_3 is present together with α-Al_2O_3. The product termed K- is probably a mixture, since ν-Al_2O_3 and η-Al_2O_3 have also been observed. Analysis of the diffraction data leads to the conclusion that χ- has probably a close-packed hexagonal type structure with $a=5.57$, $c=8.64$ Å, $a=1.551$. The principal component of 'κ-' has a large hexagonal cell, with $a=16.7$ Å. The continuity of crystallographic orientations in these reactions is clearly demonstrated by the electron diffraction diagrams.

INTRODUCTION

The thermal reactions of gibbsite

The work of de Boer and his colleagues (1954a, b, 1956), of Tertian and Papée (1958), and of other investigators has shown that the thermal reactions of gibbsite are dependent on many variables, and in particular on the crystal size of the gibbsite, on the atmosphere, and on the rate of heating. Prior to the realization of the importance of these variables, the results were conflicting and poorly understood.

In the present work, fine crystal size, normal atmospheres and slow heating rates are employed. For crystals finer than about 1 micron, it is considered by Tertian and Papée (1958), de Boer, Fortuin, Steggerda (1954*a*, *b*), and others, that the following reactions take place:

$$\text{Gibbsite} \rightarrow \chi\text{-}Al_2O_3 \rightarrow \kappa\text{-}Al_2O_3 \rightarrow \alpha\text{-}Al_2O_3 \qquad \text{(Series I)}$$

For coarse-grained gibbsite, as Brown, Clark and Elliott (1953) first clearly recognized, boehmite is the first product to be formed as a result

* Contribution No. 60-1 from the College of Mineral Industries, The Pennsylvania State University, University Park, Pa.

of the development of a hydrothermal condition in the gibbsite crystals. Subsequently a fissuring of the crystals occurs and the remaining gibbsite then follows reaction series I. The boehmite independently gives rise to a second reaction series, so that two parallel series of reactions take place.

$$\text{Gibbsite} \rightarrow \text{Boehmite} \rightarrow \gamma\text{-}Al_2O_3 \rightarrow \theta\text{-}Al_2O_3 \rightarrow \alpha\text{-}Al_2O_3 \qquad \text{(Series II)}$$

$$\searrow\ \chi\text{-}Al_2O_3 \longrightarrow \kappa\text{-}Al_2O_3 \rightarrow \alpha\text{-}Al_2O_3 \qquad \text{(Series I)}$$

Crystallographic aspects of the reactions

Ervin (1952) emphasized the concept of structural continuity in relation to the numerous intermediate products formed when gibbsite and other hydrated aluminas are converted to the final stable α-alumina, corundum. His arguments were based principally on the continuity of certain dominant reflections in the x-ray powder diagrams. Much earlier, Deflandre (1932) had shown that diaspore transforms to corundum by a crystallographically ordered process, without intermediate products. This reaction takes place at a relatively low temperature, 450–600° C. The sequence of crystallographic changes, gibbsite→boehmite→γ-Al_2O_3 →θ-Al_2O_3, exhibited by coarse gibbsite has been studied by single crystal techniques by Saalfeld (1958, 1959), who has demonstrated the following dimensional relationships:

$$a(\text{gibbsite}) \rightarrow a(\text{boehmite}) \rightarrow [1\bar{1}0]\gamma\text{-}Al_2O_3 \rightarrow a, \theta\text{-}Al_2O_3$$

$$2.88 \qquad 2.86 \qquad 2.81 \qquad 2.81$$

The crystallographic relations between the phases or products formed from fine-grained ($<1\mu$) gibbsite have not been analyzed previously, largely because the fine-grained nature of the material precludes the use of single-crystal x-ray analysis, and the x-ray powder data show mainly broad and ill-defined reflections. Tertian and Papée (1958) especially have attempted to clarify the particular features characterizing the χ- and κ-Al_2O_3 which have been designated as the principal intermediate stages in the reaction series of fine-grained gibbsite.

Present Studies

The present studies have been aimed at elucidating in more detail the reaction series I for fine-grained gibbsite heated under normal atmospheric conditions. For this purpose, electron diffraction (E.D.) analysis which can be applied to single crystals of micron dimensions, has major advantages over x-ray powder studies. It is also necessary to follow in detail the removal of 'water' from the structure, and for this purpose differential thermal analysis, thermo-gravimetric measurements and infra-red absorption measurements have been made.

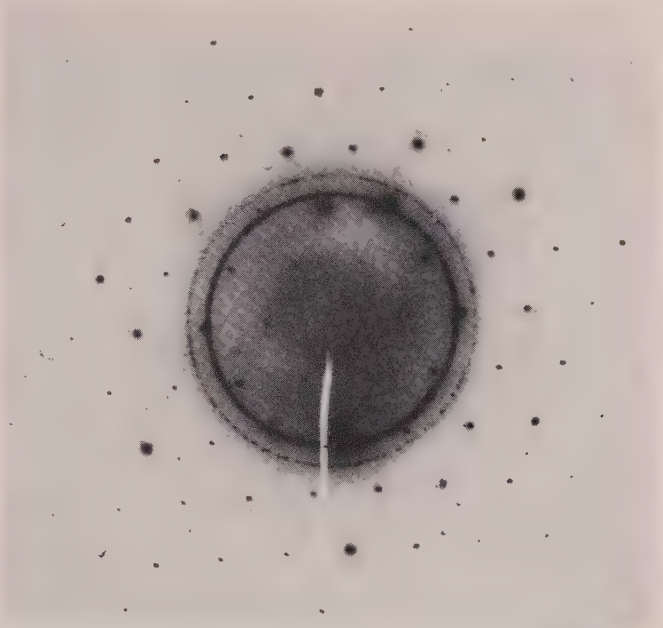

FIG. 1. Electron diffraction pattern of a single crystal of gibbsite "shadowed" with aluminum metal.

Electron-diffraction procedures

Single crystal diagrams were obtained by using well-dispersed samples and an R.C.A. instrument, Type EMU, with a diaphragm for isolating single crystals in the field of view. Spacing calibration of the single-crystal diffraction patterns was obtained by lightly shadowing the samples with metallic aluminum which gave ring patterns of the metal. Fig. 1 shows a typical single crystal spot pattern with superposed calibration rings.

Specimen preparation

Suitable fine-grained gibbsite is essential for these studies. A fine-grained material with particle size <1 micron supplied by the Reynolds Metals Company gave a clear x-ray powder diagram of gibbsite, but proved unsuitable for E.D. study; the particles were shaped so that they took up random orientations in the E.D. camera. By grinding under water a coarse 'platy' gibbsite supplied by the Aluminum Company of America, thin platy crystals of sub-micron size were obtained, which were separated from coarser material by sedimentation in water at a con-

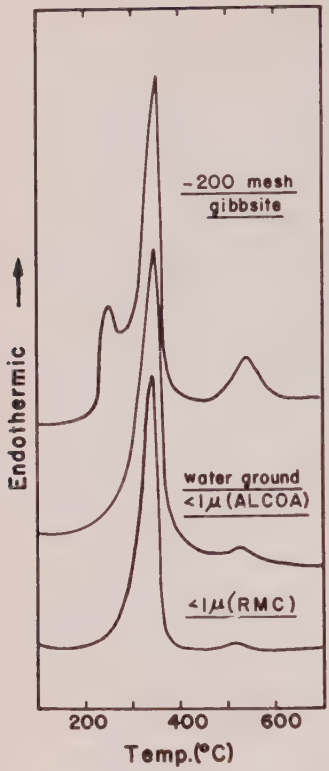

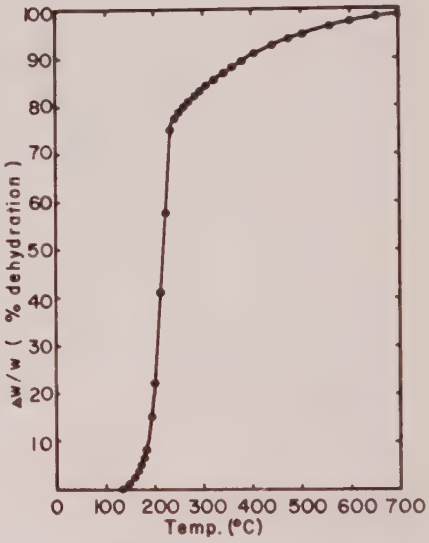

FIG. 2. (Left) Differential thermal analysis curves of (i) −200 mesh gibbsite ("Alcoa"), (ii) sample (i) water ground to less than 1μ particle size, (iii) gibbsite, 1μ particle size (Reynolds Metals Co.).

FIG. 3 (Right) Progressive weight-loss/temperature curve for <1μ gibbsite; 12 hr. heat-treatment at each temperature.

trolled pH of 6.8–7.2. These crystals were well oriented in the diffraction instrument and gave good E.D. patterns (see Fig. 1).

Following heat-treatment, the products were stored in sealed tubes over P_2O_5. Preparation of specimens for electron microscope and diffraction study was carried out using amyl acetate as the dispersion medium. Fine gibbsite crystals, oriented on a glass plate, were covered by a thin collodion film, and subsequently by a more substantial Formvar film. The combined film was stripped from the glass with the aid of Scotch tape and immersed in ethylene chloride. The Formvar film is dissolved and the thin collodion film with gibbsite attached is caught on grids for insertion in the microscope.

Dehydration studies

Whereas reaction series I is characterized by essentially the single endothermic dehydration reaction, series II is characterized by two dehydration processes. Therefore 'fine' gibbsite is differentiated from 'coarse' gibbsite by having one endotherm rather than three endotherms (see Fig. 2). However, the slow loss of water after an initial rapid loss can be followed more precisely by thermo-gravimetric measurements, and also (though less quantitatively) by infra-red absorption measurements.

Therefore all these techniques have been applied to obtain an understanding of the lower temperature reactions in which 'water' is involved.

X-ray powder measurements

These have been made with a Philips Norelco diffractometer adapted so that a stream of dry air passed over the sample during the recording of data.

Experimental Results

Differential thermal analysis data

Figure 2 shows curves obtained with relatively coarse gibbsite supplied by the Aluminum Company of America, micron-sized gibbsite obtained by grinding the 'ALCOA' material, and micron-sized gibbsite supplied by the Reynolds Metals Company.

The micron-sized powders show traces of an endotherm at about 500° C. which may arise from a small amount of boehmite. However, the more prominent boehmite peak at about 250° C. is not observed from the fine-grained materials.

X-ray powder analysis shows that only a trace of boehmite is formed from the micron-sized powders, and this small amount does not affect adversely the interpretation of the results. Boehmite was not detected in the E.D. diagrams, despite the fact that its pattern is quite distinct from the other patterns observed in these experiments.

Thermo-gravimetric data

Step-wise temperature increments of the order of 5–10° C. at 12 hr. intervals gave the dehydration curve shown in Fig. 3, where $(\Delta w/w_0)$ represents weight loss as a fraction of total weight loss. Dehydration proceeds rapidly in the temperature interval 190–240° C. up to about 75%, and thereafter goes very slowly to completion at about 800° C.

Isothermal dehydration curves show similar features. Sample size is important, as was shown previously for kaolinite and halloysite by

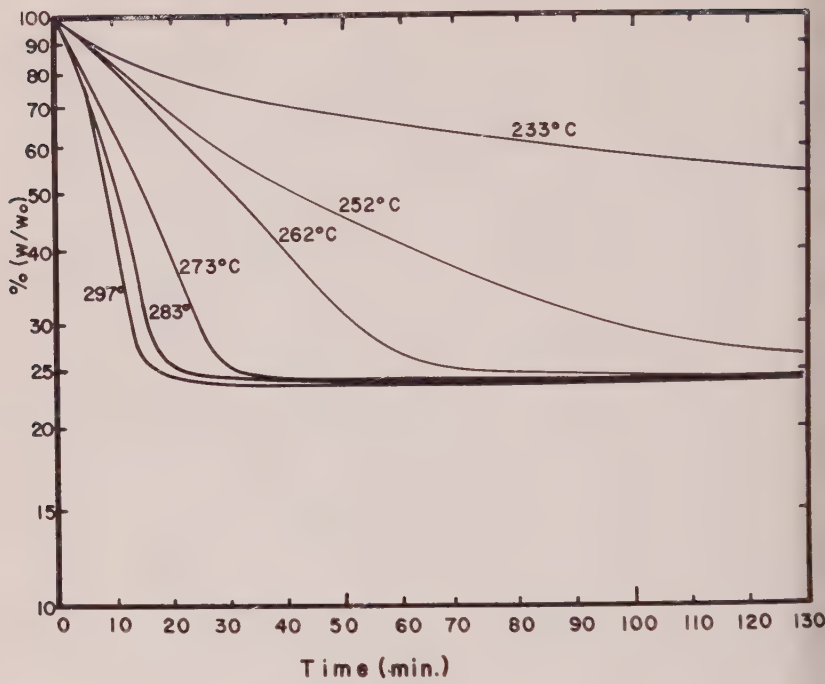

FIG. 4. Isothermal dehydration curves for $<1\mu$ gibbsite.

Brindley and Nakahira (1959). Figure 4 shows typical curves for $(w - w_0)$ where w is the weight of unreacted material, plotted logarithmically against time for thin powder layers heated isothermally at various temperatures. The initial parts of these curves are not strictly linear, so that the reaction proceeds only approximately according to first-order kinetics. When the reactions are about 75% complete, in all cases the reaction rate is reduced almost to zero at the temperatures employed.

Single crystal, electron diffraction data

Figure 5(A–F) shows a series of diagrams illustrating the various spot patterns which have been observed, together with the aluminum calibration rings, for samples heated to various stages of reaction between room temperature and 1180° C. All the patterns are hexagonal in character and exhibit certain features which are constant or nearly constant throughout the reaction series. Hexagonal axes a_1^* and a_2^* are shown in each diagram corresponding to the smallest unit cell compatible with the data.

Table 1 lists the hexagonal parameters, a_H, calculated from the various

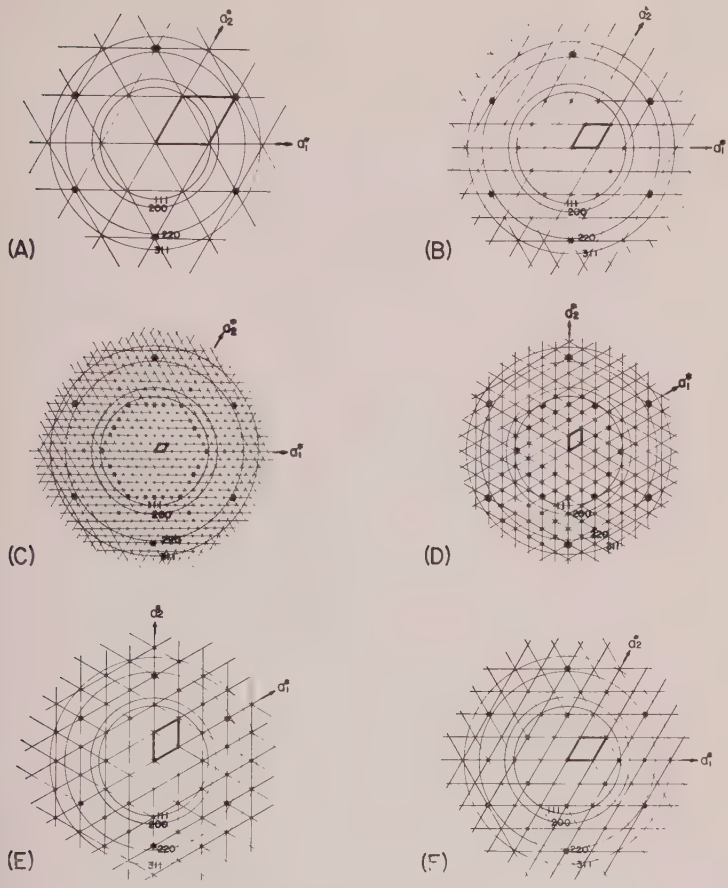

FIG. 5. Single-crystal electron diffraction patterns, with aluminum calibration rings, for transition aluminas.

(A) χ-Al_2O_3 at 270° C.; approximate formula, Al_2O_3 0.75 H_2O; $a_H = 2.77$ Å
(B) χ-Al_2O_3 at 830° C.; formula Al_2O_3; $a_H = 5.53$ Å
(C) κ(?)-Al_2O_3 at 970–1180° C.; $a_H = 16.78$ Å
(D) (?)-Al_2O_3 at 1030–1180° C.; $a_H = 9.70$ Å
(E) ξ′-Al_2O_3 at 1180–1350° C.; $a_H = 5.37$ Å
(F) υ-Al_2O_3 at 1030–1180° C.; $a_H = 5.54$ Å

E.D. patterns. The smallest cell, $a_H = 2.77$ Å (Figure 5A), is obtained on heating at 270° C., with about 75% bulk dehydration. This parameter is about 4% smaller than the corresponding value for gibbsite, namely a(monoclinic)/3 = 2.87 Å. Continued heating and dehydration produces only small changes in the E.D. patterns up to 830° C., when dehydration is virtually complete. At this stage, illustrated by Fig. 5B, weak addi-

Table 1. Values of Hexagonal Parameter, a_H, for Heated Aluminas Derived from Fine-Grained Gibbsite

Temperature, ° C.	Probable designation	E.D. pattern	Parameter, Å	
270	χ (initial)	Fig. 5A		$a_H=1.77$
830	χ (final)	Fig. 5B	$a_H=5.53$	$a/2=2.76_5$
970–1180	κ (?)	Fig. 5C	$a_H=16.78$	$a/6=2.79$
1130–1180	—	Fig. 5D	$a_H=9.70$	$a/(4\sin 60)=2.80$
1030–1180	ν	Fig. 5F	$a_H=5.54$	$a/2=2.77$
1180–1350	ξ'	Fig. 5E	$a_H=5.37$	$a/2=2.69$
>1000	α	—		

tional spots are observed corresponding with $a_H=5.53$ Å, or $a_H/2=2.76_5$ Å. Some reorganization of the structure, probably of the cations, and a slight contraction have occurred.

In the temperature interval 860–1180° C., further reorganization of the structure takes place with the emergence of reflections on a finer scale in the E.D. diagrams, Figs. 5C and D, corresponding to larger unit cells which, however, are related in a simple way to the original parameters.

At temperatures in the range 1030–1350° C., patterns are occasionally found (Figs. 5E, F) agreeing closely with E.D. patterns described by Cowley (1953) which he labelled ξ'-alumina ($a=5.23$ Å) and ν-alumina ($a=5.53$ Å). These patterns are simpler than those obtained in the temperature range 860–1180° C. X-ray patterns show that α-Al_2O_3 forms at temperatures of about 1000° C., but satisfactory E.D. patterns of the final stage were not obtained, probably owing to sintering of the material.

A statistical survey of the results observed after various heat-treatments is given in Table 2, from which it appears that the principal stages in the reaction series are as follows: From 270–870° C., E.D. patterns

Table 2. Single-Crystal E.D. Patterns of Transition Aluminas Observed at Various Temperatures

Temperature, °C.	Number and type of pattern observed
270°	37 patterns, Fig. 5A
470°	9 patterns, Fig. 5A
830–875°	52 patterns, Fig. 5B
970°	7 patterns, Fig. 5B; 24 patterns, Fig. 5C
1030°	21 patterns, Fig. 5C; 2 patterns, Fig. 5D; 2 patterns, Fig. 5F
1180°	9 patterns, Fig. 5C; 2 patterns, Fig. 5D; 2 patterns, Fig. 5E; 2 patterns, Fig. 5F
1350°	5 patterns, Fig. 5E

of the type shown in Figs. 5A, B are obtained and these may correspond with the material usually labelled χ-Al_2O_3. This result agrees broadly with the conclusion of Tertian and Papée (1958) who gave 200 400° C. up to 900° C. as the temperature range for χ-Al_2O_3. In the temperature range 950–1180° C. more complex patterns are obtained, with Fig. 5C mainly occurring. This material may correspond with κ-Al_2O_3. At 1000° C. and higher temperatures, α-Al_2O_3 (corundum) is formed but satisfactory E.D. patterns of this phase were not obtained.

Rare occurrences of ν- and ξ'-alumina (Figures 5E, F) were found in the temperature range 1030–1350° C.

X-ray powder data

Following the disappearance of gibbsite at about 200–220° C., the *x*-ray powder diagrams are mainly diffuse until α-Al_2O_3 makes its appearance at about 1000° C. From about 270–800° C., the diagram resembles mainly that of χ-Al_2O_3 as described by Tertian and Papée (1958). At 470° C., slight traces of the strongest boehmite reflections can be detected as stated earlier. At 470° C., the diagram appears to be solely that of χ-Al_2O_3, and no further changes occur until about 830° C., when additional broad reflections are observed which may be attributed to κ-Al_2O_3. As the temperature approaches 1000° C., the reflections become clearer, but the development of α-Al_2O_3 at this temperature hinders the analysis of the κ-Al_2O_3. At 970° and higher temperatures, the E.D. patterns have shown that more than one crystalline form develops so that considerable caution is required in the interpretation of *x*-ray powder patterns.

An important result obtained from *x*-ray powder data is that when the intensity of the very strong (002) gibbsite reflection at $d = 4.85$ Å, is plotted against percentage dehydration of the sample, the intensity falls smoothly and rapidly to zero at 75% dehydration (See Fig. 6). If the remaining 25% of unreacted material were present as undecomposed gibbsite, it would be very easily detected by *x*-rays. The intensity of the (002) gibbsite reflection is such that a few per cent of gibbsite could be detected easily. The conclusion seems inescapable that about 25% of the initial 'water' content is associated with the first reaction product formed from the gibbsite. This agrees exactly with the composition $Al_2O_3 \cdot 0.75\ H_2O$ given previously by Papée and Tertian (1955).

The *x*-ray powder data obtained from material heated at 470° C., which is believed to be χ-Al_2O_3, are given in Table 3, together with corresponding data by Tertian and Papée (1958), and by Stumpf *et al.* (1950) as amended by Russell *et al.* (1956). The agreement is as good as can be expected for such poorly crystalline material.

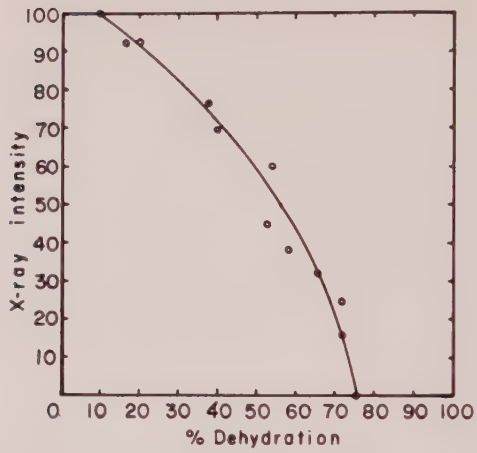

FIG. 6. *X*-ray intensity of (002) gibbsite vs. percentage bulk dehydration.

Infra-red absorption data

Absorption spectra were recorded for representative samples from the various heat-treatments, and the following are the main results achieved. Material heated at 270° C. no longer shows the sharp absorption peaks in the 9.5–15μ range obtained with gibbsite and the strong hydroxyl absorption in the neighborhood of 2.9μ is considerably reduced. The latter is reduced still further at 470° C. and is eliminated at 830° C. The results are consistent with progressive removal of 'water' from about 25% of the initial amount at 270° C. to complete removal by about 800° C.

TABLE 3. DIFFRACTION DATA FOR χ-ALUMINA

d = spacings, in Å (I) = estimated intensity

Tertian & Papée (1958) d(I) (500° C.)	Russell *et al.* (1956) d(I)	Present data 470° C. d(I), observed		calculated	
		X-ray	E.D.	$(hk, l)_H$	d
		4.80±0.15 (4)	—	100	4.822
2.848 (8)	—	2.88±0.02 (8)	—	003	2.880
	—	—	2.794	110	2.785
2.404 (15)	2.40 (4)	2.41±0.01 (15)	2.401	200	2.411
—	2.27 (2)	—	—		
2.126 (15)	2.11 (3)	2.12±0.01 (15)	—	202	2.106
—	1.98 (2)	1.96±0.01 (10)	—	104	1.971
1.91 (5)	—	—			
—	1.53 (1)	—			
1.394 (35)	1.39 (10)	1.395±0.005 (30)	1.397	220	1.393

Discussion

Electron diffraction data

The group of six strong reflections lying near the Al(220) ring is a constant and important feature of the E.D. patterns of the transition aluminas. The lattice spacing corresponding to these reflections is about 1.395 Å. *X*-ray powder studies have shown a consistently strong reflection at 1.39–1.40 Å (cf. Rooksby (1951); Ervin (1952); Russell *et al.* (1956)). Gibbsite (see Fig. 1) also gives a similar reflection with $d = 1.451$ Å.

Ervin (1952) pointed out that this spacing corresponds to the oxygen ion radius in a cubic close-packed system of oxygen ions, and is the spacing of the (440) planes of the spinel structure. This observation is important because the γ- and η-forms are considered to have a spinel-type structure. The reflection is particularly strong because all octahedral and tetrahedral cation sites lie in the (440) planes of the oxygen anions, and therefore the intensity of the reflection is independent of the particular distribution of cations in these sites. However, quite apart from this particular type of structure, one can say that a strong reflection at about $d = 1.395$ Å will arise from planes of the type (220) from cubic close-packed oxygen arrangements.

It is equally important to observe that a similar situation exists with hexagonal close-packing. The oxygen anions lie wholly in the $(11\bar{2}0)$ planes, the spacing of which is the oxygen ion radius, and also all the octahedral and tetrahedral cation sites lie in the $(11\bar{2}0)$ planes of anions.

Therefore, while the existence of a strong reflection at $d \simeq 1.395$ is evidence for close-packing of oxygen ions with the aluminum ions in interstitial sites, it does not differentiate between the hexagonal and cubic arrangements.

Indexing of electron diffraction patterns

Care is needed in drawing conclusions from the hexagonal spot patterns given by electron diffraction. Gibbsite provides a warning since this is a monoclinic structure.

Hexagonal diffraction patterns do not exclude cubic structures, because in hexagonal-to-cubic transformations, the plane $(0001)_H$ is likely to become $(111)_C$ with $[111]_C$ replacing $[001]_H$. Any rhombohedral lattice (including as a special case the cubic lattice with $[111]_C$ as the trigonal axis) can be referred to hexagonal axes with the following index relations:

$$\begin{aligned} h_C &= h_H + l_H/3 \\ k_C &= k_H + l_H/3 \\ l_C &= -h_H - k_H + l_H/3 \end{aligned}$$

A cubic structure oriented with $[111]_C$ parallel to the electron beam gives a zero-order reciprocal array satisfying the relation

$$h_C + k_C + l_C = 0$$

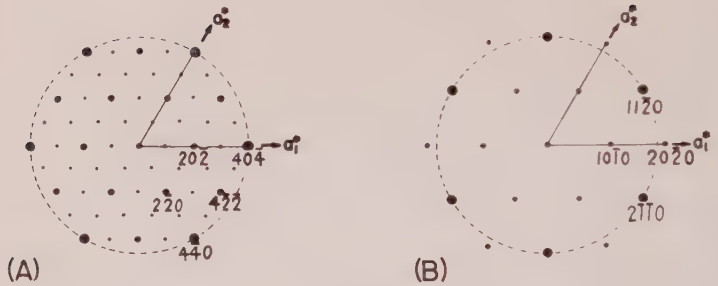

FIG. 7. Zero-level reciprocal lattice diagrams for (A) cubic lattice with respect to [111] axis, and (B) hexagonal close-packed lattice. In (A), small dots refer to simple lattice, large dots to face-centered lattice; cubic indices are given.

or, the cubic indices will be of the type $(h, k, \overline{h+k})_C$. In the zero-level of the hexagonal reciprocal lattice, $l_H=0$ and therefore $h_H=h_C$, $k_H=k_C$, and $(\overline{h+k})_H=l_C$. In other words, zero-level reflections assigned indices $(h, k, h+k, 0)_H$ with respect to hexagonal axes, may also have the indices $(h, k, \overline{h+k})_C$ with respect to cubic axes.

Reflections from a *simple* cubic lattice satisfying the relation $h_C+k_C+l_C=0$ are as follows:

$$(1\bar{1}0),\ (11\bar{2}),\ (2\bar{2}0),\ (12\bar{3}),\ (3\bar{3}0),\ (22\bar{4}),\ (13\bar{4}),\ (4\bar{4}0)\cdots$$

For a *face-centered* cubic lattice, which corresponds to cubic close-packing, only the following reflections occur:

$$(2\bar{2}0),\ (22\bar{4}),\ (4\bar{4}0)\cdots$$

Figure 7A shows these two sets of reflections referred to hexagonal axes, with the face-centered cubic reflections emphasized and with the strong reflections of type $(4\bar{4}0)$ strongly emphasized.

Figure 7B shows the zero-order array of reflections to be expected from an hexagonal close-packed system with the strong $(11\bar{2}0)$ reflections strongly emphasized in the diagram.

It is evident that the close-packed cubic and close-packed hexagonal arrangements give rise to similar E.D. patterns in the projection considered here, but the very strong reflections corresponding to planes with $d=r$ (anion) lie *on* the a_1^*, a_2^*, axes in Figure 7A, and *between* these axes in Figure 7B.

Comparison of observed and calculated E.D. patterns

Figure 5A for material heated to 270° C. corresponds exactly with Fig. 7B and it may be inferred that the gibbsite has transformed into an hexagonally close-packed arrangement of oxygen anions.

Figure 5A gives place to diagrams of the type shown in Fig. 5B at about

800° C., having weak, additional spots requiring the hexagonal net to be drawn on half the scale on Fig. 5A. It is inferred that the structure is still essentially hexagonally close-packed with the aluminum ions taking up preferential positions which require a doubling of the hexagonal a parameters.

As the temperature approaches 1000° C., the E.D. patterns remain hexagonal, but become more complex. The pattern most commonly seen is that of Fig. 5C, in which the axes have the same directions as in Figs. 5A and 5B, but the parameters are changed by a factor of 6 with respect to Fig. 5A.

In Figs. 5D and 5E, which occur much less frequently, the strong reflections at about $d = 1.39$–1.40 now lie *on* the a_1^*, a_2^* axes and to this extent correspond with Fig. 7A, but the indices are of the type $(6\bar{6}0)$ in Fig. 5D and $(3\bar{3}0)$ in Fig. 5E, and do not correspond with $(2\bar{2}0)$ or $(4\bar{4}0)$ as would be expected for cubic close-packing.

In Fig. 5F, which occurs rarely in material heated to 1180° C., the axes are oriented as in Figs. 5A, B, and C, but the pattern is simpler than in 5C; it approximates to 5B found at lower temperatures, but with more and better defined reflections.

Indexing and unit cell parameters for χ-Al_2O_3

Table 3 lists the present observed E.D. and x-ray data for χ-Al_2O_3. These have been indexed graphically on the basis of an hexagonal cell, using the indices obtained from the E.D. patterns. The following lattice parameters are obtained:

$$a = 5.57 \text{ Å} \qquad c = 8.64 \text{ A}, \qquad c/a = 1.551.$$

The axial ratio is somewhat less than the ideal value for hexagonal close-packing, 1.632, and suggests a contraction of the structure parallel to c due to the interstitial aluminum ions.

The hexagonal indices and the calculated d-values are listed in Table 3; the observed and calculated spacings are in satisfactory agreement.

The persistence of 'water' to high temperatures

The marked retardation of the dehydration reaction when about 75% complete has been observed by previous investigators (cf. Papée and Tertian, 1955). The thermo-gravimetric and the infra-red data show that the remaining 25% of 'water' is lost gradually over the temperature range from 270–800° C. In rapid heating, as in thermal analysis, the slight endothermic effect observed around 500° C. may be connected in part with this retained water. Although there are traces of boehmite formed from the fine-grained gibbsite, these traces are insufficient to produce the first boehmite endotherm (see Fig. 2).

The absence of any significant change in the E.D. and x-ray patterns between 270° and about 800° C. suggests that the structure remains essentially constant in type, although the crystallinity is obviously very poorly developed. At 830° C., when the dehydration is complete, there is an additional set of spots in the E.D. pattern which can be considered indicative of a more ordered arrangement of the Al cations. The progressive release of the water apparently does not make the structure sufficiently unstable until the temperature reaches 800° C., or thereabouts, and the 'recrystallization' (if it can be so described) still does not alter the main structural pattern which is set by the hexagonal close-packing of the anions. The 'recrystallization' probably takes the form of a re-distribution of Al ions giving a lattice parameter six times as large as that set by the oxygen ions alone.

This recalls the persistence of water in metakaolin discussed in some detail by Stubičan (1959), although the amount is much less than in χ-Al_2O_3 which might almost be described as a 'meta-gibbsite.'

Conclusions

The investigation is concerned with the thermal reactions of submicron sized gibbsite, which are confirmed to be different from those of coarser-sized gibbsite.

The disappearance of the x-ray and electron diffraction patterns of gibbsite when the material is about 75% dehydrated provides strong evidence for the retention of appreciable 'water,' probably hydroxyl ions, in the first reaction product, χ-Al_2O_3. This 'water' is lost gradually in the temperature range 270–800° C., but the diffraction patterns show little change. The diffraction data are interpreted in terms of a close-packed hexagonal type arrangement of oxygen anions, with $a = 5.57$ Å, $c = 8.64$ Å. $c/a = 1.551$.

Continuity of the structural changes occurring in the transition aluminas is shown clearly by the electron diffraction diagrams. At 970° C., a more complex structure with a large hexagonal cell, $a = 16.78$ Å, is observed which may be the form designated κ-Al_2O_3. Above this temperature α-alumina (corundum) forms, but during its formation, from 970–1180° C., other transition aluminas are recorded, in particular the forms ξ' and ν previously found by Cowley. Therefore it is believed that powder data must be interpreted with considerable caution.

Acknowledgments

This study forms part of a program on high-temperature reactions supported by a grant (G-5799) to one of us (G.W.B.) from the National Science Foundation.

J. O. Choe wishes to thank the International Cooperation Administration, Washington, D. C., for a travel grant to the U.S.A., and also the National Industrial Research Institute, Seoul, Korea, for leave of absence.

Thanks are due also to the Aluminum Company of America, and the Reynolds Metals Company for materials used in these studies.

References

Boer, J. H. de, Fortuin, J. M. H., and Steggerda, J. J. (1954a), The dehydration of alumina hydrates, *Proc. Kon. Ned. Akad. Wetensch., Amsterdam*, **B.57,** 170–180.

Boer, J. H. de, Fortuin, J. M. H., and Steggerda, J. J. (1954)b, The dehydration of alumina hydrates, II, *Proc. Kon. Ned. Akad. Wetensch., Amsterdam*, **B.57,** 434–444.

Boer, J. H. de, Steggerda, J. J., and Zwietering, P. (1956), The dehydration of alumina hydrates III. *Proc. Kon. Ned. Akad. Wetensch., Amsterdam*, **B.59,** 434–444.

Brindley, G. W., and Nakahira, M. (1957), Kinetics of dehydroxylation of kaolinite and halloysite, *J. Am. Ceram. Soc.*, **40,** 346–350.

Brown, J. F., Clark, D., and Elliott, W. W. (1953), The thermal decomposition of alumina trihydrate, gibbsite, *J. Chem. Soc.*, 84–88.

Cowley, J. M. (1953), Structure analysis of single crystals by electron diffraction. III. Modifications of alumina, *Acta Cryst.*, **6,** 846–853.

Deflandre, M. (1932), La structure cristalline du diaspore, *Bull. Soc. Franç. Min.*, **55,** 140–165.

Ervin, G. (1952), Structural interpretation of the diaspore-corundum and boehmite-γ-Al_2O_3 transitions, *Acta Cryst.*, **5,** 103–108.

Papée, D. and Tertian, R. (1955), Etude de la decomposition thermique de l'hydrargillite et de la constitution de l'alumine activée, *Bull. Soc. Chim. France*, 983–991.

Rooksby, H. P. (1951), Oxides and hydroxides of aluminium and iron, Chapter 10 of "X-Ray Identification and Crystal Structures of Clay Minerals," G. W. Brindley (Editor), Mineralogical Society, London.

Russell, A. S., *et al.* (1956), "Alumina Properties," Technical paper No. 10 (revised), Aluminum Co. of America, Pittsburgh, Pa.

Saalfeld, H. (1958), The dehydration of gibbsite and the structure of a tetragonal γ-Al_2O_3 *Clay Min. Bull.*, **3,** 249–257.

Saalfeld, H. (1959), Einkristalluntersuchungen zum Problem der Hydrargillit-Entwässerung, *Z. Krist.*, **112,** 88–96.

Stubičan, V. (1959), Residual hydroxyl groups in the metakaolin range, *Miner. Mag.*, **32,** 38–52.

Stumpf, H. C., *et al.* (1950), Thermal transformations of aluminas and alumina hydrates, *Ind. Eng. Chem.*, **42,** 1398–1403.

Tertian, R. and Papée, D. (1958), Transformations thermiques et hydrothermiques de l'alumine, *J. Chim. Phys.*, 341–353.

Manuscript received July 13, 1960.

Note added in press: Since this work was completed, a further contribution by H. Saalfeld has appeared (N. Jb. Miner., Abh., 95, 1–87, June 1960) which also discusses the χ-κ reaction series. His results and those reported here agree in some respects, but not in others.

VONSENITE AT THE JAYVILLE MAGNETITE DEPOSIT, ST. LAWRENCE COUNTY, NEW YORK*

B. F. LEONARD, *U. S. Geological Survey, Denver, Colorado*

AND

ANGELINA C. VLISIDIS, *U. S. Geological Survey, Washington, D. C.*

ABSTRACT

The opaque mineral vonsenite, a high-temperature borate of the ludwigite-vonsenite series having the composition $(Fe''_{1.92}Mn_{.01}Mg_{.04})(Fe'''_{.96}Al_{.07}Ti_{.004})B_{.98}O_5$, occurs in skarn in the pyrometasomatic magnetite deposit at Jayville, New York. One magnetite zone contains 4.80% B_2O_3, perhaps equivalent to 36 weight per cent vonsenite. Major associates are biotite, dark clinoamphiboles, salite, and hypersthene. Quartz, fluorite, zircon, chlorite, ferroan talc, hematite, pyrite, chalcopyrite, goethite, and unidentified minerals are sparingly present. Fluorite and ferroan anthophyllite are locally abundant in neighboring skarns. Vonsenite is also present, though rare, at the Clifton mine, near Degrasse, New York.

In hand specimen, Jayville vonsenite is black, metallic to adamantine, granular, weakly magnetic, and indistinguishable from associated magnetite. In polished section, vonsenite forms polygonal aggregates and occasional stubby prisms having a diamond shaped cross section; reflection-pleochroism very strong, gray or brown to blue, slightly intensified in oil; anisotropism very strong, black to fiery orange, slightly reduced in oil; $\bar{R}_{air}=13\%$ (green), 12.5% (orange), 12% (red); $\bar{R}_{oil}=3\%$ (orange); hardness F or >; HCl (+), aqua regia (+) but weak, other standard reagents (−). G.=4.77. Cell dimensions: $a_0\sim9.47$, $b_0\sim12.31$, $c_0\sim3.07$ Å (from *x*-ray powder data).

The chemical composition of Jayville vonsenite, corrected for sparse impurities, is: FeO 54.04, MnO 0.28, MgO 0.56, Fe_2O_3 30.14, Al_2O_3 1.48, TiO_2 0.13, B_2O_3 13.37; sum 100.00 weight per cent. Spectrographic analysis shows 0.x% Sn. In composition, this vonsenite closely approaches the $Fe''Fe'''BO_5$ end-member of the ludwigite-vonsenite series.

INTRODUCTION

In the winter of 1947, Leonard found an unidentifiable metallic mineral in ore from two drill holes at the Jayville magnetite deposit, New York. The striking optical properties of the unknown set it apart from other metallics that had been investigated mineragraphically and described in the literature. It was thought for a while that the unknown might be ilvaite. In the spring of 1950, G. G. L. Henderson, then of Princeton University, investigated the unknown under the direction of Edward Sampson. Henderson made the usual etch tests and bored from the polished specimen enough fairly pure material for spectrographic analysis and *x*-ray study. His *x*-ray work showed that the unknown was not ilvaite, but attempts to identify the mineral were fruitless for want of matching *x*-ray data. During January 1951, samples isolated by Henderson were studied by J. M. Axelrod and Janet D. Fletcher of the U. S.

* Publication authorized by the Director, U. S. Geological Survey.

Geological Survey. *X*-ray work by Axelrod and spectrographic analysis by Miss Fletcher identified the unknown as vonsenite (ferrous ferric borate). Later, W. T. Schaller purified a 3-gram sample of the vonsenite, determined its specific gravity, and arranged for further chemical and *x*-ray study.

Vonsenite at first appeared to be something of a mineral curiosity at Jayville. However, the routine assays for one core interval known to contain vonsenite showed a very high soluble Fe content (about 38%) for the nonmagnetic fraction.* The quantity of hematite visible in the cores was far too small to account for so much soluble nonmagnetic Fe. With some hesitation, we ascribed it to vonsenite. Lacking material for a detailed mineralogic study of this core interval, we obtained cuts of the ground samples originally used for iron assay. Upon analysis, the composite sample of crude ore showed B_2O_3 equivalent to about 36 wt. per cent vonsenite. The nonmagnetic fraction (tails) showed B_2O_3 equivalent to about 42 wt. per cent vonsenite. Some iron-rich boron-bearing mineral is thus a major constituent of part of the ore zone, and it seems reasonable to conclude that most if not all the boron is present in vonsenite.

Vonsenite has been found in one specimen of ore from the Clifton magnetite deposit, 13 miles northeast of Jayville, but it has not been identified in other ores from the district. Possibly, traces of other borates occur in a few of the many ore specimens examined, but confirmation of this suspicion is still lacking.

A preliminary note on the Jayville vonsenite was recently published (Leonard and Vlisidis, 1960). Vonsenite, first described and analyzed by Eakle (1920), is now known to be isostructural with ludwigite (W. T. Schaller, *in* Leonard and Vlisidis, 1960). The crystal structure of ludwigite was first determined by Takéuchi, Watanabé, and Ito (1950). A more refined determination was made by daSilva, Clark, and Christ (1955). Takéuchi (1956) determined the crystal structure of vonsenite. Federico (1957) determined the crystal structure of breislakite and showed that this disputed mineral is identical to vonsenite. Members of the ludwigite-vonsenite series are orthorhombic, with space group *Pbam*. The structural formula $4[Mg_2Fe'''BO_3O_2]$ reported by daSilva, Clark, and Christ (1955) may be generalized for the series to $(Mg, Fe'')_2\,(Fe''', Al)BO_5$. In this paper, the name ludwigite is given to members of the series in which Mg atoms > Fe″ atoms, and vonsenite to members in which Fe″ atoms > Mg atoms. Only a few published analyses of vonsenite were known

* *Soluble Fe* is iron soluble in HCl. *Magnetic Fe* is HCl-soluble Fe determined on a magnetic concentrate made in a Davis tube. For magnetite ores of the sort found in St. Lawrence County, magnetic Fe determined by the Davis tube method corresponds very closely to the iron content of magnetic concentrates milled from the same ore.

in 1960. These represent material from the River Dogdo, Chersky Range, Siberia (Vakar, Knipovich, and Shafranovskii, 1934); Riverside, California (Eakle, 1920); Monte Cimino, Italy (Federico, 1957); Kamaishi mine, Iwate prefecture, Japan (Watanabé and Ito, 1954); and Jayville, New York. The compound $4FeO \cdot Fe_2O_3 \cdot B_2O_3$, a synthetic Fe″-vonsenite, has been synthesized by Andrieux and Weiss (1944), Chevallier, Mathieu, and Girard (1948), Bertaut, Bochirol, and Blum (1950), and Federico (1958).

A subsequent paper will consider the distinction of vonsenite from ilvaite.

The Magnetite Deposit

The Jayville magnetite deposit, west-central ninth, Oswegatchie quadrangle, St. Lawrence County, New York, is 1.25 miles east of the hamlet of Kalurah. The mine workings are on the east and west flanks of a low north-trending hill, just west of the former Jayville railroad station. The deposit, opened and abandoned in the latter half of the 19th century, yielded a small tonnage of iron ore from scattered pits and underground workings. The ore shipped ranged in grade from 40 to 60% Fe. The deposit was explored in 1941 by the Jones and Laughlin Steel Corporation, whose eight drill holes tested parts of the deposit to a vertical depth of about 250 feet. Drilling showed that the main ore body was a short lens, 6 to 17 feet thick, averaging 43 to 46% soluble Fe. Phosphorus, sulfur, and titanium are low. Other magnetite-bearing zones of similar grade were encountered, but these are smaller and thinner. The possibility of finding commercially significant tonnages of medium- or low-grade iron ore seems slight.

The main ore body appears to be a shoot, plunging moderately northward in steeply-dipping metasedimentary rocks on the northwest limb of a compound, overturned, isoclinal syncline enclosed by granitic rocks. (Figs. 1 and 2). The metasediments are mainly skarn (metasomatized limestone or dolomite), though some biotite-quartz-plagioclase gneiss and amphibolite are also present. These rocks are referred to the Grenville series, which, together with the granitic rocks, is of Precambrian age. Pertinent aspects of regional geology are treated by Buddington (1939), Dale (1935), and Engel and Engel (1953, 1958). The magnetite deposits and regional geology of the district are described in forthcoming Geological Survey reports (Buddington and Leonard, in preparation; Leonard and Buddington, in preparation). The geologic description of the Jayville deposit found therein is based on an excellent, unpublished report by Tyler and Wilcox [1942], supplemented by the studies of Buddington and Leonard.

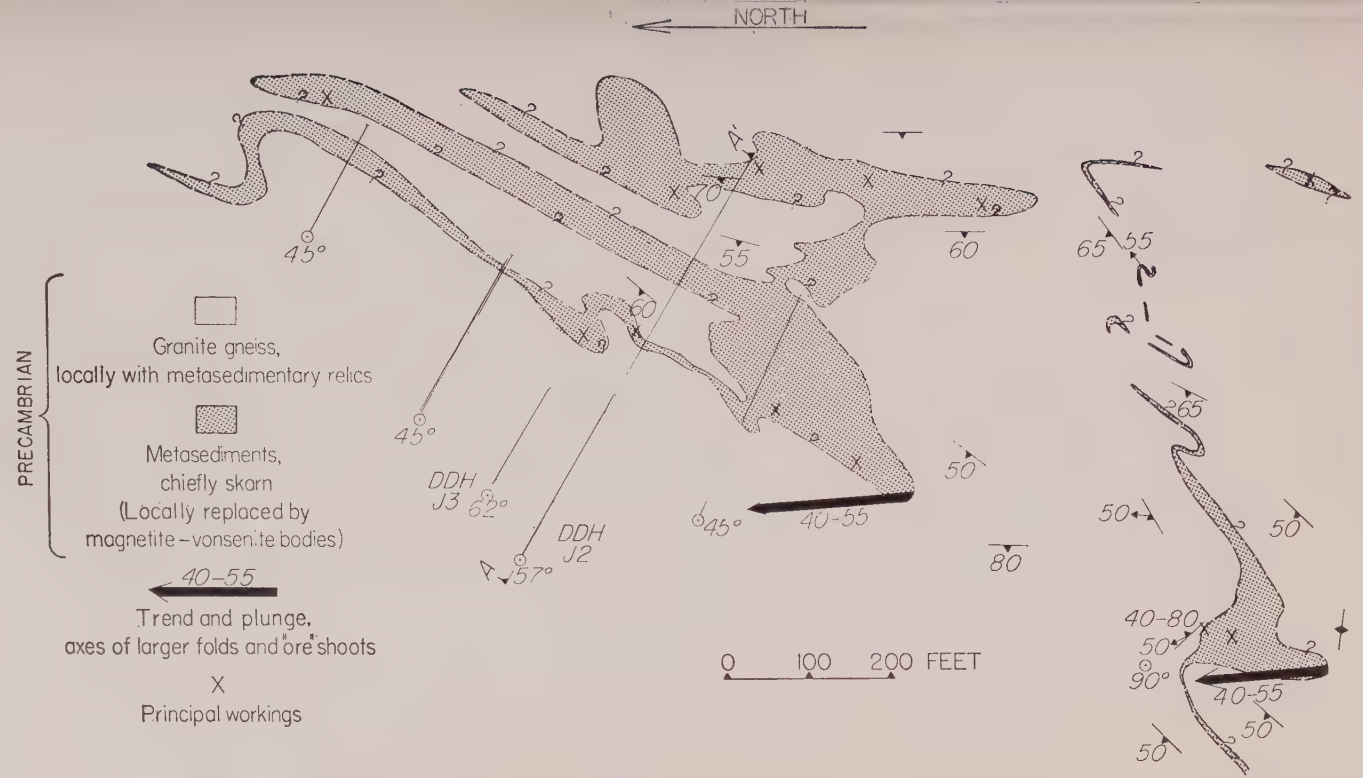

FIG. 1. Geologic sketch map of Jayville magnetite deposit, New York.

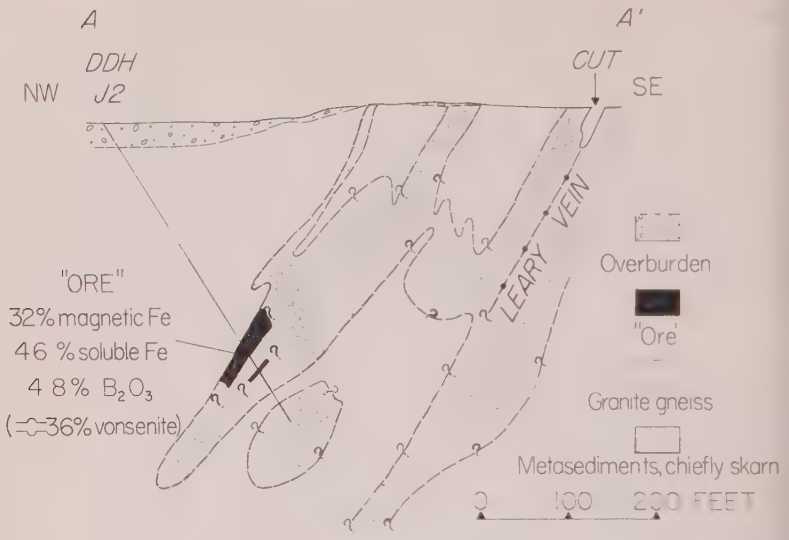

FIG. 2. Cross section of Jayville magnetite deposit.

Magnetite, the chief ore mineral at Jayville, is accompanied in place by vonsenite and by supergene hematite. The ore minerals selectively replace dark mica sköls*, pyroxene-amphibole skarn, and quartz-bearing amphibole skarn in dark skarn zones, predominantly pyroxenic, flanked by contaminated alaskite gneiss and soda granite. Parts of the skarn and ore are rich in fluorite. Anthophyllite skarn is prominent locally. The Jayville deposit is the unique example, among iron deposits of the district, of intense boron-fluorine metasomatism comparable to that described by Geijer (1939), Watanabe (1943, 1953), and Tilley (1951).

The quantitative importance of vonsenite in at least one part of the main ore zone is indicated by the data in Tables 1 and 2. From the known mineralogy of the cores, their high B_2O_3 content, and the high soluble Fe content of the nonmagnetic fraction, we infer that vonsenite is a major constituent of this part of the ore zone. This is the only part of the zone for which samples were magnetically separated and the soluble Fe content of the tails determined by the Jones and Laughlin Steel Corporation; for all other samples taken during exploration, only the soluble Fe content of the crude ore was determined. Thus there are in

* A feature of some skarns is the presence of mica as contorted, streaky masses, thick selvages, partings, or thin films in skarn or magnetite ore. The selvages and partings are analogous to one type of sköl -or, mnemonically, shell—often noted by Fennoscandian geologists.

TABLE 1. GRADE (WT. PER CENT) OF MAIN ORE ZONE, JAYVILLE DEPOSIT, WHERE SAMPLED BY HOLE J2, INTERVAL 293.5–311 FEET[1]

	Crude ore	Magnetic concentrate[2]	Tails[3]
Soluble Fe	45.73	70.09	38.61
Magnetic Fe	32.05	—	—
P	0.013	—	—
S	0.110	—	—

Apparent thickness 17.5 ft.
True thickness 14.5 ft.

Analysts, chemists of Jones and Laughlin Steel Corporation.

[1] Data from Tyler and Wilcox [1942].
[2] Davis-tube concentrate.
[3] Nonmagnetic fraction from Davis tube.

sufficient chemical clues to the distribution of vonsenite throughout the magnetite shoots. However, vonsenite has been identified optically in other parts of the ore zones at Jayville, as well as in specimens from the dumps. It seems that the mineral is a major one for that deposit.

The chemical analyses of crude ore and tails (Table 2) cannot safely be recalculated in terms of ideal mineral composition, for it seemed probable

TABLE 2. PARTIAL CHEMICAL ANALYSES (WT. PER CENT) OF CORE FROM MAIN ORE ZONE, JAYVILLE DEPOSIT, HOLE J2, INTERVAL 293.5–311 FEET

	Crude ore	Magnetic concentrate	Tails
B_2O_3	4.80	0.32	5.66
Fe_2O_3	28.67	62.45	20.09
FeO	33.50	32.15	34.81
MnO	0.23	0.10	0.22
TiO_2	0.40	0.54	0.55
Insol. residue	18.93	1.93	20.93
Total	86.53	97.49	82.26
≐ Soluble Fe	~46	~69	~41
≐ Vonsenite*	~36	~ 2	~43

Analyst, Angelina C. Vlisidis.

* Based on B_2O_3 content of analyzed vonsenite, sample J2.21, Table 3, No. 1, and Table 7.

during the analytical work that the silicate minerals were considerably attacked by the acid treatments given the samples. No sharp distinction could thus be made between the acid reactivity of the vonsenite and magnetite, and that of the associated silicates. The low totals of the analyses are to be expected, owing to the high content of volatiles in the gangue minerals. (See petrography, below.)

The Vonsenite

Physical Properties in Hand Specimen

In hand specimen, vonsenite is indistinguishable from the fine-grained magnetite with which it commonly occurs. The vonsenite forms dark-gray to black, granular aggregates with metallic (locally adamantine) luster. On rough-sawn surfaces, vonsenite looks black and adamantine against magnetite, the latter appearing dark gray and metallic. Stubby prisms of vonsenite are sometimes distinguishable on sawn surfaces. Powdered vonsenite is weakly magnetic, but because of the intimate association of vonsenite and magnetite, this property is not of much use in distinguishing the two minerals where they constitute ore. If one examines polished specimens of ore with the naked eye, one sees that the vonsenite is definitely metallic. Relative to magnetite, the vonsenite appears bluish; and its reflectivity or "brightness" relative to magnetite is about the same as the reflectivity of magnetite relative to primary crystalline hematite.

Microscopic Occurrence

The quantity of vonsenite, as well as its mineral association, varies considerably in the specimens studied. The approximate modes of three specimens are given in Table 3, and the optical properties of their major skarn silicates are given in Table 4. Details of the crystal habit of vonsenite are given in a separate section.

A thin section of "high-grade ore" (Table 3, No. 1) from a biotite sköl shows magnetite and vonsenite (both gray and opaque, but the vonsenite darker) replacing a crystalloblastic aggregate of pale-green biotite and strongly pleochroic hypersthene. A few grains of blue pargasite are also present, as well as traces of zircon and one or more unidentified accessories. The paragenetic sequence inferred from the shapes of the constituent minerals is: hypersthene→pargasite and biotite→magnetite and vonsenite. Vonsenite has replaced biotite in preference to hypersthene, though it has also attacked the latter. The polished section of this rock shows aggregates of magnetite and vonsenite, generally as polygonal grains, replacing the nonopaques. Vonsenite also occurs as scattered sub-

TABLE 3. MINERAL COMPOSITION (VOL. PER CENT) OF SOME VONSENITE-BEARING ORES AND SKARN AT JAYVILLE[1]

	1	2	3
	J 2.21	J 3.11	J 3.10
Vonsenite	35	25.4	0.8
Magnetite	27	—	58.0
Hematite	<1	—	x
Pyrite	—	—	1.0
Chalcopyrite	—	tr.	—
Goethite	—	0.4	—
(Metallics)	(62)	(25.8)	(59.8)
Quartz	—	—	5
Biotite	25	—	<1
Clino-amphibole	1	22	35
Clinopyroxene	tr.	52	—
Orthopyroxene	12	—	—
Zircon	tr.	—	—
Fluorite	—	tr.	—
Unidentified accessories	tr.	x	x
Chlorite	x	x	x
Talc	—	x	—
Unidentified alteration product	x	x	—
(Gangue)	(38)	(74)	(40)
Total	100	100	100

[1] Because of holes in the thin sections, values for nonopaque minerals are crudely approximate. All specimens are generally medium-grained.

No. in table	*Specimen no.*	*Description*
1	J 2.21	"High-grade ore" from dark-green biotite sköl, hole J2, depth 299 ft.
2	J 3.11	"Low-grade ore" from medium-green pyroxene-amphibole skarn, hole J3, depth 267 ft.
3	J 3.10	"High-grade ore" from dark-green amphibole skarn, hole J3, depth 258 ft.

hedral and euhedral crystals in the gangue. (See crystal habit, below.) The magnetite and vonsenite appear to be contemporaneous. A few hair-thin veinlets of secondary hematite cut both gangue and vonsenite. Ragged, crudely bladed patches of hematite replace the vonsenite locally. Some vonsenite grains show thin partial rims of hematite. Commonly the hematite rim is confined to a single edge of a vonsenite grain, has a smooth outer edge and a ragged inner edge, and occurs between vonsenite and gangue.

TABLE 4. OPTICAL PROPERTIES OF SOME SKARN SILICATES ASSOCIATED WITH VONSENITE AT JAYVILLE

	1*a* J 2.21 Hypersthene	1*b* J 2.21 Pargasite	1*c* J 2.21 Biotite	2*a* J 3.11 Actinolite	2*b* J 3.11 Talc	3 J 3.10 Hornblende
α[1]	1.738	1.647	1.551	1.616	~1.560	1.652
β	1.750	1.655	1.588	1.628	1.600	1.666
γ	1.756	1.667	1.588_5	1.639	1.600	1.675
γ-α	0.018	0.020	0.037_5	0.023	~0.040	0.023
Optic sign	(−)	(+)	(−)	(+)[3]	(−)	(−)
$2V_{meas.}$	$69\frac{1}{2}° \pm 1°$[2]	$81\frac{1}{2}° \pm 2°$	11°	87° ± 1°	5° or <	78° ± 3°
Dispersion of optic axes	1st axis: $r<v$, strong 2nd axis: $r<v$, very strong	A: $r<v$, weak B: $r<v$, weak	$r<v$, weak	A: $r<v$, weak B: $r<v$, strong	—	A: $r>v$, moderate B: $r>v$, strong
$Z \wedge c$	~0°	$21\frac{1}{2}° \pm 1\frac{1}{2}°$	—	$21\frac{1}{2}° \pm 1°$	—	$22\frac{1}{2}° \pm 2°$
X	pink	very pale greenish yellow	colorless	very pale yellow	colorless	pale yellow
Y	yellowish pink	green	very pale greenish gray	pale yellowish green	colorless	dark gray-green
Z	green	blue	very pale greenish gray	pale greenish blue	colorless	dark blue or greenish blue
Absorption	Z>X>Y	Z≈Y>X	Z≈Y>X	Z≈Y>X	—	Z>Y>X
Orientation	X=one crystal axis	Y=*b*	—	Y=*b*	—	Y=*b*
Lamellae	{100}	{001}	—	—	—	{001}[4]

[1] Refractive indices, determined in Na light, are ±0.002 for 1*a*, ±0.001 for the rest.

[2] Other values of 74°, obtained indirectly.

[3] Sign obtained by U-stage. Negative sign obtained by differences in refractive indices is incorrect, owing to low accuracy (±0.001) of index determinations.

[4] Also rare pair twins with composition plane {100}.

The biotite (Table 4, No. 1*c*) is a variety common in the sköls at Jayville. Its optical properties, intermediate between those of analyzed phlogopite and biotite from sköls of the district (Leonard and Buddington, in preparation) suggest that it is moderately ferroan.

The hypersthene (Table 4, No. 1*a*) is unusual. Hypersthene is a rare mineral in skarns in the district. Moreover, the Jayville hypersthene has peculiar properties; namely, anomalously high interference colors, abundance of prominent partings, and comparative rarity of {110} cleavage. Identification of the mineral as hypersthene has been confirmed by an *x*-ray powder diagram (Richard Marquiss, 1956, personal communication). Diagnostic optical properties suggest a composition near $Mg_{25}Fe_{75}$. (Cf. Fig. 2 of Hess, 1952.) In the terminology adopted by Poldervaart and Hess (1951, p. 474), the mineral is a *eulite*.

The hypersthene shows combinations of a number of very strong, regular, parallel, planar cracks that one would suppose to be cleavages. Some of these cracks are paralleled by minute, elongate opaque inclusions. Within 1°–3°, as determined by universal stage, these cracks are referable to the {100}, {010}, and {001} partings of hypersthene, and to the {110} cleavage. The {100} parting was observed most frequently. Equally well developed cracks could be referred to an assortment of pyramidal forms. A feature strongly resembling polysynthetic twinning of non-normal type is prominent in some grains. Its orientation corresponds to {100} of hypersthene. Ordinarily, one would interpret the features as exsolution lamellae of a ferroan clinopyroxene near hedenbergite in composition. Though some properties of the lamellae are consistent with that interpretation, others are not.

The lamellae are best seen on sections $\perp$ X of the host. In plane-polarized light, the lamellae are all but invisible, their color and refringence being virtually indistinguishable from those of the host. With nicols crossed and the host at extinction, the lamellae generally appear as fine to very fine, bright, straight, parallel bands that extend across the entire grain. A few lamellae pinch out toward the edges of the host. Lamellae are also visible on sections $\perp$ Z of the host. The lamellae are generally too thin to permit determination of their internal optical orientation. However, a few grains have lamellae in which the orientation of the principal optical planes can be established within about 5°. These lamellae seem to have $2V_Z$ moderate or large, optic plane about 10° (?) from the optic plane of the host. These observations are inconsistent with the known relation between orthopyroxene (host) and clinopyroxene (exsolved lamellae), wherein the optic planes of the two pyroxenes are perpendicular. If the lamellae are due to exsolution, then the exsolved phase is not the expectable one —a clinopyroxene of the diopside-hedenbergite series.

If the lamellae are due to twinning, the "orthopyroxene" must be very slightly monoclinic or triclinic. H. H. Hess (1958, personal communication) examined the hypersthene and suggested that the lamellae might represent an unusual exsolved amphibole, though the data were inconclusive.

Pargasite (Table 4, No. 1*b*) is not known to be a common constituent of amphibole skarns in the district. Its recognition at Jayville is made more difficult because some of the skarns contain an optically negative hornblende of similar color, extinction angle, and α. (Cf. Table 4, No. 3.) Both varieties commonly show partial or complete lamellae (twinning, rather than exsolution?) $\parallel \{001\}$. Pargasite similar to No. 1*b* has been found at the Clifton mine, where amphibole skarns are very sparse.

Vonsenite without magnetite occurs in a specimen of actinolite-salite skarn logged as low-grade iron ore (Table 3, No. 2). The fine- to medium-grained skarn has a strong foliation given by subparallel alignment of actinolite prisms and by layers alternately rich in actinolite, salite, or vonsenite, the last replacing both silicates. In polished section, most of the vonsenite occurs as nearly equant, roundish, elliptical, or polygonal grains, locally highly elongate. Some pairs of roundish grains are connected by narrow bridges. A few diamonds and laths of vonsenite are also present. (See crystal habit.) The very rare chalcopyrite replaces silicates and perhaps vonsenite as well. Filigree-like goethite, presumably supergene, partly replaces silicates near clusters of vonsenite. Rarely, goethite replaces vonsenite.

The pyroxene, a very pale green salite, has $\alpha = 1.686$, $Z \wedge c \sim 43°$. Presumably it is near $Ca_{50}Mg_{36}Fe_{14}$ in composition. (Cf. plate 6 of Hess, 1949.) Though some of the salite is fresh, much of it is partly or almost wholly altered to aggregates of very fine grained talc, locally accompanied by small patches of blue-green chlorite, limonite, and an unidentified isotropic, amber-colored mineral of low refractive index. Megascopically, the talc is visible as white specks, commonly somewhat stained by limonite. The optical identification of the talc (Table 4, No. 2*b*) was confirmed by an *x*-ray powder diffraction pattern (A. J. Gude, 1957, personal communication). The high refractive indices of the talc suggest a ferroan variety approaching minnesotaite in composition. This deduction regarding composition is borne out by the *x*-ray film, whose strong background Gude attributed to iron fluorescence.

The actinolite (Table 4, No. 2*a*) is uniformly fresh. Its grains—larger than those of pyroxene—are relatively stubby, not acicular. Though this amphibole is optically positive, its other characteristics are those common to actinolite.

Vonsenite is present as an accessory in "high-grade ore" whose host rock is quartz-bearing hornblende skarn (Table 3, No. 3). Pale-green biotite flakes and green chlorite patches are sparingly present in the skarn. The geometry of the fabric suggests that quartz, hornblende, and biotite grew simultaneously, the biotite perhaps forming late in the sequence. Magnetite and vonsenite replace hornblende, biotite, and quartz. Subhedral vonsenite grains, usually attached to magnetite, appear to be contemporaneous with or slightly younger than the magnetite. Pyrite replaces magnetite and gangue. Sparse secondary hematite is present as flecks and as crack fillings in gangue. Relations between chlorite and the opaque minerals are indeterminate.

The hornblende (Table 4, No. 3) is representative of one principal variety of clinoamphibole found in the Jayville skarns, the other being a ferrohastingsite of very similar color and extinction angle but having higher refractive indices and much smaller 2V.

Crystal Habit

Though the vonsenite is mostly granular (Figs. 3*a* and 5*b*), some euhedral and subhedral grains are present (Figs. 4*a* and 4*b*). In two dimensions, these are lath-, wedge-, and diamond-shaped, commonly with rounded corners. The crystals are relatively stubby, not showing the highly elongate or fibrous habit usually regarded as typical of members of the ludwigite-vonsenite series, including the synthetic Fe″ end-member. The observed forms of the Jayville vonsenite are {001}, {010}, {100}, {3.10.0}, {380}(?), {250}, {120}, {590}(?), and {320}, in the setting adopted by Eakle (1920, p. 142; $a:b \approx 0.76:1$) for Riverside vonsenite.* In cross section, most crystals are single prisms, locally modified by a front or side pinacoid. Domes have not been recognized. The forms were identified on suitably oriented crystals that were measured in their matrix in polished sections viewed microscopically. We were unable to isolate good crystals for measurement by goniometer.

The form {100} has not previously been reported for natural members of the ludwigite-vonsenite series, though Chevallier, Mathieu, and Girard (1948) observed it on synthetic vonsenite.

Rare grains show a few broad lamellae, resembling twins. Adjacent lamellae plainly differ in optical orientation; their crystallographic orientation could not be determined.

* The same setting was adopted by Chevallier, Mathieu, and Girard (1948) for synthetic $4FeO \cdot Fe_2O_3 \cdot B_2O_3$. This setting is consistent with all the *x*-ray data subsequently reported. Accordingly, it is adopted here, in preference to the setting used in Dana VII, 2 1951, p. 322, 324; $a:b \approx 0.66:1$). Transformation, Dana VII to Eakle, 010/200/001.

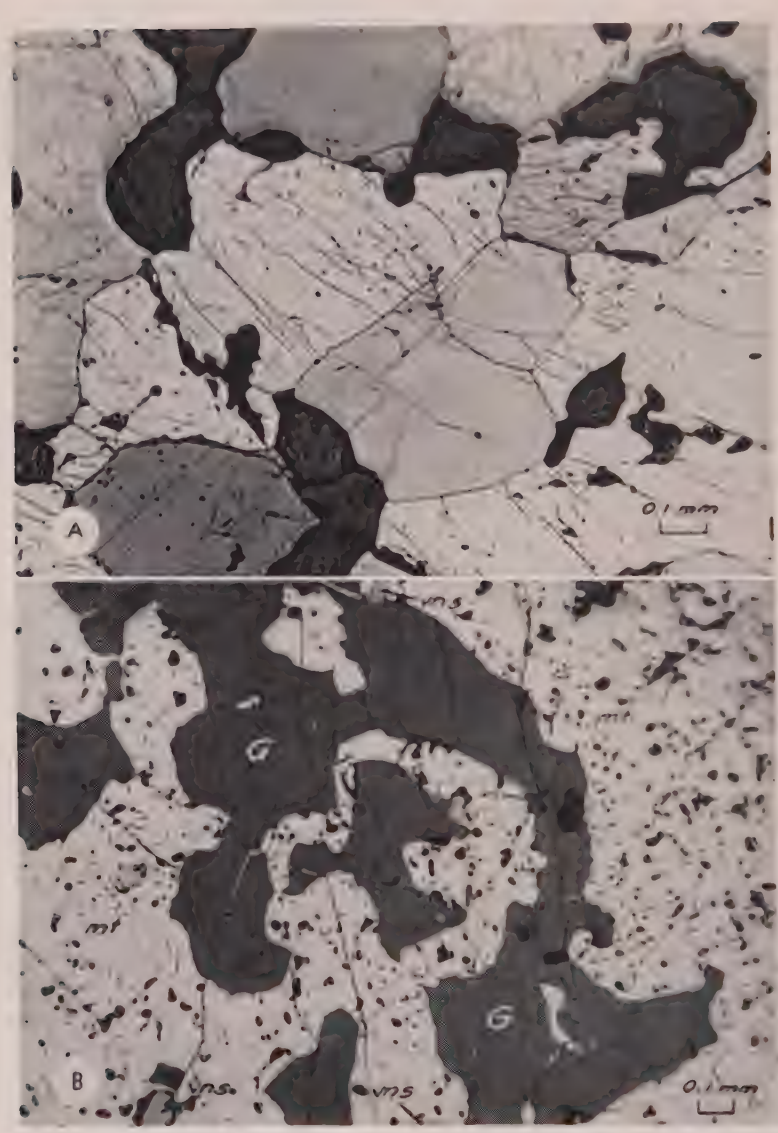

FIG. 3. Photomicrographs of polished sections of Jayville vonsenite.

(A) Granular habit of vonsenite. All but rough, nearly black material is vonsenite, in part slightly etched by HCl. Nicols partly crossed.

(B) Magnetite (mt) replacing gangue (G). Sparse vonsenite (vns) has intermediate reflectivity. Single nicol.

Optical Properties and Etch Tests

The vonsenite is opaque in thin section and in very finely crushed fragments. Crushed fragments are irregular, lacking distinctive shape. Their refringence is very high but indeterminate in oils, owing to complete absorption. In polished sections examined with the reflecting microscope, the vonsenite shows the following properties. *Color*—very strongly pleochroic from light gray or light brown to light blue-gray, slightly intensified by the oil-immersion objective ("in oil"). The brown color approaches that of magnetite; the blue-gray color looks very bluish against the brown of magnetite. Diamond-shaped vonsenite crystals—{001} sections bounded chiefly by {120}—look brown ‖ the long axis and blue-gray ‖ the short axis. Lath-shaped crystals are brown ‖ their length and gray or blue-gray across it. More fully stated, the reflection-pleochrosim is: a = gray (looks brown relative to b, but blue relative to c), b = blue or blue-gray, c = brown or pinkish brown. These relations were determined on specially cut sections of vonsenite from Riverside, California, as they could not be established on the Jayville material. Because the color of adjacent, variously oriented grains so markedly affects the apparent color ‖ a, the observer sees only bluish and brownish tones in an aggregate of vonsenite grains. *Reflectivity*—less than that of magnetite, but much greater than that of polished iron-rich pyribole and biotite. (See Figs. 3*b* and 5*a*.) Reflectivity measurements for vonsenite are reported in Table 5. These reflectivity measurements are part of a set whose relation to the data of other workers was previously established (Leonard, 1960). *Anistropism*—very strong, slightly diminished in oil. No internal reflection. Extinction ‖ long edges of laths but symmetrical in wedges and diamonds. Extinction details: with nicols set at 90°, four extinction positions per 360° rotation. The mineral is black at extinction; in the position of maximum illumination, it is fiery orange, somewhat resembling covellite as seen in the analogous position. With nicols nearly crossed, at 82°, two positions of extinction. The mineral is blue at extinction and pink or reddish brown at maximum illumination. The blue color seen between nearly crossed nicols corresponds to the blue-gray color seen in light from a single nicol; the pink or reddish brown corresponds to the light brown. Grains that show zero anisotropism under nicols set at 90°, are blue-gray in light from a single nicol. *Twinning*—broad twin lamellae are present in some grains.

Polarization figures—The polarization figures (Table 5) were obtained with a conventional ore microscope and strain-free high-power dry objective 6FL. The glass plate was inserted in place of the reflecting prism in the vertical illuminator, the ocular was removed, and the apparent

FIG. 4. Photomicrographs of polished sections of Jayville vonsenite.

(A) Vonsenite "diamond": {001} section showing {120} prism and {100} pinacoid Bright grains at left is chalcopyrite (cp). Single nicol.

(B) Vonsenite "lath" (left): section $\parallel c$, truncated at beveled top by {001}. Part of a "diamond" shows at upper left. Other prism sections to right of center. Single nicol.

Reflectivity (per cent) and orientation[1]

	Green	Orange	Red
Air			
Rg∣c	14.5	14.5	14.5
Rm∣a	12.5	12.5	12
Rp∣b	11.5	10.5	9.5
Rg−Rp	3	4	5
$\overline{R}$[2]	13	12.5	12
Oil			
$\overline{R}$	—	3	—

Instrument: Hallimond visual microphotometer.
Standard: In air, quartz {0001}. Accepted R_0=4.61% (green), 4.58 (orange), 4.54 (red), as reported by Hallimond (1953, p. 179).
In oil, galena from the Maggie M. mine, Central City district, Colorado (P. K. Sims' specimen S-543,53). R_{air}=39.9% (red), using quartz standard. For oil (n_{Na}=1.5145 at 24.0° C.), accepted standard value R_{oil}=27.13% (orange), determined by Cissarz (1932, p. 449).
Filters: green—Chance OGR 1; $\lambda_{max.}$=530 mμ, T_{max}=42%, HW=90 mμ.
orange—Ilford Spectrum Orange 607; $\lambda_{max.}$=590 mμ, $T_{max.}$=16%, HW=40 mμ.
red—Ilford Spectrum Red 608; $\lambda_{max.}$=730 mμ, $T_{max.}$=86%, HW>200 mμ.
blue (for rotational properties)—Schott PAL 660509; $\lambda_{max.}$=478 mμ, $T_{max.}$=54%, HW=20 mμ.
Filter characteristics determined in air by spectrophotometer by F. N. Ward. Data reported for visible spectrum only.

Polarization figures and rotational properties[3]

	Relative dispersion of reflection rotation (DR_r)	Apparent angle of rotation (A_r)			Relative dispersion of A_r (DA_r)	Amount of dispersion	Figure after rotation of analyzer	Figure at 45° position; × nicols
		Blue	White	Red				
{001} section, Spc. J3.11	v>r, weak	obs.[4] 1.9°	2.3°	3.1°	r>v, moderate	obs. 1.2°	Isogyres black; concave gray, convex reddish brown.	Isogyres black; v>r, strong; concave slightly greenish gray, convex brownish; center of field gray.
		corr.[5] 1.5°	2.1°	2.8°		corr. 1.3°		
		$e_{calc.}$[6] n.d.	1.9°	3.2°		n.d.		
Section∣c; grain showing maximum anisotropism, Spc. J3.11[7]	v>r, weak or moderate	obs. 2.8°	3.5°	4.6°	r>v, strong	obs. 1.8°	Isogyres black; concave bluish gray, convex brownish red, grading to central field of brownish gray.	Isogyres black; v>r, strong; concave grayish blue; convex brownish red, grading to central field of brownish gray.
		corr. 2.2°	3.0°	4.0°		corr. 1.8°		
		$e_{calc.}$ n.d.	4.0°	6.0°		n.d.		
Grain showing maximum anisotropism, Spc. J2.21[7]	v>r, weak or moderate	obs. 2.4°	3.1°	4.6°	r>v, strong	obs. 2.2°	Isogyres gray; concave blue to grayish blue, convex brownish red.	Isogyres black; v>r, strong; concave blue, convex brownish red. Center of field dark brownish gray.
		corr. 1.9°	2.7°	4.0°		corr. 2.1°		
		$e_{calc.}$ n.d.	n.d.	n.d.		n.d.		

[1] Crystallographic orientation is that of Eakle (1920), which agrees with subsequent x-ray data.
[2] $\overline{R}=(Rg+Rp)/2$.
[3] Methods and notation are those of Cameron and Green (1950).
[4] Observed angle.
[5] Angle corrected for rotation induced by reflecting glass plate. (See Cameron, Hutchinson, and Green, 1953, p. 587.)
[6] Angle calculated from the equation e (in radians) $=\frac{1}{2}(\rho-1)/(\rho+1)$, where $\rho=Rg/Rp$, and R is expressed as a decimal ratio, not per cent. (Cf. Hallimond, 1953, p. 120.) The value of e reported for white light represents $\frac{1}{2}(e_{orange}+e_{green})$.
[7] Data for most strongly ansiotropic grain found. Photometry shows that no single grain in the polished section shows true maximum bireflection; hence the discrepancy between $e_{calc.}$ and A_r.

angle of rotation was measured by rotating the analyzer. The methods and notation are those of Cameron and Green (1950).

The agreement between A_r (measured, uncorrected) and e (calculated) is rather good for the one grain, the {001} section, that had a crystallographic axis parallel to the microscope axis. The values for A_r measured on grains having apparent maximum anisotropism, also shown in Table 5, are the best obtainable on dozens of grains checked. However, reflectivity measurements show that no single grain in these specimens is so oriented as to exhibit true maximum bireflection. Rg and Rp can, of course, be measured and confirmed on separate grains, but the true maximum value of A_r can be measured only on an Rg–Rp section, which was not found here.

By the technique he devised, Capdecomme (1946, p. 35) found the maximum angle of rotation ω_M of ludwigite from Banat to be $<3°$ (blue), $\sim 3°$ (yellow), and $\sim 5°$ (red). His values of ω_M for ludwigite are slightly lower than the e's of Jayville vonsenite, a relation to be expected because of the lower Fe″ content of ludwigite.

Hardness –scratching hardness F or >, or about 6 on Mohs' scale; powder is black, opaque, and dull to moderately reflecting. The polishing hardness is less than that of hematite, and about equal to that of magnetite.

Magnetism pure mineral powder is attracted to a magnetized sewing needle.

Etch tests, originally made by Henderson and confirmed by Leonard, give the following reactions: HCl positive; aqua regia weakly positive; HNO_3, KCN, $FeCl_3$, KOH, $HgCl_2$, H_2O_2 negative. With HCl, no reaction at 30 seconds. At about 40 seconds, drop turns yellow. Etching begins at about 1 minute. A good etch, emphasizing cracks and scratches, requires 2 minutes. With aqua regia, no reaction in 1 minute. At about 2 minutes, drop turns yellow and some grains are faintly etched. Other grains are not etched after 3 minutes. The other reagents are negative, regardless of time.

All qualitative mineragraphic properties of Jayville vonsenite are identical with those of vonsenite from the type locality at Riverside, California. The quantitative mineragraphic properties of the two vonsenites are slightly different, in accordance with the known differences in Fe″ content. The ore microscopy of Riverside vonsenite, never reported by Eakle (1920), will be presented subsequently in a summary paper on the distinction of vonsenite from ilvaite.

Brief accounts of the ore microscopy of other vonsenites have been given by several workers. Chevallier, Mathieu, and Girard (1948), in their monograph on synthetic $4FeO \cdot Fe_2O_3 \cdot B_2O_3$, used unpolished crystal

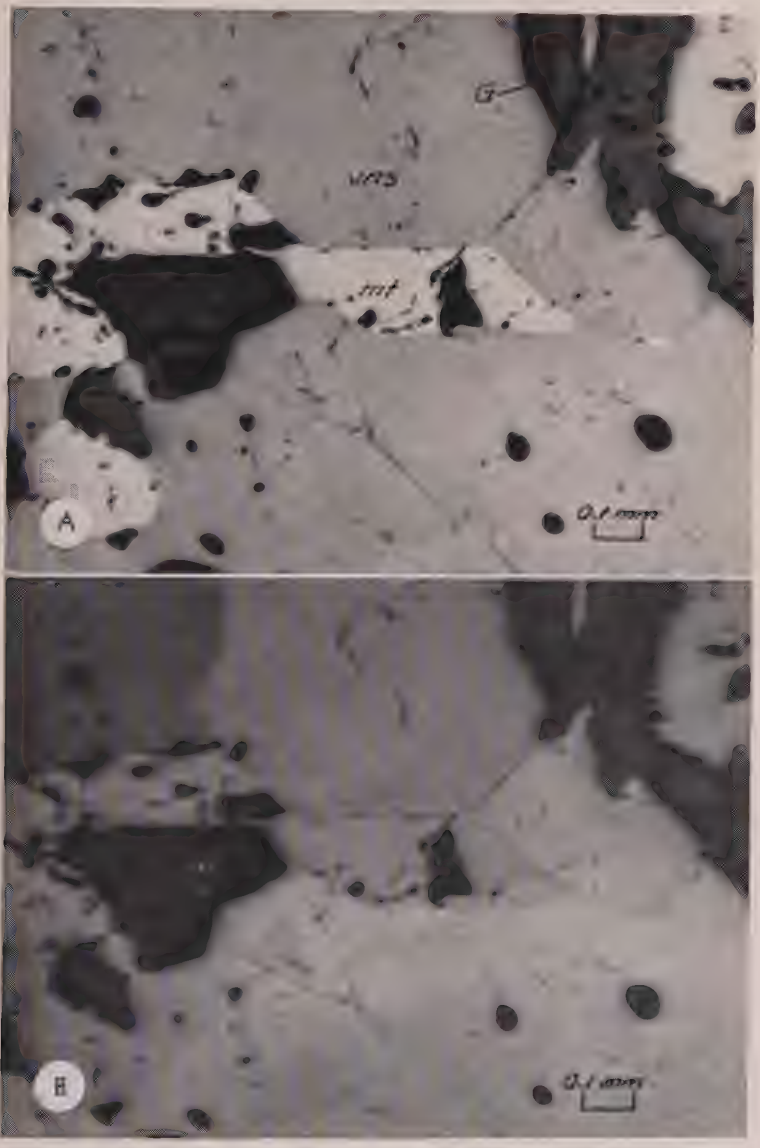

FIG. 5. Photomicrographs of polished sections of Jayville vonsenite
(A) Vonsenite (vns), showing reflectivity intermediate between that of magnetite (mt) and gangue (G). Single nicol.
(B) As above, but nicols partly crossed.

faces for observing reflection-pleochroism and anisotropism, and for measuring reflectivity. Watanabe and Ito (1954) presented the first useful description of natural vonsenite, their "paigeite" from Kamaishi. The only mineragraphic property noted by Vakar, Knipovich, and Shafranovskii (1934) for vonsenite from the Chersky Range was its anisotropism. The ore microscopy of ludwigite is reported in detail by Ramdohr (1955, p. 811).

X-Ray Powder Data

An *x*-ray powder diffraction diagram of the Jayville vonsenite was prepared by Fred A. Hildebrand, using material purified for chemical analysis. Hildebrand's data are given in Table 6, no. 1, together with data on vonsenites from Monte Cimino, Italy (Federico, 1957), and Riverside, California (Thompson and Gower, 1954). Federico's data (1958) for synthetic $4FeO \cdot Fe_2O_3 \cdot B_2O_3$ are included. The table is fully annotated. Thompson and Gower (1954, p. 523) give *x*-ray powder data for some other anhydrous borates, including ludwigite from Philipsburg, Montana. Watanabe and Ito (1954, p. 87) give indexed data for ludwigite from Hol Kol, Korea, and Kilbride, Scotland. Shabynin (1955) gives *x*-ray powder data for ludwigites from Hungary, eastern transbaikal region, and California, the last presumably representing a vonsenite. The data for Shabynin's ludwigite from the eastern Transbaikal region are unfortunately attributed to ilvaite in one abstract (Zbl. Mineralogie, Jahrgang 1956, pt. I, p. 170–171, 1958). Powder data for ludwigite are also given by Serdyuchenko (1956 -analyzed sample) and by Barsukov and Kuril'chikova (1957).

Chemical Composition

A chemical analysis of 1.9 grams of nearly pure vonsenite, separated by W. T. Schaller, is given in Table 7. (The sample is field no. J 2.21, hole J 2, depth 299 feet; laboratory sample no. 144483; laboratory report IWC-473.) For a mode of the host, see Table 3, no. 1.

The insoluble residue reported in Table 7 is hypersthene with less than one per cent of biotite and a trace of an unidentified accessory mineral. G. of eulite of composition $Mg_{27}Fe_{73}$ is 3.77. (Cf. Hess, 1952, Fig. 2.) This value was used to obtain the corrected G. for the vonsenite.

The recalculated analysis yields the oxide ratios 4.01:1.07:1.00, close to the ideal $4FeO \cdot Fe_2O_3 \cdot B_2O_3$. The composition may be expressed as $4[(Fe''_{1.92}Mn_{.01}Mg_{.04})(Fe'''_{.96}Al_{.07}Ti_{.004})B_{.98}O_5]$, based on the structural formula of daSilva, Clark, and Christ (1955). In chemical composition, the Jayville vonsenite closely approaches the $Fe_2''\ Fe'''BO_5$ end-member of the ludwigite-vonsenite series.

TABLE 6.—*X*-RAY POWDER DIFFRACTION DATA FOR VONSENITES

	(1) Vonsenite, Jayville, N. Y. $Fe''_{1.92}Mn_{.01}Mg_{.04}/O_6$ $a_0=9.47\pm.02$, $b_0=12.31\pm.01$, $c_0=3.07\pm.01$ Å (B.F.L.) FeKα; λ=1.93728 Å Mn filter F. A. Hildebrand			(2) Synthetic vonsenite Fe''_2/O_6 $a_0=9.44$, $b_0=12.26$, $c_0=3.065$ Å FeKα Bertaut (1950) Federico (1958)		(3) Vonsenite, Riverside, Cal. $Fe''_{1.33}Mg_{.64}$ to $Fe''_{1.17}Mg_{.85}/O_6$ $a_0=9.33$, $b_0=12.31$, $c_0=3.04$ Å (B.F.L.) FeKα, Mn oxide filter (λ=1.937 Å) Thompson and Gower (1954)		(4) Breislakite, Monte Cimino, Italy. $Fe''_{\sim 1.87}Mn_{.06}Mg_{.21}/O_6$ $a_0=9.50$, $b_0=12.40$, $c_0=3.10$ Å FeKα Federico (1957)	
hkl	d_{calc}	d_{obs}	I_{obs}	d_{obs}	I_{obs}	d_{obs}	I_{obs}	d_{calc}	I_{obs}
110	7.51	7.52	3			7.42	4	7.55	4
020	6.16	6.16	2			6.16	2	6.20	8
—	—	5.66 (β-120)	3	5.63 (β)	vw	5.63 (β)	1		
120	5.16	5.16	50	5.19	m	5.12	7	5.20	100
200	4.735	4.73	13	4.72	w	4.70	1	4.75	72
210	4.42	—							
—	—	4.13	0.3						
130	3.77	3.77	4	3.75	w	3.74	1	3.80	9
220	3.75	—							
—	—	3.38	0.3						
—	—	3.221*	0.3						
—	—	3.135	0.5						
230	3.101	—							
040	3.078	—		3.06	w	3.04	4	3.10	8
310	3.059	3.061 br	3					3.08	8
140	2.927	2.938	2			2.92	1	2.95	8
—	—	2.846 (β-240)	18			2.83 (β)	5		
320	2.809	2.805	4	2.83	ms	2.75	3	2.82	9
021	2.746	2.753	9	2.76	w				
—	—	2.622 (β)	0.5						
240	2.580	2.580	100	2.56	vs	2.56	10	2.64	100
330	2.502	2.494	0.5					2.52	6
150	2.383	2.372 br	25	2.36	ms	2.36	5	2.40	6
400	2.368					2.33	½	2.38	72

(*Continued on next page*)

* Hypersthene?

1. Analyzed sample—field no. J 2.21, Schaller series no. V-15. Film no. W-8495, made by F. A. H. with a Debye-Scherrer powder camera (114.59 mm. diameter); Straumanis technique; cut-off at $2\theta\sim5°$. α_1 and α_2 were not sufficiently resolved to measure separately. Measurements were made with a Hilger-Watts film-measuring rule with a vernier precision of 0.05 mm. A shrinkage correction was determined and appropriately applied to the measurements. Intensities were measured with calibrated film strips. The powdered mineral (~2 mg.) was mixed with a binder of granular ethyl cellulose dissolved in toluene and was rolled into a thin rod for mounting in the camera. Pattern indexed by B.F.L. Spacings calculated only for lines observed in films of the various vonsenites. Hypersthene is the only known contaminant of this analyzed vonsenite. Hypersthene lines tentatively assigned by B.F.L. after comparison with Marquiss' film of hypersthene J 2.21. Other major hypersthene lines coincide with observed vonsenite lines.

2. Synthesized, Fe_2O_3/FeO confirmed, and *x*-rayed by Federico (1958). Indexed by B.F.L on the basis of Bertaut's (1950) unit cell for synthetic $4FeO\cdot Fe_2O_3\cdot B_2O_3$.

3. Their "paigeite" (vonsenite); not chemically analyzed. Indexed by B.F.L. The line $d=1.068$ indexes as 821 and 3·10·1 only. The lattice constants of another vonsenite from Riverside are, according to Takéuchi (1956), $a_0=9.37_6$ [correction for typographic error in the original], $b_0=12.35_7$, $c_0=3.05_5$ Å.

4. Her microchemically analyzed breislakite, which she showed to be "paigeite" (vonsenite). Original Fe'' content uncertain, owing to partial oxidation of breislakite to hematite (cf. Federico, 1958). Indexed by Federico (1957). $d_{calc.}$ by B.F.L., using mean values derived from her sin θ's (λ not stated) and unit-cell dimensions. I reduced by B.F.L. from her $I_{max.}=47400$.

TABLE 6. (*continued*)

(1) Vonsenite, Jayville, N. Y. $Fe''_{1.92}Mn_{.01}Mg_{.04}/O_5$ $a_0=9.47\pm.02$, $b_0=12.31\pm.01$ $c_0=3.07\pm.01$ Å (B.F.L.) FeKα; $\lambda=1.93728$ Å Mn filter F. A. Hildebrand				(2) Synthetic vonsenite Fe''_2/O_5 $a_0=9.44$, $b_0=12.26$, $c_0=3.065$ Å FeKα Bertaut (1950) Federico (1958)		(3) Vonsenite, Riverside, Cal. $Fe''_{1.33}Mg_{.64}$ to $Fe''_{1.17}Mg_{.86}/O_5$ $a_0=9.33$, $b_0=12.31$, $c_0=3.04$ Å (B.F.L.) FeKα, Mn oxide filter ($\lambda=1.937$ Å) Thompson and Gower (1954)		(4) Breislakite, Monte Cimino, Italy. $Fe''_{\sim 1.87}Mn_{.06}$ $Mg_{.21}/O_5$ $a_0=9.50$, $b_0=12.40$, $c_0=3.10$ Å FeKα Federico (1957)	
hkl	d_{calc}	d_{obs}	I_{obs}	d_{obs}	I_{obs}	d_{obs}	I_{obs}	d_{calc}	I_{obs}
410	2.325	2.331	0.5	2.28	vw	2.27	½	2.33	3
—	—	2.279 β*	2						
250	2.184	—		2.16	m	2.17	6	2.20	72
311	2.167	2.171 br	25			2.14	4		
—	—	2.137*	0.3						
321	2.072	2.074	18	2.06	m	2.05	7		
060	2.052	—						2.07	<1
430	2.051	—						2.06	<1
160	2.005	2.001	4	2.00	w	1.998	2	2.02	17
241	1.975	—				1.961	½		
350	1.941	1.937	18	1.93	m	1.926	7	1.954	9
331	1.940								
260	1.882	—				1.878	1	1.898	8
440	1.876	1.875	3	1.87	w	1.857	½	1.885	17
510	1.872	—						1.880	<1
520	1.810	1.810	2	1.79	w				
341	1.790	1.793	4			1.776	4	1.817	9
251	1.780	—							
—	—	1.764 β?	1						
170	1.729	1.728 doublet	2	1.72	vw			1.744	8
530	1.720	1.719	2					1.728	1
360	1.720	—						1.732	4
450	1.707	1.699 (or β)	1						
431	1.705								
161	1.679	1.678	1	1.65	w	1.670	1		
270	1.648	1.660 br (or β)	0.7						
540	1.613							1.621	1
261	1.605	1.602	13	1.60	m	1.586	5		
511	1.598								
600	1.578	1.579	0.5					1.584	8
521	1.559	1.558	3						
080	1.539	1.538	18	1.55	w	1.538	1	1.551	72
370	1.536			1.53	m	1.528	6	1.546	6
180	1.519							1.531	4
171	1.507	1.507	13			1.505	5		
550	1.501			1.50	m	1.487	4	1.510	8
531	1.500	1.499	13						
630	1.473	1.472	1						
280	1.464	1.456	0.7			1.466	½	1.475	<1
271	1.452								
541	1.428	1.426	0.7						
640	1.404	1.403	9	1.40	mw	1.388	5	1.411	72
611	1.395	—				1.366	½		
560	1.392	—						1.400	<1
380	1.383	1.375	2	1.37	w			1.393	1
371	1.373								

TABLE 6. (*continued*)

	(1) Vonsenite, Jayville, N. Y. $Fe''_{1.92}Mn_{.01}Mg_{.04}/O_5$ $a_0=9.47\pm.02$, $b_0=12.31\pm.01$ $c_0=3.07\pm.01$ Å (B.F.L.) FeKα; $\lambda=1.93728$ Å Mn filter F. A. Hildebrand			(2) Synthetic vonsenite Fe''_2/O_5 $a_0=9.44$, $b_0=12.26$, $c_0=3.065$ Å FeKα Bertaut (1950) Federico (1958)		(3) Vonsenite, Riverside, Cal. $Fe''_{1.38}Mg_{.64}$ to $Fe''_{1.17}Mg_{.85}/O_5$ $a_0=9.33$, $b_0=12.31$, $c_0=3.04$ Å (B.F.L.) FeKα, Mn oxide filter ($\lambda=1.937$ Å) Thompson and Gower (1954)		(4) Breislakite, Monte Cimino, Italy. $Fe''_{\sim 1.87}Mn_{.05}$ $Mg_{.21}/O_5$ $a_0=9.50$, $b_0=12.40$, $c_0=3.10$ Å FeKα Federico (1957)	
hkl	d_{calc}	d_{obs}	I_{obs}	d_{obs}	I_{obs}	d_{obs}	I_{obs}	d_{calc}	I_{obs}
190	1.354	1.349	0.5			1.352	½	1.369	4
551	1.349					1.339	½		
650	1.329	—				1.315	6	1.335	3
720	1.321	1.321	9	1.31	mw	1.300	½	1.326	8
290	1.314	—							
480	1.290	—		1.29	w	1.283	3	1.299	17
570	1.289	1.289	4					1.296	3
730	1.285	—						1.290	3
390	1.255	1.258 br	1			1.251	2	1.264	8
660	1.251	—						1.258	1
740	1.238							1.244	<1
711	1.232								
0·10·0	1.231	1.231	0.7			1.217	2	1.241	3
1·10·0	1.221	1.221	0.7						
721	1.214	—				1.200	1		
—	—	1.203	0.5						
580	1.194								
2·10·0	1.191	1.189	2			1.183	2	1.201	<1
490	1.184								
800	1.184	1.182	3	1.18	ms	1.166	3	1.188	72
670	1.175	1.171	0.5						
661	1.158	1.158	0.3						
3·10·0	1.147	1.147 br	0.7	1.14	w	1.144	½	1.156	3
1·11·0	1.111	—						1.120	<1
—	—					1.131 (β?)	½		
590	1.109					1.105	½	1.116	3
680	1.102							1.108	<1
671	1.097	1.094	0.3						
4·10·0	1.092			1.09	vw	1.087	4	1.100	17
2·11·0	1.089	1.089 br	2						
821	1.087	1.087 br	2						
082	1.087					1.068	1		
3·10·1	1.074	1.073 br	0.5						
3·11·0	1.055	1.054	1			1.052	½	1.063	8
1·11·1	1.045	1.045 br	2			1.044	2		
591	1.043								
920	1.037	1.036	4	1.04	w			1.041	3
690	1.034	—				1.028	6	1.040	1
5.10·0	1.032	—						1.039	4
4·11·0	1.012	1.012	2						
—	—	1.009	1						
2·12·0	1.003	1.002	2			1.003	3		
—	—	1.000	1			.997	3		
—	—	.997	1			.992	1		
940	.996	.995	0.7			.983	4		
870	.982	.988 br	2						

Table 7. Chemical Analysis of Vonsenite from Jayville, New York

	Wt. per cent	Wt. per cent (recalc.)
FeO	53.06	54.04
MnO	0.27[a]	0.28
MgO	0.55[b]	0.56
Fe_2O_3	29.59	30.14
Al_2O_3	1.45	1.48
TiO_2	0.13	0.13
SnO_2	Present[c]	Present
B_2O_3	13.13	13.37
CaO	None	100.00
Acid insoluble	1.80	
	99.98	

Angelina C. Vlisidis, analyst, 1955

G. of analyzed sample = 4.75
G. corrected for acid insoluble = 4.77 } W. T. Schaller

[a] Amount of MnO recovered from the Mg precipitate. Total amount not determined.

[b] Corrected for the contained MnO (0.27 per cent).

[c] Not determined gravimetrically. Spectrographic determination (see below) indicates a small quantity, about 0.x per cent.

Spectrographic analysis, made in 1951 by Janet D. Fletcher, shows (report IWS-156):

	Per cent
Fe, B	>5
Mg, Si, Al	1–5
Sn, Pb, Zn, Mn, Ti	0.x
Cu, Cr, Zr, Ba, Ca	0.0x
Ag, Co, Ni	0.00x

Looked for but not found: As, Bi, Be, Au, Pt, Mo, W, Ge, Sb, Cd, Tl, Ga, V, Y, La, Th, Cb, Ta, U, Sr, Na, P.

The sample analyzed by Miss Fletcher was drilled from the surface of a polished section. The presence of Sn is of interest, for that element is a major constituent of the chemically related minerals hulsite and paigeite. Ludwigite from the Zheleznyi Kryazh deposit, Kalgan district, Chita region, U.S.S.R., contains 0.03 0.3% Sn, according to semiquantitative spectrographic analysis (Efimov, 1955, p. 1308).

Vonsenite at Clifton

Vonsenite was identified in a single specimen from the Clifton magnetite deposit, hole 51, depth about 143 feet. The sparse vonsenite is asso-

iated with martitized magnetite, cobaltoan loellingite, colloform graphite, pyrrhotite, sphalerite, chalcopyrite, and chalcocite(?) in mica-pyroxene-calcite marble from a weakly mineralized zone of diopside skarn. Mineralogical details are given in the forthcoming report by Leonard and Buddington. Optical identification of the vonsenite was confirmed by *x*-ray by A. J. Gude (1957, personal communication). Gude notes that the pattern from the very small sample confirms the presence of a mineral of the ludwigite-vonsenite series, though it does not permit an estimate of the relative position of the Clifton mineral in that series.

Acknowledgments

We wish to thank the Jones and Laughlin Steel Corporation and the Benson Iron Ore Corporation for permission to use data in an unpublished report by S. A. Tyler and R. E. Wilcox on the geology of the Jayville deposit. Messrs. Tyler and Wilcox themselves contributed additional information during our investigation. Cuts of Jones and Laughlin's analyzed samples of Jayville drill core were obtained through the kindness of Messrs. R. M. Crump, W. M. Fiedler, and W. F. Smith. Michael Fleischer encouraged a careful study of the vonsenite. I. J. Mittin translated some of the Russian literature. P. K. Sims provided galena suitable for use as a standard for reflectivity measurements. Wendell Walker made the photomicrographs of vonsenite in Figures 3 and 4. Frank Spence made the photomicrographs in Figure 5. The contributions of other colleagues are noted in the text.

W. T. Schaller would, except for his modesty, be appropriately listed as co-author of this paper. His generous contributions of advice, encouragement, data, and specimens are gratefully acknowledged.

References

Andrieux, J. L., and Weiss, Georges (1944), Sur l'attaque anodique du fer et la formation d'un boroferrite par électrolyse ignée: *Acad. Sci. Paris, Comptes rendus*, **218,** 615–617.

Bursukov, V. L., and Kuril'chikova, G. E. (1957), Ob usloviyakh obrazovaniya endogennogo asharita: *Geokhimiya*, 312–319. (English summary, p. 319: On the conditions of endogene ascharite formation.)

Bertaut, E. F. (1950), Structures des boroferrites: *Acta Cryst.*, **3,** 473–474.

Bertaut, Félix, Bochirol, Louis, and Blum, Pierre (1950), Synthèse et groupe d'espace des boroferrites: *Acad. Sci. Paris, Comptes rendus*, **230,** 764–765.

Buddington, A. F. (1939), Adirondack igneous rocks and their metamorphism: *Geol. Soc. America Mem.* **7,** 354 p.

Cameron, E. N., and Green, L. H. (1950), Polarization figures and rotation properties in reflected light and their application to the identification of ore minerals: *Econ. Geology*, **45,** 719–754.

Cameron, E. N., Hutchinson, R. W., and Green, L. H. (1953), Sources of error in the

measurement of rotation properties with the ore microscope: *Econ. Geology*, **48,** 574–590.

Capdecomme, L. (1946), Propriétés optiques nouvelles de quelques minerais de fer orthorhombiques: *Soc. franç. mi éralogie Bull.*, **69,** 24–41.

Chevallier, Raymond, Mathieu, Suzanne, and Girard, Jean (1948), Monographie du boroferrite ferreux: *Bull. Soc. Chim. France, ser.* 5, **15,** 611–615.

Cissarz, Arnold (1932), Reflexionsmessungen an absorbierenden Kristallen, mit besonderer Berücksichtigung der Erzmineralien, III: *Zeit. Krist.*, **82A,** 438–450.

Dale, N. C. (1935), Geology of the Oswegatchie quadrangle: *New York State Mus. Bull.* **302,** 101 p.

daSilva, J. C., Clark, J. R., and Christ, C. L. (1955), Crystal structure of ludwigite, $Mg_2Fe'''BO_5O_2$ [abs.]: *Geol. Soc. America Bull.*, **66,** 1540–1541.

Eakle, A. S. (1920), Vonsenite, a preliminary note on a new mineral: *Am. Mineral.*, **5,** 141–143.

Efimov, I. A. (1955), O nalichii bornoi mineralizatsii na mestorozhdenii Zheleznyi Kryazh [The presence of boron mineralization in the Zheleznyi Kryazh deposit]: *Akad. Nauk SSSR Doklady*, **105,** 1306–1308.

Engel, A. E. J., and Engel, C. G. (1953), Grenville series in the northwest Adirondack Mountains, New York. Part 1. General features of the Grenville series: *Geol. Soc. America Bull.*, **64,** 1013–1047.

——— (1958), Progressive metamorphism and granitization of the major paragneiss, northwest Adirondack Mountains, New York. Part 1. Total rock: *Geol. Soc. America Bull.*, **69,** 1369–1413.

Federico, Marcella (1957), Sulla breislakite: Periodico di Mineralogia, **26,** 191–214.

——— (1958), Il processo di alterazione della breislakite: *Periodico di Mineralogia*, **27,** 293–303.

Geijer, Per (1939), The paragenesis of ludwigite in Swedish iron ores: *Geol. fören. Stockholm Förh.*, **61,** 19–33.

Hallimond, A. F. (1953), Manual of the polarizing microscope, 2d ed : York, England; Cooke, Troughton & Simms, 219 p. [Reprinted 1956, with Appendices 5 and 6.]

Hess, H. H. (1949), Chemical composition and optical properties of common clinopyroxenes. Part 1: *Am. Mineral.*, **34,** 621–666.

——— (1952), Orthopyroxenes of the Bushveld type, ion substitutions and changes in unit cell dimensions: *Bowen vol. Am. Jour. Sci.*, 173–187.

Leonard, B. F. (1960), Reflectivity measurements with a Hallimond visual microphotometer: *Econ. Geology*, **55,** 1306–1312.

Leonard, B. F., and Vlisidis, A. C. (1960), Vonsenite from St. Lawrence County, northwest Adirondacks, New York: *Am. Mineral.*, **45,** 439–442.

Palache, Charles, Berman, Harry, and Frondel, Clifford (1951), Dana's System of mineralogy, 7th ed., **2,** New York, John Wiley and Sons, 1124 p.

Poldervaart, A., and Hess, H. H. (1951), Pyroxenes in the crystallization of basaltic magma: *Jour. Geology*, **59,** 472–489.

Ramdohr, Paul (1955), Die Erzmineralien und ihre Verwachsungen, 2d ed.: Berlin, Akademie-Verlag, 875 p.

Serdyuchenko, D. P. (1956), Mineraly bora i titana v nekotorykh osadochno-metamorficheskikh porodakh [The minerals of boron and titanium in certain metasedimentary rocks]: *Akad. Nauk SSSR, Trudy Geol. Inst., vyp.* **5,** 53–124.

Shabynin, L. I. (1955), Ob asharite i drugikh boratakh v magnetitovykh rudakh kontaktovo-metasomaticheskikh mestorozhdenii [Szaibelyite and other borates from magnetite ores of contact-metasomatic deposits]: *Akad. Nauk SSSR Doklady*, **101,** 937–940.

TAKÉUCHI, YOSHIO (1956), The crystal structure of vonsenite: *Mineralog. Jour.* (*Mineralogical Soc. Japan*), **2,** 19–26.

TAKÉUCHI, Y., WATANABÉ, TAKÉO, AND ITO, T. (1950), The crystal structures of warwickite, ludwigite and pinakiolite: *Acta Cryst.*, **3,** 98–107.

THOMPSON, R. M., AND GOWER, J. A. (1954), A magnesium borate from Isère, France, and Swift River, Yukon Territory, with X-ray powder data for some anhydrous borates: *Am. Mineral.*, **39,** 522–524.

TILLEY, C. E. (1951), The zoned contact-skarns of the Broadford area, Skye: a study of boron-fluorine metasomatism in dolomites: *Mineralog. Mag.*, **29,** 621–666.

TYLER, S. A., AND WILCOX, R. E. [1942], Geological report on the Jayville area, Pitcairn township, St. Lawrence County, New York: private rept. prepared for Jones and Laughlin Steel Corp.

VAKAR, V. A., KNIPOVICH, E. V., AND SHAFRANOVSKII, I. I. (1934), Lyudvigit iz polyarnoi Yakutii: *Vseross. Mineral. Obshchestvo Zapiski, ser. 2,* **63,** 381–385. (English summary, p. 385: Ludwigite in polar Yakutia.)

WATANABE, TAKEO (1943), Geology and mineralization of the Suian district, Tyôsen (Korea). The geology of the Suian gold mining district (3d report): *Hokkaido Univ., Fac. Sci. Jour., ser. 4,* **6,** 205–303.

— — (1953), Genesis of the contact metasomatic iron ore deposits in Japan, with special reference to those of the Kamaishi iron mine: *Internat. Geol. Cong., 19th Algeria, Comptes rendus, sec.* **10,** *fasc. 10,* 51–61.

WATANABE, TAKEO, AND ITO, JUN (1954), Paigeite (ferroludwigite) from the Kamaishi iron mine, Iwate prefecture, Japan: *Mineralog. Jour.* (*Mineralogical Soc. Japan*), **1,** 84–88.

Manuscript received September 11, 1960.

Note added in proof: Robert Carpenter, University of Wisconsin, reports the following values of A_r for Vonsenite in specimen J 3.11:

λ(mμ)	A_r(obs.)	A_r(corr.)
470	2.17°	1.70°
589	4.19°	3.41°
650	5.83°	4.82°

Carpenter obtained these by a more refined technique than ours. We are indebted to him for the data and to Professor Cameron for his interest in the problem.

X-RAY STUDY OF AUTUNITE

YUKIO TAKANO, *Institute of Earth Science, College of General Education, University of Tokyo, Tokyo, Japan.*

ABSTRACT

The autunite-meta-autunite I—meta-autunite II series was studied by *x*-ray diffraction. In America and Europe, autunite is usually found as the meta-autunite I phase, whereas in Japan it occurs as autunite. By studying the process by which autunite is dried and heated until it finally forms a high temperature phase, the writer has determined the diffraction pattern of each phase. Single crystals were analyzed by the Weissenberg method, and the lattice constants and space groups were determined. The large cell proposed by Donnay and Brichard for meta-autunite was not found. Meta-autunite II is orthorhombic, with $a_0=6.55$, $b_0=7.05$ and $c_0=8.16$ Å. This c_0 value is smaller than the c_0 of meta-autunite I, contrary to the values hitherto reported.

INTRODUCTION

The first *x*-ray study of autunite was attempted in 1938 by J. Beintema, who found it to be tetragonal. *X*-ray study of this mineral has been active since 1955, and reports have been published by G. Donnay and J. D. H. Donnay (1955); C. Frondel, D. Riska and J. W. Frondel (1956); P. B. Gechebe (1957); and H. Brichard and H. Brasseur (1958), and others, One of the latest is A. Volborth (1959), who studied strontian meta-autunite. Table 1 summarizes the *x*-ray data on the autunite series.

The crystal structures of the members of the autunite series have not yet been determined, and the views on the hydration state of each phase are varied. Most of the research since 1955 has been concentrated on meta-autunite, which is regarded as the most stable mineral in this series, and very little data on autunite and meta-autunite II have been pub-

TABLE 1. SPACE GROUP AND CELL DIMENSIONS OF AUTUNITE SERIES

Name	Autunite	Meta-autunite I	Meta-autunite II
Chemical formula	$Ca(UO_2)_2(PO_4)_2 10\sim 12H_2O$	$Ca(UO_2)_2(PO_4)_2 2\sim 6H_2O$	$Ca(UO_2)_2(PO_4)_2O\sim 2H_2O$
Crystal system	Tetragonal	Tetragonal	Orthorhombic
Space group	*I*4/*mmm*	*P*4/*nmm*	*P mmm*
Cell dimensions	a_0 6.989 b_0 — c_0 20.63	6.972 — 8.47	6.45 6.97 8.65

ished since Beintema's work. Hence, the writer's study was focussed on hese lesser-known minerals.

Transitional Relation

The samples used in the present study are from Ningyō Pass, on the order between Okayama and Tottori Prefectures, Japan, and from the Daybreak Mine, Washington, U.S.A. The samples are all micaceous, etragonal platy crystals. Those from Ningyō Pass are light greenish ellow and transparent, or yellow and translucent, mostly 4 mm. in the maximum diameter, having tetragonal outlines, whereas those from Daybreak are yellow to dark green or greenish black and many of them re rectangular and platy, occasionally as large as 1 cm. or more in diamter. Of the Daybreak mine specimens, only the yellow portions were elected and used in the experiments. From these samples, pure thin lakes of crystals were separated under petrographic and binocular icroscopes. The flakes were ground in a mortar, and x-rayed with a iffractometer operated as follows: Cu/Ni, 35 K.V., 15 M.A., and scaning speed 1° per 1′. The results (lower part of Fig. 1) disclose that almost all the samples from both Ningyō Pass and Daybreak are autunite. According to Volborth (1959), most of the autunites occurring in nature re supposed to be meta-autunite, but the writer has found that the samles from Ningyō Pass in humid Japan are autunite, and contain almost o meta-autunite. Moreover, the Daybreak samples, collected at the ame locality as those by Volborth, gave more diffraction patterns of utunite than of meta-autunite, when the samples were examined in apan. Hence the geographical situation of Japan is favorable for this ind of experiment. Accordingly the writer has carried out various exeriments in order to obtain diffraction patterns of pure autunite. Figure shows the results of one of these experiments, in which a powdered ample was placed in a holder, water was then added, and gradually llowed to dry up. In this experiment, the samples from both localities, hen soaked in water, first showed diffraction patterns of low temerature type autunite, but gradually changed into meta-autunite I, beinning with a dried part. This fact indicates that autunite, which reains relatively stable in Japan, becomes meta-autunite I without being eated when it is pulverized and soaked in water. The samples that have one through this transitional process become autunite again if water is dded, but as they dry up the transition from autunite to meta-autunite takes place at a faster rate than before. On the other hand, if autunite amples were not soaked in water they would remain stable for more than year, even after they were pulverized. When a sample that has transionally altered to meta-autunite I is placed in the air bath at 110° C. to

FIG. 1. *X*-ray diffractometer traces of transition in the autunite series. Samples from Ningyō-Pass.

A—autunite; B—meta-autunite I; C—meta-autunite II.

TABLE 2. X-RAY DATA FOR AUTUNITE

I4/mmm
a_0=6.969 Å c_0=20.76 Å (Ningyō-Pass)
a_0=6.872 Å c_0=20.73 Å (Daybreak Mine)

Calculated values		Ningyō-Pass		Daybreak Mine		Mt. Spokane	
hkl	*d* (Å)	*I*	*d* (Å)	*I*	*d* (Å)	*I*	*d* (Å)
002	10.37	100	10.48	100	10.31	160	10.4
101	6.61	6	6.74	4b	6.52	10	6.67
004	5.19	86	5.19	36	5.21	84	5.19
110	4.92	35	4.91	30	4.93	39	4.96
103	4.91						
112	4.45	15	4.46	9	4.46	29	4.48
105	3.567	83	3.565	53	3.574	70	3.58
200	3.486	18	3.495	29	3.495	31	3.51
202	3.304	22	3.317	18	3.315	28	3.33
204	2.893	8	2.899	5b	2.915	8	2.91
213	2.842	13	2.861	6	2.854	12	2.86
107	2.729	16	2.727	10	2.722	17	2.73
008	2.598	5	2.596	—	—	3	2.60
215	2.492	3	2.495	4b	2.492	5	2.50
220	2.464	5	2.440	6	2.454	5	2.48
206	2.454						
222	2.397	7b	2.418	5	2.411	8	2.41
118	2.299	9	2.299	—	—	5	2.30
224	2.225	14	2.219	6	2.214	8	2.22
310	2.203	26	2.193	11	2.203	10	2.19
109	2.187	22	2.181	11	2.177	9	2.17
312	2.157	16	2.161	10	2.146	12	2.15
217	2.146	17	2.143				
208	2.080	45	2.080	15	2.072	24	2.08
0·0·10	2.076						
314	2.028	9	2.033	7	2.033	9	2.039
305	2.028						
1·1·10	1.914	10	1.917	5	1.910	7	1.918
219	1.854	5b	1.857	—	—	—	—
307	1.829	5b	1.835	4	1.828	2	1.834
1.0.11	1.822	4b	1.820	—	—	—	—
2.0.10	1.784	5b	1.785	—	—	4	1.787
325	1.755	4b	1.754	5	1.751	4	1.761

be heated intermittently for short periods, and then cooled, the resulting X-ray diffraction pattern gradually shows the phase of meta-autunite II. The transitional process, as shown in the left side in Fig. 1, was determined by assuming that the samples used in the experiment are admixtures of the three phases, and by calculating the mixing ratio by the

TABLE 3. *X*-RAY DATA FOR META-AUTUNITE I

*P*4/*nmm* a_0=6.972 Å c_0=8.47 Å (Volborth)

Small cell	Calculated values†	Takano (1959)		Volborth (1959)		Brichard (1958)			Frondel (1956)		Large cell‡	Gechebe (1957)	
						Synthetic		Natural					
hkl	*d* (Å)	I	*d* (Å) meas.	I	*d* (Å) meas.	I	*d* (Å) meas.	*d* (Å) I	I	*d* (Å) meas.	*HKL*	I	*d* (Å) meas.
001	8.47	100	8.54	100	8.47	s	8.465	8.52	10	8.51	001	10	5.98
101	5.38	32	5.37	44	5.38	s	5.39	5.41	7	5.39	221	2	5.35
110	4.93	14	4.93	21	4.93	s	4.92	4.95	5	4.96	040	0.5	4.84
111	4.26	16	4.28	—	—	vf	4.42	—	—	—	240*	—	
002	4.24	30	4.25	69	4.23	m	4.25	4.26	6	4.28	002	2	4.12
102	3.62	86	3.62	85	3.61	m	3.64	3.64	8	3.63	222	10	3.56
200	3.49	28	3.50	31	3.48	s	3.48	3.51	9	3.50	440	5	3.44
201	3.22	18	3.24	23	3.22	—	—	—	—	—	—	—	—
112	3.21	10	3.20	—	—	s	3.23	3.24	8	3.24	042	5	3.19
211	2.93	11	2.93	15	2.93	m	2.93	2.94	4	2.94	621	4	2.98
003	2.82	—	—	—	—	—	—	—		—	—	—	
202	2.69	—	—	—	—	vf	2.70	2.705	1	2.68	213*	—	—
103	2.62	48	2.62	35	2.61	—	—	2.62	3	2.61	—	—	—
212	2.51	7	2.51	6	2.51	f	2.52	2.52	2	2.51	323*	5	2.58
220	2.47	—	—	4	2.47	w	2.47	2.48	2	2.47	—	—	—
113	2.45	9	2.45	4	2.45	—	—	—				—	
221	2.37	3	2.38	8	2.37	w	2.38	2.38	3	2.38	423*	—	—
301	2.24	4	2.25	5	2.24	w	2.24	2.25	2	2.25	523*	—	—
310	2.21	7	2.21	10	2.21	m	2.21	2.215	3	2.21	480	2	2.19
203	2.19	6	2.19	—	—	—	—				—		
311,222	2.13	—	—	—	—	w	2.13	2.14	3	2.14	613*	—	—
004	2.12	63	2.11	71	2.11	—	—	—	—		—		
213	2.09	18	2.095	—	2.04	f	2.10	2.10	3	2.10	623	7	2.08
302	2.04	8	2.037	9	2.04	w	2.05	2.05	3	2.04	633*	2	2.01
104	2.03	17	2.020	14	2.02	—	—	—	—	—	—	—	—
114	1.946	22	1.943	14	1.943	—	—	—	2	1.941	—	4	1.92

* Where Brichard's indexing does not agree with Volborth's, the *HKL* indices are marked with an asterisk.
† In this table all calculated *d* values larger than 2.00 Å for small cell are given.
‡ Large cell, a_0=19.72, c_0=8.47; by the transformation $2\bar{2}0$, 220/001.

Alexander Klug method. Unlike single crystals, transition of powder samples occurs sporadically, beginning with scattered grains within the holder, and continues as water escapes, until the transition is completed.

The above-mentioned experiments were repeated and diffraction patterns of the respective phases were separated, as shown by Tables 2, 3 and 4. In the *x*-ray data hitherto reported, autunite diffraction patterns were generally commingled with several meta-autunite patterns, and meta-autunite patterns contained some of autunite lines. Consequently, there may have been many cases where the diffraction pattern of one phase was erroneously indexed as the other phase, so that the resultant calculated values became identical incidentally. Therefore, even about the phase of meta-autunite I which has been studied best of all in this series, discussions are still going on whether or not the a_0 value should be

TABLE 4. X-RAY DATA FOR META-AUTUNITE II

Pmmm

$a_0=6.55_1$ Å $b_0=7.05_3$ Å $c_0=8.16_4$ Å (Ningyō-Pass)

Calculated values		Ningyō-Pass		Mt. Spokane		U.S.S.R.	
hkl	*d*	I	*d*	I	*d*	I	*d*
001	8.16	100	8.17	150	8.21	10	7.90
100	6.55	6	6.57	9	6.58	—	—
011	5.35	5	5.30	9	5.33	2	5.25
110	4.80_5	9	4.81	11	4.81	2	4.42
111	4.14	32	4.14	—	—	—	—
002	4.08	57	4.08	70	4.08	10	4.03
—	—	—	—	5	3.60	—	—
020	3.53_5	13	3.51	17	3.53	5	3.50
200	3.28	6	3.28	8	3.27	—	—
—	—	—	—	6	3.21	4	3.21
112	3.11	4	3.10	2b	3.12	—	—
210	2.972	8	2.963	10	2.97	4	2.94
121	2.907	5	2.926	—	—	—	—
003	2.722	14	2.718	16	2.72	7	2.69
202	2.555	4	2.556	2	2.58	—	—
013	2.539	4	2.542	—	—	—	—
103	2.220	5	2.205	5	2.21	1	2.19
300	2.182	4	2.179	—	—	—	—
033	2.157	4	2.156	—	—	—	—
004	2.041	10	2.040	7	2.04	7	2.02
213	2.008	6	2.007	—	—	—	—
230	1.914	3	1.916	2	1.90	2	1.87
—	—	—	—	—	—	1	1.84
040	1.768	3	1.778	—	—	1	1.74
005	1.633	8	1.630	5	1.63	1	1.63
401	1.605	8	1.601	3	1.61	—	—
025	1.482	4	1.480	3	1.48	2	1.47

$2\sqrt{2}$ times as great. The writer's experiments by *x*-ray diffraction may give a fairly precise answer to the above question.

AUTUNITE

Detailed numerical data on autunite have been very few since the study of Beintema (1938). It is probably because of the fact that autunite seldom occurs in nature as it easily alters to meta-autunite II. Unless the region where autunite occurs is moist and relatively cool, like Japan and Soviet Russia, experiments on natural autunite at room temperature are difficult.

Table 2 shows the x-ray diffraction patterns of autunite obtained from the above-mentioned experiments. The experiments reveal that the samples from Ningyō Pass have slightly larger c_0 values than those from Daybreak. At room temperature in Japan, each of the samples showed the (001) peak of meta-autunite I on the outer side of (002). This phenomenon was especially noticeable in the Daybreak samples. Nevertheless, in the experiments on the samples fully soaked in water (Fig. 1 *b*-2), this peak disappeared, and it coincided with the diffraction pattern of meta-autunite I. Thus, it has been confirmed that the peak does not belong to the autunite phase.

Small flakes of autunite were separated from the Ningyō Pass samples and more than sixty flakes were tested by x-ray oscillation photographs. Autunite flakes, no matter how thin, are considered to consist of aggregation of parallel crystals with interspaces parallel to (001). It is, therefore, very difficult to obtain specimens suitable for single crystal tests. The writer was able to find seven such autunite flakes, and made a- and c-axis Weissenberg photographs. The cell dimensions of autunite were confirmed as $a_0=6.97$, $c_0=20.76$ Å. Only reflections with $h+k+l=2n$ were found. Hence the space group is $I4$ mmm, and the indexing of the powder patterns was confirmed. Figure 2 shows the 0-level Weissenberg photograph with rotation around the a axis.

Meta-Autunite I

Table 3 shows the experimental values obtained by the writer from the Ningyō Pass samples and the values converted from the calculated values of Volborth (1959). With a marked increase of data on meta-autunite I, two different theories concerning the value of a_0 are being advocated; one is represented by Beintema and Volborth who maintain that a_0 is 6.97 Å, while the other is supported by Donnay and Brichard who insist that a_0 is 19.8 Å, which is $2\sqrt{2}$ times the former. However, the present experiments were convenient for studying this problem, for the writer was observing the transitional stages of autunite. The experiments revealed, as indicated in Table 3, that the index (B) of large cell of meta-autunite I reported by Donnay, Brichard and others corresponds to index (A) of autunite, *i.e.*, B(240) is Å(112), B(213) is A(107), B(613) is A(217) and A(312), and B(633) is A(0·0·10) and B(302). As the diffraction patterns representing large cells are all weak, it may be appropriate to think that autunite phase is included there, and the small cell theory of Volborth seems to be right. The samples from Ningyō Pass even showed (111), (112), (203) and (213) lines which do not occur among the experimental values by Volborth although they are found among his calculated values. In addition, almost all diffraction lines which did not disappear, were those of the space group P4/nmm, whereas no diffrac-

FIG. 2. *X*-ray diffractometer traces of transition in the autunite series. Samples from ...ybreak Mine.

A—autunite; B—meta-autunite I; C—meta-autunite II.

...on lines supporting the large cell theory of Donnay and others were ...und.

META-AUTUNITE II

Important new data on meta-autunite II have been contributed by a ...cent study by Leo (1960). Since he did not index the powder photo-...aphs, the present writer has carried out the indexing. The results are

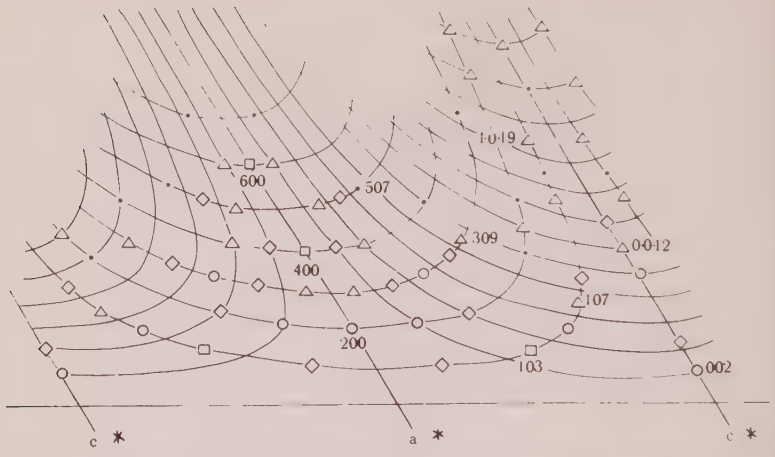

FIG. 3. Weissenberg photograph of autunite; 0-level, rotation around a axis. Symbols: ○-very strong; □—strong, ◇—medium; △—weak; •—faint.

shown in Table 4, along with the new data obtained in this paper. The cell dimensions obtained $a_0=6.55$, $b_0=7.05$, and $c_0=8.16$ Å; space group *Pmmm*. According to Crystal Data (Donnay and others, 1954), $a_0=6.97$, $b_0=8.65$, and $c_0=6.45$ Å, while Beintema reported $a_0=6.45$, $b_0=6.97$, and $c_0=8.65$ Å. However, in the writer's precise experiments, the basal reflection (001) of meta-autunite II appeared as one of the double lines on the outer side of (001) of meta-autunite I. It has become clear, therefore, that c_0 of meta-autunite II should have a smaller value than $c_0=8.47$ Å of meta-autunite I. Thus, c_0 of meta-autunite II becomes 8.16 Å, instead of 8.65 Å.

Using the lattice constants of meta-autunite II obtained in the present experiments, indices cannot be assigned to 3.60 and 2.31 A of Leo's data. However, (102) and (201) of meta-autunite I are fairly strong reflections, and roughly correspond to the two above-mentioned values, so it is possible that Leo's data resulted from the mis-indexing of these reflections.

When meta-autunite II is measured at high temperatures, diffraction patterns of a different lattice having 7.6 to 8.0 Å basal reflections can be obtained. This cell is probably an orthorhombic cell in which $a_0=5.58$, $b_0=6.36$ and $c_0=7.95$ Å. Its lattice constant becomes shorter with increase in temperature, and when cooled it returns to the initial state of meta-autunite II.

DISCUSSION

As x-ray study of single crystals of autunite has been limited, in many cases reflections have been assigned indices impossible for an I lattice.

n powder data for fully hydrated autunite by Leo (1960, Table 6), the eported indices (009), (140) and (029) are an example. In the writer's xperiments (1959) using Buerger's precession camera, it seemed that the hk0) reflections appeared with $h+k+1=2n+1$. However, when hk1) and hk2 levels were obtained, it was found that reflections from more than one level were being recorded. An autunite plate may look like single crystal because of the very perfect cleavage, but in fact it is an ggregation of several pseudo parallel-grown crystals with markedly arge dimensions of c_0. Consequently, reciprocal lattice points of different evels of other slightly inclined crystals give such effect as mentioned bove.

Previously the writer made precise measurements of the crystal structure, morphology and optical character of xanthophyllite, and found hat pseudo-hexagonal plates of the mineral consists of many-sectored tructures of varied orientation (Takano and Takano, 1958, Fig. 4). Then, micaceous autunite having such structures, he unraveled a similar relaion from precession photographs (Takano and Takano, 1959*b*, Figs. 4). These results have been practically verified by Leo's detailed optical easurements (Leo, 1960, Fig. 3*a*). That the space group of autunite is $I4/mmm$ has been confirmed by the recent analysis of the Weissenberg hotographs.

It is important, but very difficult, to determine quantitatively the deree of hydration at each stage of the autunite series, because the minals of this series change easily under nearly normal temperature and umidity. Besides, as is known from the writer's experiments, separation f quite pure specimens of the respective minerals is almost impossible. is anticipated also that in the transition experiments under temperaure of little variance, some portion of the specimen may remain unffected on account of the fact that a plate is usually composed of several akes due to cleavage and sectoral structure. For example, calculated alues of hydration of autunite would become smaller than the theoretal value 12 H_2O, as a result of intermixture of some meta-autunite I. he writer has entrusted M. Tsuboi and K. Takano with the measureent of the hydration state of autunite by infrared absorption, so the sult will be reported in the near future.

Acknowledgments

The present writer is greatly indebted to Professor Nobuo Katayama College of General Education, University of Tokyo, for his valuable ggestions during this study of autunite, as well as for his criticism on e manuscript. In the *x*-ray work and related calculations, much help nd advice were given by Mrs. Kotoyo Takano of Chemical Institute,

Science Department, University of Tokyo, to whom the writer's thanks are due.

The writer also wishes to express his sincere thanks to Dr. Kichinosuke Henmi of Okayama University for his discussion throughout the study, and to Dr. Akiho Miyashiro of Geological Institute, Science Department, University of Tokyo, for his cordial offer of a sample of autunite from the Daybreak Mine.

References

Beintema, J. (1938), On the composition and the crystallography of autunite and the meta-autunites: *Rec. Travaux Chim. Pays-Bas*, **57,** 155–175.

Brichard, H., and Brasseur, H. (1958), Sur les autunites naturelles et synthetiques: *Bull. Soc. Franç. Miner. Crist.*, **81,** 4–10.

Donnay, G., and Donnay, J. D. H. (1955), Contribution to the crystallography of uranium minerals: *U.S.A.E.C. Tech. Inf. Serv., Oak Ridge, TEI-***507,** 42.

Frondel, C., Riska, D., and Frondel, J. W. (1956), *X*-ray powder data for uranium and thorium minerals: *U. S. Geol. Survey Bull.*, **1036-G,** 91–153.

Gechebe, P. B. (1957), Pykobogembo no onepegelehubo ypahobeix nuheparob: Bonpocor reolomu yparea, Mockba, 143.

Heinrich, E. W. (1958), Mineralogy and geology of radioactive raw materials: McGraw-Hill Book Company, Inc., New York, 654 p.

Katayama, N., and Sato, Y. (1957), The sedimentary environment of the uraniferous bed of the Ningyo-pass: *Sci. Pap. Coll. Gen. Educ. Univ. Tokyo*, **7,** 131–144.

Leo, G. W. (1960), Autunite from Mt. Spokane, Washington: *Am. Mineral.*, **45,** 99–128.

Nuffield, E. W., and Milne, I. H. (1953), Studies of radioactive compounds: VI. Meta-uranocircite: *Am. Mineral.*, **38,** 476–488.

Palache, C., Berman, H., and Frondel, C. (1951), The System of Mineralogy, 7th ed., vol. 2: John Wiley and Sons, Inc., New York, 1124 p.

Soma, T. (1957), Autunite from the Ningyo-pass on the boundary between Tottori and Okayama prefectures, Japan: *Jour. Miner. Soc. Japan*, **3,** 214–217.

Takano, Y., and Takano, K. (1958), Apparent polytypism and apparent cleavage in micas: *Jour. Miner. Soc. Japan*, **3,** 674–692.

Takano, Y., and Takano, K. (1959a), The relation between optical anomaly and crystal structure: *Jour. Geol. Soc. Japan*, **65,** 236–247.

Takano, Y., and Takano, K. (1959b), The problem of the stability of the reciprocal main axis in polysynthetic twin: *Jour. Jap. Ass. Miner. Petro. Econ. Geol.*, **43,** 194–202.

Volborth, A. (1959), Strontian meta-autunite from the Daybreak mine, Mt. Spokane, Washington: *Am. Mineral.*, **44,** 702–711.

THE AMERICAN MINERALOGIST, VOL. 46, JULY–AUGUST, 1961

DIFFERENTIAL THERMAL PYROSYNTHESIS

EDGAR M. BOLLIN AND PAUL F. KERR, *Department of Geology, Columbia University, New York, New York.*

ABSTRACT

Differential thermal pyrosynthesis may be considered a modification of differential thermal analysis which allows investigation under closed system conditions. A record is obtained of thermal reactions which occur during synthesis by heating elemental constituents to the fusion point. The equipment provides a continuous curve which records exothermic and endothermic reactions during formation; at higher temperatures, up to and above the fusion point; and subsequent cooling of synthetic compounds. The relative kinetics of the reactions are readily observable providing information applicable to other types of thermal study.

Modifications of the equipment design, changes in the technique, and alteration of physical parameters combine to provide sensitive thermal data. Pyrosynthesis curves of several synthetic minerals demonstrate the range of the method.

INTRODUCTION

Pyrosynthesis has been utilized in the studies of the differential thermal analysis of the system PbS–PbSe (Dunne and Kerr, 1961) to obtain supplemental data on this system. Rapid fusion of elemental constituents in a Bunsen burner or hotter flame (Earley, 1949, 1950) is undesirable since there is little control of the environment of synthesis and the thermal shock of rapidly applied heat and the rapid increase in the internal pressure produced by some reactions causes the failure of glass vials. Fixed temperature equilibrium synthesis studies used by the majority of the investigators of synthetic systems is similarly restricted by the length of time and the number of syntheses required for a complete determination of equilibria. Neither of the previous methods readily provides information concerning the relative kinetics of the reactions.

In this study, the thermal environment during synthesis is controlled by an electric furnace adjusted to a reproducible linear heating rate, and differential thermal analysis (D.T.A.) equipment is employed to indicate the temperatures at which reactions occur within the system.

Elemental constituents are confined in an evacuated glass vial with a molded depression at one end, which forms the contact with reacting products and a thermocouple. A similar vial filled with thermally inert material and a second thermocouple completes the pair of differential elements. An envelope of granular aluminum oxide holds the vials in a massive metal head. This arrangement provides a stabilized temperature distribution from the furnace to the sample and reference vials.

The technique is well adapted to the investigation of previously synthesized materials and naturally occuring minerals. The method is non-

destructive for compounds with thermally reversible reactions and repeated analyses of the same sample are possible. Trial syntheses have shown that the method is capable of recording reactions within vials with sufficient sensitivity to justify refinement and standardization of the technique (Bollin, Dunne, and Kerr, 1960).

Differential thermal pyrosynthesis (D.T.P.) is a highly flexible and reasonably accurate method for the investigation of a large number of minerals. Anhydrous synthesis of the majority of naturally occurring sulfide minerals directly from their elemental constituents and the observation of the kinetics of the reactions is possible. The method is not only adapted to synthesis studies, but also furnishes a sensitive method of investigation of reactions such as melting and transition relations which are not readily observable by other means. As a reconnaissance investigation preliminary to fixed temperature equilibrium studies of a system, or to furnish specific or comparative data on specific minerals, the method is rapid, easily implemented, and is a necessary corollary to the investigation of many systems.

Instrumentation and Technique

Instrumentation

The recording and heating units are largely the same whether used for D.T.A. or D.T.P. Modification of D.T.A. facilities for D.T.P. merely requires a fast response time in the recording equipment. However, continuous recording is essential and multiple point recorders, such as used by Kerr and Kulp (1948), are unsatisfactory because of the rapid rate of some reactions.

One Leeds and Northrup Speedomax H, model S recorder is used to record the amplified potential of a differential pair of chromel-alumel thermocouples, while another similar unit is used to record the temperature of one of these thermocouples. The potential recorder has a scale range of -5, 0, $+5$ mv, and the temperature recorder has a scale of 0 to 1200° C. The potential recorder is modified to allow variable suppression of the range at any position along the scale by replacing the (E) fixed resistor of the emf bridge* with a variable potentiometer of 4 ohms. This allows the recorder to be offset if either drift or a large thermal peak tends to drive it offscale. A chart speed of six inches per hour is normally used for both recorders. The response time of the potential recorder is one second, while the temperature recorder has a response time of five seconds.

Preamplification of the differential pair of thermocouples is provided

* Leeds and Northrup Manual #077990, p. N-2.

by a Leeds and Northrup No. 9835 B microvolt preamplifier. Two of the available ranges of preamplification may be used with the present configuration of thermal head and thermocouples. Low sensitivity results in 5 mv deflection of the recorder with a 0.5 mv input (10X) while high sensitivity produces a 5 mv deflection with 0.25 mv input (20X).

The response time of the preamplifier appears rapid enough to record D.T.P. reactions, and is slow enough to suppress the electrical pulses applied to the furnace by the on-off controller. Use of the extremely fast response direct current amplifiers now commercially available necessitates proportional type control of furnace input or a reduction of their response by capacitive loading. A Beckman Model 14 breaker amplifier has been modified for fast response by using 60 cycle choppers and direct current feedback. The configuration and magnitude of the D.T.P. curves are not affected during a fast deflection, although the baseline is considerably broadened by current pulses of the furnace controller.

The program controller provides a linear heating rate of 12.5° C. per minute from room temperature to 1200° C. A linear cooling rate at the same speed is also provided. The program controller consists of a Leeds and Northrup Micromax recorder-controller and a M.E.C. two position time-proportional anticipation unit. The control point is driven upscale or downscale by a synchronous motor. Contact pitting, noise, and maintenance associated with standard heavy duty control relays have been eliminated by the use of an Ebert mercury plunger relay to control the current supplied to the furnace.

The furnaces are constructed of internally wound cores supplied by the Mevi-Duty Electric Co., Milwaukee, Wisconsin (type MK-3712, 3″ bore, 12″ long, 1205° C. maximum continuous operating temperature). These cores have a 1900 watt rating when operated on 230 volt alternating current. One-half inch thick transite discs at each end of a five gallon drum constitute the external shell of the furnace. Fiberfrax, ceramic fiber (Carborundum Co., Niagara Falls, New York), packed 6 lbs./cu. ft., is used for insulation.

Four two-inch water pipe vertical supports attached to $\frac{1}{4}$ inch thick boiler plate, above and below, form a substantial frame within which the furnaces are suspended by a pulley mounted sash cord and counter weight. Standard, threaded water pipe floor flanges are used to attach the pipe to the boiler plate.

The power input of the furnace is considerably above that necessary to maintain a 1200° C. terminal temperature;* however, the high input provides a useful excess of available heat. This is highly desirable since other-

* Norton Company Catalog No. 485, The Construction of Laboratory Electric Furnaces, p. 9.

wise furnace limitations may affect the linearity of the program controller. Continuous input to the furnace yields a heating rate of approximately 28° C. per minute with sufficient linearity of the program throughout most of the range to allow rapid reconnaissance investigations.

Low resistance, high current furnaces, such as the Hoskins 305 previously used by Kerr and Kulp (1948) produce a higher heating rate at lower temperatures than the furnaces now in use; however, linearity is poor above 800° C. Heating rate curves exhibit a high temperature nonlinearity when insufficient insulation is provided for these temperatures. Such furnaces, however, have a considerable advantage for investigations in the low temperature range since their rapid low temperature heating rate allows the program controller to establish a linear heating rate earlier in the cycle. The furnaces now in use have a low initial heat, which does not allow a completely linear curve to be established below approximately 100° C. with the size of the thermal head now in use. Since most of the critical reactions are above this temperature in the present study, the slight deviation from linearity in this range is not considered critical.

Thermal Head

The thermal head (Fig. 1) is constructed of 18-8 chrome-nickel stainless steel, which is essentially as heat resistant as the nickel used in some equipment.* Stainless steel produces no curie effect, is more easily machined, and is more readily obtainable than nickel. A further consideration in the selection of the stainless steel is its oxidizing properties. A uniform dull black oxide film is formed by heating in excess of 1000° C. and subsequent heating to 1050° C. under normal conditions of analysis does not produce appreciable scaling.

The black oxide layer tends to smooth out the transition from the conduction and convection mode of heat transfer to the radiation mode of heat transfer between furnace windings and head by increasing the radiation absorptivity at a lower temperature. The porosity of the oxide also furnishes a bonding surface for cementing thermocouple insulator tubes in the head.

If the metal is purchased in rod form, machining of the head is reduced to cutting to desired length, preferably with a power hack saw, and facing the ends in a lathe. The center hole is drilled, and the center line of the sample and reference wells is scribed while the rod is still centered in the lathe chuck in order to assure accuracy of hole location.

The upper half of the head serves as a heat shield for the exposed tips

* Publication No. 266, Heat Resistant Castings, Corrosion Resistant Castings, Their Engineering Properties and Applications: International Nickel Co., Inc., 60 p.

f the vials which protrude from the lower portion. This two piece con- truction of the head is of considerable advantage when placing the vials n the head as it allows each vial to be seated firmly on the thermo- ouples and concentric with the thermal wells. The open space in the ower half of the head is packed with granular aluminum oxide to hold the rials in position before placing the top half in place. The two piece head lso allows rapid removal of the vials for quenching. A further advantage f the two piece head is the maintenance of a heat gradient between the

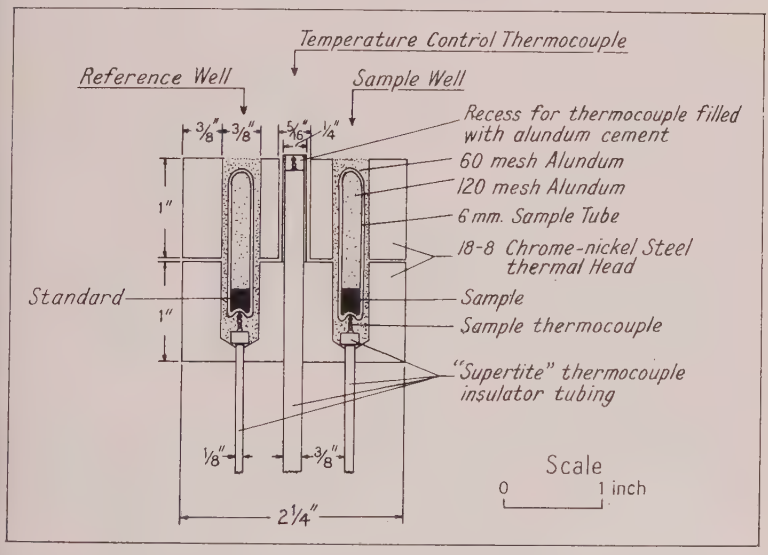

Fig. 1. Cross-section of the thermal head. Sealed, evacuated glass vials are concen- ically located in alundum packed apertures in a stainless steel head. Thermocouples fit n indented base.

p and bottom of the vial during convection cooling of the furnace. The ncomplete heat transfer between the two portions of the head under nese conditions allows the lower portion of the vial to cool first. This radient is sufficient to cause single crystal growth within the vial in the ase of a number of compounds.

The thermal head is mounted on a Norton RA 98 alundum tube two aches in diameter with a $\frac{1}{4}$ inch wall thickness. The length of the tube is uch that the head is located at the center of the furnace and concentric ith the vertical axis of the furnace. When the furnace is lowered over ne thermal head, the whole assembly is aligned automatically by the en- osing furnace frame, which restricts horizontal displacement to main- in exact concentricity of the thermal unit with the axis of the furnace.

Much importance is attached to the alignment and the vertical arrangement of the furnace to assure symmetrical convection distribution of heat in the thermal head. Convection currents are reduced to a minimum by a plug on the top of the furnace, and a mechanical seal is provided at the bottom by the insulation in which the thermal head support tube is mounted.

The head should be brought to the exact thermal center of the furnace by a simple procedure. The transite discs at the bottom of the furnace support frame are drilled slightly oversize so that the alundum head support tube may be slightly tilted. The thermal wells are filled with granular alundum, and the furnace is brought to approximately 600° C. The alundum support tube is tilted slightly in different directions and the furnace lowered so that the system comes to an equilibrium condition. Experimental tilting is continued until a minimum base line offset on the differential potential recorder is obtained. This places the head in the exact thermal center of the furnace windings. Base line offset may now be reduced to zero by rotating the alundum support around its vertical axis so that both thermal wells are symmetrically disposed with respect to the vertical furnace windings. The support tube is next cemented permanently in this position. This procedure results in a minimum overall base line drift throughout the heating cycle.

During controlled cooling cycles, convection cooling is accomplished by removing the top plug closure of the furnace and raising the furnace approximately two inches. The temperature controller is left at the highest temperature until a convection equilibrium is established with the thermal head. This is indicated by a return of the base line of the differential record to a normal position. As the convection current cools the furnace at a rate faster than 12.5° C. per minute, the program controller is able to maintain a linear cooling rate by adding heat.

Preparation of Thermocouples

The thermocouples are prepared from B & S No. 22 gauge chromel-alumel wires. A simple arc welding process allows rapid and uniform fabrication without the equipment and skill necessary in gas-oxygen torch welding. The thermocouple welder is shown in Fig. 2. Construction dimensions are not critical, and a considerable modification is possible without affecting results appreciably. The current during the arcing process may be controlled by either a series resistor as shown, or by a Variac. The series resistor of 5 ohms in the present unit is wound with furnace resistance wire on a $\frac{1}{4}$ inch ceramic thermocouple insulator tube and covered with Insalute No. 1 cement. Considerable heat is dissipated

by the resistor if welding is prolonged, and ventilation should be provided or the construction should be open. The mercury cup may be made of plastic sheet and tubing. Size is of minor importance as long as sufficient depth is provided to maintain at least a minimum layer one inch thick of mineral oil over the mercury. The cover should have a hole just sufficient to admit the thermocouple wires in order to reduce splattering of oil during welding.

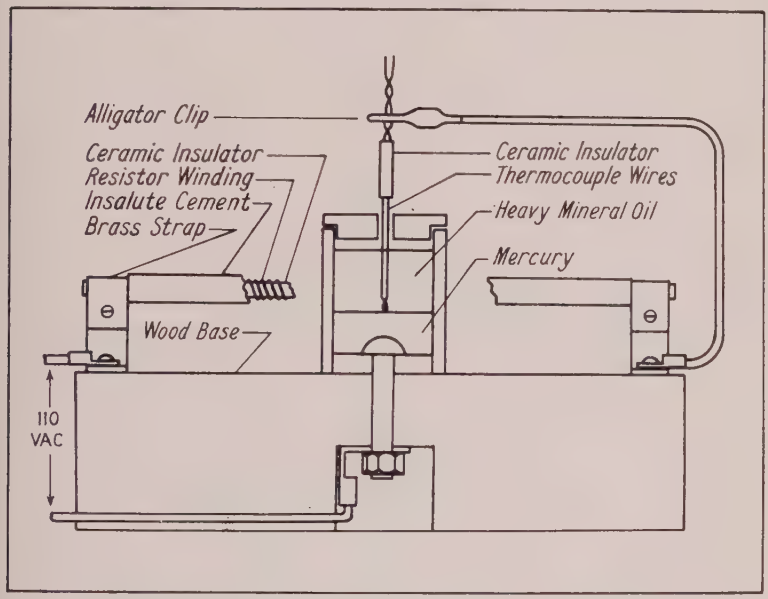

FIG. 2. Thermocouple arc-welding device. A cup containing mercury covered with oil forms one 110 volt A.C. terminal. The thermocouple wires form the other. On contact, the two wires are fused to form a small sphere.

The thermocouple wires are threaded through a short piece of ceramic insulator tubing and the ends uniformly twisted together. An alligator clip is then attached to the wires protruding through the other end of the insulator, and the twisted end is lowered through the mineral oil allowing momentary contact with the mercury. The thermocouple is immediately raised very slightly allowing an arc to form for a second or two; then the contact is broken by lifting the thermocouple slightly higher into the overlying mineral oil. The thermocouple is removed from the mineral oil after approximately ten seconds so that the temperature is low enough to prevent oxidation. The mineral oil serves to reduce the amount of mer-

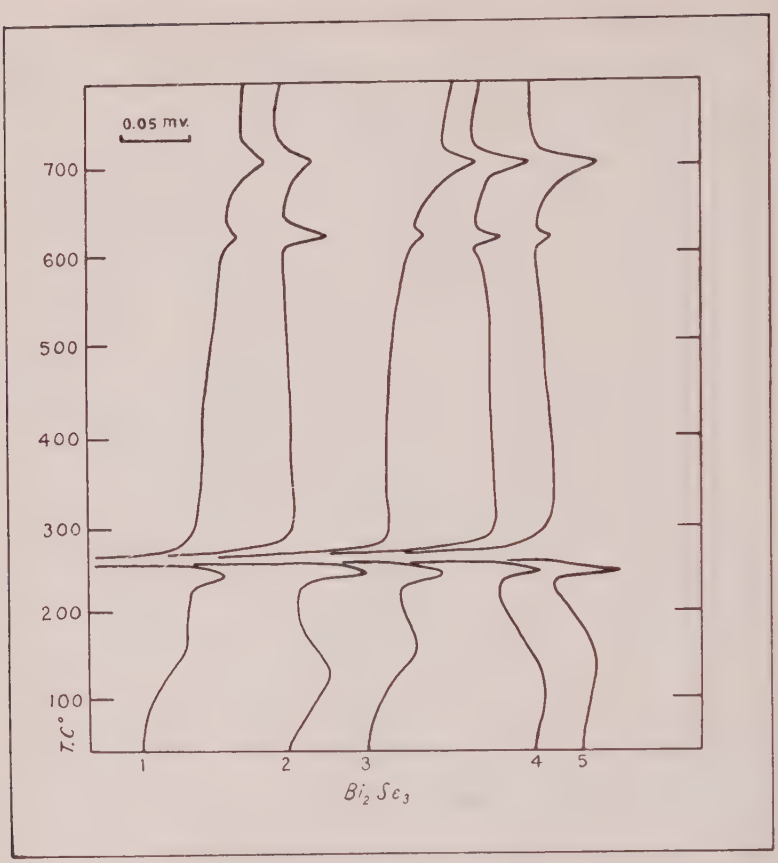

FIG. 3. Pyrosynthesis curves for Bi_2Se_3 for vials with different basal configuration for thermocouple contact. (1) A round bottom with a point thermocouple contact. (2) A flat bottom with a point thermocouple contact. (3) Base indented $\frac{1}{8}$ inch. (4) Base indented $\frac{3}{16}$ inch. (5) Base indented $\frac{1}{4}$ inch.

cury vapor produced during the welding and allows the surface tension of the molten thermocouple to produce a spherical shape. The size of the thermocouple junction can be readily controlled by the amount of arc time, and after a few experiments uniform couples may be produced with little difficulty. A sphere approximately twice the size of the wire diameter is used to provide a good contact with the sample vials. In standard D.T.A. investigation, where thermal contact is provided by the sample completely surrounding the junction, a weld which shows no increase or decrease in size at the junction is desired to obtain optimum response time commensurate with longevity.

Preparation of Sample and Reference Vials

A somewhat similar thermal technique has been used by Jensen (1942) and Kracek (1946). However, the construction of the double re-entrant vials, used by these workers to allow placement of the thermocouples in the center of the reactants, requires considerable glass blowing technique and provides less strength than the vials used in this study. The increased thermal transfer by placing the thermocouple in the center of the reactants is of doubtful value, and may be even less effective than in the present construction. In the present design the thermocouple recess is molded around the end of the thermocouple junction, providing intimate physi-

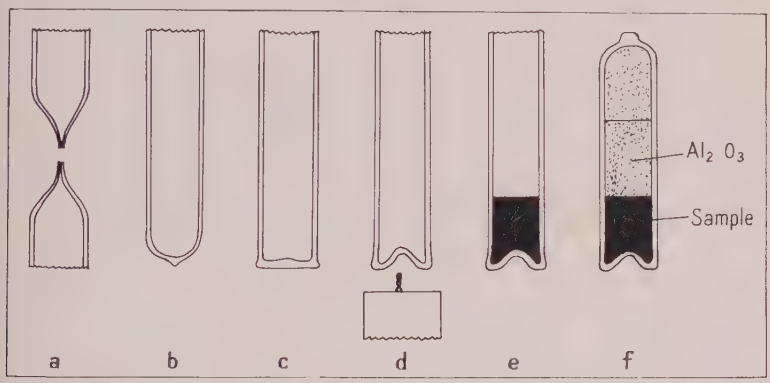

FIG. 4. Successive steps in the preparation, filling, and sealing of a sample vial.

cal contact. The complexity of fabrication of the double re-entrant vials and the associated multiple seals of the previous designs has probably prevented wide adoption of the method. The effect of thermocouple penetration into the reactants, as shown for Bi_2Se_3 (Fig. 3) demonstrates that reactions may be observed in simplified vials with excellent results.

The sample vials may be constructed of Pyrex, Vycor, or fused quartz tubing 6 mm. in diameter, depending upon the highest temperature to which the tubing is to be subjected. A tube wall 1 mm. thick is normally used where internal pressures are not excessive. Pyrex tubing remains rigid to 600° C. and is easily worked with a gas-air torch. Vycor and fused quartz tubes require the use of an oxygen torch for fabrication and are usable to at least 1200° for short periods.

A tube twice as long (8 inches) as the final length is heated and pulled into a fine capillary in the middle, providing two tubes (Fig. 4*a*). The capillary is necessary, as fusion of a tube with a normal diameter often produces an imperfect vacuum seal. The capillary is fused, and, as the

tubing approaches a spherical shape, caused by surface tension (Fig. 4*b*), it is flattened against a heat resistant surface (Fig. 4*c*). The closure is reheated to softening temperature, and a cold thermocouple is pushed into the bottom of the tube until approximately a $\frac{1}{8}$ inch re-entrant is formed (Fig. 4d). A thermocouple is used as a mold and is mounted in a large diameter ceramic tubing from which it extends the required $\frac{1}{8}$ inch. This procedure results in a uniform thermocouple recess depth which conforms to the size and shape of the thermocouple used in analysis. The vials are thoroughly heated at a temperature below softening to anneal the seal and drive off any entrapped moisture, then are cooled in a desiccator and kept until ready for use.

A measured volume or weight (1–2 mg.) of reactants is placed in the bottom of a vial (Fig. 4*e*) and tapped on a solid surface until no further compaction is noted in order to reduce the pore space to a minimum without mechanical pressure. A uniform volume of 120 mesh granular aluminum oxide is placed on top of the sample to fill the open space in the vial and to protect the sample during the sealing operation. The aluminum oxide filling of the tubes may be omitted if a pure sample is desired for *x*-ray analysis. The alundum filler is likewise omitted where cooling curves are to be examined to prevent reactants from being trapped in the pore space or on the surface area of the alundum. Closely fitting glass rods may be used where volume considerations are more important than base line drift.

The vial is evacuated to approximately 50 microns of mercury pressure with a Cenco Megavac vacuum pump. While under vacuum the vial is heated and sealed by rapidly twisting the plastic portion of the vial. Any open space above the aluminum oxide is eliminated by continued twisting while the seal is still plastic. The seal is then drawn out to separate the tube from the pump and flattened against a heat resistant surface (Fig. 4*f*). The aluminum oxide filler in the vial not only serves to mark a consistent length for the seal, but also protects the sample from coming into contact with the heated portion of the vial in handling. When sealing Vycor or fused quartz vials there is a tendency for the vacuum trapped with the reactants to bulge the tubing inward at the seal. Until facility is gained in the sealing process, failure of the vials may result unless the inward bulging is prevented by contact with the aluminum oxide filler or glass rods.

Internal standards may be used in the reference vial to provide check points on curves by which the emf record may be indexed over the temperature record and traced on a light table. From the differential standpoint, it is of no consequence which vial contains the standard. From the chemical standpoint, the standard in the reference vial removes a source

of possible sample contamination and spurious reactions from interaction between the sample and the standard.

Electrical Wiring of the Thermal Head

In wiring the thermal head, the reference thermocouple of the differential pair also serves as the temperature recording thermocouple. A further reduction in the number of thermocouples may be made by using this thermocouple to activate the program controller. However, the program control thermocouple is located in the center of the head and serves to maintain alignment of the two halves. In this position it does not disturb the thermal symmetry of the head.

If the thermocouples are reduced to two, the temperature of the reference vial is controlled and not the furnace. Because of the thermal inertia of the head surrounding the reference vial, some difficulty caused by control overshoot may be expected unless the temperature controller has sufficient latitude of adjustment, or a very small thermal head is used.

The reference thermocouple of the differential pair is used as the temperature recording thermocouple for several reasons.

(1) The addition of another thermocouple mounting for a separate head temperature thermocouple, as used in some D.T.A. arrangements, would disturb the thermal symmetry of the head.

(2) Maintaining an exactly symmetrical heat flow distribution for a third thermocouple increases the number of uncontrolled variables in the system and increases the difficulty of construction.

(3) The temperature of the head is of no significance, since there is a slight difference between the head temperature and the actual sample temperature caused by the imperfect heat transfer through the aluminum oxide surrounding the sample and the reference vials.

(4) The reference thermocouple has a more nearly linear heat rise than the sample thermocouple, as there is a slight deviation of linearity in the sample well caused by the reactions produced. It may be argued that the temperature in the two wells is not exactly the same because of differing rates of heat absorption of the reactants in the sample well and the aluminum oxide or the reference in the reference well. However, the amounts of reactants used are so small that this effect is negligible. The actual temperature difference between the two vials may be computed from the displacement of the base line of the emf recorder from zero by dividing actual displacement by the preamplifier gain. In properly designed and aligned thermal heads and furnace configurations, the distinction concerning which thermocouple is the valid temperature recording couple is not significant. The temperature difference between the two vials in the present instrumentation, when a reaction is not in progress, is in the range of 0° to 0.25° C., which is too small to be resolved on the temperature record.

(5) Thermal deviations from linearity produced by some reactants during a reaction are large enough to slightly distort the temperature curve and give anomalous temperatures of reaction when the sample thermocouple is used to record temperature. Self heating or self cooling during strong reactions may cause the actual sample temperature to be slightly different from that recorded in the reference well. Since relative temperatures based

upon a specific linear heating rate are a basic assumption in this method of analysis, the temperatures as expressed by the reference vial more nearly approach a valid figure for comparison. An otherwise linear temperature curve, which is distorted at the point of measurement, is not susceptible to interpolation of small differences in temperature.

(6) The presence of a standard in the reference vial does not interfere with the temperature record because the amount may be regulated to avoid affecting the temperature curve. The difference in the sensitivity of the temperature and the differential recorders makes this procedure possible.

Physical Factors in Thermal Methods

The control of environmental variables encountered in differential thermal analysis applied to the study of clay minerals (Kerr and Kulp, 1948); thermal analysis applied to the study of metallurgical problems (Jensen, 1942); and the utilization of fixed temperatures held until equilibrium is attained (Kullerud and Yoder, 1959), all involve factors which must be considered in applying the D.T.P. method. The technique for the standardization of D.T.A. has been treated extensively by Mackenzie (1957) and is applicable for most methods in which an open sample is in contact with the thermocouple. A number of parameters which affect D.T.A. also affect D.T.P., and only those with characteristics which are essentially changed by D.T.P. procedures need be discussed.

The major modifications which occur in D.T.P. involve the enclosure of the sample within a sealed vial and the method of heat transfer to the thermocouples. Also, extension of investigations to include the liquid and vapor state requires control of pressure influence and a thermal head design which must enclose the sample and reference vials.

Effect of Grain Size

The components should be as finely divided as possible, although the particle size employed depends upon the physical and chemical nature of the elemental constituents of the mineral under investigation. Several factors determine grain size, other than the complete physical homogenization obtainable with extremely fine-grained powdered mixtures. The optimum grain size for any single combination of elemental constituents should be experimentally determined for each system.

The initial reaction temperature in forming a specific chemical compound may influence the choice of grain size. Three basic types of reactions predominate (Fig. 12): (1) reaction in the solid state (Ag+S or Cu +S); (2) reaction with one component in the solid state and the other component in the liquid state (majority of the compounds studied); (3) reaction with both components in the liquid state (Zn+S). All three of these types of reactions may occur to a greater or lesser degree in any system. As the temperature increases, the vapor state reaction enters into

all three divisions to an increasing degree. The effect of the vapor state is easily demonstrated, even for condition (1) above, by the marked increase in the reaction of Cu+S at room temperature in evacuated vials compared with vials at normal pressure. Considerable reaction takes place in a week at one atmosphere pressure; whereas the same grain size material produces an equivalent amount of reaction overnight when sealed in evacuated vials. However, the slowness of the reaction rate in the unsealed vials may be in part due to the presence of oxygen which substitutes for sulfur in the lattice sites and decreases the diffusion rate within the structure (Hannay, 1959, p. 281). Grain size has little influence on those components which become liquid before reaction occurs.

The extremely fine grain size, which is important in obtaining homogeneity of the constituents, presents several specific problems. A decreasing accuracy of chemical composition is caused by increased weighing and transfer losses, especially with elements which develop a static charge which causes adherence to weighing instruments, vials, etc. These difficulties may be eliminated by weighing the constituents directly into the vials; however, the problem of removing portions of the constituents which adhere to the walls of the vial still remains. Care must be exercised to prevent these particles from being removed from the vial during the sealing of the vial.

Difficulty is also encountered in evacuating vials since trapped air pockets expel constituents by their rapid escape. This problem can be alleviated to some extent by including an adjustable air bleed to allow gradual application of the vacuum or by placing a relatively large container in the vacuum line. This container may also be used as a trap to prevent foreign particles from entering the pump. Tightly packed glass fiber may also be used between the vial and the pump to act as a trap and to allow gradual application of the vacuum. An electromagnetic or ultrasonic vibrator coupled to the vial is also helpful in preventing air pocket "explosions" during pumping.

Compaction of the constituents is desirable if glass rods are inserted into the vials before sealing to reduce the volume of the vapor space. However, incomplete compaction is less desirable than a loosely packed mixture because the escape of the air pockets through partially compacted material becomes violent during pumping.

The study of inversions of previously synthesized or naturally occurring minerals may be enhanced by the use of a single grain of material to avoid the effects of multiple nucleation of the transition.

Fine grain size is important because the heating rate limits the time available to attain equilibrium during any specific temperature interval. Thus the state of division of the constituents is more important in D.T.P.

than in fixed temperature equilibrium studies. Effects such as mobility of reacting ions; the chemical gradient toward reaction as a function of the relative chemical activity of the constituents; or the tendency of the reactants to form partial reaction barriers around the individual grains, must be evaluated in relation to grain size.

Partial reaction products, which may occur at grain boundary interfaces and tend to prevent further reaction, depend in many respects upon the physical characteristics of the reaction product and of the host grain. The tenacity, porosity, relative thermal coefficient of expansion of the host and its rim, film adherence between rim and host, and the ductility of the film affect the duration of the reaction rim as the temperature increases. The ductility of the film, in a large measure, determines the tolerance of a relatively large difference in thermal expansion properties of the film and host before rupture occurs allowing further reaction.

The effect of reaction rim or barrier development may be observed in Figure 5. Here, and in other compounds, reaction rim development tends to break down in a stepwise manner as the temperature increases. The composition range from CuS to Cu_2S was made with coarse grains of copper and sulfur to eliminate weighing and transfer losses and to provide as much accuracy in chemical composition as possible. Some combination occurred during sealing and storage of the vials before heating; also, the time during which constituents were in contact was not controlled as the dissociation and melting relations were of major interest in this experiment. The series was synthesized, starting with the CuS end where a major development of exothermic peaks is shown accompanied by the endothermic melting of sulfur at 115° C. The decrease in intensity of these peaks is a function of the time the constituents were in contact, as all vials were sealed at the same time. The similarity of the stepwise exothermic peaks indicates that a characteristic development of reaction rim breakdown occurs. Analysis of this appears feasible under controlled conditions of sample preparation.

Limited conclusions concerning some of the reactions indicated by Fig. 5 appear justified. The endothermic peak at 505° C. is the incongruent melting point of covellite to digenite+liquid+vapor, which as determined by Kullerud (1956) occurs at 507°±3° C. at about 880 mm. Hg pressure. The temperatures obtained by D.T.P. are within the limits of error of reading the temperature scale and thermocouple variations (±5° C.). The magnitude of the endothermic peak decreases toward extinction at a composition of $Cu_{1.8}S$, which is the composition of digenite. The decrease results as less and less covellite becomes present. The temperature of the reaction is constant up to a copper to sulfur ratio of 1.6:1, which indicates that the volume of the vapor space in the vials is such that liquid sulfur is always present at this temperature. The reac-

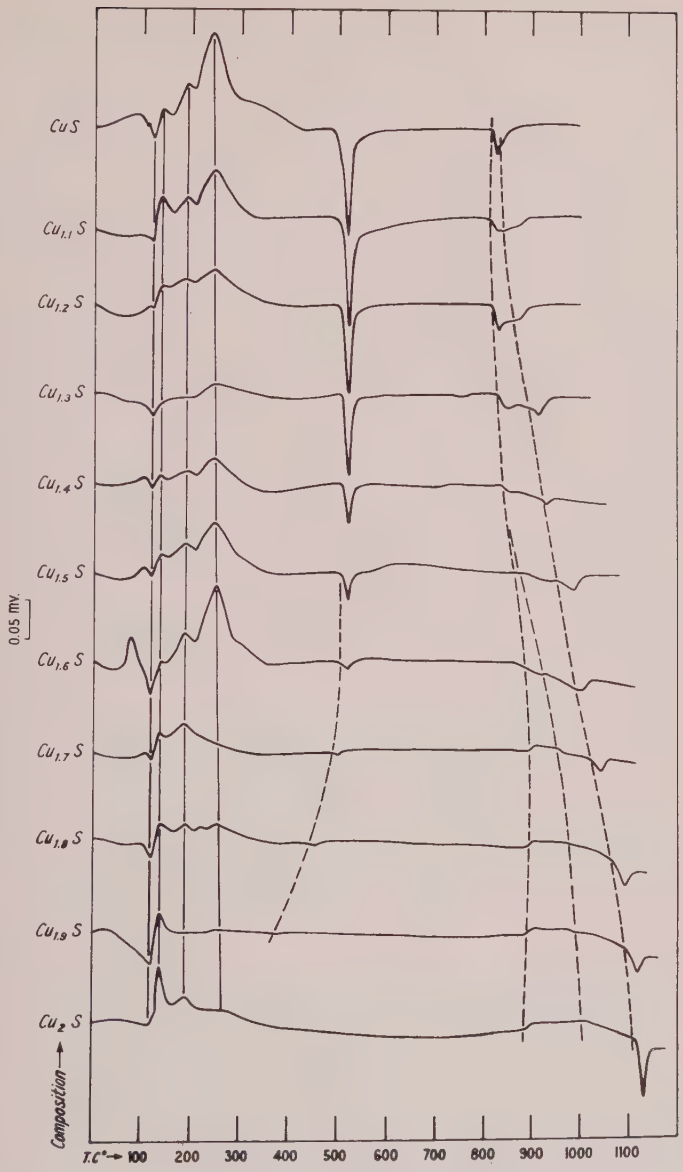

FIG. 5. Pyrosynthesis curves for the system CuS-Cu_2S.

tion is observable to a copper to sulfur ratio of 1.9:1. The peaks at the composition of $Cu_{1.8}S$ and the copper to sulfur ratio of 1.9:1 are attributed to non-equilibrium formation of a small amount of covellite during synthesis. The decrease in the temperature of dissociation from the

copper to sulfur ratios of 1.6:1 to 1.9:1 graphically demonstrates that the vapor pressure was less than that over liquid sulfur, and that the effects of changes of sulfur pressure within the vials are observable.

The dissociation of covellite to digenite+sulfur at vapor pressures less than that of liquid sulfur is extremely sensitive to bulk composition and the relative proportions of covellite, digenite, and chalcocite which may be formed during synthesis under non-equilibrium conditions. Factors such as grain size, degree of homogenization of the sample during mixing, partial reaction during sealing and storage, and the heating rate all contribute to the degree of equilibrium attained during analysis. Therefore, these peaks are non-reproducible from sample to sample and the smooth curve drawn through the peaks in Fig. 5 from $Cu_{1.6}S$ to $Cu_{1.9}S$ merely indicates that the majority of the steps in the sample preparation of this series were closely controlled.

Exothermic peaks of copper and sulfur using extremely finely divided constituents, not mixed until immediately before heating, show an abrupt single peak immediately following the melting of sulfur. The copper used in this case was electrolytic dust. The exothermic peak using this material appears much like the exothermic peak of Cu_2S in Fig. 12. The electrolytic dust has not been used in composition dependent reactions because of the difficulty experienced in removing it from weighing instruments, vial walls, etc.

Each of the previously mentioned factors of reaction rim development may become significant under special circumstances of chemical composition, but in other compositions may be of little consequence. The precise interpretation of the range and significance of each of these factors has not been attempted. However, in the detailed study of a particular system the effect of non-equilibrium reaction rim development must be considered and procedures to minimize its occurrence should be evaluated.

In some systems, the formation of reaction rims, with the attendant suppression of a reaction at the true initial temperature of combination, may be a source of trouble in fixed temperature equilibrium studies. Where a reaction rim develops which is thermally and chemically metastable, repeated grinding and reheating may be necessary to achieve complete reaction. Such repeated handling increases the possibility of changing bulk composition.

In numerous studies of the formation of double sulfides, difficulty has been encountered in achieving the reaction of the second molecule of sulfur with the cation. This has caused some investigators to form the monosulfide by reaction for long periods of time with repeated grinding and reheating. The disulfide is usually formed by adding sulfur in excess,

and reheating. The present study has encountered little difficulty in the synthesis of disulfides directly, using stoichiometric bulk compositions, and avoids the above procedure by using fine-grained, well mixed, non-oxidized elemental constituents. It is believed that many of the obstacles in difficult syntheses may be eliminated by thorough precautions to eliminate substitution of oxygen in the sulfur lattice sites. Some reaction rims may be dissipated more readily by a cyclic temperature program rather than fixed temperature equilibria programs by differential expansion and contraction of the reaction rim and unreacted material.

Extremely pure metals may now be obtained in the form of refined rods intended for use in the semi-conductor industry. The synthesis of compounds from these highly purified materials is highly desirable if precision determination of any parameter is contemplated. The reduction of these materials to a fine grain size without contamination is readily achieved by the method described by Van der Lann and Nicholls (1960). A spray of molten metal from a nozzle is forced into a free falling column under the pressure of nitrogen or hydrogen gas. Relatively perfect spheres of 10 to 100 microns in diameter may be formed by this method. The possibility of rapid oxidation of these fine-grained materials may be overcome if the free falling column is constructed so that the metal freezes in an oxygen free atmosphere derived from the nozzle. The materials should be immediately transferred to, and held in, evacuated vials until used. The original apparatus was constructed of metal, limiting its use to low melting point metals. The apparatus may be readily adapted to higher temperatures by cementing nozzles and gas lines of fused quartz to the rod of metal with ceramic cement and enclosing the assembly in castible ceramic. This procedure also reduces possible contamination from metallic parts of the apparatus.

Effect of Heating Rate

The heating rate has a pronounced effect upon the thermal curve. The intensity of the peaks is altered and the temperature at which the reactions occur is affected by a rate change. Two examples were used to show their relative effect upon the D.T.P. curves. The compositions FeS to FeS_2 first were synthesized in ten per cent mol increments at the standard D.T.A. rate of 12.5° C. per minute, and then at a continuous furnace input which yielded a semi-linear heating rate of approximately 28° C. per minute. The family of curves for the slower heating rate is shown in Fig. 6. The faster heating rate curve is as reproducible as the slower heating rate curve and the comparison of the two heating rates for the bulk composition $FeS_{1.5}$ (Fig. 7) is valid for all compositions of both heating rates. The faster heating rate curve shows an increase in resolution above

FIG. 6. Pyrosynthesis curves for the system FeS-FeS_2.

275° C. where a single broad peak in the slower heating rate curve is resolved into three distinct peaks. The intensity of the peaks is not only increased, but also the deflection at the initial point is considerably sharper. The possibility exists that the three peaks represent a rapid removal of reaction rims which are gradually broken down in the broad peak of the slower heating rate curve.

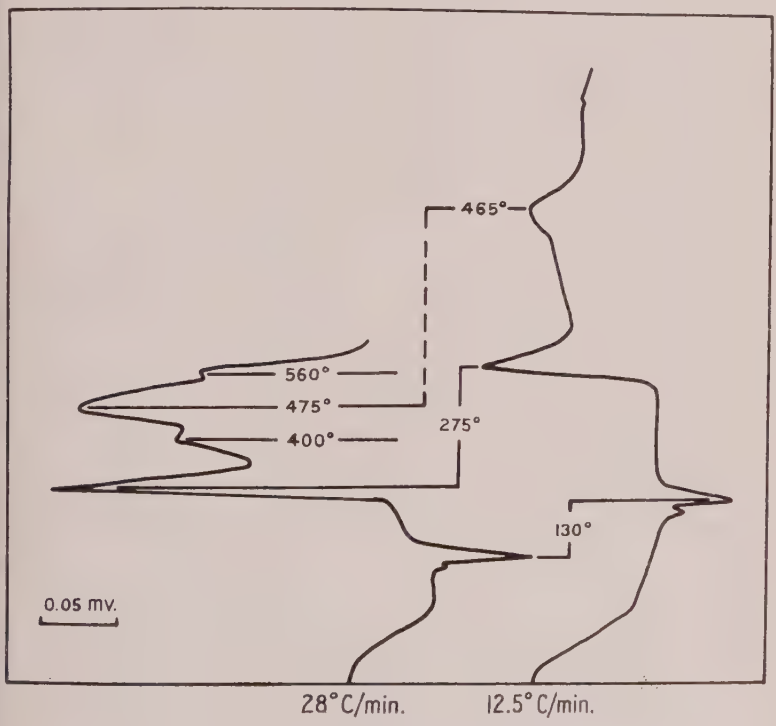

FIG. 7. Change in configuration of pyrosynthesis curves of $FeS_{1.5}$ with differing heating rates.

High heating rates yield an increased intensity of temperature dependent reactions, and are most likely to produce temperature differentials within the samples, cause an upscale shift of true reaction temperatures, and a compression of the temperature scale reducing accuracy. Kingery (1959, p. 284) also points out the existence of " . . . nonequilibrium temperature indications for phase changes, such as undercooling or possible complete suppression of solid state transformations." High heating rates also impose stringent requirements upon furnace capacity and furnace insulation. They also require a small thermal head, which in

turn reduces reproducibility and increases base line drift. A higher rate of sealed vial failure occurs with the faster heating rate which may be caused by the thermal shock or the increased rate of pressure produced within the vials because of faster reactions. However, the heating rate of 28° C. per minute is of interest in a preliminary study of a system or in the study of decompositions and similar rate dependent reactions which tend to be broad and undifferentiated from the base line when slower heating rates are used.

A slow heating rate, in the range of 0.5° to 5° C. per minute, is preferable for the study of liquidus-solidus relations and with powdered samples to increase the precision of temperature determination. The slow rates are necessary in the study of some samples to prevent the overlap of two successive peaks (Fig. 5) for nonequilibrium conditions, such as undercooling or the suppression of solid state reactions.

A heating rate of 12.5° C. per minute is used, unless otherwise indicated, since it represents a compromise which has been standardized in D.T.A. as giving the most adequate resolution of all differing types of reactions for a single heating rate and is available in most laboratories engaged in thermal analysis.

The use of a wide range of heating and cooling rates is mandatory if all types of reactions which are observable by the instrumentation are to be analyzed. The optimum heating or cooling rate for a specific reaction in a specific system can be recommended only if the kinetics of the reaction are known. As this type of information is usually not available, experimental variation of the heating rate is the best solution to the problem. In many studies it is of extreme importance to determine if a reaction rate is sufficiently high to allow attainment of equilibrium under dynamic conditions of observation. The degree to which the thermal curves are affected by various heating rates gives considerable information toward this end, and in many cases it is necessary to ascertain these effects in order to allow the correct emphasis to be placed upon the results obtained.

Optimum resolution of the thermal curves for different types of reactions depends to a considerable degree on different heating or cooling rates. High-low displacive transformations tend to be rapid and may be studied at high heating rates. Reconstructive transformations involving the breaking of chemical bonds, and structural rearrangement or diffusion are generally sluggish and require slow heating rates if they are to be observed at all (Buerger, 1951, p. 189).

Similar reactions, such as liquidus-solidus relations, in differing types of materials may proceed at different rates. Bivariant transformations, such

as the freezing of solid solutions may result in a shift of the base line rather than a distinct peak. Univariant equilibria, such as the freezing of a eutectic, are isothermal and are therefore not as rate dependent as other liquidus-solidus relations. Hypo- and hyper-eutectic alloys yield curves that have intermediate characteristics of the solid-solution and eutectic type curves. Peritectic alloys produce a sharp deflection of the thermal curve with a gradual return to the base line. Undercooling is usually more pronounced in eutectoid transformations than in eutectic or monotectic reactions and tends to be even more pronounced in peritectic transformations. These reactions and thermal characteristics are described in detail by Rines (1956). Even greater variance in the liquidus-solidus relations is found when comparing metals and alloys to intermetallics and especially to silicates.

The physical state of the material under observation further affects the kinetics of the reaction. Whether the material is in a single crystal, polycrystalline, or in powdered form influences the rate at which equilibrium is attained; thereby necessitating adjustment of the heating rate for proper observations.

Non-equilibration shifts of the true temperature of reaction may be compensated for to some extent by approaching the reaction from both directions, heating and cooling. The observed range in the temperature between the liquidus and the solidus, minimizing the influences of undercooling and overheating can be narrowed by slow heating rates. The magnitude of undercooling and overheating can be estimated by the use of different heating rates in observing these phenomena.

Reactions which change the thermal conductivity or the heat capacity of the sample may be observed by shifts in the base line of the thermal curve, although a distinct peak is not produced. In such reactions the heating rate is important if the reaction is to be observed. The differences in thermal conductivity and heat capacity between the sample and the reference largely regulate the drift of the base line for any specific heating rate. This is especially true if the thermal distribution of the head and the symmetry of the head and furnace are not perfect. A combination of different heating rates, reference materials, and deliberate slight misalignment of the head and furnace can be used to enhance the observation of these reactions.

In addition to the variation of the heating or cooling rates to emphasize a specific reaction, it is necessary to employ extremely non-linear heating programs for some reactions. In determination of some solidus temperatures it is important to equilibrate the sample for long periods of time just below the melting point. In determination of the liquidus of

viscous melts it is also necessary to equilibrate just above the freezing point.

Effect of Thermal Head Design

The thermal head design is predicated upon an exact symmetry of disruption of heat flow in the head by the placement of the thermal wells. The dimensions of the head do not appear to be critical if symmetry is maintained. Modifications in the head size depend upon: the size of the furnace available; heat input available; smoothness of program control action; size of sample vials to be enclosed; and the magnitude of the peaks necessary for a particular problem under investigation.

The apparent simplicity of the thermal head is somewhat misleading. Several factors enter into the design which are not obvious and exert a profound influence upon the data obtained.

Examination of the influences on head design has indicated that the original head design (Fig. 1) is not optimum for the complete range of D.T.P. investigations. However, as the design produces a maximum uniformity of results, it has been retained for the remainder of the investigation as a major change would invalidate continuity of the analysis. As a general survey type of head, certain practical advantages are inherent which allow a rather wide margin of control of several parameters without severe distortion of the D.T.P. curves.

The major thermal requirement of optimum head size is a head with sufficient thermal mass to equalize differences in temperature distribution from the furnace windings, and with small enough thermal mass to minimize absorption of temperature differences produced by reaction within the vials. A head with sufficient mass to completely equalize temperature differences within the furnace tends to suppress the magnitude of the reactions and smooth abrupt step-functions of heat change produced in the sample if the thermal conductivity between the sample vial and the thermal head is high. The design (Fig. 1) used in the present study provides a high thermally conductive metal head to smooth out temperature gradients, and a partial barrier of aluminum oxide of much lower thermal conductivity between the sample vial and the head, to reduce dissipation of the heat of reaction in the head.

The decrease in the amplitude of the peaks, by dissipation of heat to the head, may be balanced by preamplifier gain because of the reduced base line offset produced by a high conductive head. However, this procedure is to be avoided because rapid reactions are appreciably broadened, and the curves approach a function which represents a characteristic of the heat capacity of the head rather than of the reaction which is produced in the sample. The initial reaction point becomes a broad gentle

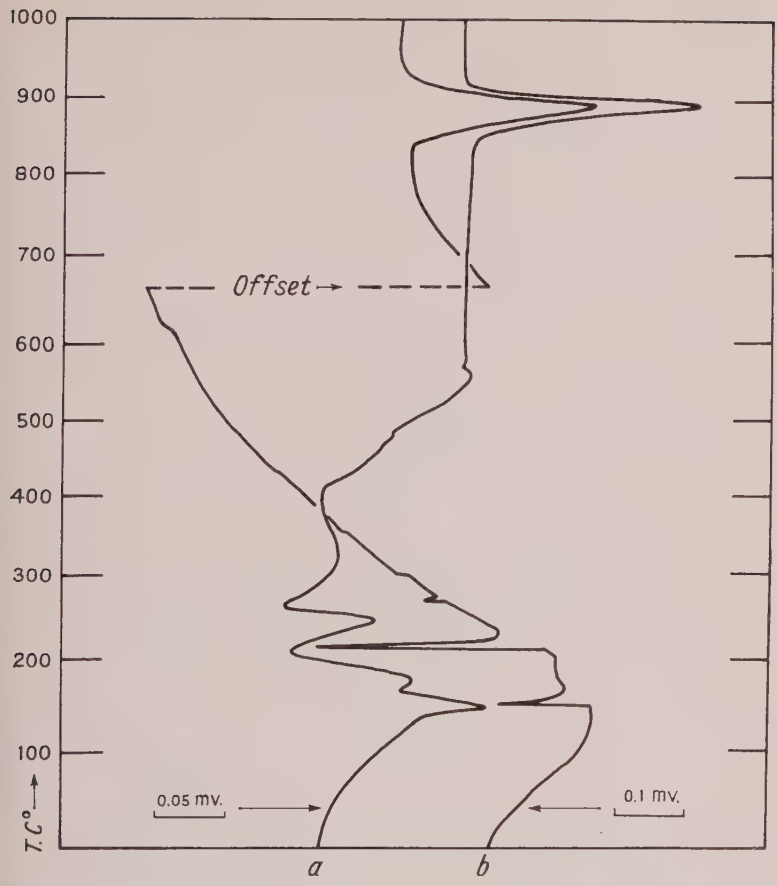

FIG. 8. Pyrosynthesis curves for $CuFeS_2$ (chalcopyrite) showing change in configuration of curves using thermal heads with differing heat capacities: (a) metal head; (b) ceramic head.

ope and not an abrupt deviation from the base line. This results in de-reased accuracy of data and has been one of the major factors in the non-eproducibility between differing types of thermal heads in D.T.A. in-estigations.

The differences produced with a change in the head material are illus-rated in Fig. 8, which shows the nature of the reactions produced by the omposition $Cu+Fe+S_2$. Figure 8*a* is the normal head used throughout ie investigation, and Fig. 8*b* is the ceramic head shown in Fig. 9. The oints of initial reaction are not only distinctly resolved in curve 8*b*, but is also evident that endothermic reactions do not occur on either side of e exothermic peak at approximately 200° C. The differences in the ap-

parent initial temperature of the exothermic reactions are ascribable to reaction development and differences in sample preparation.

In some respects, however, the ceramic head is not as sensitive to small reactions as the metal head. The lowered preamplification necessitated by the increased base line drift is responsible for this loss in sensitivity. The inversion at approximately 565° C. in Fig. 8*a* does not appear on the curve produced by the ceramic head. Thus it becomes apparent, as in the case of variation of heating rates, that different types of reactions are

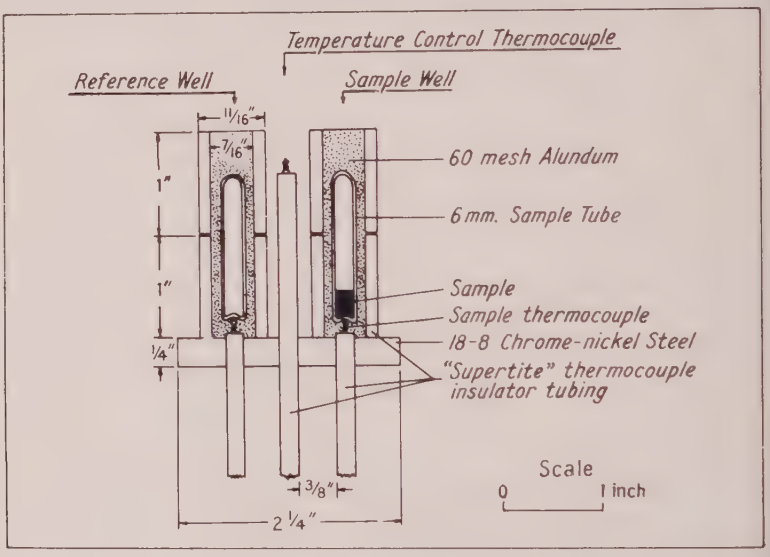

FIG. 9. Cross-section of low thermal mass ceramic head.

best investigated by thermal heads with differing heat capacities and equalizing characteristics.

Ceramic heads have been considered unsatisfactory by many workers. Kingery (1959, p. 258) states: "Because of its lower thermal conductivity the ceramic holder gives increased sensitivity, but results are less reproducible than with a high thermal conductivity metal block which is preferred." As indicated from the previous discussion, this statement may be modified. A more accurate evaluation of the low thermal conductivity head would be that reactions greater than the threshold limitation imposed by base line drift result in greater sensitivity not only in amplitude of the peaks, but also in increased sensitivity to variations in technique. The high thermal conductivity head tends to make all reactions greater than a certain threshold value, assume the characteristics of the head which is a fixed quantity. Thus reproducibility appears to be better. To

reat a reproducibility is a reflection of the inability to respond to small ifferences in reactions. Unavoidable differences in sample preparation nd technique require a certain amount of non-reproducibility. Com- lete reproducibility indicates that the instrumentation lacks resolution. eramic heads clearly require a much higher order of precision of tech- ique, fabrication, and alignment than metal heads.

The head design in Fig. 1 may be considered to be a composite metal nd ceramic head. The alundum filling of the metal thermal wells con- itutes the ceramic portion of the head. Characteristics approaching ther a metal head or a ceramic head may be achieved by a variation in ne diameter of the thermal well. Even greater variation is possible in the ead shown in Fig. 9 by replacing the ceramic tubing which forms the ermal wells with stainless steel tubing. The tube wall thickness and iameter may be modified to produce a head with thermal characteristics hich are suitable for nearly any type of reaction.

The effect of the thermal mass of the head may be indicated by a series f sample volumes in increments of 0.05 cc of ZnS in a fixed vial length of .5 inches. The series was produced to analyze the effect of sample volume n the initial temperature of reaction. Reaction temperatures were iden- al, and five volumes of ZnS produced only slightly greater amplitude of eak height than a single volume. The thermal head was evidently ab- rbing the extra heat of reaction produced by the increase of material in ne vial. The thermal wells in the present head design are therefore too ose to the sample vial for the total amount of heat produced in the sam- le to be recorded by the thermocouple. The optimum ratio of sample al diameter to thermal well diameter has not been determined. As a gen- al rule, to reduce excessive heat of reaction dissipation in the thermal ead, the distance from any point on the sample to the thermocouple unction should be less than the distance to the thermal head.

Thermocouple Lead Wires

Considerable concern about the dissipation of the heat of reaction by ne thermocouple lead wires has been shown by workers in D.T.A. ingery (1959, p. 259) indicates that total heat dissipation may amount 75 to 80 per cent for practical configurations. However, if the thermal lations are considered in a normal D.T.A. head, the greatest amount of f heat is dissipated where the walls of the thermal wells are in direct con- ct with the sample. Since the thermal masses of the thermocouple lead ires are nearly insignificant in comparison to the thermal mass of the ead, the amount of heat dissipated in the head is proportionately much reater. The amount of reacting materials in contact with the thermal ead is a fixed quantity which does not lend itself to systematic study

without changing the head. This usually reduces reproducibility to such an extent that the factor may not be analyzed statistically. Materials such as powdered clay mineral usually studied by D.T.A. are such poor thermal conductors that the reaction of the portion of the sample in contact with the thermal wells is not recorded. The portion of the charge which is recorded is that part immediately surrounding the thermocouple itself.

The lead wires may be considered an extension of the thermal head and, since only the minor portion of the charge in contact with the thermocouple is recorded, this effect is multiplied to such an extent that the assumption of a 75 to 80 per cent loss ascribed to thermocouple wires is understandable. Thus it becomes apparent that the thermal efficiency of the head used in D.T.P., with a single point contact of the thermocouple with the sample, may be nearly equal to standard D.T.A. configurations.

In effect, the standard D.T.A. sample forms its own heat barrier to the dissipation in the thermal wells by poor thermal conductivity. Factors such as sample packing assume magnitudes of importance well beyond their actual validity. The thermal barrier formed by the sample is highly susceptible to a large range in thermal conductivity and is modified greatly by packing and composition of each sample analyzed. The analysis of this problem is beyond the scope of this investigation, but a standardized method of packing normal D.T.A. and corrosive D.T.A. samples is being described separately, which incorporates the alundum heat barrier used in D.T.P. heads (Bollin and Kerr, 1961).

The effect of loss of the heat of reaction by thermocouple wires and their insulator tubes in the D.T.P. arrangement may be illustrated by Fig. 10, which shows the difference in curves obtained by a relatively small change in the path length from the thermocouple junction to the head. The initial deflection of the exothermic reaction of Fe+S at approximately 240° C. is rounded to such an extent by the extra heat capacity of the $\frac{1}{8}$ inch path length that an estimate of initial temperature of reaction is only approximate. The higher temperature portion of the curve, showing the reaction of the additional sulfur to form pyrrhotite +pyrite is similarly of little value. The short path length from the thermocouple junction to the head allows a substantial amount of the heat of reaction to be transferred to the head increasing the heat capacity of the assembly.

The thermal path from the thermocouple junction to the head may be disrupted to a considerable degree by the following factors: (1) the use of thermocouple insulator tubing with a bore considerably larger than the wires, permitting as little physical contact as possible; (2) increase in the

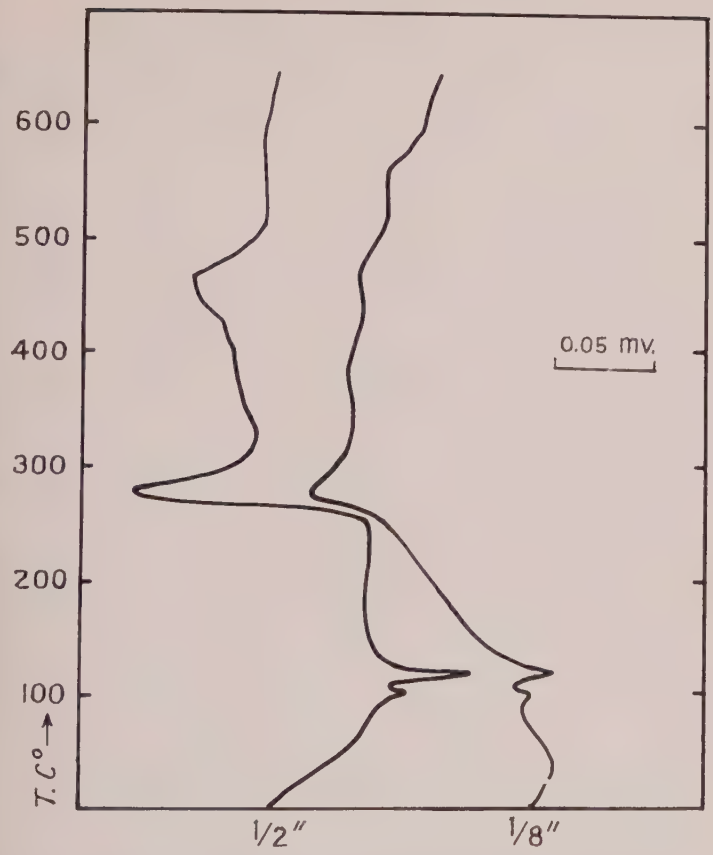

FIG. 10. Spacing of thermocouple from bottom of thermal well. Pyrosynthesis curves showing relative effect of differing path lengths from thermocouple junction to thermal head for the composition $FeS_{1.5}$.

utside diameter of the thermocouple insulator tube to make the radial ath length from the wire to the head as great as possible in the low conuctivity ceramic, or the use of a second ring of ceramic at the point of ontact between the insulator and head, allowing the use of small insutor tubing; (3) reduction of the wire diameter to the lowest dimension mpatible with optimum thermocouple life; (4) increase of the distance om the thermocouple junction to the metal head by a deeper thermal ell; (5) increase in depth of the thermal well to obtain a minimum mount of metal to support the thermocouple insulator tubing; (6) the se of four hole insulator tubing to reduce the amount of ceramic in the ube.

The thermocouple insulator tubes may be prepared by casting a ring of

ceramic* around the tube the same size as the diameter of the thermal well. The thermal well is then drilled completely through the head at a single diameter further increasing the low conductivity thermal path to the head. The casting of the tube and the ceramic ring is then cemented into the bottom of the thermal well.

Effect of Volume of Sample Vials

Many reactions observable in D.T.P. are dependent upon the vapor pressure of the anion. The volume of the sample, the volume of the sample vial, the composition of the reactants, and the temperature are effective in determining whether the internal pressure within the vials is equal to that over liquid sulfur, or equal to some lesser pressure, thereby causing differences in the observed reactions. If thermodynamic extrapolations are to be made of the data obtained by D.T.P. it is necessary to determine, within limits, the pressure effects upon the reactions.

The majority of the reactions in D.T.P., those below approximately 500° C., are little affected by the range of sample vial volume permissible in the present head design. Two factors are responsible for this. Sulfur has a relatively low vapor pressure at these temperatures, and the dissociation pressure of many sulfides is less than that of sulfur vapor in equilibrium with liquid sulfur at these temperatures. In this range of temperature, the low vapor pressure of sulfur readily allows the formation of a liquid phase which determines the pressure relations at any specific temperature, and the volume of the vial is not critical, within limits.

In compositions, where the ratio of sulfur to bulk composition is small so that negligible free sulfur is present, insufficient sulfur may be present to form a liquid phase. In these compositional ranges the effects of vapor pressure less than that over liquid sulfur are readily apparent, as in the lowered temperature of the dissociation of covellite in the Cu_2S end of the compositions in Figure 5.

In compositional ranges where sufficient sulfur is present to assure a liquid phase at 507° C., as shown by the constant temperature of the incongruent melting of covellite in the CuS end of the compositions of Fig 5, it might be assumed that a liquid phase of sulfur is present at higher temperatures. However, the liquid-vapor curve as given by Kullerud and Yoder (1959, p. 541) shows an increasingly rapid rise in the pressure necessary to maintain a liquid phase above 600° C. Thus the pressure-volume relations become more critical as the temperature is increased.

The use of excess anion, such as sulfur to produce saturation vapor pressure within the system by the formation of a liquid phase, can be

* Sur-Grade S-2, Castible Ceramic, Duramic Products Company, Palisades Park, New Jersey.

pplied to end members of an anion substitution series of disulfides, or in e case where high sulfides do not exist, on monosulfides. Where anion bstitution is a function of the composition, such a procedure is not pos- ble, and the per cent equivalent of the partial pressures of the anions ust be estimated.

The use of closely fitting glass rods to fill the space above the reactants preferable to the alundum filling of the vials when pressure relations e studied.

A series of sample vials was prepared from one inch to two inches in ngth (Fig. 11) to determine the effect of vial volume on the dissociation, incongruent melting, of FeS_2. A constant weight (0.2399 gms.) of ele- ental constituents of the composition FeS_2 occupied approximately e-half inch of each vial. The one inch vial (Fig. 11*a*) is too short to ow sealing without partial reaction by overheating of the constituents, d the two inch vial (Fig. 11*e*) extends beyond the top of the head. One he normal length vials was filled with 120 mesh alundum to provide a inimum volume of the series (Fig. 11*d*).

The exothermic peaks of the above series below 600° C. show some riation which is primarily a result of non-equilibrium obtained at these ating rates as was indicated in Fig. 7. The large endothermic peak at 3° C. is the incongruent melting of pyrite to pyrrhotite+liquid+vapor ullerud and Yoder, 1959). No variation in peak temperature was ob- rvable. Thus it is assumed that liquid sulfur was present, determining e pressure relations at these temperatures.

An important feature is indicated by the data obtained from the above ries. A gradual decrease in peak amplitude occurs with increasing vial ume, or, in other words, a decrease in the amount of alundum in the ermal well. If volume relations of the vial were responsible for this ange, as would be the situation in the absence of liquid sulfur, the tem- ratures of dissociation would be affected as was the dissociation of vellite; within the limits imposed by the relative sensitivity of the dis- iation pressures of CuS and FeS_2 to vapor pressure of sulfur. It is ap- rent that the heat flow from sample to the thermocouple junction is not stricted to the point of contact with the vial. The alundum envelope rrounding the vial and the thermocouple, as well as the walls of the l, serve as heat transfer media. Thus the length of the sample vials ould be closely controlled, thereby maintaining the same amount of ndum and silica in the thermal well, if peak areas or amplitudes are to used for comparative data.

The decrease in the amplitude of the peaks in Figure 11 with increasing l size may be caused by an increased heat capacity of the vial. As heat w is in all directions from the reaction point, a certain amount of the

FIG. 11. Pyrosynthesis curves representing variation of sample vial length with constant weight of FeS_2. (a) 1 in. (b) $1\frac{1}{4}$ in. (c) $1\frac{1}{2}$ in. (d) $1\frac{1}{2}$ in. with Al_2O_3 filling empty portion of vial. (e) 2 in.

heat of reaction is carried to the upper part of the vial and is dissipated. The higher thermal conductivity of the vial, in comparison to the thermal conductivity of the granular aluminum oxide allows a greater part of the reaction to be carried away from the thermocouple with the larger vials.

The vial in Figure 11*d*, which is filled with alundum above the reactants, should transfer a greater portion of the reaction to the upper end of the vial and thus be dissipated. This is undoubtedly true; however, the short path length from the top of the reactants to the thermocouple allows more of the heat of reaction to be registered by the thermocouple than is dissipated at the top of the vial. In the absence of the alundum filler within the vial, the reaction of the top surface of the sample is not transferred effectively to the thermocouple or to the walls of the vial. The increase in the transfer of heat of reaction from the top of the sample, and the short path length to the thermocouple, more than compensate for the loss to the upper portion of the vial.

The relative heat flow distribution when silica rods are used to fill the vial has not been investigated; however it is believed that the rods would tend to transmit a greater portion of the reaction to the top of the vial because of the undisrupted flow along the rod. The disruption of the heat flow by the interface between the sides of the rod and the wall of the vial may also reduce the effectiveness of the short path length to the thermocouple. Thus the relative heat flow distribution would be greatly influenced by the closeness of fit between the rod and the vial. Loosely fitting rods should be avoided, and would be less preferable than an empty vial, if measurement of the heat of reaction is of more importance than pressure relations in a specific study.

The influence of volume-pressure relations in the higher temperature regions of Fig. 5 is complicated by multiple reactions and incomplete knowledge of the nature of the reactions. Early work on the Cu-S system (Allen and Lombard, 1917) assumed that covellite dissociated directly to chalcocite. Kullerud (1956) with the knowledge of the intermediate compound, digenite, from the work of Buerger (1942) recognized that the reaction was the dissociation of covellite to digenite and not chalcocite. Kullerud also stated, "Further experiments on the stability of this compound have shown that digenite, which decomposes to chalcocite and vapor, is stable up to about 925° C. in the presence of excess sulfur (liquid and vapor). . . , it is likely that the upper stability curve of digenite, similiar to the stability curves of covellite and pyrite, is very steep. Thus even under 30,000 psi of sulfur pressure, the breakdown temperature of digenite would probably not exceed 950° C. (1958, p. 217)." These statements refer to a digenite of a composition of $Cu_{1.8}S$ at these temperatures. The temperature at which digenite would dissociate to chalcocite under low vapor pressures of sulfur was not determined.

A tentative interpretation of the high temperature reactions shown in Fig. 5 may be attempted, although additional data would be necessary for complete evaluation. The unresolved double endothermic peak at ap-

proximately 815° C., at a composition of CuS may represent the incongruent melting of digenite and fusion of chalcocite. The upper peak of this pair rises to approximately 1105° C. and is explained by the data given by Kullerud and Yund (1960). At 815° C. a two liquid field appears in the system for compositions ranging from about 25.5 to more than 95.5 weight per cent sulfur. The maximum melting point of chalcocite at 1129° C., which occurs at a composition of $Cu_{1.989}S$ (Jensen, 1947, p. 9) is not shown in Fig. 5 as this composition is straddled by the sample compositions.

The lower peak of the above mentioned pair appears to split into two branches at a copper to sulfur ratio of 1.5:1. These are not well resolved because of a non-optimum heating rate. The lower part of these two branches may represent the dissociation of digenite as it appears to decrease in temperature toward the CuS end of the compositions. This would be the expected direction if the dissociation of digenite is affected by low vapor pressures of sulfur in a manner similar to the dissociation of covellite to digenite. The upper curve of these two branches may represent the change in the composition of the solid phase with incongruent melting to a digenite approaching the composition of chalcocite.

To investigate the effects of the vapor pressure of sulfur on the reactions a continuously evacuated vial was analyzed. In this procedure, previously synthesized covellite was placed in a vial six inches long which was not sealed. The thermal head was moved upward in the furnace allowing attachment of a vacuum line. The vacuum pump was operated continuously during the run. Sulfur vapor, evolved during dissociation, moved to the cooler portion of the vial extending out of the furnace and condensed. The melting point under vacuum had an initial deflection of 1130° C. This is in agreement with the melting point obtained by Posnjak, Allen and Merwin (1915) under similar conditions. Jensen (1947, p. 10) has indicated that their analyses of products with this melting point agrees with the maximum melting point composition, $Cu_{1.989}S$, and that the dissociation of digenite under vacuum conditions does not proceed beyond this composition. Similarly he indicates that the melting point of pure Cu_2S begins at 1107° C. and is not completed until 1127° C. which may be interpreted as the breakdown of Cu_2S on melting in a melt which is richer in copper and a solid which is richer in sulfur, or in other words, the final product approaches the maximum melting point composition, $Cu_{1.989}S$ from both sides of this composition.

In view of the complicated reactions in this portion of the temperature and composition range the recorded reactions in the upper part of Fig. 5 serve to indicate the complexity of the problem rather than to clarify the relations. Optimum heating rates, closely controlled volume relations,

fixed temperature equilibirum studies, and high temperature *x*-ray diffraction studies are necessary to completely define the reactions in this portion of the figure. Further analysis was not attempted, as the purpose of the explanation of Fig. 5 is to attempt to show the use of the curves obtained by the instrumentation and not to define the system Cu-S.

The series CuS to CuSe and Ag_2S to Ag_2Se both show linear changes in fusion and upper dissociation temperatures from one end of each series to the other. This may be partially an effect of pressure and partially an effect of composition. The lower temperature dissociation, or incongruent melting, peaks of these two series also show a linear change from one end of each series to the other, in contrast to the nearly fixed temperature of incongruent melting of covellite to digenite in the range CuS to $Cu_{1.8}S$. By analogy with the composition range from $Cu_{1.6}S$ to $Cu_{1.9}S$ which shows a marked decrease in the temperature of this reaction with lowered pressure of sulfur vapor, the change in the temperatures of these incongruent melting points with the substitution of selenium for sulfur is mainly a function of the pressure change produced by the different proportions of the partial pressures of sulfur and selenium. Analyses of these three systems is not complete, and assumptions made are to be considered approximate until further data are collected.

Survey of Minerals

A number of sulfides, selenides, tellurides, arsenides, and antimonides have been produced to determine the range of the D.T.P. method in the synthesis of these minerals. A number of the curves resulting from these syntheses are reproduced in Fig. 12. Each curve is worthy of more detailed investigation than has been possible in the present study. Each synthesis properly requires such investigation to assure that parameters affecting peak configuration have been minimized and closely controlled. However, a general survey of the type attempted is a necessary prelude to the more detailed studies which should follow.

X-ray diffraction of the final products has shown that nearly all syntheses were successful. Inversions below the formation temperatures of synthetic minerals are observable in cooling curves and in reheating curves of previously formed synthetics. The instrumentation is also readily adaptable to the study of naturally occurring minerals.

The cooling curves of recombination of dissociated phases were somewhat unexpected. The recombinations, in nearly every case, were as rapid and sharply defined as the dissociation peaks. These rapid recombinations occur in decomposed phases that have been fused and recrystallized. The anion vapor, trapped in the vial during dissociation diffuses through the solid regulus in a very rapid manner upon cooling.

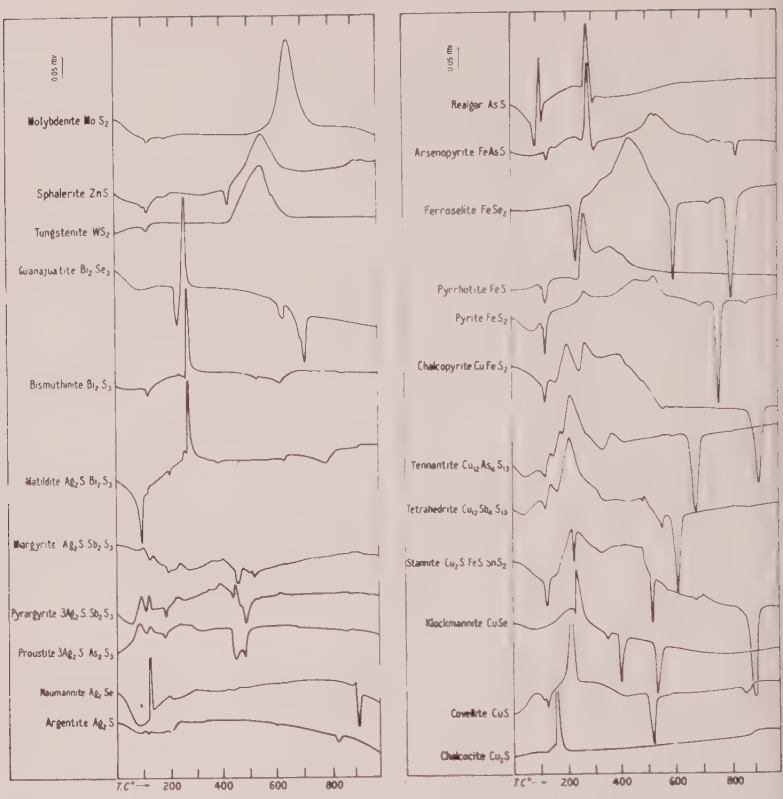

FIG. 12. Pyrosynthesis curves showing a survey of 23 minerals.

Cooling curves of powdered material that has been heated above the decomposition temperature, but not to the melting point, have not been studied yet. Comparison of the recombination of powdered material with fused material may give indications of the relative rate of diffusion of the liquid and vapor. However, the rapidity of the recombinations observed at 12.5° C. per minute indicates that the limiting factor is the slow rate of cooling and not the time required for diffusion through the crystal structure. It must be noted, however, that the diffusion under discussion has a considerable chemical gradient caused by the undersaturated, dissociated structures with a very high percentage of vacant lattice sites. The rate of recombination of some of the dissociated phases caused difficulty in quenching studies as many of the high temperature phases could not be quenched rapidly enough to prevent considerable recombination even when vials were dropped into water from temperatures far in excess of the dissociation temperature.

Conclusions

This study has shown that the instrumentation used for D.T.P. is able to furnish sensitive thermal data on processes which tend to give off or absorb heat during mineral synthesis and mineral stability studies. These processes include chemical combination, crystallization, dissociation, fusion, and inversion of one structure to another. The range of the method is large and it is readily adaptable to studies of differing types of reactions. The conflicting requirements of dissimilar reactions indicate that a rigid standardization of the technique is not justifiable; and that each system under study presents problems which somewhat alter the requirements of the instrumentation.

Data obtained from D.T.P. are in many cases directly applicable to a better understanding of processes which occur in the deposition of sulfide and mineralogically related ore bodies. It is believed that studies in the non-aqueous environment of D.T.P. and other "dry" studies can furnish much useful information in the study of mineral genesis and, when combined with hydrothermal methods, give a clearer understanding of the possible range of mineral deposit formation.

Acknowledgments

This study was made possible through the assistance of the National Science Foundation and the United States Atomic Energy Commission. The writers express their appreciation to Dr. G. Kullerud, Geophysical Laboratory, Carnegie Institution of Washington, and Dr. Philip M. Bethke, United States Geological Survey for critically reading the manuscript and offering many helpful suggestions.

References

Allen, E. T., and Lombard, R. H., 1917, Method for the determination of dissociation pressures of sulphides: *Am. Jour. Sci., 4th Ser.*, **43,** 175–195.

Bollin, E. M., Dunne, J. A., and Kerr, P. F., 1960, Differential thermal study of pyrosynthesis: *Science,* **131,** 661–662.

——, and Kerr, P. F., 1961, Die-extruded samples and calorimetric accuracy in D.T.A.: *Am. Mineral.*, in press.

Buerger, N. W., 1942, *X*-ray evidence of the existence of the mineral digenite, Cu_9S_5: *Am. Mineral.*, **27,** 712–716.

Buerger, M. J., 1951, in Smoluchowski, R., Phase Transformations in Solids: John Wiley and Sons, Inc., New York, 660 p.

Dunne, J. A., and Kerr, P. F., 1961, Differential thermal analysis of galena and clausthalite: *Am. Mineral.*, **46,** 1–11.

Garley, J. W., 1949, Description and synthesis of the selenide minerals: *Am. Mineral.*, **34,** 337–364.

——, 1950, Studies of the natural and artificial selenides: I—Klockmannite, CuSe: *Am. Mineral.*, **35,** 435–440.

HANNAY, N. B. (Ed.), 1959, Semiconductors: ACS Monograph No. 140, Reinhold Publishing Corporation, 767 p.

JENSEN, E., 1942, Pyrrhotite: melting relations and composition: *Am. Jour. Sci.*, **240,** 695–705.

———, 1947, Melting relations of chalcocite: *Avhand. Norske Videnskaps-Akademi, Oslo, Mat.-Naturv.*, **6,** 1–14.

KERR, P. F., AND KULP, J. L., 1948, Multiple differential thermal analysis: *Am. Mineral.*, **33,** 387–419.

KINGERY, W. D., 1959, Property Measurements at High Temperatures: John Wiley and Sons Inc., New York, 416 p.

KRACEK, F. C., 1946, Phase relations in the system sulfur-silver and the transitions in silver sulfide: *Am. Geophys. Union Trans.* **27,** 364–373.

KULLERUD, G., 1956, The Cu_2S-CuS system: Ann. Rept. Geophys. Lab., 1955-1956, *Paper 1265, Carnegie Inst. Wash.*, 215–218.

———, AND YODER, H. S., 1959, Pyrite stability relations in the Fe S system: *Econ. Geol.*, **54,** 533–572.

———, AND YUND, R., 1960, Cu-S system: *Program of 1960 Ann. Meetings, Geol. Soc. Amer.*, 143–144.

MACKENZIE, R. C., 1957, The Differential Thermal Analysis of Clays: Central Press, Aberdeen, 456 p.

POSNJAK, E., ALLEN, E. T., AND MERWIN, H. E., 1915, The sulphides of copper: *Econ. Geol.*, **10,** 491–535.

RHINES, F. N., 1956, Phase Diagrams in Metallurgy: McGraw Hill Book Co., Inc., 340 p.

VAN DER LAAN, H., AND NICHOLLS, 1960, Simple apparatus for making 10–100 cu. spheres of low melting point metals: *Rev. Sci. Instr.*, **31,** 212.

Manuscript received Sept. 19, 1960.

THE AMERICAN MINERALOGIST, VOL. 46, JULY-AUGUST, 1961

THE SYSTEM $NaAlSiO_4$ (NEPHELINE)-$NaAlSi_3O_8$ (ALBITE)-H_2O*

PRASENJIT SAHA†, *Department of Geophysics and Geochemistry, The Pennsylvania State University.*

ABSTRACT

The system $NaAlSiO_4$-$NaAlSi_3O_8$-H_2O has been investigated in the temperature range 700°–700° C. at pressures of 5000 to 45,000 psi. The following minerals and compounds were synthesized and their stability investigated: nepheline solid solutions, albite, analcite solid solutions, nepheline hydrate I, paragonite, zeolite "B" and species "Y". Natrolite was found to be unstable in the presence of excess water vapor under the pressure and temperature conditions utilized. Experimental investigations and theoretical calculations indicated that the alkali-rich portion of the system does not remain ternary at low temperatures under the conditions of the experiments.

The following transitions, within the P-T-X region involved, were studied in detail:

(1) nepheline hydrate=nepheline+water.

(2) analcite solid solution=nepheline solid solution+albite+water.

(3) analcite solid solution (comp.—$NaAlSi_3O_8 \cdot 1.5H_2O$)=albite+water.

Analcite was found to exhibit solid solution through an extensive range of composition, but field and laboratory evidence suggests that part of it may be metastable. The range of solid solution found in nature is more restricted than the range determined experimentally.

Petrogenetic implications of the investigation are discussed. Preferential solubility of soda and alumina in the vapor in runs made with glasses whose compositions lie in the alkali-rich portion of the system, indicates a possible mode of nephelinization of country rocks surrounding bodies of alkaline rocks. Experimental work carried out on the formation of the assemblages analcite solid solution+nepheline solid solution and analcite solid solution+albite may be useful in ascertaining the temperature and pressure of development of these assemblages in nature. The origin of analcite in deeply buried slightly metamorphosed rocks derived from pyroclastic materials is discussed.

INTRODUCTION

Experimental determinations of the stability of minerals have been useful in laying down the basic principles necessary for the interpretation of petrological features associated with igneous activity. In the late stages of igneous activity and in metamorphism and weathering, where water plays a very important role, experimental determination of the stability of hydrous minerals and the stability of anhydrous minerals in the presence of water becomes important. Phase-equilibrium relations in the system $NaAlSiO_4$-$NaAlSi_3O_8$-H_2O, both stable and metastable, have been investigated and will be described in this paper. An attempt will be made to interpret the petrological significance of minerals occurring in this system.

* Mineral Industries Experiment Station Contribution No. 59–80.

† Present address: Central Glass & Ceramic Research Institute, Jadavpur, Calcutta-32, India.

The following ternary compounds are found in the system $NaAlSiO_4$-$NaAlSi_3O_8$-H_2O: nepheline ($NaAlSiO_4$), albite ($NaAlSi_3O_8$) and jadeite ($NaAlSi_2O_6$), all of which occur as minerals in nature. All of these minerals have been synthesized by different workers in different laboratories. The following quaternary compounds have been reported in this system: analcite ($NaAlSi_2O_6 \cdot H_2O$), natrolite ($Na_2Al_2Si_3O_{10} \cdot 2H_2O$), nepheline hydrate I ($NaAlSiO_4 \cdot \frac{1}{2}H_2O$), nepheline hydrate II ($NaAlSiO_4 \cdot \frac{1}{4}H_2O$), zeolite "A" ($NaAlSiO_4 \cdot 2.35H_2O$), and zeolite "B". Among these, analcite and natrolite occur as minerals in nature. Analcite forms readily in hydrothermal runs, but natrolite has only recently been synthesized (Hoss and Roy, 1959). Hydronephelite has been reported to occur as an alteration product of nepheline (Thugutt, 1892; Tilley and Harwood, 1931; Dunham, 1933). Barrer and White (1952) suggested that it may be the same as nepheline hydrate I. Nepheline hydrate II, zeolite "A" and zeolite "B" have been synthesized by different workers, but have not yet been reported from nature.

Greig and Barth (1938) investigated liquidus relations in the system $NaAlSiO_4$-$NaAlSi_3O_8$, and the extent of solid solution of albite in nepheline and vice versa. They found that nepheline is relatively insoluble in albite, but takes up a large amount of albite in solid solution (33% by wt.). They found the eutectic temperature to be at $1068° \pm 5°$ C. at a composition $Ab_{76}Ne_{24}$ (by wt.). Their conclusions in regard to the extent of solid solution were tentative, because they suspected that the glasses did not crystallize completely. MacKenzie (1954), while working in the system $NaAlSiO_4$-$NaAlSi_3O_8$-H_2O at 1000 bars, found the minimum melting temperature to be at $870° \pm 5°$ C. at the composition $Ab_{72}Ne_{28}$ (by wt.). He also found the limit of nepheline solid solution to be about $Ne_{75}Ab_{25}$ (by wt.) at 750° C.

Jadeite was first synthesized by Coes (1953), by the reaction between sodium sulfate, kaolin and silica at a pressure of 20,000 kgm/cm², at 900° C. Later, several other workers were able to synthesize jadeite and determine its stability (Robertson, Birch and MacDonald, 1957; Griggs, Kennedy and Fyfe in Fyfe, Turner and Verhoogen, 1958, p. 175). Yoder studied the system $NaAlSi_2O_6$-H_2O in an attempt to synthesize analcite and jadeite and determine their fields of stability (Yoder, 1950, 1954). Sand, Roy and Osborn (1957) studied the stability of minerals in the quaternary system Na_2O-Al_2O_3-SiO_2-H_2O. They were able to synthesize analcite from gels of albite composition at low temperatures, but according to them, " . . . this converted gradually to albite at temperatures above 290° C. indicating that the latter is the stable phase." Fyfe, Turner and Verhoogen (1958) determined part of the boundary for the reaction analcite+quartz=albite+quartz+water. They worked with

oxide mixes of composition $NaAlSi_4O_{10}$ in the presence of water vapor. Coombs *et al.* (1959) also studied the same reaction with oxide mixes ($NaAlSi_3O_8+SiO_2$) and with $NaAlSi_3O_8$ glass.

Barrer and White (1952) heated gels ranging in composition from $Na_2O \cdot Al_2O_3 \cdot 2SiO_2$ to $Na_2O \cdot Al_2O_3 \cdot 10SiO_2$ at different temperatures and atmospheric pressure, frequently in the presence of excess NaOH solution. In the range $Na_2O \cdot Al_2O_3 \cdot 2\text{–}6SiO_2$, they were able to synthesize the following minerals and compounds: nepheline, nepheline hydrate I, nepheline hydrate II, analcite, albite, paragonite, compound L ($2Na_2O \cdot Al_2O_3 \cdot 6SiO_2 \cdot 2H_2O$), "basic" sodalite, "basic" nosean, "basic" cancrinite and compound N. Nepheline hydrate I and nepheline hydrate II could be synthesized from gels of $NaAlSiO_4$ composition, and they gave the following compositions for these two compounds: $Na_2O \cdot Al_2O_3 \cdot 2SiO_2 \cdot H_2O$ for nepheline hydrate I and $Na_2O \cdot Al_2O_3 \cdot 2SiO_2 \cdot \frac{1}{2}H_2O$ for nepheline hydrate II. Paragonite was also synthesized from $NaAlSiO_4$ gel. Analcite was synthesized from gels of a wide range of composition ($Na_2O \cdot Al_2O_3 \cdot 3\text{–}10SiO_2$). From gels of $NaAlSi_3O_8$ composition, analcite was synthesized below 300° C., a mixture of analcite and albite in the range 300°–420° C., and only albite above 450° C. This work cannot be considered as phase-equilibrium investigations in the system $NaAlSiO_4$–$NaAlSi_3O_8$-H_2O as they often used excess NaOH solution for the synthesis of the minerals and compounds. Thus for example, nepheline hydrate II, compound L, compound N, etc., were synthesized only in the presence of excess NaOH. MacKenzie (1957), while investigating the transformation high albite→low albite, reported the presence of some analcite at 400° C. and only analcite at 300° C. in runs made with glass of $NaAlSi_3O_8$ composition in the presence of water. Guyer, Ineichen and Guyer (1957) synthesized analcites from compositions within the range $Na_2O \cdot Al_2O_3 \cdot 2\text{–}10SiO_2$ in order to study their sorbing properties. Some sodalite was present together with analcite in the products of crystallization of $NaAlSiO_4$ gel. Breck *et al.* (1956) were able to synthesize two zeolitic compounds, zeolite "A" and zeolite "B", from $NaAlSiO_4$ gel in the presence of water.

Techniques

Investigations in the system $NaAlSiO_4$-$NaAlSi_3O_8$-H_2O were carried out using gels and glasses.

Gels were prepared by a method described by Roy (1956). Some other gels were prepared by mixing together Ludox* silica sols, standardized aluminum nitrate and sodium hydroxide solutions and evaporating to

* duPont Co. trade name.

dryness. Only rarely were the gels used as such; in most cases they were melted at high temperatures to give homogeneous glasses. Glasses varying from $Na_2O \cdot Al_2O_3 \cdot SiO_2$ to $Na_2O \cdot Al_2O_3 \cdot 6SiO_2$, were made by these methods.

$NaAlSiO_4$ and $NaAlSi_3O_8$ glasses were also prepared by the method described by Schairer and Bowen (1956). Glasses intermediate in composition were prepared by repeated fusion and grinding of these two end members. The composition and refractive index of the glasses prepared by this method are listed in Table I.

Table I. Refractive Indices of Glasses

	Composition of Glasses (Mol. Ratio)						n
	Na_2O	:	Al_2O_3	:	SiO_2		
1	1	:	1	:	2.00		1.515±0.002
2	1	:	1	:	2.25		1.512±0.002
3	1	:	1	:	2.50		1.510±0.002
4	1	:	1	:	2.75		1.508±0.002
5	1	:	1	:	3.00		1.506±0.002
6	1	:	1	:	3.25		1.504±0.002
7	1	:	1	:	3.50		1.502±0.002
8	1	:	1	:	3.75		1.500±0.002
9	1	:	1	:	4.00		1.498±0.002
10	1	:	1	:	5.00		1.493±0.002
11	1	:	1	:	6.00		1.490±0.002

The runs were made in cold-seal pressure vessels described by Tuttle (1949). Approximately 20 mg. of the charges were sealed in small gold tubes with about 20 mg. of water. Care was taken to add excess water, since the scope of the investigation did not extend to the water-deficient region. The runs were considered to be good only when the samples appeared to be wet on opening the tubes after the runs. External hydrothermal pressure was applied to the sealed tubes by means of a Sprague Electric Company air-operated pump and a system of valves. The temperature was controlled by a Brown Electronic Controller. The products of the runs were examined by standard microscopic and x-ray powder diffraction procedures.

Phases Synthesized

Runs were made in the systems $NaAlSiO_4$-H_2O, $NaAlSi_3O_8$-H_2O, $Na_2Al_2Si_3O_{10}$-H_2O and $NaAlSiO_4$-$NaAlSi_3O_8$-H_2O (Saha, 1959b). Attempts were also made to determine the stability of the different phases by the decomposition of synthetically prepared and natural crystalline

phases. The following phases have been synthesized: nepheline, nepheline hydrate I, paragonite, zeolite "B," analcite, albite and species "Y." X-ray powder diffraction patterns of all the phases synthesized, except for albite, are shown in Fig. 1. Brief descriptions of the phases will be given here.

Nepheline: The nepheline crystals synthesized from glass of $NaAlSiO_4$ composition were apparently identical with the low-temperature form of nepheline described by Smith and Tuttle (1957). They appeared as hexagonal basal plates and prismatic laths. The maximum grain-size recorded was 0.18 mm×0.04 mm. Nepheline synthesized from glasses richer in silica than $NaAlSiO_4$ had a somewhat different habit; the crystals occurred as short square prisms and hexagonal basal plates full of vapor inclusions.

Nepheline Hydrate I: Nepheline hydrate I (the convention adopted by Barrer and White (1952) has been retained here) appeared as small irregular grains, never more than 35 microns in diameter and rarely with crystalline outlines. The crystals were determined to be biaxial, and the refractive indices were $\alpha = 1.499 \pm 0.002$, $\gamma = 1.503 \pm 0.002$. The values are somewhat lower than the values given by Barrer and White ($\alpha = 1.503$, $\beta = 1.506$, $\gamma = 1.508$).

Albite: Albite occurred as well crystallized euhedral grains when prepared from compositions near the silica-deficient boundary of the solvus ($Na_2O \cdot Al_2O_3 \cdot 3SiO_2$), but became blocky and full of inclusions in preparations having compositions on the albite side of the solvus boundary ($Na_2O \cdot Al_2O_3 \cdot 3\text{-}4SiO_2$). Fine clusters of needles and plates of albite formed readily in runs made with $Na_2O \cdot Al_2O_3 \cdot 4\text{-}6SiO_2$ glasses at high temperatures. The maximum dimensions of the albite laths synthesized in this range were: 0.04 mm. in length and 0.014 mm. in width. From *x*-ray powder diffraction patterns, they were found to be identical with the high-temperature modification of albite synthesized by Bowen and Tuttle (1950).

Analcite: Analcite was synthesized from glasses of compositions within the range $Na_2O \cdot Al_2O_3 \cdot 2\text{-}6SiO_2$. In very long runs (21 days—90 days) at low temperatures (200° C.), made with glass of $NaAlSiO_4$ composition as starting material, analcite began to appear as round isotropic grains, replacing zeolite "B." Microscopically the grains were too small and too intimately mixed with zeolite "B" to make refractive-index determinations; but the characteristic reflections of analcite were present in the *x*-ray powder diffraction patterns. Analcite prepared from $Na_2O \cdot Al_2O_3 \cdot 2.25\text{-}5SiO_2$ glasses had similar habit of growth, the size of the individual crystals attaining a maximum diameter of 0.09 mm. in products of runs made with $Na_2O \cdot Al_2O_3 3SiO_2$ glass. Analcite formed very readily from glass of $NaAlSi_3O_8$ composition in runs made below 400° C. The crystals had a maximum diameter of 0.04 mm. Complete crystallization of the glass to a fine-grained aggregate of analcite crystals (except for $\simeq 1\%$ paragonite) indicates that the analcite has the composition $NaAlSi_3O_8$ together with zeolitic water (Saha, 1959a).

The synthetic crystals were isotropic, and the refractive index changes considerably with SiO_2 content as shown in Table II.

It was not possible to measure the refractive index of analcite synthesized from glasses within the range of composition $Na_2O \cdot Al_2O_3 \cdot 2\text{-}3SiO_2$ because of the presence of paragonite flakes, which surround the analcite grains.

The author would like to correct an error in a previous paper (Saha, 1959a) concerning the *x*-ray investigation of analcite. Inadvertently, tables for CuKα radiation were used for calculating the lattice parameter of analcite of different compositions, instead of tables for CuKα_1 radiation. Table III shows the displacement of (639) peak for analcite of different compositions, both synthetic and natural, and in this the lattice parameters have been calculated correctly. Fig. 2 shows the displacement of the (639) peak. Some new data have

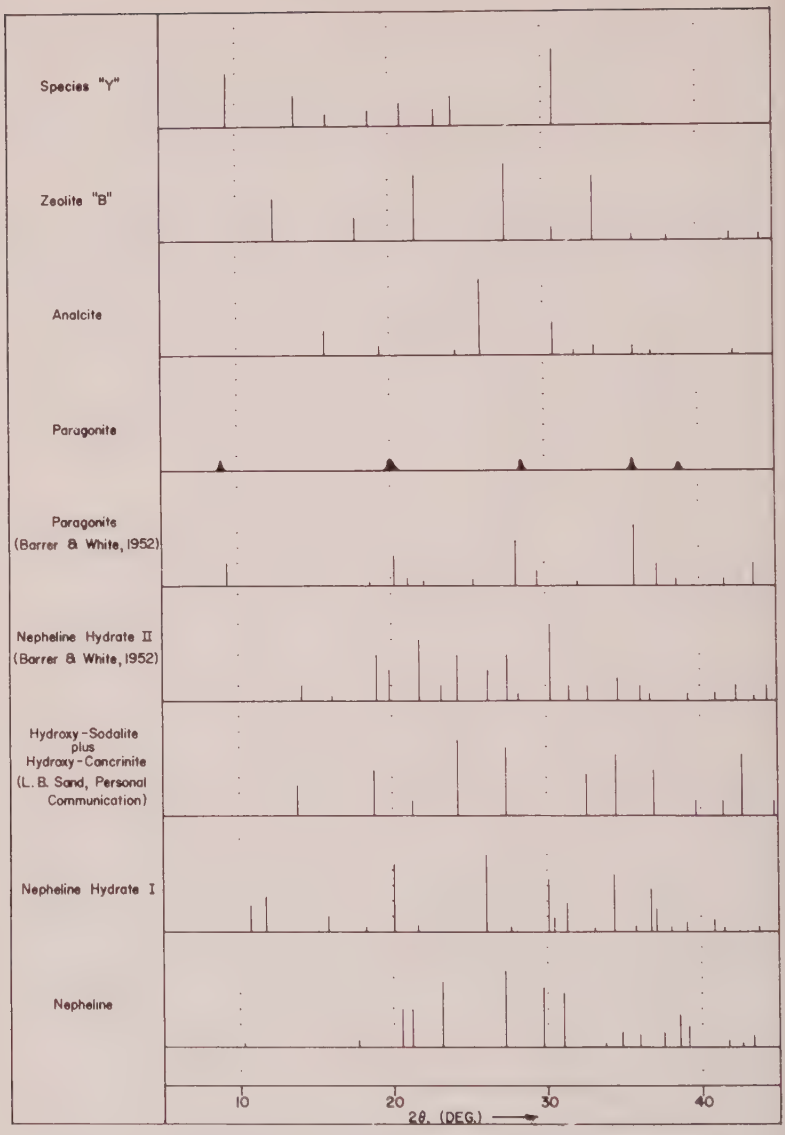

FIG. 1. *X*-ray powder diffraction patterns of crystalline phases synthesized in the system $NaAlSiO_4$-H_2O and related systems.

also been incorporated, on the basis of which a break in the curve for the displacement of (639) peak of analcite, approximately at the composition $Na_2O \cdot Al_2O_3 \cdot 2.75SiO_2$, can be postulated. This break represents the limit of solid solution of analcite for the alkali-rich portion of the system.

Species "I": At very low temperatures (200° C.) in comparatively short runs (2–8 days)

TABLE II. REFRACTIVE INDICES OF ANALCITE

	Composition of Glasses (Mol. Ratio)					n
	Na_2O	:	Al_2O_3	:	SiO_2	
1	1	:	1	:	3.00	1.494±0.002
2	1	:	1	:	3.25	1.492±0.002
3	1	:	1	:	3.50	1.491±0.002
4	1	:	1	:	3.75	1.489±0.002
5	1	:	1	:	4.00	1.488±0.002
6	1	:	1	:	5.00	1.484±0.002
7	1	:	1	:	6.00	1.482±0.002

TABLE III. DISPLACEMENT OF (639) PEAK OF ANALCITES OF DIFFERENT COMPOSITIONS

No.	Composition					$2\theta_{An(639)} - 2\theta_{Si(331)}$ (CuKα_1 radiation)		a_0 (Å)
	Synthetic analcites:							
	Na_2O	:	Al_2O_3	:	SiO_2[1]			
1	1	:	1	:	2.25	1.550		
2	1	:	1	:	2.50	1.525		
3	1	:	1	:	2.75	1.530		
4	1	:	1	:	3.00	1.500[4]		
5	1	:	1	:	3.00	1.530	1.540	13.75_1
6	1	:	1	:	3.00	1.550		
7	1	:	1	:	3.25	1.610		
8	1	:	1	:	3.50	1.680		
9	1	:	1	:	3.75	1.770		
10	1	:	1	:	4.00	1.765		
11	1	:	1	:	4.00	1.745	1.763	13.71_8
12	1	:	1	:	4.00	1.780		
13	1	:	1	:	5.00	1.940		13.69_5
14	1	:	1	:	6.00	2.150		
15	1	:	1	:	6.00	2.140	2.123	13.66_5
16	1	:	1	:	6.00	2.080		
	Natural Specimens:							
	Na_2O	:	Al_2O_3	:	SiO_2 : H_2O			
17	1	:	1	:	5.45 : 2.70[2]	2.010		
18	1	:	1	:	5.45 : 2.70[2]	2.075		
19	Natrolite converted to analcite[3]					1.575		

[1] Composition of glasses used as starting material.

[2] Two specimens of analcite from Yavapai County, Arizona; compositions assumed to be average of two analyses given by Ross (1928).

[3] Natural natrolite from Habstein, Bohemia, Specimen No. 453.6, Genth collection.

[4] α_1 and α_2 peaks of d(639) not well resolved. Cannot be measured accurately.

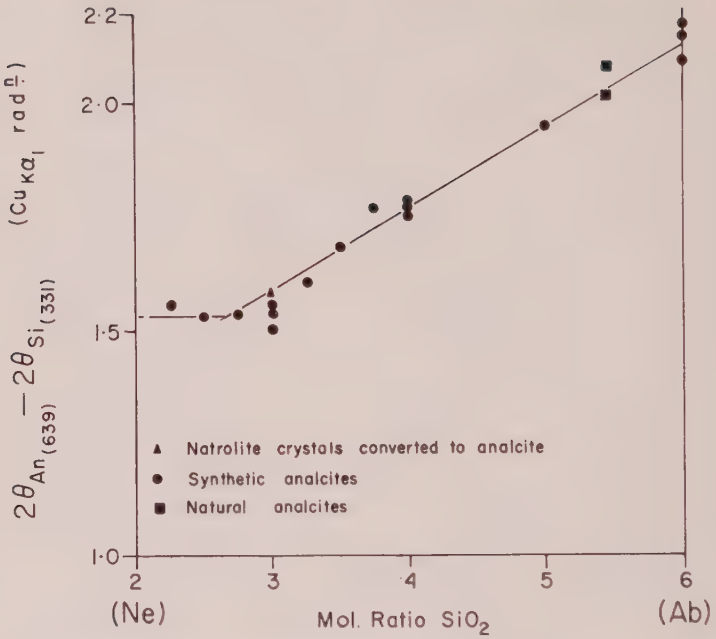

FIG. 2. Variation of $d_{(639)}$ spacing of synthetic analcites with variation of SiO_2 content.

made with glasses of compositions in the range $Na_2O \cdot Al_2O_3 \cdot 2\text{–}3SiO_2$, a mixture of two phases appeared, which were too fine grained to be identified optically. Certain lines appearing in the powder diffraction spectrometer charts (Fig. 1) have been assigned to zeolite "B_1" and the other lines have been assigned to species "Y." In longer runs (21 days), the lines for species "Y" disappeared, the intensities of the lines for zeolite "B" decreased, and analcite started to appear, indicating that both zeolite "B" and species "Y" are metastable phases. Glasses of composition $Na_2O \cdot Al_2O_3 \cdot 4SiO_2$ crystallized directly to zeolite "B" in short runs (8 days), which was replaced by analcite in longer runs (21–90 days). It is possible that species "Y" is a mixture of more than one phase.

Zeolite "B": Zeolite "B" was synthesized from glasses within the range $Na_2O \cdot Al_2O_3 \cdot 2\text{–}6SiO_2$ at low temperature (200° C.) in short runs (1½–21 days). Crystallization was best in runs made with $Na_2O \cdot Al_2O_3 \cdot 2SiO_2$ glass, but some glass remained in short runs made with glasses of $Na_2O \cdot Al_2O_3 \cdot 3\text{–}4SiO_2$ compositions. $Na_2O \cdot Al_2O_3 \cdot 6SiO_2$ glass did not crystallize appreciably in runs of short duration. Some zeolite "B" appeared in longer (21 days) runs. Still longer runs (90 days) proved that zeolite "B" is definitely metastable with respect to analcite, as it is totally ($Na_2O \cdot Al_2O_3 \cdot 3\text{–}4$ glasses) or partially ($Na_2O \cdot Al_2O_3 \cdot 2SiO_2$ and $Na_2O \cdot Al_2O_3 \cdot 6SiO_2$ glasses) replaced by it. The compound appeared to be weakly birefringent, and the average refractive index decreased toward the silica-rich end as shown in Table IV.

This suggests that there is a solid-solution relationship. However, the *x*-ray powder diffraction spectrogram of zeolite "B" synthesized from glasses of different compositions did not indicate any appreciable displacement of the peaks. The cell dimension for the pseudocubic unit cell was measured, and found to be 10.05 ± 0.05 Å.

Paragonite: Small platy grains of paragonite, 22-7 microns in length and 7-1 microns in

diameter, appeared in intimate association with nepheline hydrate I at the stability range of the latter. They could be very easily distinguished from nepheline hydrate I by their much higher refractive indices, but it was impossible to identify them by the x-ray diffraction spectrometer alone, because of the small quantity available. Weak, diffuse reflections were obtained at $2\theta = 9°$ (CuKα), corresponding to the basal plane of paragonite, and $2\theta = 20°$ (CuKα), which also corresponds to another strong paragonite peak (Barrer and White, 1952). Two other peaks could be observed in an electron diffraction photograph which also correspond to paragonite (Fig. 1).

Paragonite also appeared quite frequently in association with analcite in runs made with glasses of compositions within the range $Na_2O \cdot Al_2O_3$. 2–$3SiO_2$, but the amount decreased quite considerably in runs made with glasses higher in silica than $Na_2O \cdot Al_2O_3 \cdot 3SiO_2$. This phase was mentioned as an "unidentified phase" in a previous paper by the author (Saha, 1959a). The mineral occurred as very fine flakes forming clusters around analcite grains.

Phase-Equilibrium Studies in the System $NaAlSiO_4$-H_2O

Figure 3 has been drawn using the data obtained (Saha, 1959b, Table II). The crystalline phases, stable and metastable, obtained in the products of the runs, have been marked with different symbols. The curve for the transition: nepheline hydrate I + water = nepheline + water has been drawn as a solid line. Nepheline hydrate I crystallized readily below the curve from runs made with glass of $NaAlSiO_4$ composition. At 15,000 psi and 445° ± 10° C., nepheline hydrate I decomposes to yield nepheline and vapor; Sand, Roy and Osborn (1957) found the transition temperature to be 460° C. at this pressure.

Efforts made to synthesize nepheline hydrate I by the reaction of nepheline crystals with water below the curve resulted only in the appearance of analcite. On the other hand, even in very long runs (3 months) made with glass and with nepheline hydrate I crystals, only nepheline hydrate I crystals could be detected. It was therefore impossible to establish the stability of nepheline hydrate I.

In runs made in the lower stability range of nepheline hydrate I, platy grains of a phase identified as paragonite appeared. Barrer and White (1952) also reported the synthesis of paragonite from gels of $NaAlSiO_4$ composition.

Table IV

	Composition of Glasses (Mol. Ratio)			Average Refractive Index of Zeolite "B"
	Na_2O :	Al_2O_3 :	SiO_2	
1	1 :	1 :	2	1.501 ± 0.002
2	1 :	1 :	3	1.493 ± 0.002
3	1 :	1 :	4	1.485 ± 0.002

Barrer and White (1952, Fig. 1-f), while working with gels of $NaAlSiO_4$ composition, were able to synthesize another hydrated phase, which they designated as nepheline hydrate II ($Na_2O \cdot Al_2O_3 \cdot 2SiO_2 \cdot \frac{1}{2}H_2O$), just above the stability field of nepheline hydrate I. They were able to synthesize this phase only in the presence of excess NaOH solution, and nepheline always appeared with this phase (1952, Table I). Subsequent investigators (Sand, Roy and Osborn, 1957) failed to synthesize this

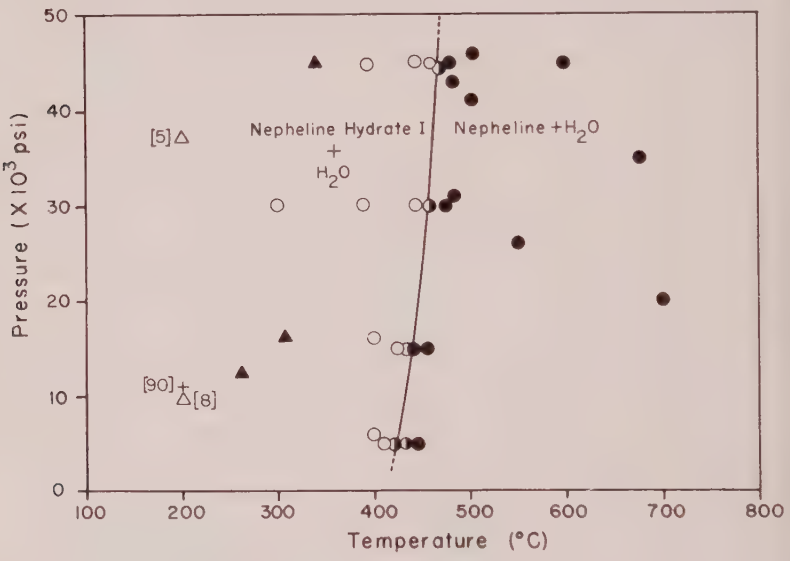

FIG. 3. The system $NaAlSiO_4$-H_2O
●—nepheline, ○-nepheline hyrdate I,
▲—nepheline hydrate I+paragonite,
+—analcite+zeolite "B," △—zeolite "B"+species "Y,"
[x]—duration of runs in days.

phase. Attempts were made to synthesize this phase during this investigation, but without success.

A compound of the composition $Na_2O \cdot Al_2O_3 \cdot 2SiO_2 \cdot 4.5H_2O$ designated by Breck *et al.* (1956) as zeolite "A" was reported to have been synthesized in very short runs (approximately 3 hours, personal communication with Dr. Breck). Since the minimum duration of any runs made during the present investigation was one day, zeolite "A" was not synthesized. Zeolite "A" is replaced by zeolite "B" in longer runs (Breck, personal communication). This suggests that zeolite "A" is a metastable phase under this condition.

Species "Y" and zeolite "B" are metastable phases which were partly

replaced by analcite in relatively longer runs (21 days –3 months). Analcite was very imperfectly crystallized in these runs, and it was not possible to determine the composition of analcite by the method of measuring the position of (639) peak, as described in a previous paper (Saha, 1959a). It seems possible that analcite is the stable phase at low temperatures crystallizing from a glass of $NaAlSiO_4$ composition. The presence of the metastable phases made it impossible to determine the transition curve: analcite solid solution $+ H_2O =$ nepheline hydrate I $+ H_2O$, if such a curve exists. A great deal of additional work must be done before this curve can be located accurately.

Thus experimental investigations suggest that nepheline is not stable below 400°–500° C. at moderate to high pressures in the presence of excess water. Glasses of nepheline composition, heated within the range 265°–450° C. and at various pressures, crystallize directly to nepheline hydrate I and some paragonite, the latter possibly due to some loss of soda and alumina and probably silica in the vapor. Also nepheline crystals are directly converted to analcite when heated at 300°–395° C. and 30,000–45,000 psi. These facts have an important bearing on the petrogenesis of alkaline rocks, which are known to be markedly rich in volatiles (Shand, 1947). It is expected that nepheline hydrate I or analcite would be abundant as alteration products, where there has been sufficient time for the magma to cool down slowly and yet retain a considerable amount of water under high pressure in the fissures. It is also expected that analcite rather than nepheline hydrate I will be abundant as a replacement product in volcanic rocks, rich in alkalies and glass, and where there is a chance for the alkali- and alumina-rich vapor phase to escape.

Reports on the occurrence of any natural counterpart of nepheline hydrate I are rare. As Barrer and White state, "hydronephelite" reported by Thugutt (1892) may well be nepheline hydrate I, but he did not give any identifying physical data. Walker and Parsons (1926) have described the presence of a zone ($\frac{1}{2}$–1″) of white to pink porcelaneous hydronephelite surrounding cancrinite in the nepheline syenite area of French River, Ontario. But the analysis of the mineral, even after deducting 11.19% calcite, contains too much alumina (28.88%) to be called hydronephelite. Tilley and Harwood (1931) have described the alteration of nepheline to fibrous masses of hydronephelite in titanaugite rocks. The mineral is uniaxial, elongation positive and the refractive indices ($\omega = 1.490$, $\epsilon = 1.500$) can be compared to those of synthetic nepheline hydrate I ($\alpha = 1.499$, $\gamma = 1.503$). Dunham (1933) also reported the occurrence of "hydronephelite" in undersaturated rocks from Hawaii. Jeremine (1948) has described the occurrence of "hydronephelite" derived from nepheline in association with aegirine-augite, apatite, sphene, soda

amphibole and biotite in a rock which has been named mestigmerite b Lacroix. No *x*-ray data for natural "hydronephelite" have been pub lished.

The rare occurrence of nepheline hydrate I in nature is in contrast t the observation that it can be grown readily from glass or gel of nephe line composition in the laboratory. A possible explanation of this can b offered only when the crystallization behavior of glasses of other compos tions in the system $NaAlSiO_4$-$NaAlSi_3O_8$-H_2O are considered. The dat obtained (Saha, 1959b, Tables II, VIII and IX) show that nephelin hydrate I can be crystallized from glass of $NaAlSiO_4$ composition only A little excess silica completely inhibits its growth, and since normal a kaline rocks contain more silica than end-member nepheline, this ca explain why nepheline hydrate I is such a rare mineral. Also the possibi ity that nepheline hydrate I appears as a metastable phase in the hydr thermal runs cannot be excluded.

On the other hand, analcite has quite often been reported from unde saturated rocks, sometimes in close association with nepheline, and h drothermal treatment of synthetic nepheline at low temperatures alway yielded a mixture of nepheline and analcite. An explanation of th peculiar behavior, *i.e.*, loss of soda and alumina, will be discussed in mo detail later. At low temperatures, it is possible that structural contr plays an important part in the crystallization of multi-component glass and gels. It is very difficult and in some cases impossible to determine t stability of different phases at these low temperatures. Moreove volatile associated with alkaline rocks contain not only water vapor, b also other compounds bearing Cl^-, F^-, $SO_4^=$, etc., and it is quite like that the presence of minerals like cancrinite, sodalite, etc., will restri the stability field of nepheline hydrate I. As a matter of fact, these mi erals do form very readily in undersaturated plutonic and volcanic rock

Phase-Equilibrium Studies in the System $NaAlSi_3O_8$-H_2O

Figure 4 has been drawn on the basis of the hydrothermal runs.* Son complications arose when it was found that analcite is a phase whi crystallized very rapidly from glass of $NaAlSi_3O_8$ composition in the pre ence of water vapor, and once formed, it was very difficult to decompo it below 450° C. Even in runs brought up to temperature and pressure ten minutes, some analcite grains were always observed under the micr scope, though characteristic analcite peaks were not observed in the *x*-ray diffraction spectrometer chart. The runs near the transition te peratures were not conclusive because of the presence of both the phas

* The complete data are given in Saha, 1959b.

in the product. The dotted line has been drawn on the basis of the proportion of the two phases present, and it is quite possible that the transition curve may be raised or lowered by as much as 25° C.

Several long runs (3 months) were made to investigate the stability of analcite solid solution of $NaAlSi_3O_8$ composition. Very finely ground specimens of high-, low-, and authigenic albite were used to see whether they would change over to analcite of $NaAlSi_3O_8$ composition. Runs were made at 300° C. and 30,000 psi, within the range of crystallization of analcite solid solution from $NaAlSi_3O_8$ glass. No change in the specimens was observed. On the other hand, only analcite crystallized from identical runs made with $NaAlSi_3O_8$ glass. Thus it cannot be said that analcite

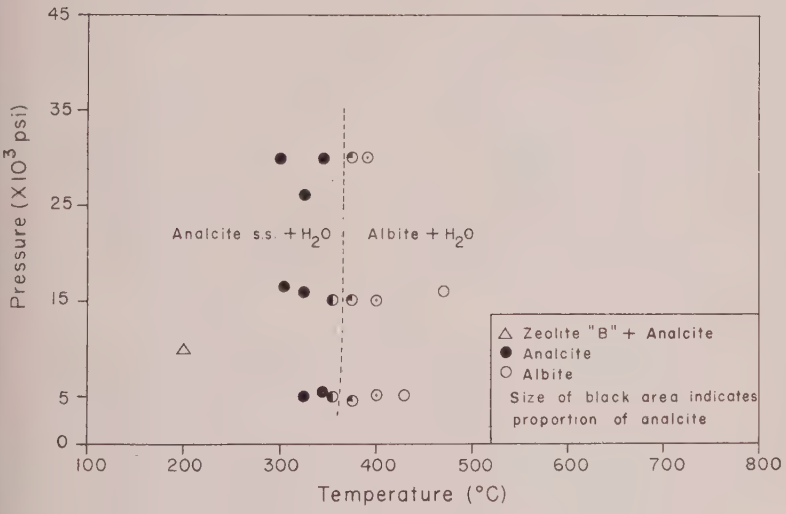

FIG. 4. The system $NaAlSi_3O_8$-H_2O.

solid solution of $NaAlSi_3O_8 \cdot 1.5H_2O$ composition is the stable phase at these temperatures.

Fyfe, Turner and Verhoogen (1958) determined the position of the pressure-temperature curve for the reaction analcite + quartz = albite + quartz + water (1). Their transition curve appears to be somewhat lower ($\simeq$50° C.) than the curve for the reaction analcite(ss) = albite + water (2) determined by the author (Fig. 4), even after allowing the rather uncertain nature of the curve for reaction (2). This can be explained readily because they were working with oxide mixes of composition $NaAlSi_4O_{10}$, richer in silica than the composition of albite ($NaAlSi_3O_8$). It is possible that the extent of analcite solid solution does extend beyond $NaAlSi_3O_8$ but not quite up to the composition $NaAlSi_4O_{10}$, and hence the transition

curve was lowered and quartz was obtained as a stable phase both above and below the transition curve for reaction (1). Fyfe, Turner and Verhoogen did not specify the composition of analcite synthesized in their experiments.

The appearance of analcite in runs made with glass of $NaAlSi_3O_8$ composition at low temperatures obviously has important geochemical significance in the petrogenesis of saturated igneous rocks, if the experimental results represent stable equilibrium. Analcite of $NaAlSi_3O_8 \cdot 1.5H_2O$ composition has not been reported from nature, but analcite intermediate in composition between $NaAlSi_2O_6$ and $NaAlSi_3O_8$ has been reported from sedimentary rocks (Ross, 1928, 1941). In one instance (Ross, 1941) the sedimentary series is composed almost exclusively of analcite together with a small proportion of glauconite and plagioclase. Keller (1952) also reported authigenic analcite intermediate in composition between $NaAlSi_2O_6 \cdot H_2O$ and $NaAlSi_3O_8 \cdot 1.5H_2O$ from the Popo Agie member of the Chugwater formation. Extensive deposits of analcite also occur in the Green River formation of Utah, Colorado and Wyoming (Bradley, 1928) associated with other zeolites, but its chemical composition is not known. These occurrences suggest that natural analcite approaching $NaAlSi_3O_8 \cdot 1.5H_2O$ composition should be looked for in sedimentary rocks.

Transitions from zones rich in analcite to zones rich in albite in thick formations of slightly metamorphosed sedimentary rocks have been observed in some places (Coombs, 1954). The pressure probably does not play a very important role in the case $P_{total} = P_{H_2O}$, as is evident from the nature of the transition curve (Fig. 4, cf. Coombs *et al.*, 1959, fig. 7), but the geothermal gradient associated with the increase in depth and pressure is very important. Investigation of environmental conditions of deposition and application of phase-equilibrium data on the transition analcite ($NaAlSi_3O_6 \cdot 1.5H_2O$) = albite + water may be helpful in defining a temperature within the assemblages of the recently proposed "zeolite facies." The work of Coombs *et al.* (1959) on the reaction analcite + quartz = albite + quartz + water will be more helpful in the case of analcime + quartz assemblages described by Coombs (1954).

Stability of Minerals and Compounds in the System $NaAlSiO_4$-$NaAlSi_3O_8$-H_2O

Phase-equilibrium relationships in the system $NaAlSiO_4$-$NaAlSi_3O_8$-H_2O can be conveniently represented by means of a series of isobaric triangles, as indicated in Fig. 5. They are based on the runs made at 15,000 psi (Saha, 1959b). $NaAlSi_3O_4$, $NaAlSi_3O_8$ and H_2O constitute the three components; it has been assumed that the system is ternary. This hold

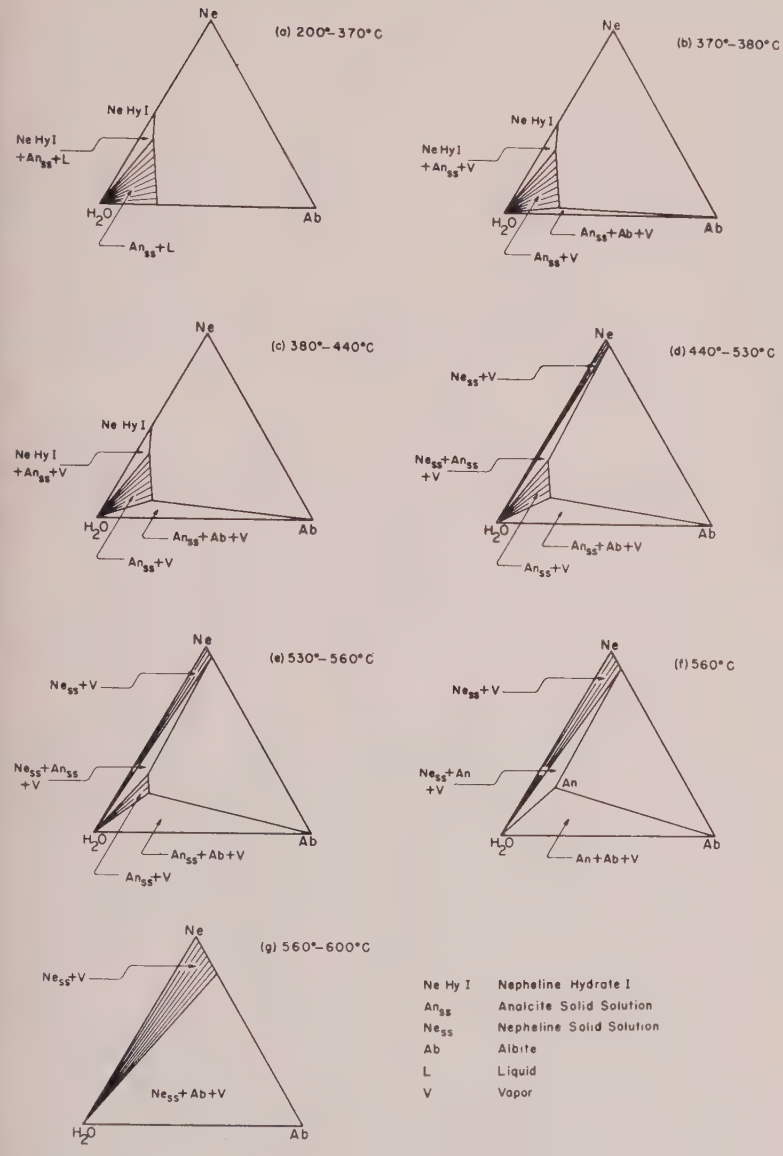

FIG. 5. Isobaric (15,000 psi.), isothermal sections for the system $NaAlSiO_4$-$NaAlSi_3O_8$-H_2O. Data plotted in mol.%.

true in general, except, perhaps, for glasses within the range $Na_2O \cdot Al_2O_3$ 2-2.75SiO_2, at low temperatures (200°–400° C.). The limit of solid solu tion of analcite ($Na_2O \cdot Al_2O_3 \cdot 2.75SiO_2$) has been drawn on the basis o the curve for the shift in (639) peak position of analcite (Fig. 2).

Nepheline Solid Solution

The extent of solubility of albite in nepheline has been determined. It was found that a 600° C. and 15,000 psi, nepheline can take up to 33% by wt. of albite into solid solution MacKenzie (1954) placed the solvus position at 25% by wt. of albite at 750° C. and 100 bars water vapor pressure. The displacement of peaks in *x*-ray powder diffraction spectro grams, of the order of $2\theta = 0.06°$ ($CuK\alpha$) for the (21.0) reflection from Ne_{100} to Ne_{75}, wa not sufficient for accurate measurement of composition. The position of the solvus on th nepheline side (Fig. 5) has been drawn primarily on the basis of microscopic determinatio of the first appearance of albite, which has certain characteristic growth habits quite di tinct from that of nepheline.

Jadeite

The maximum pressure (45,000 psi) obtained during the present investigation was to low for the synthesis of jadeite, and the mineral never appeared in the products of th runs.

Analcite-Water

The system $NaAlSi_2O_6$-H_2O was investigated by Yoder (1950), who presented a trans tion curve, part of which was based on Morey's data (personal communication with D Yoder), for the reaction:

$$\text{analcite}_{(NaAlSi_2O_6 \cdot H_2O)} = \text{nepheline} + \text{albite} + H_2O.$$

Another curve, based on revised data, was published by the same author several years lat (1954). Yoder found the transition temperature to be 550° C. at 15,000 psi. The results the present investigation suggest a somewhat lower temperature ($\simeq$530° C.) This compar favorably with Sand, Roy and Osborn's (1957) data (525° C. at 1000 atm). The results we further verified by making a run with glass of $NaAlSi_2O_6$ composition at 400° C. and 15,0 psi for four days, when only analcite could form, and then raising the temperature to 54 C. and 15,000 psi, and making the run for four more days. The products of the runs ind cated the presence of analcite together with clusters of albite laths. Moreover, it shou be noted that the maximum temperature of stability of analcite solid solutions does not co respond to $Na_2O \cdot Al_2O_3 \cdot 4SiO_2$ composition, but rather to $Na_2O \cdot Al_2O_3 \cdot 3.25SiO_2$ compos tion (Saha, 1959b, Tables VIII, IX). These data have been incorporated in the triangul diagrams of Fig. 5.

Natrolite-Water

Runs were made at different temperatures and pressures (Fig. 6), in an attempt to sy thesize natrolite ($Na_2Al_2Si_3O_{10} \cdot 2H_2O$), which has been found mostly in amygdules in bas volcanic rocks often in association with analcite and other zeolites. However, all these a tempts were unsuccessful. The association of natrolite with minerals like analcite and oth zeolites, calcite, etc., suggests that natrolite should be stable at relatively low temperatur and pressures. Natrolite and other zeolites are known to have been deposited in the wa work of Roman baths at Plombieres at a temperature of 70° C. (Coombs *et al.*, 1959). Hc

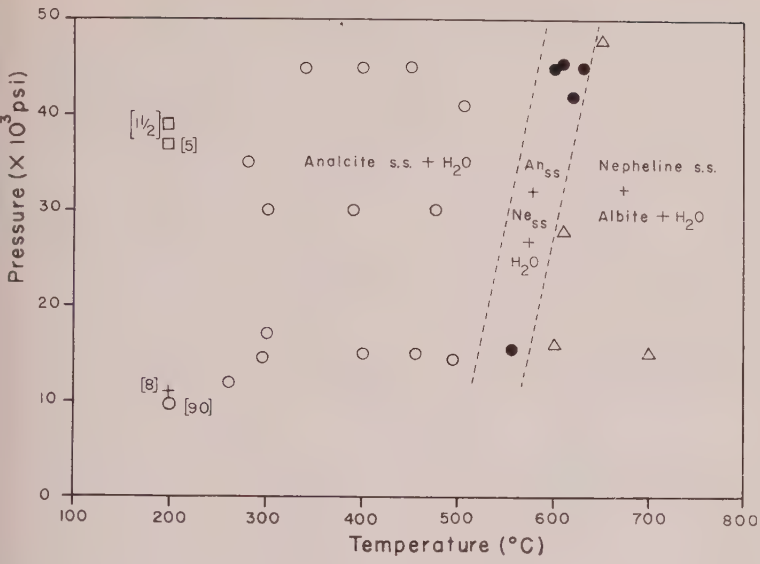

FIG. 6. The system $Na_2Al_2Si_3O_{10}$-H_2O. Dotted lines are projections of a P-T surface, not univariant P-T curves.

△—nepheline+albite, ● —analcite+nepheline,
○—analcite, □—zeolite "B"+species "Y,"
+—zeolite "B,"
[x]—duration of runs in days.

and Roy (1959) produced natrolite by the breakdown of Ca-type zeolite "A." Apparently structural control plays an important part in the formation of natrolite. It was possible to convert natrolite into analcite in a long run (3 months) at 300° C. and 30,000 psi, suggesting that it is not stable at this temperature and pressure. The analcite crystals formed by the decomposition of natrolite show peak positions in the *x*-ray diffraction data (Fig. 2) similar to that of analcite synthesized from $Na_2O \cdot Al_2O_3 \cdot 3SiO_2$ glass. Assuming that the natural natrolite used for the run has the ideal composition, this suggests that natrolite was converted to analcite of its own composition, except perhaps for the amount of water that it contains.

Albite-Water

It has already been mentioned that long runs (3 months) were made with albite crystals at 300° C. in the presence of water vapor in order to investigate whether it can be converted to analcite of albite composition. The products of the runs did not indicate the presence of analcite. Runs (15 days) have also been made at 300° C. with mixtures of synthetic ($Na_2O \cdot Al_2O_3 \cdot 4SiO_2 \cdot 2H_2O$) and natural analcites and silica in different forms, *i.e.*, silica gel, silica glass and Ludox silica sol, in order to investigate whether any shift in the (639) peak position of analcite can be produced. Within the experimental error no shift could be detected. This makes it impossible to determine the stability of analcite solid solution, and the triangular diagrams at the low temperature region of Fig. 5 may, perhaps, represent only metastable equilibrium.

Non-Ternary Nature of the System When Paragonite Appears as a Crystalline Phase

As shown in Figure 5(*a*), (*b*) and (*c*), a three-phase field nepheline hydrate I + analcite solid solution-liquid (or vapor) is present. Thus in runs made with glasses within the range $Na_2O \cdot Al_2O_3 \cdot 2.25$–$2.75SiO_2$, a mixture of nepheline hydrate I and analcite solid solution ($Na_2O \cdot Al_2O_3 \cdot 2.75SiO_2 \cdot 1.5H_2O$) would be expected. However, only analcite solid solution and paragonite could be recognized in the products, indicating that a third unrecognized phase must be present.

Microscopic examination of the charges showed no evidence of glass or amorphous material, and it was suspected that the third phase must be a vapor or a liquid which appeared as an aqueous solution after quenching (the quenched charges were observed to be wet and the liquid was alkaline). The experimental method did not permit using a large sample to collect the hydrous phase for analysis. All runs were made in sealed gold tubes and approximately equal weights of water and glass were put into the tubes, and as the hydrous phases (analcite, nepheline hydrate I and paragonite) required only a few weight per cent of water, the remaining water was present as a liquid or a vapor during the runs.

Morey and Hesselgesser (Morey, 1957a) have shown that at 2000 bars of steam pressure and at 500° C., 0.27% of albite was dissolved by the superheated steam, and the molecular ratio of the dissolved material was that of albite, within experimental error. This confirms the fact that for the composition $NaAlSi_3O_8$, the composition of vapor falls within the plane $NaAlSiO_4$-$NaAlSi_3O_8$-H_2O, and only one phase, albite or analcite solid solution of composition $Na_2O \cdot Al_2O_3 \cdot 6SiO_2 \cdot 3H_2O$, crystallizes. No experimental results are available for any of the other phases, *i.e.* nepheline, nepheline hydrate I or analcite solid solution. Morey (1957) assumed that the compositions of the liquid and gas phases remain within the ternary plane for the crystallization of jadeite, nepheline and analcite. From the present investigation, it appears that this may be approximately true for nepheline, nepheline solid solution, and analcite solid solution within the range $Na_2O \cdot Al_2O_3 \cdot 2.75$–$6SiO_2$, since very little paragonite (~1–3%) appeared in the runs. But for nepheline hydrate I and analcite solid solution synthesized from glasses within the range $Na_2O \cdot Al_2O_3 \cdot 2.25$–$2.75SiO_2$, paragonite was present in more than trace amount. Optical and *x*-ray evidence suggests that the amount of paragonite increased from ~3% in runs made with $Na_2O \cdot Al_2O_3 \cdot 3SiO_2$ glass to ~20% in runs made with $Na_2O \cdot Al_2O_3 \cdot 2SiO_2$ glass, and consequently the composition of the vapor changes drastically and deviates from the ternary plane.

The question now arises, can this hydrous vapor or liquid phase dissolve the excess solid materials not accounted for by the analcite and paragonite found in the charges? Table V illustrates the approximate composition of the vapor phase in the case of runs made with $Na_2O \cdot Al_2O_3 \cdot 2–2.75SiO_2$ glasses, calculated after making the following assumptions: (1) analcite solid solution of composition $Na_2O \cdot Al_2O_3 \cdot 2.75SiO_2 \cdot 1.5H_2O$ and paragonite crystallize from glasses within the range $Na_2O \cdot Al_2O_3 \cdot 2.25–2.75SiO_2$, (2) nepheline hydrate I ($Na_2O \cdot Al_2O_3 \cdot 2SiO_2 \cdot H_2O$) and paragonite crystallize from $Na_2O \cdot Al_2O_3 \cdot 2SiO_2$ glass, (3)

TABLE V. COMPOSITION OF VAPOR PHASE

Composition of glass (Mol. ratio)			Phases present after run	Composition of vapor (Wt. %)			
Na_2O	Al_2O_3	SiO_2		Na_2O	Al_2O_3	SiO_2	H_2O
1	1	2.75	Analcite[1] (95%)+Paragonite[2] (5%)	0.91%	0.00%	0.96%	98.14%
1	1	2.50	Analcite[1] (90%)+Paragonite[2] (10%)	2.89%	1.85%	0.00%	95.26%
1	1	2.25	Analcite[1] (85%)+Paragonite[2] (15%)	5.00%	4.48%	0.00%	90.52%
1	1	2.00	Nepheline Hydrate I[3] (80%)+Paragonite[2] (20%)	3.39%	0.00%	0.00%	96.61%

[1] Composition—$Na_2O \cdot Al_2O_3 \cdot 2.75SiO_2 \cdot 1.5H_2O$.
[2] Composition—$Na_2O \cdot 3Al_2O_3 \cdot 6SiO_2 \cdot 2H_2O$.
[3] Composition—$Na_2O \cdot Al_2O_3 \cdot 2SiO_2 \cdot H_2O$.

about equal proportion of glass and water is assumed to be present in each case, (4) alumina, not silica, is lost in the case of glasses of composition $Na_2O \cdot Al_2O_3 \cdot 2.25–2.50SiO_2$.

The calculations indicate that the amount of soda, alumina and silica dissolved by the vapor is quite reasonable if one takes into account the fact that while working in the system H_2O-$Na_2O \cdot 2SiO_2$, Morey and Hesselgesser (1952) found that at 400° C. and 2200 bars, the vapor contained 80.6% H_2O and 19.4% dissolved solid, and a liquid at the same temperature and pressure contained 34.0% H_2O, 66.0% solid. While working in the system H_2O-Na_2O-SiO_2-Al_2O_3, Friedman (1951) also found that liquids exist which can dissolve a fairly large amount of alumina.

It must be emphasized that Table V shows only the minimum amount of soda, alumina and silica in the vapor phase, when either silica in some cases or alumina in others has been assumed to be totally insoluble in the vapor phase. This is probably not true in the actual case, and all the

three oxides, *i.e.*, soda, alumina and silica are lost to the vapor phase t some extent.

Thus the system is no longer ternary when paragonite appears as stable phase, as the paragonite composition falls off the $NaAlSiO_4$-$NaAlSi_3O_8$-H_2O plane in the quaternary system Na_2O-Al_2O_3-SiO_2-H_2O. At low temperatures, the runs made with glasses within the rang $Na_2O \cdot Al_2O_3 \cdot 2$–$2.75SiO_2$ do not, therefore, represent ternary equilibri It is suggested that as a result of the above calculations on the vapor com position, the alkali-rich portion of the system becomes quaternary onl because of the excess vapor present during the experiments. It seems u likely, however, that equilibrium could be attained in a reasonable tim at these low temperatures if the water content of the charges were r duced to the stoichiometric amount.

Petrological Significance of the System $NaAlSiO_4$-$NaAlSi_3O_8$-H_2O

The non-ternary nature of the alkali-rich portion of the syste $NaAlSiO_4$-$NaAlSi_3O_8$-H_2O in the presence of excess water at low ten peratures (250°–500° C.) and pressures indicates that preferential sol bility of soda and alumina over silica in the vapor may be an importa feature, geochemically. Many alkaline rocks have been found to posse characteristic features (Smyth, 1927; Tilley, 1958), such as (1) speci tectonic environment, (2) abundance of volatile constituents. Smyt (1927) contended that the volatile constituents have the power to d velop alkali fractions from calc-alkali magma, but that this ability effective only under especially favorable conditions. Tilley (1958) h discussed the metasomatic development of alkaline rocks by the proce of nephelinization. From the present investigation, it seems possible th the volatiles escaping from the crystallizing alkaline rocks in a restricte range of composition may be quite enriched in soda and alumina a may be effective in the process of alkalization of the surrounding count rocks. No estimate of the importance of this process can be made un the composition of the vapor phase is known.

Paragonite appears quite frequently in runs made with glasses with the range $Na_2O \cdot Al_2O_3 \cdot 2$–$2.75SiO_2$, but it has very rarely been report from nature (Winchell and Winchell, 1951), possibly because optically resembles muscovite very closely. Eugster and Yoder (1954) studied mica-bearing schists from the Lincoln Mountain and Hyde Park qua rangles (Vermont) by the powder *x*-ray diffraction method, and fou that 33 samples contained paragonite in amounts up to 60% of the tot mica content.

The partial determination of the extent of analcite solid solution (an

icites having silica in excess of that of albite have not been investigated) indicated that information about the (1) compositions of the analcite and nepheline or albite crystals and (2) the approximate depth of burial and nature of the overlying rock formations would be helpful in estimating the temperatures attained in slightly metamorphosed rocks buried at moderate depths.

Analcite and natrolite have been reported from rocks which can be broadly classified into the following groups: (1) in igneous rocks, either as phenocrysts or in the groundmass, (2) in amygdules in volcanic rocks, and (3) in sedimentary beds.

Tyrrell (1928) has described the occurrence of analcite-syenites in the form of differentiated sills, schlierens and veins in Ayrshire along with analcite-olivine-dolerites. The schlierens and veins have been thought to have formed from the residual magmatic liquids. Where the analcite-olivine-dolerites are relatively rich in analcite, there has been only small developments of analcite-syenite, but the great development of analcite is concomitant with the impoverishment of the associated analcite-olivine-dolerite in analcites.

Tilley and Harwood (1931) have shown that vesicles in pyroxene-rich dolerites and pyroxenites from Scawt Hill were filled with thomsonite, some analcite, stilbite and natrolite. Thomsonite and analcite were also recorded in the groundmass of rocks, though never in large amounts. Tilley and Harwood concluded that these minerals in the groundmass of the rocks were formed by the alteration of the plagioclase. Larsen and Buie (1938) have described the occurrence of analcite as phenocrysts in analcite basalt from Highwood Mountains, Montana. They have been thought to have formed by primary crystallization from the magma. Roques (1947) has described the occurrence of fist-sized analcite crystals in nepheline-syenite-pegmatite on Kassa Island. Povarennyka (1954) has studied the replacement of nepheline by natrolite and albite by analcite in alkaline rocks and discussed the zeolitization of rocks during the late magmatic stage.

The commonest occurrences of analcite and natrolite in igneous rocks are in amygdules, and here there is no doubt about their secondary origin.

Extensive and comprehensive work on the occurrence of zeolites in thick sedimentary beds has been reported by Coombs (1954; Coombs in Coombs *et al.*, 1959). He described the occurrence of thick formations of marine Triassic and late Paleozoic sedimentary beds, a total thickness of about 30,000 ft., containing several members of the zeolite group of minerals, in Taringatura District, New Zealand. Zeolites are abundantly developed here; (1) fresh analcite is common in the upper 20,000 ft., and only pseudomorphs after analcite are present in the lower 10,000 ft., (2)

members of the heulandite-clinoptilolite group are very common in th upper 20,000 ft., and diminish considerably in the lower 10,000 ft., (3 laumontite is common only in the lower 10,000 ft. Among other mineral the upper 20,000 ft. is rich in detrital lime-bearing plagioclase, whereas i the lower 10,000 ft. the plagioclase is albitized, with local patches of relic calcic plagioclase. Most of the albite was generated by the breakdow and hydration of calcic plagioclase to albite and laumontite. Other min erals present are prehnite, pumpellyite, etc., more common in the lowe 10,000 ft. At shallow depths, analcite was formed by reaction betwee glass and saline waters, and with increasing depth the analcite was re placed by authigenic albite.

The occurrence of authigenic zeolites, especially analcite, in pyroclast rocks deposited in shallow basins, has been recorded by many invest gators. Tyrrell and Peacock (1926) described the occurrence of analci associated with faujasite in alteration products of palagonite tuff. Brad ley (1928, 1929) has described thin beds consisting almost wholly euhedral analcite crystals in the Eocene Green River formation of Uta Colorado and Wyoming. Field and microscopic evidences suggested th the analcite crystals were formed " . . . in place on the lake bottom as result of interactions between various salts dissolved in the lake wat and the dissolution products of volcanic ash that fell into the ancie Green River lakes." Ross (1928) has described a bed of "sedimenta analcite" from Yavapai County, Arizona, and concluded that the ana cite grains were formed either (*a*) by the reaction between volcanic a showers and sodium salts in the playa lakes, or (*b*) by the reaction b tween sodium salts concentrated in the playa lake and the hydrous al minium silicates in the playa mud. Later (Ross, 1941) he supported t former possibility.

During borehole investigations of the Upper Geyser Basin of Yello stone Park, Fenner (1936) described the frequent occurrence of analcite distinct veinlets and as impregnations and replacement of the gene mass in fragments of rhyolite and obsidian. Analcite occurs in the ran 86 to 216 ft. The temperature range measured by Fenner was 115 141° C. Heulandite, on the other hand, appears at 62 ft. and disappea at 86 ft., just above the zone of analcite. At the Weirakei thermal spri area, Steiner (cited in Coombs *et al.*, 1959) observed that the temperatu of occurrence of albite is 160°-240° C. at a depth of 100–600 m. It is inte esting to note that both the temperature and depth of formation of albi here are higher than the temperature and depth of formation of analci at Yellowstone Park. Raw (1943) concluded that analcite has be formed in palagonite tuffs in Jamaica by the reaction between the salt the sea and silicates, especially volcanic dust under volcanic heat.

Thus a survey of the literature on "authigenic zeolites" indicates that in many cases they were formed under unusual circumstances. They were formed in sedimentary rocks (1) often composed of pyroclastic materials, (2) often under conditions of high salinity, (3) moderate temperatures, (4) and where metamorphism played any part at all, depth of burial and not stress during metamorphism was most important. Comparison with the conditions of laboratory investigation of the system $NaAlSiO_4$-$NaAlSi_3O_8$-H_2O brings out several points of interest. Analcite crystallizes readily from most of the glasses used as starting materials for the runs, and appears to be very stable at low temperatures, and in cases of particular compositions deficient in silica is stable even up to 560° C. at 15,000 psi. This would suggest that low temperature metamorphism of volcanic rocks would give rise to analcite and other zeolites, as in the case of laboratory experiments. This is in complete accord with the field occurrences of "authigenic" zeolites, described in the previous paragraphs. Moreover, with increasing temperature and pressure, *i.e.*, increasing depth of burial, we would expect analcite to be replaced by albite, and this has been found to be the case in New Zealand (Coombs, 1954). As regards salinity, water extracted from the gold tubes after the experimental runs was found to be quite alkaline, though the pH was not measured. Barrer and White (1952) measured the pH of solutions after making runs with gels of compositions $Na_2O \cdot Al_2O_3 \cdot nSiO_2$ in the presence of water only, and they also found that the solutions were quite alkaline, the pH decreasing with rise in temperature (10.0 at 150° C. and 7.4–7.0 at 450° C.). This is probably due to the leaching of some soda from the glasses, as mentioned before.

Authigenic zeolites have also been found in sedimentary beds which may or may not have been derived from volcanic ash. Rengarten (1940) found authigenic analcite deposited around fragments of decomposed porphyrite in Permian sandstones from Russia and as minute crystals in the gypsum and carbonate matrix. It was considered to have been formed during the deposition of the sandstone. Foster and Feicht (1946) have described sulfur balls from the Pittsburgh coal seam in West Virginia containing analcite, pyrite and other minerals. They concluded that calcium bicarbonate solutions percolating down from the overlying limestones might have neutralized the acids and given rise to analcite from clay-like minerals. The presence of pyrite instead of marcasite indicated alkaline conditions. Keller (1952) found it more probable that authigenic analcite in the Popo Agie member of the Chugwater formation was formed by the reaction of strong sodium-rich carbonate-sulfate solutions with clays under an oxidizing alkaline environment. A volcanic origin of the parent material was not acceptable because of the complete absence

of volcanic material, and the presence of fossil *Unio* of freshwater type suggested the absence of strongly saline environment. Van Houten and Olson (1957) have described argillites from Upper Triassic Lockatong Argillite composed of analcite and illite, and contended that analcite in samples from widely separated outcrops suggests that the mineral is authigenic.

Conclusion

The present study thus indicates the importance of determining the composition of natural analcites of varying modes of origin. Given this information, and if reasonable assumptions as to the pressures are made it is possible to fix the temperatures at which any given analcite may have been formed. In the case of the more sodic analcites, which may be expected to occur as alteration products in feldspathoidal rocks, reversal of reaction has been achieved and the reaction curve experimentally determined may represent equilibrium conditions. Reversal of reaction has not been achieved for the more siliceous analcites, but the apparent transition boundary may probably represent an upper temperature limit for the stability of these analcites.

Acknowledgment

The author is indebted to Dr. O. F. Tuttle for his constant help and guidance in carrying out this research program, to Dr. D. S. Coombs for critical reading and discussion of the manuscript, and to Dr. Rustum Roy for many helpful suggestions.

References

Barrer, R. M. and White, E. A. D. (1952), Hydrothermal chemistry of silicates. Part I. Synthetic crystalline alumino-silicates: *Jour. Chem. Soc. London*, 1561–1571.

Boswell, P. G. H. (1933), On the mineralogy of sedimentary rocks: London, Murby and Co.

Bowen, N. L. (1928), The evolution of igneous rocks: Princeton University Press, Princeton, N. J.

Bowen, N. L. and Tuttle, O. F. (1950), The system $NaAlSi_3O_8$-$KAlSi_3O_8$-H_2O: *Jour. Geol.*, **58**, 489–511.

Bradley, W. H. (1928), Zeolite beds in the Green River formation: *Science, new ser.*, **6**, 73–74.

Bradley, W. H. (1929), The occurrence and origin of analcite and meerschaum beds in the Green River formation of Utah, Colorado and Wyoming: *U. S. Geol. Survey, Prof. Paper*, **158-A**, 1–7.

Breck, D. W., Eversole, W. G., Milton, R. M., Reed, T. B. and Thomas, T. L. (1956), Crystalline zeolites. I. The properties of a new synthetic zeolite, type A: *Jour. Am. Chem. Soc.*, **78**, 5963–5971.

Coes, L. (1953), A new dense crystalline silica: *Science*, **118**, 131. (Cited in Roy, R. and Tuttle, O. F. (1956). Investigations under hydrothermal conditions: Physics and Chemistry of the Earth, vol. 1, p. 146).

COOMBS, D. S. (1954), The nature and alteration of some Triassic sediments from Southland, New Zealand: *Trans. Roy. Soc. N.Z.*, **82**, part 1, 65–109.

COOMBS, D. S., ELLIS, A. J., FYFE, W. S. AND TAYLOR, A. M. (1959), The zeolite facies; with comments on the interpretation of hydrothermal syntheses: *Geochim. et Cosmochim. Acta*, **17**, 53–107.

DUNHAM, K. C. (1933), Crystal cavities in lavas from the Hawaiian Islands: *Am. Mineral.*, **18**, 369–385.

EUGSTER, H. P. AND YODER, H. S. (1954), Stability and occurrence of paragonite (Abstract): *Bull. Geol. Soc. Am.*, **65**, 1248–1249.

FENNER, C. N. (1936), Bore-hole investigations in Yellowstone Park: *Jour. Geol.*, **44**, 225–315.

FOSTER, W. D. AND FEICHT, F. L. (1946), Mineralogy of concretions from Pittsburgh coal seam, with special reference to analcite: *Am. Mineral.*, **31**, 357–364.

FRIEDMAN, I. (1951), Some aspects of the system H_2O-Na_2O-SiO_2-Al_2O_3: *Jour. Geol.*, **59**, 19–31.

FYFE, W. S., TURNER, F. J. AND VERHOOGEN, J. (1958), Metamorphic reactions and metamorphic facies: *Geol. Soc. Am. Mem.*, **73**, 166–179.

GREIG, J. W. AND BARTH, TOM. F. W. (1938), The system $Na_2O \cdot Al_2O_3 \cdot 2SiO_2$ (nepheline, carnegieite)-$Na_2O \cdot Al_2O_3 \cdot 6SiO_2$(albite): *Am. Jour. Sci.*, **35A**, 93–112.

GUYER, A., INEICHEN, M. AND GUYER, P. (1957), Ueber die Herstellung von Kunstlichen Zeolithen und ihre Eigenschaften als Molekelsiebe: *Helvetica Chimica Acta*, **40**, 1603–1611.

HOSS, H. AND ROY, R. (1959), Relative stability of some zeolites (Abstract): *Program, 1959 Annual Meeting, Geological Society of America*, p. 62A.

JEREMINE, E. (1948), Sur quelques roches provenant du Maroc oriental. Aiounite et mestigmerite: *Notes and Mem. Serv. Geol. Varoc., No. 71*, 67–71. (M.A. 11–40).

KELLER, W. D. (1952), Analcime in the Popo Agie member of the Chugwater formation: *Jour. Sed. Pet.*, **22**, 70–82.

LARSEN, E. S. AND BUIE, B. F. (1938), Potash analcime and pseudoleucite from the Highwood Mountains of Montana: *Am. Mineral.*, **23**, 837–849.

MACKENZIE, W. S. (1954), The system $NaAlSiO_4$-$NaAlSi_3O_8$-H_2O: *Carnegie Inst. of Washington, Year Book, No.* **53**, p. 119.

MACKENZIE, W. S. (1957), The crystalline modifications of $NaAlSi_3O_8$: *Am. Jour. Sci.*, **255**, 481–516.

MOREY, G. W. AND HESSELGESSER, J. M. (1952), The system H_2O-Na_2O-SiO_2 at 400° C.: *Am. Jour. Sci.*, Bowen Volume, Part II, 343–371.

MOREY, G. W. (1957), The system water-nepheline-albite: a theoretical discussion: *Am. Jour. Sci.*, **255**, 461–480.

MOREY, G. W. (1957a), The solubility of solids in gases: *Econ. Geol.*, **52**, 225–251.

POVARENNYKA, A. S. (1954), On the question of zeolitization of alkali rocks: *Doklady Acad. Sci. U.S.S.R.*, **94**, 761–764. (M.A. 12–482).

RAW, F. (1943), Some altered palagonite tuffs from Jamaica and the origin and history of their chlorites: *Jour. Geol.*, **51**, 215–243.

RENGARTEN, N. V. (1940), Authigenic analcyme in the Kazanian sandstones of the Kirov region: *Mem. Soc. Russe Min., ser.* **2**, **69**, 50–53. (English summary, p. 53).

ROBERTSON, E. C., BIRCH, F. AND MACDONALD, G. J. F. (1957), Experimental determination of jadeite stability relations to 25,000 bars: *Am. Jour. Sci.*, **255**, 115–137.

ROQUES, M. (1947), Edifices mimetiques et symetrie triclinique de l'analcime des iles de Los (Guinee Francaise): *Compt. Rend. Acad. Sci. Paris*, **225**, 946–948. (M.A. 10–294).

ROSS, C. S. (1928), Sedimentary analcite: *Am. Mineral.*, **13**, 195–197.

Ross, C. S. (1941), Sedimentary analcite: *Am. Mineral.*, **26,** 627–629.

Roy, R. (1956), Aids in hydrothermal experimentation: II, Methods of making mixture for both "dry" and "wet" phase-equilibrium studies: *Jour. Am. Cer. Soc.*, **39,** 145–14

Saha, P. (1959a), Geochemical and *x*-ray investigations of natural and synthetic analcite *Am. Mineral.*, **44,** 300–313.

Saha, P. (1959b), "Subsolidus Studies in the System $NaAlSiO_4$ $NaAlSi_2O_6$ H_2O"; Ph.I dissertation, The Pennsylvania State University, June, 1959.

Sand, L. B., Roy, R. and Osborn, E. F. (1957), Stability relations of some minerals in th Na_2O-Al_2O_3-SiO_2-H_2O system: *Econ. Geol.*, **52,** 169–179.

Schairer, J. F. and Bowen, N. L. (1956), The system Na_2O-Al_2O_3-SiO_2: *Am. Jour. Sc* **254,** 129–195.

Shand, S. J. (1947), Eruptive Rocks, John Wiley and Sons, Inc., New York.

Smith, J. V. and Tuttle, O. F. (1957), The system $KAlSiO_4$-$NaAlSiO_4$-I. The crystalli phases: *Am. Jour. Sci.*, **255,** 282–305.

Smyth, C. H. (1927), The genesis of alkaline rocks: *Proc. Am. Phil. Soc.*, **66,** 535–58 (Cited in Tilley, C. E. (1958), Problems of alkali rock genesis: *Geol. Soc. Lond Quart. Jour.*, **113,** 324).

Thugutt, St. J. (1892), Mineralchemische Studien: *Zeits. Anorg. Chem.*, **2,** 65–107. (Cit in Barrer, R. M. and White, E. A. D. (1952), Hydrothermal chemistry of silicat *Jour. Chem. Soc. London*, p. 1565).

Tilley, C. E. and Harwood, H. F. (1931), The dolerite-chalk contact of Scawt Hill, C Antrim: *Min. Mag.*, **22,** 439–468.

Tilley, C. E. (1958), Problems of alkali rock genesis: *Geol. Soc. London Quart. Jour.*, **1** 323–360.

Tuttle, O. F. (1949), Two pressure vessels for silicate-water systems: *Bull. Geol. Soc. A* **60,** 1727–1729.

Tyrrell, G. W. and Peacock, M. A. (1926), The petrology of Iceland: *Trans. Roy. S Edin.*, **55,** 57–76. (Cited in Coombs, D. S. (1954), The nature and alteration of so Triassic sediments from Southland, New Zealand: *Trans. Roy. Soc. N.Z.*, **82,** part 1. 78).

Tyrrell, G. W. (1928), On some dolerite-sills containing analcite-syenite in central A shire: *Quart. Jour. Geol. Soc.*, **84,** 540–569.

Van Houten, F. B. and Olson, R. C., Jr. (1957), Lithology of Upper Triassic Lockatc Argillite (Abstract): *Bull. Geol. Soc. Am.*, **68,** 1808.

Walker, T. L. and Parsons, A. L. (1926), Minerals from the new nepheline syenite ar French River, Ontario: *Univ. of Toronto Studies, Geol. Ser.*, No. **22,** 5–14. (M 3–302).

Winchell, A. N. and Winchell, H. (1951), Elements of optical mineralogy. Part Description of minerals. John Wiley and Sons, Inc., New York.

Yoder, H. S. (1950), The jadeite problem: *Am. Jour. Sci.*, **248,** 225–248 and 312–334.

Yoder, H. S. (1954), Zeolites analcite: *Carnegie Inst. of Washington Year Book*, No. 121–122.

Manuscript received August 16, 1960.

THE AMERICAN MINERALOGIST, VOL. 46, JULY–AUGUST, 1961

NOVÁKITE, $(Cu,Ag)_4As_3$, A NEW MINERAL*

Z. JOHAN, *Dept. of Mineralogy, Charles University, Prague,*

AND

J. HAK, *Institute for Ore Research, Kutná Hora, Czechoslovakia.*

ABSTRACT

Novákite is a new copper arsenide with the formula $(Cu, Ag)_4As_3$. It forms steel-gray granular aggregates in carbonate veins found in Černý Důl, in the Giant Mts., northern Bohemia. Density 6.7. Hardness 3–3.5. It shows medium strong anisotropism. Diagnostic etching: HNO_3 1:1 positive; NCl 1:1 positive; $FeCl_3$ 20% positive; HgCl 5% negative (film); KOH 40% negative; KCN 20% negative. The indexed x-ray powder photograph gives $a_0=9.99$, $c_0=14.03$Å, $c/a=1.405$. The cell is pseudocubic ($a_0\sqrt{2}=14.12$). $G_{calc}=6.75$. $Z=12$. It is associated with arsenic, arsenolamprite, koutekite, silver, löllingite, mineral X, chalcocite, smaltite, chalcopyrite, bornite and pitchblende.

INTRODUCTION

A new mineral was found during an investigation of the waste dumps of deserted mine-works in Černý Důl in the Giant Mountains. It is a copper arsenide, and was named in honor of Dr. Jiří Novák, Professor of Mineralogy at the Charles University in Prague.

The locality is about 3.5 km. north of the village of Černý Důl, in the valley of Stříbrný potok (Silver Creek), near Berghaus. The novákite was found associated with arsenic, arsenolamprite, koutekite (Johan, 1958), silver, löllingite, mineral X,† chalcocite, smaltite, chalcopyrite, bornite and pitchblende. All these minerals occur as inclusions in the carbonate gangue, fragments of which can be found on the dumps.

The Černý Důl locality is in a region of mica schists and gneisses (Máška, 1954; Svoboda and Kodym, 1948). The schists are garnetiferous in places, and contain abundant albite porphyroblasts. In them there lies an elongated erlan (pyroxene gneiss) body, tens of meters thick. The mica schists also contain bodies of conformable synkinematic orthogneisses. The crystalline body is highly folded, and forms an anticline near the deposit.

Carbonate veins containing the ore minerals run through the erlans, and less often through the mica schists. The veins are up to 20 cm. thick. The formation of the carbonate took place in several stages, separated by tectonic movements of the vein. The ore minerals are closely intergrown, and enclosed in the carbonate gangue. All of the ore minerals are metasomatically replaced by younger slightly manganous calcite.

* Preliminary report published in *Chemie der Erde*, Bd. XX, Heft 1, 49, 1959.

† A new copper arsenide mineral, which is still being studied.

The New Mineral

Novákite forms irregular aggregates with grains up to 3 cm. in size. I is steel-gray on a fresh surface, but soon turns iridescent and later be comes black. It weathers easily to secondary copper arsenates. Hardnes 3–3.5; streak black; cleavage none. Since the novákite is intergrown wit löllingite and chalcocite, the value of G = 6.7 is only approximate.

In reflected light novákite appears white with a light cream tint, whic is distinct from arsenic. The anisotropy is medium, with dark blue-gra and light brown ocher color effects in marginal positions. No reflectic pleochroism could be observed. The reflectivity is a little higher than th of arsenic. Small grains of novákite embedded in arsenic cannot be di tinguished microscopically without etching. No internal reflectio could be observed, even in oil immersions. On account of its low hardnes the mineral can be easily polished.

Diagnostic etching:

Etching agents according to M. N. Short (1940) were used. Time of etching wa min.

HNO_3	1:1	pos.—The mineral changes color to dark-grey with a brown tint, la varied iridescent colors appear.
HCl	1:1	pos.—The color changes to light gray-green with a brown and blu tint. This distinguishes novákite from arsenic.
$FeCl_3$	20%	pos.—The reaction is the same as with HCl 1:1.
$HgCl_2$	5%	neg.—The etching is not distinct. The mineral is covered with a yell
		(pos.) brown film, which can be washed away easily. After the f removal the polished section is intact.
KOH	40%	neg.
KCN	20%	neg.

Spectrochemical Analysis

Semi-quantitative spectrochemical analyses were carried out by Litomiský in the Institute for Ore Research in Kutná Hora.

	I	II
>10%	As, Cu	As, Cu
10–1%	Ag	Ag, Ca, Fe
1–0.1%	Ca, Si	Co
0.1–0.01%	Al, Co, Fe, Sb	Sb, Ni, Si
0.01–0.001%	Mg, Pb	Al, Cd, Mg, Mn, Y
<0.001%	Mn, Zn, Ni	Be, Pb, Yb, Zn
?	Ti	Bi

Technical conditions: Spectrograph Zeiss Q 24, a.c. arc 4 A (gener. DG 1), expos 30 sec. without pre-arcing, photoplate Foma super-ortho, slit-width 0.003 mm., car electrodes ČKD Prague, analytical gap 3 mm.

Analysis No. I was carried out on practically pure novákite. Analy No. II was on material analyzed quantitatively by chemical methods.

represents a mixture of novákite, löllingite, chalcocite and gangue carbonate.

It is assumed that the Ag replaces Cu, and the Sb replaces As. The heterogeneous, carbonate-rich gangue contains the Ca, Si, Al, Mg and Mn. The presence of löllingite in analysis II is indicated by the increased content of Fe, Co and Ni.

Chemical Analysis

The sample used for the determination of density was analyzed. The mineral was separated from a polished section, in which novákite was intergrown with calcite, löllingite and chalcocite. A 0.4 gm. sample was used for the analysis. All determinations were carried out in duplicate with the exception of S and CaO. The CO_2 content was calculated.

After dissolving the finely powdered mineral in concentrated H_2SO_4 and after adding dilute HCl, arsenic was determined directly by titrating with 0.05-N $KBrO_3$. After a suitable adjustment, the same sample was used for separating silver as AgCl, which was then dissolved in ammonia; silver was determined electroanalytically from an ammoniacal complex. After reduction and removal of arsenic by means of hydroxylamine and hydrochloric acid, iron was determined manganometrically (0.05 N $KMnO_4$) following several reprecipitations and separation as hydroxide. Copper was estimated electroanalytically from an ammoniacal solution of the filtrate, which was then used after a suitable adjustment for an electroanalytical determination of cobalt. After removal of R_2O_3 and ammonium salts and after separation of cobalt the solution was used for a complexometric estimation of calcium (0.01 N versene) with fluorexone as indicator. Sulfur was determined on a portion of the original sample as barium sulfate, after fusion of the mineral with a mixture of sodium carbonate and sodium peroxide.

The results of the chemical analysis are as follows:

As	43.30%	43.23%
Cu	41.39	41.32
Fe	5.13	5.12
Ag	1.96	1.96
Co	0.79	0.79
S	2.73	2.73
CaO	2.72	2.72
CO_2 (calc.)	2.13	2.13
	100.15%	100.00%

Percentage composition after subtraction of $CaCO_3$, (Fe, Co)As_2 and Cu_2S:

		atomic quotients	
As	45.82%	0.6117	
Ag	3.27	0.0303	0.8316
Cu	50.91	0.8013	
	100.00%		

The ratio of atomic quotients corresponds to the formula $(Cu, Ag)_{1.36}As_1$, or in integers $(Cu, Ag)_4As_3$.

X-Ray Powder Data

The character of the material allowed only the powder method to b used. Patterns were obtained on both 57.3 and 114.59. mm. cameras, wit CuKα radiation. Intensities were estimated visually. Before indexing wa undertaken, isostructural or chemically analogous compounds we looked for, but without success. Then the analogy between the tetra onal structure of Cd_2Sb_2 with a pseudocubic cell was used. The Hu Davy charts were used. When the coincidence of some of the diffracti lines with a cubic pattern was noticed, an axial ratio $c : a = \sqrt{2}$ was trie and all of the lines could be indexed. The agreement between the the retical and measured d-values is satisfactory. The cell dimensions are

$$a_0 = 9.99, \quad c_0 = 14.03\text{Å}; \qquad c/a = 1.405; \qquad Z = 12.$$
$$a_0\sqrt{2} = 14.12$$

The indexed powder pattern is given in Table I.

Synthesis and Stability of Cu_4As_3

Synthesis of the compound Cu_4As_3 was attempted by fusing a mixtu of copper and arsenic in an evacuated glass tube. After fusion the m terial was examined microscopically, chemically and by x-rays. A p mary phase consists of crystals of Cu_2As, which are embedded in a tectic of Cu_2As and an unidentified white phase.

Since the Cu_4As_3 phase could not be prepared by direct union of t elements, a stability investigation of novákite was carried out. A samp was heated in an evacuated tube to 500° C. The mineral did not melt, b a microscopic investigation revealed that the original mineral was longer present. It decomposed below its melting point to Cu_2As and t unidentifed white phase mentioned above.

Relation of Novákite to Other Minerals

Novákite is found most frequently intergrown with native arsenic. shown in Fig. 1, it forms metasomatic veinlets in arsenic. Löllingite younger origin occurs in the center of the veinlets. On account of atm pheric oxidation of the polished section, a reaction zone between novák

TABLE I. *X*-RAY POWDER PATTERN OF NOVÁKITE—$(Cu, Ag)_4As_3$
Locality: Černý Důl

Cu/Ni, $\lambda = 1.5418$ Å, camera 114.59 mm.

I	$d_{meas.}$	$d_{calc.}$	*hkl*
2	9.98 Å	9.99 Å	100
5	6.41	6.32	111
2	4.08	4.08	202
1	3.80	3.77	212
1 B	3.35	3.33	300
4	3.164	3.163	310
1	3.089	3.086	311
2–3	3.018	3.013	302
2	2.903	2.886	312
2 B	2.806	2.806	005
1	2.698	2.704	105
1	2.622	2.621	313
2	2.508	2.500	400
3	2.449	2.449	205
4	2.386	2.389	411
1	2.322	2.324	331
3 B	2.281	2.279	106
2	2.206	2.208	421
2	2.171	2.176	324
1	2.133	2.131	422
1	2.108	2.100	315
4	2.072	2.073	216
8	1.998	2.000	500
9	1.959	1.960	510
5	1.913	1.915	306
10	1.877	1.881	316
1	1.844	1.841	520
3	1.787	1.789	326
1 B	1.730	1.729	108
2	1.670	1.667	600
2	1.655	1.655	601
1	1.598	1.600	612
1	1.566	1.565	407
1	1.546	1.544	109
2	1.500	1.498	623
3–4	1.443	1.442	624
3	1.407	1.407	711, 551
6	1.351	1.353	713, 553
1	1.336	1.338	2.1.10
4	1.312	1.313	730
2	1.293	1.294	3.0.10
4	1.268	1.267	1.1.11
2	1.251	1.253	3.2.10
6	1.225	1.227	530
1	1.200	1.200	618
9	1.180	1.178	660
5	1.157	1.158	751

B—broad line.

nd arsenic is visible. The arsenic may be very extensively replaced netasomatically by novákite (Fig. 2). When rarely found without rsenic, it forms irregular aggregates partly replaced by carbonate, and

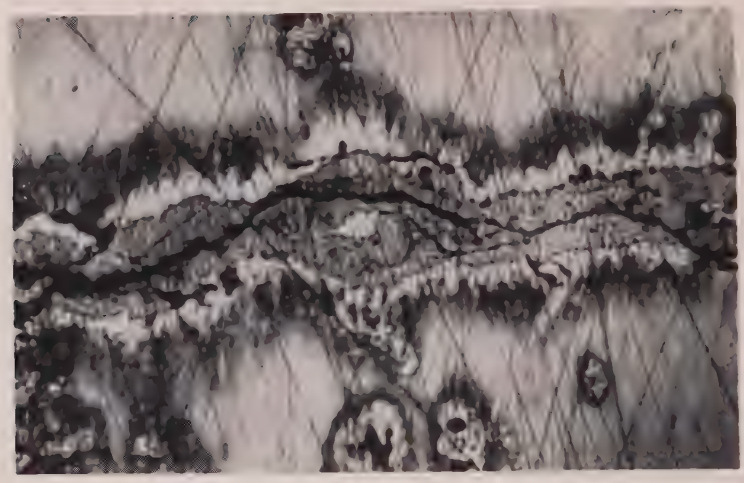

Fig. 1. A metasomatic veinlet of novákite in native arsenic. On account of atmospheri oxidation a reaction zone occurs between novákite and arsenic. Löllingite (white) appear in the center of the novákite veinlets. Polished section, etched by 1:1 HCl. Magnificatio about 160×.

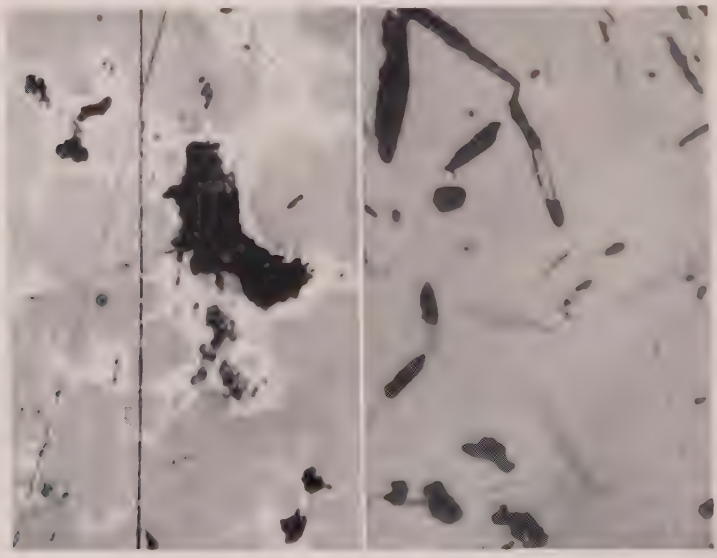

Fig. 2. (Left) Arsenic (white) is very extensively replaced by novákite (gray); unev areas appear black. Polished section, etched by 1:1 HCl. 100×.

Fig. 3. (Right) The "oleanderblätter" texture in novákite (light gray groundmass). T original mineral forming the "oleanderblätter" was replaced by carbonate (black), which is turn partly or completely replaced by relatively younger chalcocite (gray). Polished secti without etching. 500×.

surrounded by löllingite fringes. These aggregates occasionally show a texture (Fig. 3) caused by unmixing of the solid solution, called "oleanderblätter" by Ramdohr (1955).

The genesis of novákite in the Černý Důl locality was characterized by the presence of much arsenic in the hydrothermal solutions, resulting in the formation of copper arsenides with higher arsenic content than previously known.

References

Johan, Z. (1958) Koutekite a New Mineral. *Nature*, **181,** 1553, London.

Máška, M. (1954) On the Problem of Tectonic Analysis of the Crystalinic Terrains. *Library of Central Geological Survey*, **27,** Praha.

Ramdohr, P. (1955) Die Erzmineralien und ihre Verwachsungen, Berlin.

Short, M. N. (1940) Microscopic Determination of the Ore Minerals. *U.S. Geol. Survey Bull.* **914.**

Svoboda, J., Kodym, O. (1948) The Caledonian Nappe Structure of Krkonoše and Jizerské hory. *Sborník ÚÚG*, **XV,** 109, Prague.

RAPID DETERMINATION OF THE APPROXIMATE COMPOSITION OF AMPHIBOLES AND PYROXENES

RONALD B. PARKER, *Department of Geology and Mineralogy, The University of Wyoming*

ABSTRACT

Published determinative curves for amphiboles and pyroxenes have been recalculated with the use of a Bendix G 15 computer. The new curves are plots of the indices of refraction measured on a (110) cleavage flake and the extinction angle on the flake versus composition. The new curves are suggested for use in rapid reconnaissance of numerous specimens, and as a useful preliminary to more complete measurements.

INTRODUCTION

The use of refractive indices measured on cleavage flakes (n_1 and n_2) for the purpose of identification of rock-forming minerals was early suggested by Tsuboi (1923) for the plagioclase series. Later (1924), Tsuboi presented formulae for calculation of n_1 and n_2 from more fundamental optical and crystallographic parameters for a number of other mineral groups. Tomita (1934) presented additional formulae, and calculated n_1 and n_2 for a number of analyzed pyroxenes. In spite of the fact that the formulae have been available for some time, they have been little used. Pabst (1928, p. 363–367) and Wager and Deer (1939, p. 77–79) used the refractive indices n_1 and n_2 to estimate compositions of amphiboles and pyroxenes respectively. Emmons and Gates revived the use of Tsuboi's plagioclase curve (1948), but the use of n_1 and n_2 for other mineral groups has been limited.

COMPUTATIONS

It may be presumed that calculations have not been made for other mineral groups because of the time consuming nature of the computations. This element of time may now be reduced to a minimum by the use of electronic computers. The results of calculations, shown here as curves, were obtained by use of a Bendix G-15 computer, using the Intercom 500 programming language. Primary data were read from published curves noted in captions accompanying the curves. All results were spot checked with slide rule, desk calculator, and stereographic net. The formulae used are given in the appendix. Values of n_1, n_2, and extinction angle were calculated at 5 per cent composition intervals.

METHOD AND USE OF MEASUREMENTS

Care must be used to select grains which lie on (110). No convenient conoscopic test is possible; but, if small grains of uniform interferen

(*Text continued on page 899*)

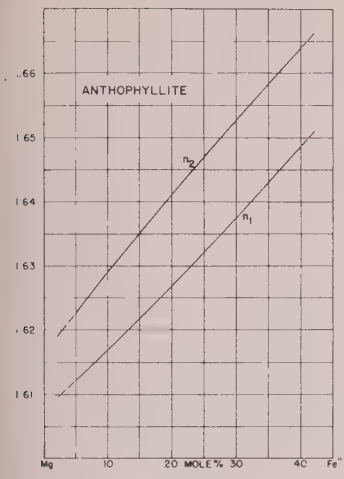

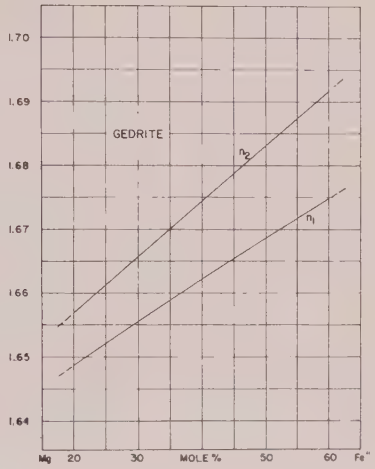

FIG. 1. (Left) The anthophyllite series. Primary data from Tröger (1956, p. 71).
FIG. 2. (Right) The gedrite series. Tröger (1956, p. 71).

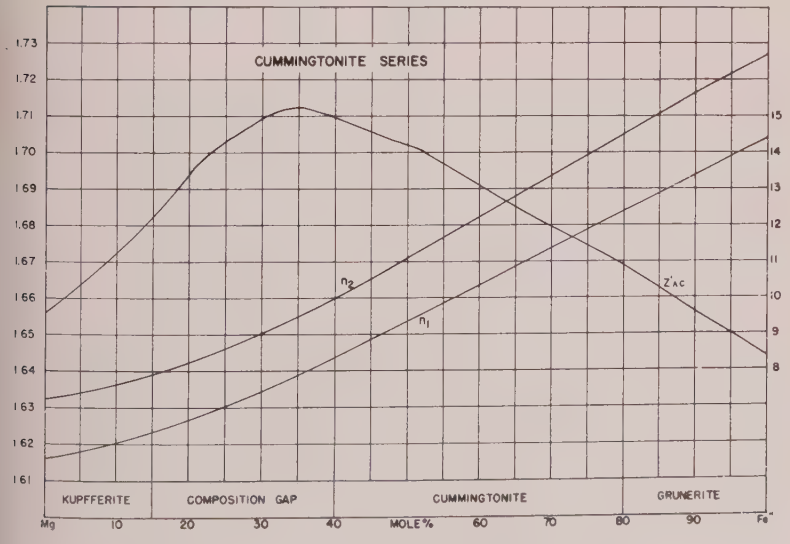

FIG. 3. The cummingtonite series. Winchell (1938, p. 332).

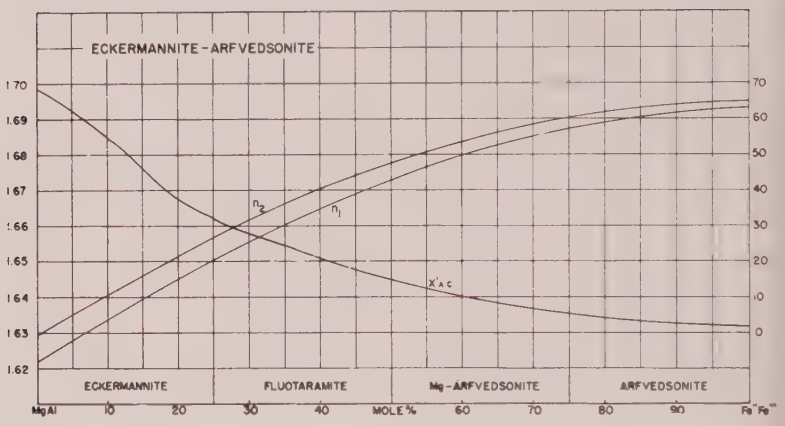

FIG. 4. The eckermannite-arfvedsonite series. Tröger (1956, p. 74).

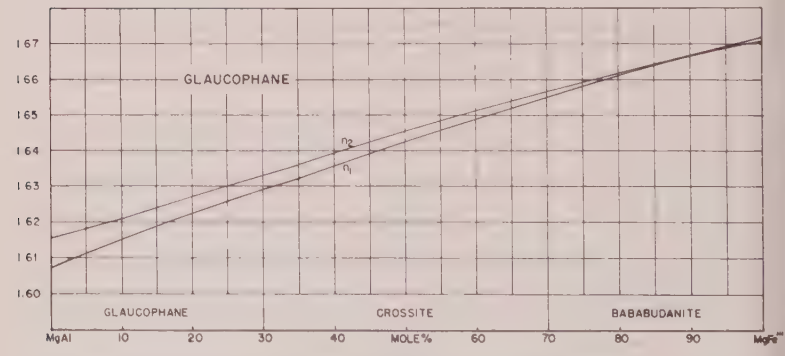

FIG. 5. The glaucophane series. Tröger (1956, p. 73). Values of δ' not given because variation is too slight to be diagnostic.

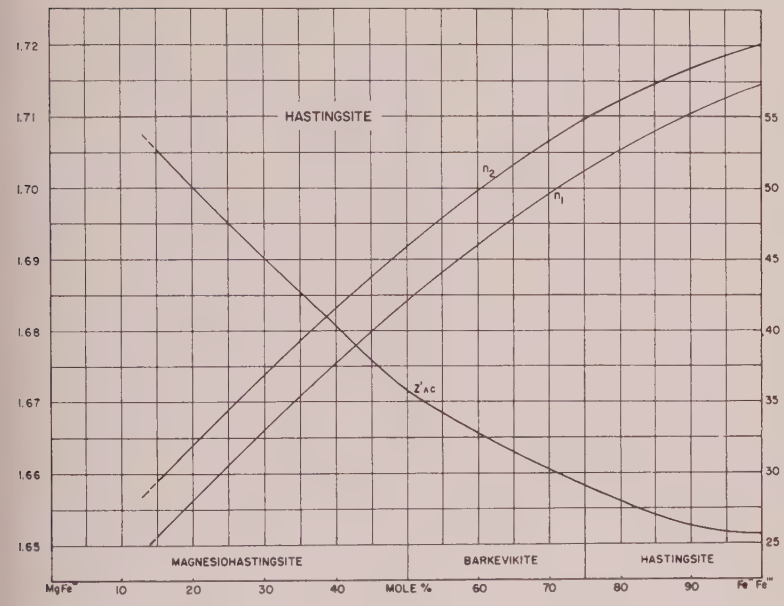

FIG. 6. The hastingsite series. Tröger (1956, p. 75).

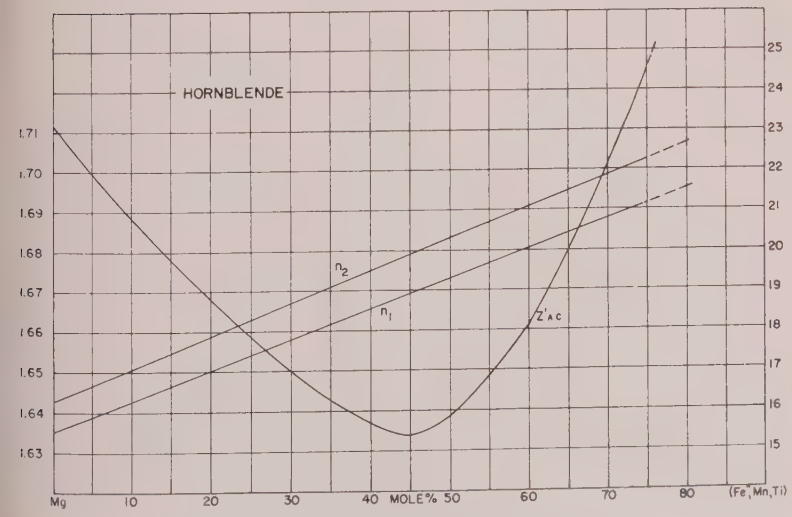

FIG. 7. The hornblende series. Tröger (1956, p. 77).

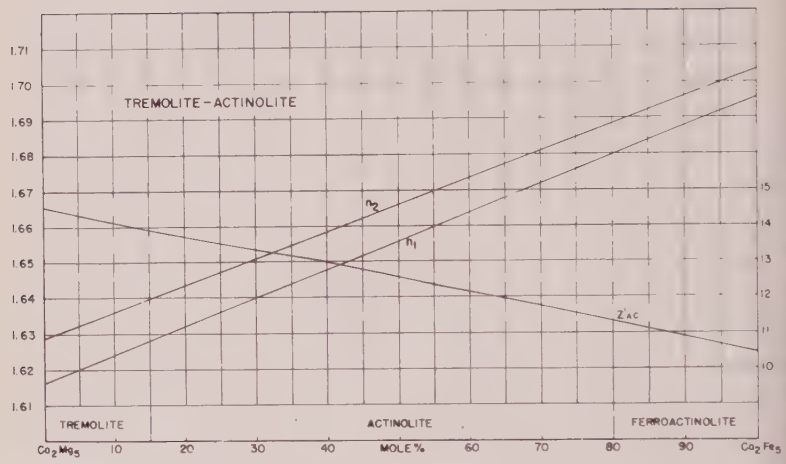

FIG. 8. The tremolite-actinolite series. Tröger (1956, p. 72).

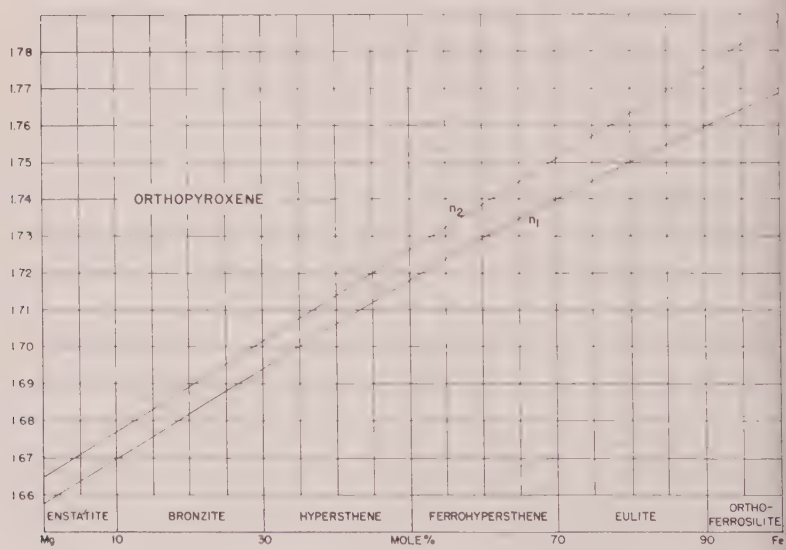

FIG. 9. The orthopyroxene series. Hess (1960, p. 27)

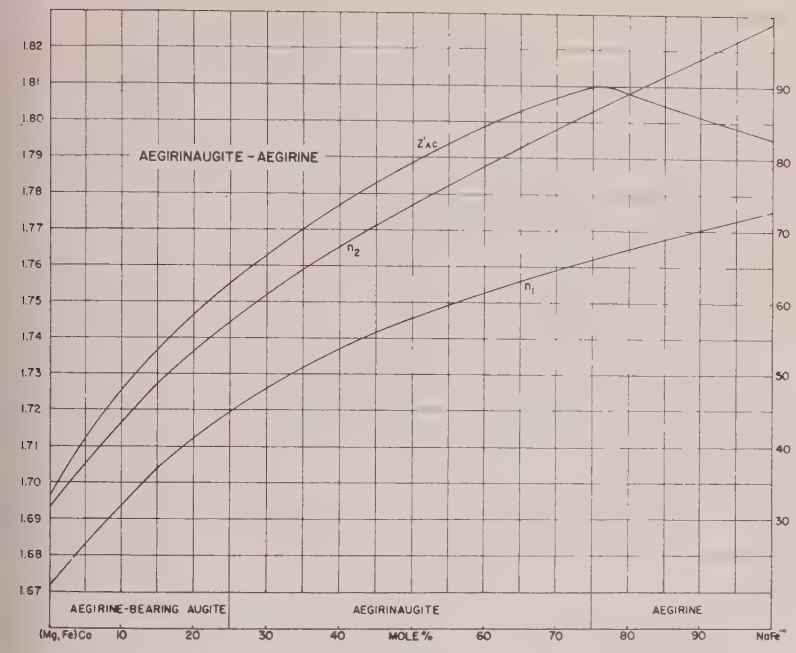

FIG. 10. The aegirinaugite-aegirine series. Larsen (1941, p. 48).

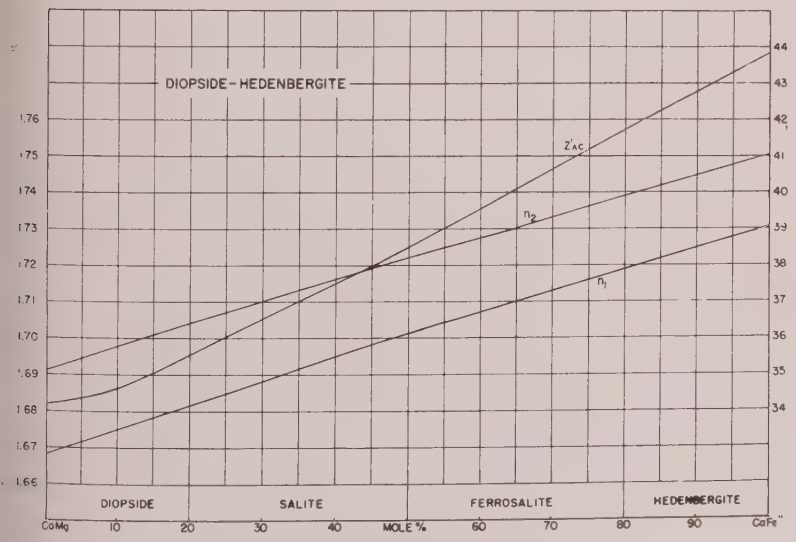

FIG. 11. The diopside-hedenbergite series. Hess (1949, p. 641–642).

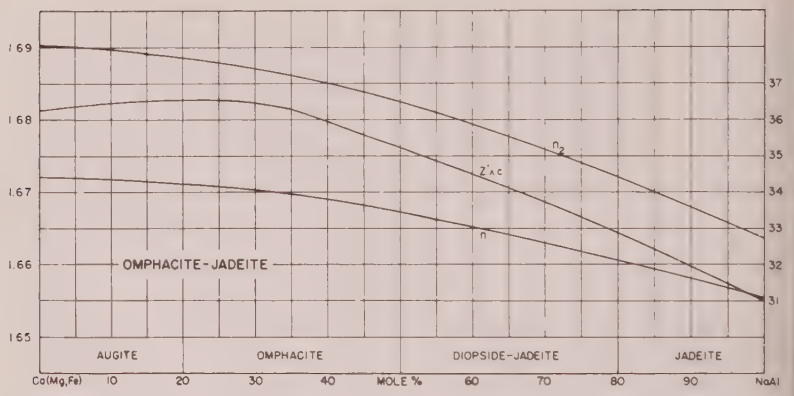

FIG. 12. The omphacite-jadeite series. Tröger (1956, p. 63).

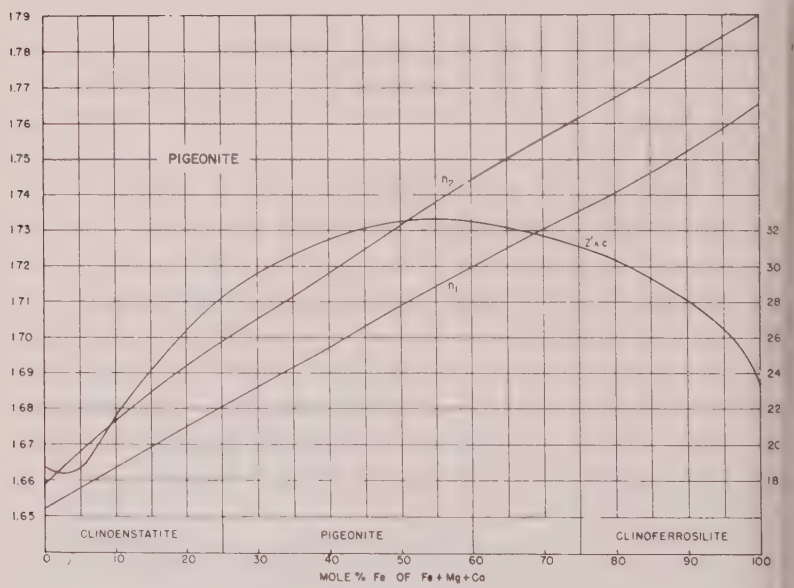

FIG. 13. The pigeonite series. Hess (1949, p. 63).

olor are selected, the results are reproducible. It is suggested that composition determinations with these curves would be useful for studies of ariation in chemical composition in which a large number of samples re to be studied, and that such determinations would be of value as a reliminary step to more precise (and laborious) determinations by ther methods. It is not suggested that measurements of n_1 and n_2 hould be considered a substitute for determination of α, β, and γ, and ther optical-crystallographic information; since these data should lways accompany mineral analyses.

Acknowledgments

The writer is indebted to Professor Adolf Pabst of the University of alifornia, Berkeley for first suggesting the utility of the method. Dr. . J. Varineau, director of the University of Wyoming Computer aboratory; and C. R. Dunrud, student at the university, both gave aluable suggestions about programming.

Appendix

Formulae used for computations are as follows: Where the optic plane is parallel to 010) and $b=y$

$$\left.\begin{aligned}(n_1)^2 &= \frac{2\gamma^2\alpha^2}{(\gamma^2+\alpha^2)+(\gamma^2-\alpha^2)\cos(\psi-\psi')}\\ (n_2)^2 &= \frac{2\gamma^2\alpha^2}{(\gamma^2+\alpha^2)+(\gamma^2-\alpha^2)\cos(\psi+\psi')}\end{aligned}\right\} \quad \text{(I)}$$

which

$$\left.\begin{aligned}\cos\psi &= -\sin(\Omega-\delta)\sin K\\ \cos\psi' &= \sin(\Omega-\delta)\sin K\end{aligned}\right\} \quad \text{(II)}$$

here

$$\Omega = Vz, \qquad \delta = c \wedge z, \qquad K = \perp(110) \wedge b \qquad \text{(Tsuboi, 1924, p. 24).}$$

here the optic plane is perpendicular to (010) and $b=x$, relation (I) applies with

$$\left.\begin{aligned}\cos\psi &= \sin\Omega\cos K+\cos\Omega\sin K\sin\delta\\ \cos\psi' &= -\sin\Omega\cos K+\cos\Omega\sin K\sin\delta\end{aligned}\right\} \quad \text{(III)}$$

(Tomita, 1934, p. 48).

here the optic plane is perpendicular to (010) and $b=z$

$$\left.\begin{aligned}(n_1)^2 &= \frac{2\gamma^2\alpha^2}{(\gamma^2+\alpha^2)-(\gamma^2-\alpha^2)\cos(\psi-\psi')}\\ (n_2)^2 &= \frac{2\gamma^2\alpha^2}{(\gamma^2+\alpha^2)-(\gamma^2-\alpha^2)\cos(\psi+\psi')}\end{aligned}\right\} \quad \text{(IV)}$$

which

$$\left.\begin{aligned}\cos\psi &= \sin\phi\cos K+\cos\phi\sin K\sin T\\ \cos\psi' &= -\sin\phi\cos K+\cos\phi\sin K\sin T\end{aligned}\right\} \quad \text{(V)}$$

ere

$$\phi = Vx \qquad T = c \wedge x, \qquad K = \perp(110) \wedge b.$$

For determination of the extinction angle, δ'; where the optic plane is parallel to (010 and $b=y$

$$\delta' = (\theta + \theta')/2 \qquad \text{(VI}$$

in which

$$\left.\begin{aligned} \tan\theta &= \tan(\delta + \Omega)\cos K \\ \tan\theta' &= \tan(\delta - \Omega)\cos K \end{aligned}\right\} \qquad \text{(VII}$$

(Tomita, 1934, p. 48

Where the optic plane is perpendicular to (010) and $b=x$, relation (VI) applies with

$$\left.\begin{aligned} \cos\theta &= \frac{\cos\delta\cos\Omega}{\sin\psi} \\ \cos\theta' &= \frac{\cos\delta\cos\Omega}{\sin\psi'} \end{aligned}\right\} \qquad \text{(VII}$$

in which ψ and ψ' may be found by relation (III) (Tomita, 1934, p. 48). Where the opt plane is perpendicular to (010) and $b=z$, relation (VI) applies with

$$\left.\begin{aligned} \cos\theta &= \frac{\cos T\cos\phi}{\sin\psi} \\ \cos\theta' &= \frac{\cos T\cos\phi}{\sin\psi'} \end{aligned}\right\} \qquad \text{(I}$$

in which ψ and ψ' may be found by relation (V).

References

Emmons, R. C., and Gates, R. M., 1948, The use of Becke line colors in refractive ind determinations: *Am. Mineral.*, **79,** 612–617.

Hess, H. H., 1949, Chemical composition and optical properties of common clinopyroxen I: *Am. Mineral.*, **34** 621–666.

———, 1960, Stillwater igneous complex, Montana: a quantitative mineralogical stuc *Geol. Soc. America Mem.* **80,** 230 p.

Larsen, E. S., 1941, Alkalic rocks of Iron Hill, Gunnison County, Colorado: *U. S. Ge Survey Prof. Paper* **197A,** 1–64.

Pabst, Adolf, 1928, Observations on inclusions in the granitic rocks of the Sierra Neva *Univ. California Pubs. in Geol. Sci., Bull.*, **17,** 325–386.

Tomita, Toru, 1934. Variations in optical properties, according to composition, in pyroxenes of the clinoenstatite-clinohypersthene-diopside-hedenbergite system: *Jo Shanghai Sci. Institute, Sec. II*, **1,** 41–58.

Trüger, W. E., 1956, Optische Bestimmung der gesteinbildenden Minerale, Teil Bestimmungstabellen: Stuttgart, E. Schweizerbart'sche verlagsbuchhandlung, **147**

Tsuboi, Seitaro, 1923, A dispersion method of determining plagioclase in cleavage flak *Mineralog. Mag.*, **20,** 108–122.

———, 1924, On the discrimination of mineral species in rocks: *Japanese Jour. Geol. Geog.*, **III,** no. 1, p. 19–26.

Wager, L. R., and Deer, W. A., 1939, Geological investigations in East Greenland, The petrology of the Skaergaard intrusion, Kangerdlugssuaq, East Greenla *Meddelelser om Grønland*, Bd. **105,** Nr. 4, 352 p.

Winchell, A. N., 1938, The anthophyllite and cummingtonite-grunerite series: *A Mineral.*, **23,** 329–333.

Manuscript received September 17, 1960.

THE AMERICAN MINERALOGIST, VOL. 46, JULY-AUGUST, 1951

THE EFFECT OF PARTICLE SIZE ON THE THERMAL PROPERTIES OF SERPENTINE MINERALS

EDWARD MARTINEZ, *Central Research Laboratories, American Smelting and Refining Company, South Plainfield, N. J.*

ABSTRACT

The effects of particle size of chrysotile and platy serpentine on the differential thermal and thermal gravimetric analyses have been investigated. It was found with DTA that decreasing the particle size decreased the starting and peak temperatures of the endothermic or dehydroxylation reaction and that the peak height of the exotherm was considerably increased although the peak temperature was not appreciably changed. As the chrysotile particle size decreased the endothermic peak temperature decreased from a maximum of 710° C. with no grinding, to a minimum of 670° C. when it was finely ground. When chrysotile samples from several sources were ground following a standard procedure, the DTA thermograms obtained were quite similar. TGA also showed the dehydroxylation (weight loss) occurring at lower temperatures when the samples were ground. The results indicate that if comparison between serpentine samples is the objective of a DTA-TGA study, the sample preparation is of utmost importance, otherwise differences noted may not be true differences but due to variations in particle size between samples. Data obtained with chrysotile and platy serpentine on a thermal increment diffractometer are given. DTA-TGA were also obtained on a brucite-carbonate sample indicating particle size has a similar effect on its endothermic reactions but it is not as large as those noted for the serpentine minerals.

INTRODUCTION

The literature contains many references to the thermal properties of the serpentine minerals, particularly chrysotile, with much of the reported data having been obtained using differential thermal and thermal gravimetric analyses. The two principal reactions with the serpentine minerals are a broad endotherm between 600° C. and 720° C. due to dehydroxylation of the mineral and an exothermic peak about 810° C. usually ascribed to the formation of olivine or forsterite. The reported results with chrysotile indicate wide differences of starting and peak temperatures for these reactions and these differences appear to be greater than the variations normally obtained due to the use of different equipment, varying size of samples, etc.

When the present DTA study of chrysotile was started, it was observed that the peak temperature for the endotherm was not constant and that occasionally shoulders occurred during the endothermic reaction suggesting the possibility that another reaction was taking place. The peak temperature for the exotherm remained fairly constant but the height and sharpness of the peak varied from run to run with the same sample. An investigation into the cause for this lack of reproducibility revealed that the particle size had a considerable effect on the endothermic and exothermic reactions for both chrysotile and platy serpentine; when

a standard grinding procedure was followed reproducible results were obtained.

Description of Equipment and Sample Preparation

Differential Thermal Analysis

The DTA unit, manufactured by the Robert L. Stone Co., Austin, Texas, utilizes the dynamic gas principle where a gas can flow through the sample and inert reference material during a run (Stone and Rase, 1957). Nitrogen was used as the flowing gas in all the tests reported. The temperature rate increase was approximately 10° C. per minute and the inert used was alundum. The Inconel sample holder is 1.5 inches in diameter by $\frac{5}{8}$ inch thick and the two cavities for the sample and inert are $\frac{1}{4}$ inch diameter by $\frac{3}{8}$ inch deep. Platinum-platinum, 10% rhodium thermocouples were used for both the differential and reference temperature thermocouples. The thermocouples were calibrated from time to time with quartz.

The differential temperature recording system contains an amplifier which is designed for adjustable range within wide limits. After grinding, the exothermic peak height of chrysotile became so large that the sensitivity of the amplifier output had to be decreased at about 750° C. to keep the recorder from running off scale during runs. In general the portion of the curve below 750° C. was run at ten times the sensitivity as that above 750° C. when ground samples of chrysotile were being run.

The chrysotile samples were obtained from crudes longer than one-half inch. The ends of the fibers were cut off with scissors and discarded to minimize contamination from the wall rock. The standard grinding procedure was as follows: A 210 mg. sample was weighed and split approximately into halves. Each half was ground in a Wig-L-Bug using a stainless steel vial with two pestles; every thirty seconds the grinding was stopped and the sample was scraped from the sides and ends of the vial to minimize packing. After grinding each half for a total of 180 seconds, the two halves were mixed and placed in the DTA holder. Approximately 500 to 550 mg. of Al_2O_3 were used as the inert.

The chrysotile samples that were not ground were pulled apart with tweezers and packed carefully around the thermocouples in the sample holder. This required great care and it is doubtful that packing from run to run was the same. When the sample was finely ground no difficulty in packing the sample around the thermocouple was experienced. Approximately 170 mg. could be packed in when the sample was unground.

Thermal Gravimetric Analysis

The gravimetric analyses were run on a Chevenard thermobalance (Duval, 1953) converted electronically for graphic recording by Gordor

and Campbell using a system similar to that described in their paper (1956). A Moseley Autograph X–Y recorder was used to plot the temperature-weight loss curves. A heating rate of 5° C. per minute was used with a one-gram sample, unless otherwise noted. A Spex Mixer/Mill was used for grinding the larger chrysotile and platy serpentine samples required for TGA.

Thermal Increment Diffractometer

The thermal increment diffractometer studies were run by Mr. William A. Bassett. The unit used has been described by Bassett and Lapham (1957). For the runs reported, copper radiation produced at 40 kilovolts and 17 milliamperes was used. While the temperature was being increased at a rate of approximately 10° C./minute, the goniometer was oscillated over one of the prominent peaks with an oscillating range of 2° 2θ. The heating was stopped and scans were made at temperatures which seemed significant.

The chrysotile specimen was ground to a fine powder in a Wig-L-Bug and the platy serpentine was ground in a mortar and pestle. The samples were prepared for the thermal increment diffractometer by sedimenting the powder onto a platinum-rhodium plate in distilled water. The water was drawn off and the specimen allowed to air dry. The plate with the layer of powder was then mounted on the heating element of the instrument. This method of preparation permitted a considerable degree of preferred orientation of flaky and fibrous minerals.

Test Results

DTA-TGA

The effect of particle size on the DTA of chrysotile was investigated by varying the time of grinding. The peak temperatures and heights of the reactions are given in Table I and the results of a microscopic examination of the ground samples in Table II. As the grinding time increased, the fiber lengths and widths decreased resulting in a decrease in the peak temperature for the endotherm from 710° C. in unground fiber carefully pulled apart with tweezers to a minimum of 670° C. with finely ground fiber; increased grinding time from 180 to 420 seconds did not decrease the endothermic peak temperature any further. The particle size did not change appreciably the peak temperature for the exotherm, but the sharpness and heights increased as grinding time increased.

Figure 1 shows the thermograms obtained with samples ground for different lengths of time. Included is a curve of a mixture of chrysotile half unground and half ground for 180 seconds resulting in two endothermic peaks.

After a standard procedure of grinding for 180 seconds was adopted,

Table I. Effect of Particle Size of Chrysotile on DTA Peak Temperatures and Heights of Exothermic and Endothermic Reactions

Grind. Time	Peak Temp., °C.		Ratio Peak Hts. Exoth./Endoth.
Seconds	Endoth.	Exoth.	
0	710	816	0.1
15	698	816	1.2
30	697	814	4.3
60	671, 693	813	11.3
90	671	812	12.0
180	670	812	13.7
420	671	812	11.4

Sample: Lake Asbestos of Quebec, Black Lake, P. Q.

extremely good reproducibility was obtained with the DTA. A number of chrysotile crude samples from other mines in Quebec gave very similar thermograms, as shown in Fig. 2.

The use of nitrogen as the dynamic gas flowing through the sample and reference resulted in a decrease of about 20° C. in the peak temperature of the endotherm compared to when no gas was used. The sweeping out of the products of reaction by the gas may be a contributing factor in obtaining good reproducibility.

Samples of ground and unground chrysotile were run on the thermobalance and the curves obtained are given in Fig. 3. The loss of weight due to dehydroxylation starts at a much lower temperature with the ground samples compared to one consisting of gross bundles of fiber. The small weight loss above 750°, the "high" temperature water, was still present after grinding.

Table II. Microscopic Examination of Ground Chrysotile

Grind. Time	Size of Bundle or Particle		Approx. Avg. Size	
Seconds	Lengths	Widths	Length	Width
15	100–5,500	40–900	3,000	400
30	30–4,000	10–600	2,000	150
60	20–2,000	8–200	1,200	50
90	10– 800	6–100	400	30
180	8– 160	4– 80	70	20
420	4– 60	<3– 30	30	9

Sample: Lake Asbestos of Quebec, Black Lake, P. Q.

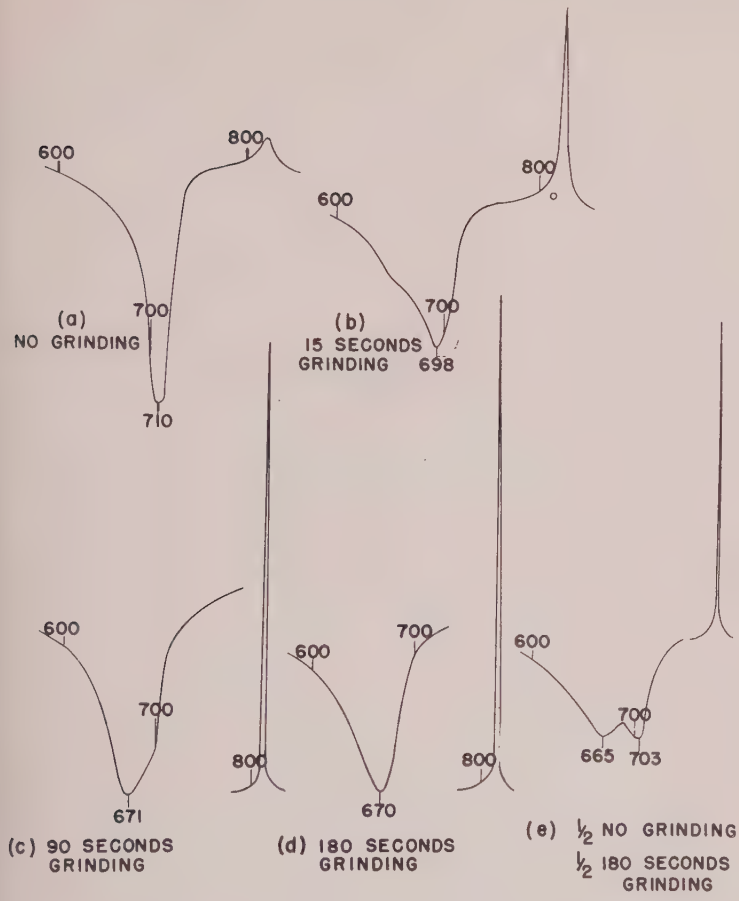

FIG. 1. Differential thermal analyses of chrysotile asbestos samples ground in Wig-L-Bug for varying lengths of time.

Platy serpentine was also run on the DTA and TGA and behaved in a very similar manner to chrysotile as indicated by the TGA curves in Fig. 4. In the DTA, grinding the sample resulted in a decrease in the starting and peak temperatures of the endotherm, and an increase in the peak height of the exotherm.

A 35×65 mesh sample of brucite containing carbonate was also run and the TGA curves are shown in Fig. 5. Decreasing the particle size reduced slightly the temperature at which the endothermic reactions in the DTA and weight losses in the TGA started for both brucite and carbonate. However, the effect was not as pronounced as those noted with

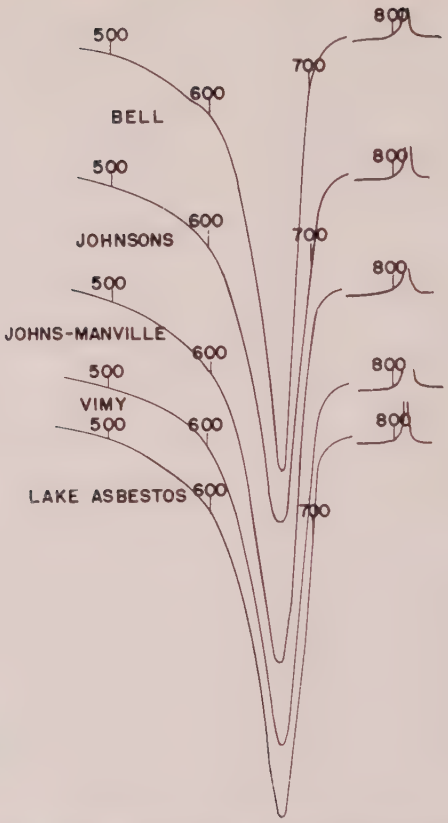

FIG. 2. Differential thermal analyses of chrysotile samples from various sour
Samples were prepared following a standard procedure of grinding for 180 seconds
Wig-L-Bug.

chrysotile. The TGA curves obtained with the brucite-carbonate sam
also include a run at a temperature rate increase of 10° C. as well as t
usual 5° C. per minute. The higher rate shifted the starting temperatu
for the weight losses to higher values. The results indicate that the p
ticle size had less effect on the starting temperatures of the breakdo
of the $Mg(OH)_2$ and carbonate than did the rate of temperature rise.

X-Ray Data

Unground samples of chrysotile were heated to 350°, 500°, 775°, 87
and 1100° C., allowed to cool to room temperature, and then *x*-ray p
terns obtained on the Picker unit. The samples heated to 350° and 500°
did not show any change from a standard unheated chrysotile; the 775°

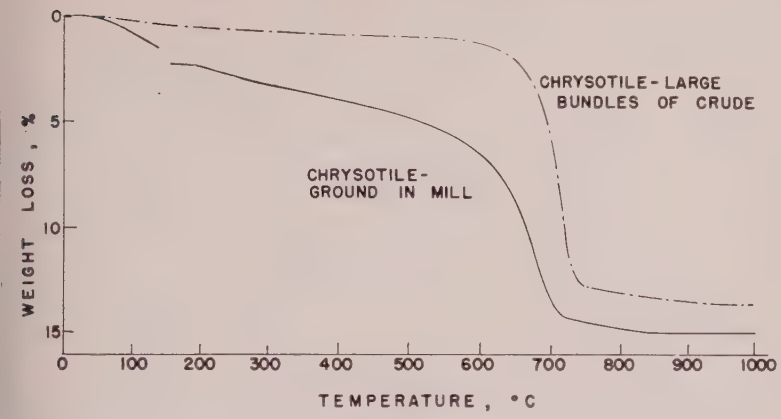

FIG. 3. Thermal gravimetric analyses of ground and unground chrysotile from the ke Asbestos of Quebec mine, Black Lake, P. Q. Thermograms very similar to the lower e were obtained when ground chrysotile samples from Asbestos and Thetford, P. Q., re run. Heating rate was 5° C./min.

mple was amorphous with some unidentified lines; and the 850° and 00° C. samples yielded sharp and well defined patterns of olivine.

Ground samples of chrysotile and platy serpentine were run on the rmal increment x-ray diffractometer. The temperature was raised at a te of approximately 10° C. per minute and the goniometer oscillated er a prominent peak. The intensity of certain peaks vs. temperature r chrysotile and platy serpentine is plotted in Fig. 6. Table III contains ta on chrysotile obtained from scans taken at 25°, 325°, and 515° C.,

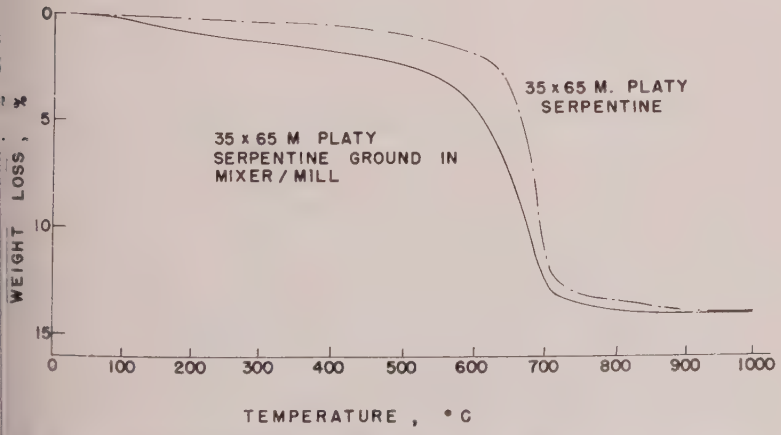

FIG. 4. Thermal gravimetric analyses of platy serpentine from Lowell, Vermont; heating rate was 5° C. per minute.

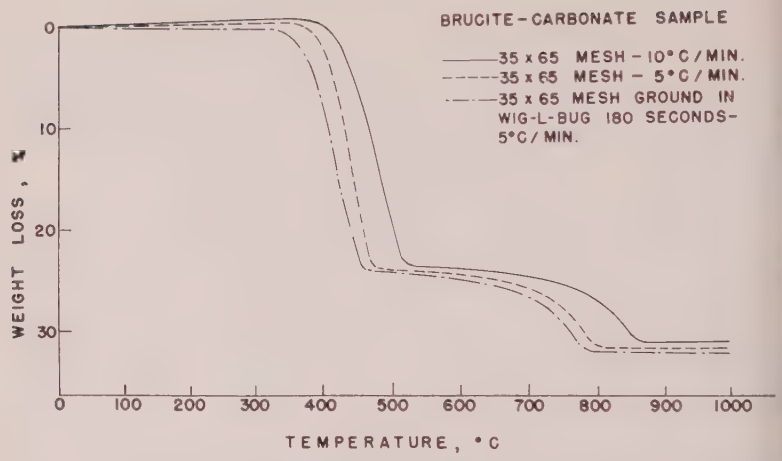

FIG. 5. Thermal gravimetric analyses of a brucite sample containing carbonate from Luning, Nevada.

and indicates that no major changes take place in chrysotile throughout this temperature range. However, the decrease in the 2.45 Å may be significant and should be more thoroughly investigated.

The *x*-ray data indicate that chrysotile and platy serpentine show little change until 475° C., above which the intensity of the 7.3 Å reflection

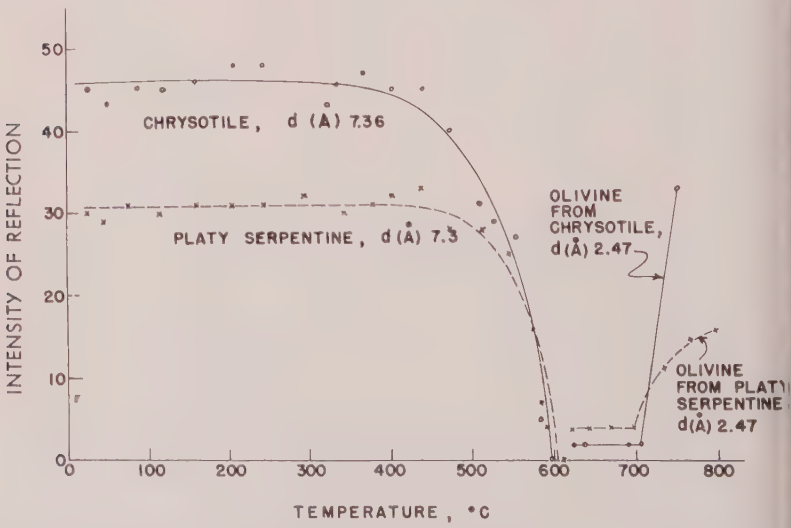

FIG. 6. Effect of temperature on reflection intensities of certain peaks of chrysotile and platy serpentine obtained on the thermal increment diffractometer.

TABLE III. THERMAL INCREMENT DIFFRACTOMETER *X*-RAY DATA ON CHRYSOTILE

25° C.		325° C.		515° C.	
d(Å)	Intensity	*d*(Å)	Intensity	*d*(Å)	Intensity
7.36	100	7.36	100	7.36	100
4.50	20	4.50	24	4.50	25
3.668	80	3.675	80	3.67	65
2.561	16	2.561	20	2.59	13
2.453	30	2.447	30	2.47	13

Sample: Lake Asbestos of Quebec, Black Lake, P. Q.

tion begins to decrease until it disappears about 600° C. when both become amorphous. In addition a slight expansion of the platy serpentine occurs above 400° C. Although weak olivine lines were noted at lower temperatures, they do not become prominent until about 740° C. The olivine produced by heating both samples appeared to be near the magnesium rich or chrysolite end of the isomorphous series chrysolite-fayalite.

DISCUSSION

That particle size can alter the shape and position of peaks in the DTA of some minerals has been recognized for some time. Smothers and Chiang (1958) and Mackenzie (1957) discuss this to some extent and give many references to investigations of various minerals where the effect of particle size on the thermal properties has been reported. There have been numerous publications on the DTA and TGA of serpentine minerals, but the effect of particle size has not been noted although Sabatier (1950) investigated this effect in the chlorites. Attempts have been made to identify the source of chrysotile samples (Pundsack, 1955; Woodrooffe, 1956) or to differentiate between fiber and matrix (Kalousek and Muttart, 1957; Lyon and Tuddeham, 1959) by means of DTA or TGA. Since the particle size has such a large effect on both reactions and the thermograms for chrysotile and platy serpentine are so similar, the sample preparation becomes of utmost importance if the objective of the study is comparison between samples. The DTA curve with half ground and half unground chrysotile resulting in two distinct endotherms (Fig. 1*e*) shows clearly the difficulty involved since such a pattern would normally be interpreted as being caused by two reactions, possibly leading to the conclusion that two minerals were present.

Pundsack has suggested that the ratios of endothermic to exothermic peak heights and areas vary depending upon the source of the chrysotile

sample. However, the ratios of exothermic endothermic peaks given in Table I indicate the dependence of this ratio on the grinding time or particle size since it varied from 0.1 with no grinding to over 13 with 180 seconds in the Wig-L-Bug. When crudes from various sources were prepared using a standard grinding procedure, no appreciable differences in ratios were obtained between the samples tested. It should be noted that when the tests with the DTA were run in duplicate, varying the length of time in the Wig-L-Bug, reproducibility was poor with insufficient grinding. The peak temperatures for the main endotherm and the position of the shoulders varied as did the peak heights of the exothermal reaction with two samples ground for the same length of time. However, samples ground very fine gave excellent reproducibility.

The TGA results obtained with the serpentine minerals (Fig. 3 and 4) indicate the difficulty in determining the starting temperature for the dehydroxylation. Comparison of TGA results obtained with samples from various sources as Woodrooffe (1956) has done is complicated by the fact that some of the differences noted may be due to particle size variations between samples. With granular material it may be possible to grind and screen the sample to produce a closely sized product giving reproducible results; however, preparing chrysotile samples having similar particle size or surface areas presents a more difficult problem.

The decrease in the starting temperatures for dehydroxylation when the serpentine minerals are ground may be caused simply by the smaller particle size producing a greatly increased surface area making it easier for the OH^- to leave the crystal. However, grinding may have altered the bond energy distribution of the particles (Stone, 1954) and thus some of the bonds usually broken by high temperatures in a large particle may have been broken or altered in grinding. The TGA curves substantiate the decrease in temperature for dehydroxylation noted in the DTA when the sample is ground. This eliminates the possibility that the DTA results were due solely to differences in conductivity or porosity between the ground and unground samples packed in the holder.

The thermal increment diffractometer data indicate a striking similarity between chrysotile and platy serpentine. Below 500° C. both minerals undergo only minor changes. Above 500° C. the changes noted were due to the dehydroxylation of the samples and correspond to the endotherm obtained in the DTA. The removal of the OH ions leaves a chaotic arrangement of magnesium, iron, silicon, and oxygen which recombine to form olivine at about 740° C.

The increased peak height of the exothermic reaction of the serpentine minerals noted in the DTA may be due to the finer size and more intimate mixture of the ground sample causing the reaction to occur over

much shorter temperature range and resulting in a much sharper reaction. However, the chrysotile structure and the reactions taking place on heating are not yet completely understood. There are indications that it may be in the form of tubes (Turkevich and Hillier, 1949; Bates, *et al.*, 1950; Noll and Kircher, 1950) with plugs of water blocking the ends (Young and Healey, 1954) and amorphous appearing material surrounding the tubes (Bates, 1958; Comer, 1959). There is a small, but reproducible weight loss occurring about 800° C. (Woodrooffe, 1956; Kalousek and Muttart, 1957) that is not completely understood, but which was not eliminated by grinding. The formation of enstatite as well as olivine on heating has been reported (Calliere, 1936; Strelov, 1953). Although the exothermic reaction at 812° C. is normally ascribed to the formation of forsterite or olivine, the thermal diffraction data show that formation of olivine starts at about 740° C. Pundsack (1956) has noted the formation of forsterite below 800° C. It would appear from the above that the thermal reactions occurring in the serpentine minerals may be more complicated than usually assumed and that further study is necessary for a better understanding of the reactions taking place.

Acknowledgments

The author is indebted to Mr. William A. Bassett for running the tests on the thermal increment diffractometer at Columbia University and interpreting the results; to Mr. Robert Haagensen of ASARCO for the microscopic study of the ground chrysotile samples; and to Dr. Max L. Hollander of ASARCO for his helpful suggestions and assistance.

References

Bassett, W. A. and Lapham, D. M. (1957), A thermal increment diffractometer, *Am. Mineral.*, **42,** 548–555.

Bates, T. F., Sand, L. B., and Mink, J. F. (1950), The tubular crystals of chrysotile asbestos, *Science*, **111,** 512–513.

Bates, T. F. (1958), Selected electron micrographs of clays and other fine-grained minerals, *Circ. No. 51, Col. of Min. Ind., Penn. State Univ.*, 21–28.

Calliere, S. (1936), Study of the serpentine minerals, *Bull. Soc. Franc. Mineral.*, **59,** 163–326.

Comer, J. J. (1959), The electron microscope in the study of minerals and ceramics, *T.P.* **257,** ASTM, 105–107.

Duval, C. (1953), Inorganic Thermogravimetric Analysis, Elsevier, N. Y., 13–30.

Gordon, S. and Campbell, C. (1956), Electronic conversion for graphic recording with the Chevenard photographically recording thermobalance, *Anal. Chem.*, **28,** 124–126.

Kalousek, G. L., and Muttart, L. E. (1957), Studies on the chrysotile and antigorite components of serpentine, *Am. Mineral.*, **42,** 1–22.

Lyon, R. J. P. and Tuddeham, W. M. (1959), Quantitative mineralogy as a guide in exploration, *AIME Trans.*, **214,** 1233–1237.

MACKENZIE, R. C. (1957), The Differential Thermal Investigations of Clays, Mineralogica Society, London.

NOLL, W. AND KIRCHER, H. (1950), The morphology of chrysotile asbestos, *Naturwissen schaften*, **37,** 540–541.

PUNDSACK, F. L. (1955), The properties of asbestos. I. The colloidal and surface chemistr of chrysotile, *J. Phys. Chem.*, **59,** 892–895.

SABATIER, G. (1950), Influence of the crystal dimensions of chlorites on their differentia thermal analysis curves, *Soc. Franc. Min. Crist. Bull.*, **73,** 43–48.

SMOTHERS, W. J. AND CHIANG, Y. (1958), Differential Thermal Analysis: Theory an Practice, Chemical Publishing Co., N. Y.

STONE, R. L. AND RASE, H. F. (1957), Differential thermal analysis: New technique fo testing silica-alumina catalysts, *Anal. Chem.*, **29,** 1273–1277.

STONE, R. L. (1954), Preliminary study of the effects of water vapor pressure on th thermograms of kaolinitic soils, *Clays and Clay Minerals, Second Nat'l Conf.*, **195.** 315–323.

STRELOV. K. K. (1953), Transformation of chrysotile asbestos on heating in the temper ture interval 500–1100° C., *Zhur. Priklad. Khim.*, **26,** 1091–1094; *C.A.* (1954), **4.** 7474C.

TURKEVICH, J. AND HILLIER, J. (1949), Electron microscopy of colloidal systems, *Ana Chem.*, **21,** 475–485.

WOODROOFFE, H M. (1956), Pyrolysis of chrysotile asbestos fibre, *Trans. Can. Inst. Min. & Met.*, **59,** 363–368.

YOUNG, G. J. AND HEALEY, F. H. (1954), The physical structure of asbestos, *J. Phy Chem.*, **58,** 881–884.

Manuscript received September 17, 1960.

THE AMERICAN MINERALOGIST, VOL. 46, JULY–AUGUST, 1961

SYNTHESIS AND CRYSTAL CHEMISTRY OF GYROLITE AND REYERITE

J. W. Meyer and K. L. Jaunarajs, *Johns-Manville Research Center, Manville, New Jersey.*

Abstract

Phase equilibria in the system $CaSiO_3$-SiO_2-H_2O have been determined by using hydrothermal techniques. These experiments combined with dehydration studies of pure compounds have shown that reyerite has a composition $Ca_2[Si_4O_9(OH)_2]$. Attempts to synthesize pure gyrolite were unsuccessful due to a gradual transformation of gyrolite to reyerite. During this inversion mixed-layer gyrolite-reyerite phases have been observed. On the basis of selected area electron diffraction patterns and (000l) diffraction intensities it is concluded that both minerals must be composed of the same structural elements which probably have trigonal symmetry. These structural elements are stacked in a perfect way to form reyerite (c=18.7 Å). Due to a 60° rotation of successive layers the expanded gyrolite lattice (c=22.1 Å) is obtained. Gyrolite having the composition $Ca_2[Si_4O_9(OH)_2]\cdot 3H_2O$ cannot be transformed into reyerite by dehydration. Therefore it has to be assumed that the elementary layers are undulating sheets. In gyrolite the layers are separated due to an improper fit so that molecular water penetrates between the sheets.

Electron microscopy and diffraction indicate that tobermorite appears as flaky and fibrous crystals.

Introduction

The mineral gyrolite was first described from Skye (Scotland) by T. Anderson in 1851. Chemical analysis indicated the mineral to be a hydrated calcium silicate with approximate composition, $2CaO\cdot 3SiO_2\cdot 3H_2O$. Gyrolite has since been found in other localities. In their comprehensive study of a natural gyrolite sample from Bombay (India), Mackay and Taylor (1953) concluded that the chemical formula of gyrolite is $2CaO\cdot 3SiO_2\cdot 2H_2O$. Their x-ray single crystal examination showed that the mineral is hexagonal with a=9.72 Å and c=132.8 Å (=6×22.13 Å). On being heated gyrolite loses water in two distinct stages. After heating to 450° C. about 75% of the water content is lost without appreciable changes in the crystal structure. The second dehydration stage is observed between 550° and 850° C., where the rest of the water is lost. This step is accompanied by complete destruction of the structure. According to Mackay and Taylor (1953) the gyrolite crystal is thereby transformed in an ordered way to pseudowollastonite and to amorphous silica.

The mineral reyerite was discovered by Giesecke in 1811 in Greenland and was described and named by Cornu (1907). In 1914 Hövig described a hydrated calcium silicate mineral having the chemical composition $3CaO\cdot 2SiO_2\cdot \frac{1}{2}H_2O$, which was named truscottite. The identity of this mineral and its relationship to reyerite was in doubt for many years until Strunz and Micheelson (1958) established that reyerite is identical

with truscottite. Although truscottite is a well established mineral name, the name reyerite actually has priority and will be used exclusively in this paper. Mackay and Taylor (1954) demonstrated that truscottite (=reyerite) from Benkulen (Sumatra) is a distinct mineral species, though one closely related to gyrolite. They confirmed Hövig's chemical formula and showed that reyerite has trigonal symmetry. The unit cell dimensions were found to be $a=9.72$ Å and $c=18.7$ Å. Dehydration characteristics of this mineral are similar to those of gyrolite. About 50 per cent of the water is lost upon heating to 450° C., apparently without affecting the crystal structure. The second dehydration step ends at about 850° C., when the remainder of the water is lost. According to Mackay and Taylor (1954), this stage is connected with the formation of an unidentified, unoriented phase. After prolonged heating at 1000° C. the main products are wollastonite and cristobalite with a little pseudo-wollastonite.

Both reyerite and gyrolite have a trigonal or hexagonal unit cell with identical a-parameters ($a=9.72$ Å). Significant differences exist in the chemical composition, in the c-axis dimension, which is 18.7 Å for reyerite and 132.8 Å ($=6\times22.13$ Å) for gyrolite, and in the dehydration characteristics. Mackay and Taylor (1954) observed that $000l$ reflections occur in strong and weak bands at similar θ values for both minerals. This and the identical a-parameters suggest that gyrolite and reyerite may have the same structural layer units. In a recent discussion by Mamedov and Belov (1958) of the crystal structures of mica-like calcium silicates the unit cell dimensions of gyrolite and reyerite reported by Mackay and Taylor (1954) were accepted. Strunz and Micheelson (1958) in a report on their study of calcium phyllosilicates indicated that gyrolite is a water-expanded reyerite. This hypothesis was reflected in the chemical formulas of the two minerals. Reyerite was assumed to have a $CaO:SiO_2$ ratio of 0.75 which leads to the idealized formula $Ca_{9.2}[(OH)_3Si_6O_{15}]$. Gyrolite presumably has the same structural units separated by molecular water ($3H_2O$ per formula unit).

Flint, McMurdie and Wells (1938) attempted a synthesis of these compounds. They reacted mixtures of lime and silica under saturated steam pressures at 250° C. for 40 days and obtained gyrolite. From x-ray powder patterns they concluded that both species were identical. Peppler's experiments (1955) led to the conclusion that gyrolite was metastable with respect to xonotlite ($6CaO\cdot6SiO_2\cdot H_2O$) and quartz. He did not observe reyerite as reaction product. Assarsson (1957) synthesized gyrolite under saturated steam conditions at temperatures between 160° and 220° C. but found no reyerite in these samples. Most synthetic preparations of these authors were carried out in short periods of time only. Therefore,

is probable that equilibrium was not attained, since hydrothermal reactions in the system $CaSiO_3$-SiO_2-H_2O are frequently very sluggish. Due to this fact one cannot deduce the exact chemical composition of gyrolite from short hydrothermal runs. The synthesis of reyerite was recently reported by Buckner, Roy and Roy (1960) in their studies in the system $CaSiO_3$-H_2O. However, the stability range and composition of reyerite or gyrolite was not discussed.

In order to study the synthesis, stability and composition of gyrolite and reyerite, a systematic investigation of the phases in the system $CaSiO_3$-SiO_2-H_2O was undertaken. The reactions were carried out mainly at saturated steam pressures for periods of time ranging from 24 hours to 4 months. Some runs were made under supersaturated steam conditions (up to 20,000 psi). The reaction products were examined using *x*-ray powder diffraction, electron microscope, electron diffraction, dehydration and infrared absorption methods. On the basis of the results obtained some conclusions have been reached about the relations between the synthetic compounds gyrolite and reyerite, and their relationship to the natural minerals. This relationship has great bearing on the chemical composition of gyrolite and reyerite.

Synthesis and Identification of Samples

Preparation of samples

Many substances which might be used as sources for silica are not suitable for hydrothermal reaction studies, either due to their low reactivity (e.g. pulverized quartz) or to undesirable impurities (diatomaceous earths). For these experiments silicic acid (Mallinckrodt, Special Bulky) was found to be sufficiently reactive and pure. It was used for most syntheses. A few runs were made using the much less reactive tripoli in order to duplicate several reactions reported by Flint, McMurdie and Wells (1938).

Calcium oxide, which was freshly prepared by igniting c.p. grade $CaCO_3$ at 1000° C. for about four hours, and c.p. grade $Ca(OH)_2$, furnished the calcium for these reactions.

The two components at the desired CaO/SiO_2 ratios were thoroughly dry mixed in sealed containers before they were used for the reactions. After addition of 35 ml. distilled water to the dry-mixed starting materials the slurry was reacted in stainless steel vessels of 70 ml. capacity. The ratio of solid to liquid was varied between 1:3 and 1:20 in order to find the most reactive conditions. The reaction vessels were placed in a constant temperature oven equipped with a fan. A few high pressure reactions were made using equipment similar to that described by Tuttle (1948) which has separate controls for pressure and temperature. Sealed

platinum tubes containing the sample-water mixture were placed in stainless steel bombs for the reaction.

Several experiments were made using a Morey bomb of 20 cc. capacity in the temperature range of 340° to 425° C. and pressures up to 5000 psi These runs were designed to determine the upper stability limit o reyerite. The starting material for these preparations was a well crystal lized synthetic reyerite.

After reaction the products were removed from the vessel, immediately filtered, washed with acetone and dried in a CO_2-free atmosphere a 105° C. for one hour.

Composition of samples

Seven ternary phases are known to exist in the system $CaSiO_3$-SiO_2 H_2O. Six of these are natural minerals or mineral groups: gyrolit ($2CaO \cdot 3SiO_2 \cdot 2H_2O$), reyerite ($CaO \cdot 2SiO_2 \cdot \frac{1}{2}H_2O$), okenite ($CaO \cdot 2SiO_2 \cdot 2H_2O$), nekoite ($CaO \cdot 2SiO_2 \cdot 2H_2O$), xonotlite ($6CaO \cdot 6SiO_2 \cdot H_2O$), an the tobermorite group ($4\text{-}5CaO \cdot 5SiO_2 \cdot nH_2O$). A synthetic ternary phas of variable composition has been called CSHI: it is related to the tober morite group minerals (Heller and Taylor, 1951), but can be distinguishe from tobermorite on the basis of its x-ray pattern. Okenite and nekoit have never been reported as synthetic phases.

Mixtures of CaO and SiO_2 having C/S ratios* from 0.5 to 1.0 were sul jected to hydrothermal treatment. A list of significant runs is given i Table 1. In order to attain equilibrium rapidly, temperature or tim must be increased, or a lower solid-to-liquid ratio may be used. Th effects of these variables can be easily studied because the reactions a quite sluggish at lower temperatures. Attempts to increase the rate reaction by employing high-pressure techniques were not successf (Table 2). A number of runs which were made to establish the upp stability limit of reyerite are also listed in Table 2.

Reaction products were obtained from samples with C/S ratios 0. 0.67, 0.74, 0.8, and 1.0, which were treated hydrothermally at temper tures between 145° and 320° C. The experiments were frequently e tended over long periods of time in order to test the stability of a pa ticular phase. If equilibrium is reached, the mineralogical composition indicative of the chemical composition of the phases.

Methods of Identification

Since most phases formed under these conditions are extremely fi grained, x-ray diffraction, differential thermal analysis, electron micr

* Lime-to-silica molar ratio.

TABLE 1. LIST OF REPRESENTATIVE RUNS

Run No.	CaO/SiO_2	Temp. ° C.	Press. psi	Time days	Solid/ liquid	Starting Materials	Phases Present
1	0.50	170	114	6	1.3	CaO+silicic acid	CSHI (G)
2	0.50	180	145	7	1.9	CaO+silicic acid	G
3	0.50	188	174	3	1.9	CaO+silicic acid	G
4	0.50	220	336	14	1.3	CaO+silicic acid	G (R)
5	0.50	220	336	14	1.9	CaO+silicic acid	G, G+R
6	0.50	220	336	42	1:3	CaO+silicic acid	R, (G)
7	0.50	220	336	42	1:9	CaO+silicic acid	R+G
8	0.50	220	336	112	1:9	CaO+silicic acid	R
9	0.50	250	576	5	1:8	CaO+silicic acid	G
10	0.50	270	797	7	1:10	CaO+silicic acid	R (G)
11	0.50	282	958	7	1:10	CaO+silicic acid	R
12	0.50	300	1245	5	1:19	CaO+silicic acid	R
13	0.50	300	1245	30	1:30	CaO+silicic acid	R (X, α)
14	0.50	320	1600	8	1:10	CaO+silicic acid	R (α)
15	0.50	320	1600	7	1:10	Sample 14	R (α, X)
16	0.50	320	1600	17	1:10	Sample 15	R, X, α
17	0.55	300	1245	30	1:10	CaO+silicic acid	R (X, α)
18	0.60	300	1245	30	1:10	CaO+silicic acid	R (X, α)
19	0.60	320	1600	8	1:10	CaO+silicic acid	R
20	0.60	320	1600	8	1:10	Sample 19	R (α)
21	0.60	320	1600	15	1:10	Sample 19	R (α, X)
22	0.60	320	1600	25	1:10	Sample 19	R, X
23	0.66	220	336	14	1:6	CaO+silicic acid	CSHI, (G+R)
24	0.66	220	336	42	1:9	CaO+silicic acid	G+R
25	0.66	220	336	112	1:9	CaO+silicic acid	R+G
26	0.66	250	576	5	1:8	CaO+silicic acid	G
27	0.66	250	576	21	1:10	CaO+silicic acid	R, (R+G)
28	0.66	250	576	40	1:20	$Ca(OH)_2$+tripoli	X, R, T, Q
29	0.66	250	576	40	1:20	CaO+tripoli	Q, X, (T)
30	0.66	250	576	40	1:20	$Ca(OH)_2$+silicic acid	R (T, X)
31	0.66	250	576	40	1:20	CaO+silicic acid	R (R+G)
32	0.66	270	797	7	1:10	CaO+silicic acid	R (R+G)
33	0.66	300	1245	5	1:19	CaO+silicic acid	R (X)
34	0.67	300	1245	30	1:10	CaO+silicic acid	R, X
35	0.74	220	336	14	1:3	CaO+silicic acid	G (X)
36	0.74	220	336	42	1:9	CaO+silicic acid	R, G, (X)
37	0.74	220	336	112	1:9	CaO+silicic acid	X, G, R
38	0.8	220	336	14	1:9	CaO+silicic acid	X, (G)
39	0.8	220	336	42	1:9	CaO+silicic acid	X (G)
40	0.8	220	336	112	1:9	CaO+silicic acid	X (G)
41	0.8	250	576	5	1:8	CaO+silicic acid	X
42	0.8	270	797	7	1:10	CaO+silicic acid	X
43	0.8	300	1245	5	1:19	CaO+silicic acid	X (R)
44	1.0	90	Atmos	6 hr	1:9	CaO+silicic acid	CSHI
45	1.0	170	100	1 hr	1:9	Sample No. 33	CSHI, (T)
46	1.0	170	100	3 hr	1:9	Sample No. 33	CSHI, T
47	1.0	170	100	4 hr	1:9	Sample No. 33	CSHI, T
48	1.0	170	100	20 hr	1:9	Sample No. 33	T, (CSHI)
49	1.0	170	100	8	1:4	CaO+silicic acid	T, (CSHI)
50	1.0	250	576	5	1:8	CaO+silicic acid	X, CSHI, $Ca(OH)_2$
51	1.0	300	1245	5	1:19	CaO+silicic acid	X

Abbreviations: G=Gyrolite X=Xonotlite
R=Reyerite R+G=Reyerite-gyrolite mixed layer material
T=Tobermorite ( )=minor amount present
α=α-Cristobalite

TABLE 2. DATA ON HIGH PRESSURE OR HIGH TEMPERATURE RUNS

Run No.	CaO/SiO_2	Temp. ° C.	Press. psi	Time hrs.	Solid/ Liquid	Starting Materials	Phases Present
52	0.50	425	4000	192		Sample 2 (R)	R, α, X, W
53	0.50	420	4000	67		Sample 2 (R)	R
54	0.50	365	3500	192		Sample 2 (R)	X, R, α
55	0.50	367	3500	38		Sample 2 (R)	R
56	0.50	362	500	12		Sample 2 (R)	R
57	0.50	340	3000	240		Sample 2 (R)	X, R, α
58	0.5	210	20,000	30	1:2.3	CaO+silicic acid	(G)
59	0.5	220	20,000	4	1:2.3	CaO+silicic acid	(G)
60	0.5	220	20,000	7	1:2.3	Sample No. 2	G
61	0.5	230	20,000	6	1:2.3	Sample No. 2	G
62	0.5	240	20,000	3	1:2.3	Sample No. 2	G
63	0.5	265	15,000	15	1:2.3	Sample No. 2	R

Abbreviations: R = Reyerite
X = Xonotilte
α = α-Cristobalite
W = Wollastonite

copy and diffraction, infrared spectroscopy and thermobalance metho were employed for identification.

X-ray powder diffraction

All phases which appear in the system $CaSiO_3$-SiO_2-H_2O can be id tified by *x*-ray powder diffraction methods. A list of powder diffract patterns of calcium silicates, which was found to be very accurate, been collected by Heller and Taylor (1956). Due to the fact that gyro and reyerite have the same *a*-parameter, all (*hki*0) reflections have id tical spacings. Differences between the two phases are most apparent their (000*l*) reflections. It was found that tobermorite and CSHI can distinguished on the basis of their strongest diffraction line, which ha spacing of 3.03 Å for CSHI and 3.07 Å for tobermorite. Kalousek (19 used the same criterion. All other phases in this system have disti powder patterns.

X-ray powder diffraction methods were used to study all react products. The results of this investigation have been incorporated Table 1. Since it is quite difficult to detect minor components with method, electron diffraction and microscopy were used to study samp which were close to the ideal composition of the phases.

Electron diffraction and microscopy

Grudemo's examination of the synthetic phases formed in the sys CaO-SiO_2-H_2O at low temperatures demonstrated the value of a c bined electron microscopy-selected area diffraction study for a r eralogical characterization of reaction products. Such compounds

equently very fine-grained, and electron microscopy allows a morpho-gical study of these phases. Many of the compounds which were in-stigated in the course of this work have similar habit; gyrolite, yerite, and tobermorite always appear as thin hexagonal flakes, fibrous obermorite" and xonotlite as fibers. CSHI is present as "crumpled ils." In order to distinguish phases of similar morphology an identifica-n of the crystals by selected area diffraction methods is absolutely cessary.

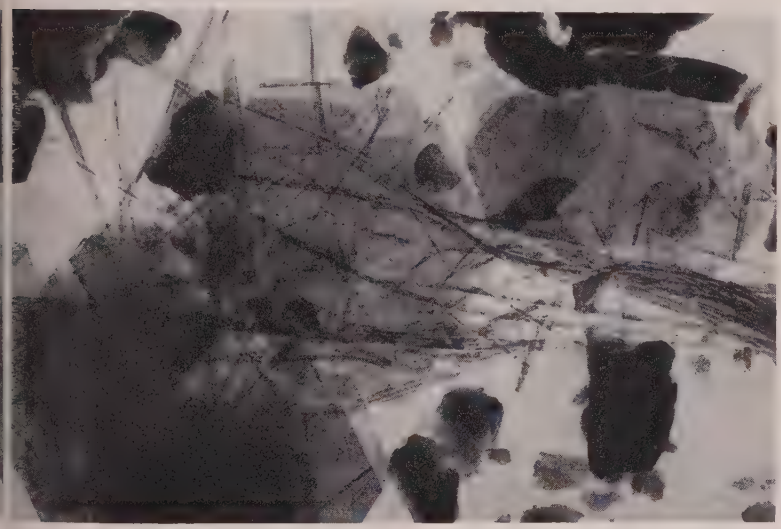

FIG. 1. Electron micrograph of synthetic tobermorite (24,000×)
Hydrothermal treatment of 0.8 C/S mixture at 170°C.

A typical electron micrograph of synthetic tobermorite is shown in g. 1. Selected-area electron diffraction of the platy phase (Fig. 2) gave sharp ($hk0$) pattern of tobermorite ($a=11.2$ Å, $b=7.3$ Å). These ystals, always lying on (001) show strong pseudo-halving of b. The ong reflections can be indexed in terms of a pseudo-cell with $a=5.6$ Å d $b=3.65$ Å. The weak reflections are elongated into streaks parallel to while the maxima on these streaks appear in positions which are in-xable on the basis of the larger unit cell. Similar features have been ob-ved by Gard, Harrison and Taylor (1959) on their synthetic materials. is interesting to note that the $00l$ spacing as determined by x-ray dif-ction is 11.0 Å and does not shift upon heating. A selected area dif-ction pattern of the fibrous phase is shown in Fig. 3. It consists of ong arcs, which suggest a b-spacing of 7.3 Å parallel to the fiber axis. ositive identification of this phase is not possible because the spacings

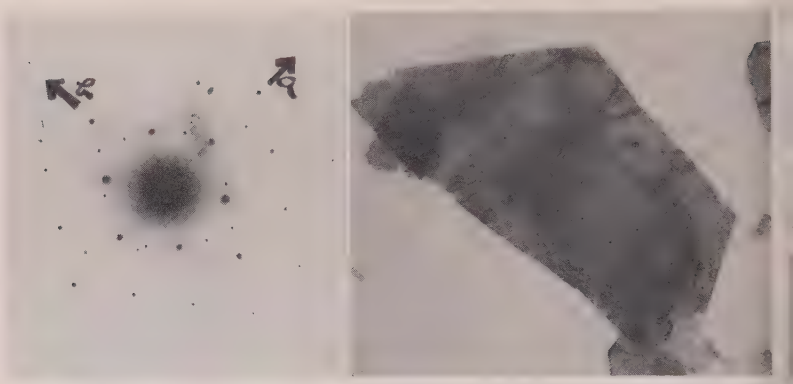

FIG. 2. Selected area diffraction pattern and corresponding micrograph (12,000×) of a platy tobermorite crystal. (C/S 0.8, 170°C.)

of the strong arcs correspond to either tobermorite or xonotlite. Sor electron micrographs seem to suggest that the platy tobermorite brea up parallel to its *b*-axis into these small fibers. Kalousek and Preb (1958) and Gard *et al* (1958) have published such micrographs. Materi consisting exclusively of crinkled foils never give clear electron diffra tion patterns. Their *x*-ray diffraction patterns always show a broad pe at 3.04 Å which is characteristic for CSHI.

Synthetic reyerite always consists of thin flakes. Selected area electr diffraction of this crystal gives a sharp, hexagonal pattern with $a = 9.7$ (Fig. 4). Intense peaks are indexed as $(20\bar{2}0)$, $(21\bar{3}0)$ and $(41\bar{5}0)$. similar pattern is obtained from a synthetic gyrolite. Since natural rey ite was found by single crystal *x*-ray diffraction methods to have trigo symmetry (Mackay and Taylor, 1953) which is in contrast to the pres

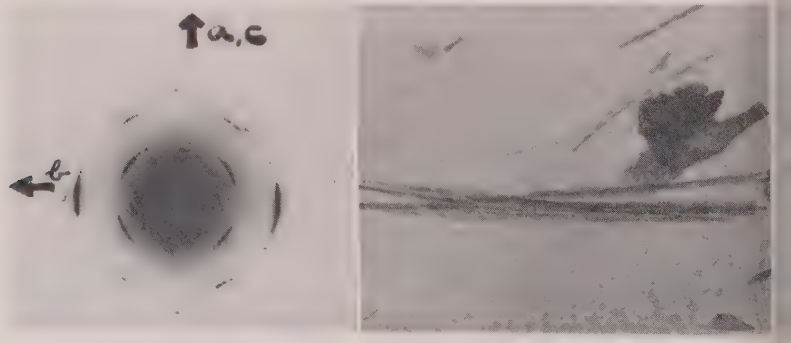

FIG. 3. Selected area diffraction pattern and micrograph (12,000×) of a bundle of tobermorite fibers (C/S 0.8, 170°C.)

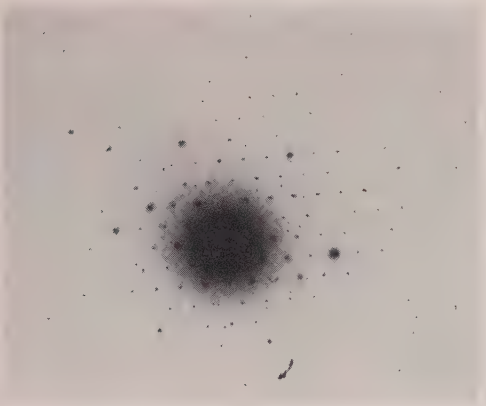

FIG. 4. Selected area diffraction pattern of synthetic reyerite (C/S 0.5, 300°C.) showing a sharp hexagonal pattern with $a=9.7$ Å.

ndings on synthetic material, natural minerals were also investigated in he course of this study. Selected area diffraction patterns of gyrolite rom Bombay, India (AMNH No. 12587) and of reyerite from Niakor-ak, Greenland (USNM No. 4016) were similar to the pattern in Fig. 4, a that both minerals have hexagonal Laue symmetry. A preliminary ingle-crystal *x*-ray study revealed that reyerite from Greenland is ctually monoclinic, pseudo-trigonal. It is quite clear that gyrolite and eyerite are structurally related because the intensities and spacings of *hki*0) peaks are very similar. This similarity of the (*hki*0) patterns is the eason why the two mineral species cannot be distinguished by selected rea diffraction methods.

Xonotlite appears under the electron microscope as a bladed mineral. lectron diffraction methods always give (*hk*0) Laue patterns with *b* as ber axis.

Thermal dehydration characteristics

Differential thermal analysis and thermobalance curves were obtained rom the synthetic phases gyrolite, reyerite, tobermorite, xonotlite and SHI. *X*-ray powder diffraction methods were used to interpret the hase changes at elevated temperatures.

Upon heating to 200° C. gyrolite loses about 7% water, which corre-onds to about two-thirds of its total water content. No structural anges were observed. The rest of the water is lost between 600° and 0° C. (about 4%). In the course of this reaction the gyrolite lattice is mpletely destroyed. After an exothermic reaction at 825° C., diffraction nes of wollastonite (β-$CaSiO_3$) appear and are strengthened by heat

treatment at higher temperatures. A trace of pseudo-wollastonite is fr quently observed.

Reyerite experiences a water loss of about 1% at 200° C. witho changes in crystal structure. The rest of the water (about 4%) is drive off between 600° and 800° C. In this temperature range the (*hki*0) r flections of reyerite, which are more stable than the (000*l*) diffractio peaks, slowly fade away while faint lines of pseudo-wollastonite ($CaSiO_3$) appear. After an exothermic reaction at 835° C. reyerite h been completely destroyed. Pseudo-wollastonite is now the major co ponent. Often a small amount of wollastonite is detected.

Due to the fact that gyrolite and reyerite have a C/S ratio of less tha 1.0, silica must be present in the high temperature phases. It was not d tected, however, as a crystalline compound by *x*-ray diffraction metho The present findings disagree with the observations on natural cryst by Mackay and Taylor (1953), who found that gyrolite is converted pseudo-wollastonite and reyerite to wollastonite upon heating to 1000° It is possible that the difference between the high-temperature produc of natural minerals and synthetic materials may be due to the grain si A small crystal size could favor a rapid inversion of the initially form pseudo-wollastonite to the stable wollastonite.

Synthetic tobermorite shows a partial dehydration if heated to abo 500° C. This dehydration is not accompanied by a one-dimensional latt shrinkage. At about 810° C. an exothermic reaction takes place duri which the material is transformed to wollastonite. The synthetic m terial seems to correspond in that respect to the tobermorite from Lo Eynort, Scotland (Gard and Taylor, 1957).

Synthetic xonotlite is converted to wollastonite at about 800° C. T reaction is connected with the loss of hydroxyl groups.

Differential thermal analysis or thermobalance methods are not sen tive enough to detect mixtures of several components. A proper ident cation of such mixtures must be made by other means.

Infrared spectroscopy

A Perkin Elmer 12C spectrometer was used to obtain spectra in t range of 2 to 15 micron wavelengths. The samples were dispersed in n eral oil on sodium chloride sample plates. The resulting spectrogra were corrected for radiation curve, mineral oil, atmospheric water vap carbon dioxide and back scattering.

Infrared absorption spectra of xonotlite and tobermorite were cussed extensively by Kalousek and Roy (1957). Since our patterns co sponded closely to the ones presented by those authors, only gyrolite reyerite curves will be presented here (Fig. 5).

The infrared absorption spectrum of synthetic reyerite (curve 1) shows that the stoichiometric water in this sample consists of hydroxyl ions (peak at 2.7 microns). In synthetic gyrolite (Fig. 5, curve 2) two kinds of (OH) can be distinguished; hydroxyl ions (peaks at 2.7 microns) and non-ionic (OH) groups (peak at 2.9 microns). The large amount of hydrogen bonding suggests that these non-ionic (OH) groups are present as water. This water is tightly bound, because the (OH) arm neither flexes nor rotates (no 6.7 micron peaks). A similar arrangement is found in layer silicates, such as vermiculite.

The main region of silicon-oxygen vibrations (between 8 and 12 micron

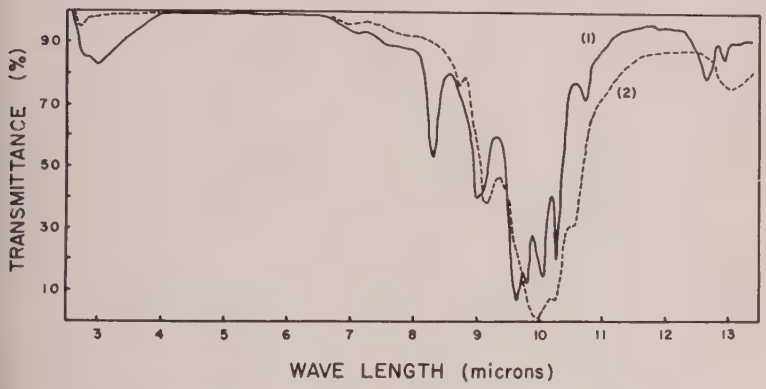

FIG. 5. Infrared absorption spectra of synthetic reyerite (curve 1) and gyrolite (curve 2).

wavelength) shows several absorption peaks. Synthetic gyrolite as well as the natural mineral exhibits broad overlapping peaks (curve 2). The natural mineral reyerite is characterized by a similar pattern. The broad absorption zones, which are indicative of gyrolite, are resolved into sharp peaks in synthetic reyerite (curve 1). The appearance of these sharp peaks suggests a perfection of the structural building plan. Since no shifts in the peak wavelengths, which would indicate changes in the effective bond strength, can be observed in the case of the most intense peaks, it has to be assumed that the structures of gyrolite and reyerite are indeed closely related.

Since gryolite and reyerite have excellent basal cleavage, preferred orientation spectrograms were obtained. Such a method has been used by Serratosa and Bradley (1958) to determine the orientation of the OH-bond axis in some layer silicates. The present investigation showed that oriented and unoriented gyrolite gave the same absorption spectrum.

Results

The composition of the samples, the reaction time and temperature the solid-to-liquid ratio, and the phases as identified by x-ray diffractio methods, of significant experiments are listed in Table 1. A reasonabl approach to evaluate such a number of experiments is achieved if th effects of temperature and time upon the course and rate of reaction ar considered. In this way the stability of a phase or a phase assemblag can be criterically studied; however, it is impossible to draw conclusion as to the chemical composition of the individual phases. Therefore th review of stability ranges will be followed by a brief discussion of th effects of varying C/S ratios upon the stable phase assemblages.

Samples with C/S=0.50

CaO and silicic acid are reacted at 320° C. (saturated steam pressure) for eight day Reyerite is the major component together with a trace of α-cristobalite. After fifteen day the amount of α-cristobalite has increased and a trace of xonotlite is observed, while reyeri is still the main constituent. A prolonged treatment results in a decrease of the amount reyerite and in a corresponding increase of the xonotlite and α cristobalite content.

At temperatures between 270° and 300° C. and saturated steam pressures, CaO a silicic acid react to form first CSHI, then gyrolite and finally reyerite. Short runs at 300° (several hours) leads to a mixture of reyerite and gyrolite. After seven days only reyeri is found. After reacting the mixture for thirty days at 300° C., reyerite is the major co ponent together with xonotlite and α-cristobalite. At lower reaction temperatures the ti for a gyrolite-reyerite inversion becomes very important. At 220° C. (saturated stea pressure) pure reyerite is obtained only after a reaction period of four months. It is interest to note that the transition of gyrolite to reyerite is characterized by the appearan of a mixed-layer phase (gyrolite-reyerite) in which the 00l reflections become broad. Tl random interlayered phase always shows fairly strong, non integral diffraction effe which are characteristic of one dimensional disorder. The (hki0) peaks always remain sha Below 220° C. the transformation time is appreciably increased. It should also be point out that a decrease in solid to-liquid ratio speeds up the reaction. The lower limit of gyrol synthesis is about 145° C.

In order to increase the rate of conversion from gyrolite to reyerite several samp were reacted at temperatures between 210° and 265° C. and at pressures between 15,(and 20,000 psi. Samples, which were prereacted under saturated steam conditions at 180° for ten days, were subjected to high pressures. The results of this study listed in Tabl indicate that the rate of conversion increased slightly. It is evident, however, that tempe ture is a much more important factor.

Samples with C/S=0.55

A hydrothermal reaction of CaO and silicic acid at 300° C. for thirty days led to t formation of reyerite with small amounts of α-cristobalite and xonotlite.

Samples with C/S=0.60

The phases obtained by reacting CaO and silicic acid at 320° C. after eight days reyerite, after sixteen days reyerite plus a trace of α-cristobalite, after thirty-three d reyerite, α-cristobalite and xonotlite. At 300° C. and saturated steam pressure reyer α-cristobalite and xonotlite are detected after thirty days.

Samples with C/S=0.67

The phases obtained by reacting CaO and silicic acid under saturated steam conditions at 300° C. are reyerite and a small amount of xonotlite. At lower temperatures reyerite-gyrolite mixed-layer phases are very common. Short reactions lead to the formation of gyrolite, which is transformed to a mixed layer phase if the experimentation time is prolonged. Xonotlite was not observed in the low temperature reaction products. Electron micrographs reveal the presence of fibrous components, which were too small for selected area diffraction studies.

Several samples having a C/S ratio 0.67 were prepared using tripoli as the source of silica and $Ca(OH)_2$ or CaO as the source of calcium. These samples were reacted for forty days at 250° C. (saturated steam pressures). The results of these experiments listed in Table 1 indicate that tripoli is much less reactive than silicic acid. In fact, quartz (unreacted tripoli) is a major constituent of the reaction product, which consequently contains hydrated calcium silicates with a higher C/S molar ratio (xonotlite, tobermorite) in addition to reyerite. In comparison CaO and silicic acid formed mainly reyerite and a small amount of interlayered material. If $Ca(OH)_2$ is used, the resulting products are reyerite and small amounts of xonotlite and tobermorite. The formation of tobermorite seems to be favored by use of $Ca(OH)_2$ as starting material. These experiments clearly show that tripoli is not a suitable material for phase equilibria studies. The stable phases at 250° C. and forty days reaction time are reyerite and small amounts of xonotlite.

Samples with C/S=0.74

Mixtures of CaO and silicic acid were reacted only at 220° C. for extended periods of time. After 2 weeks gyrolite and a small amount of xonotlite appear. Reyerite and gyrolite were the major components after six weeks. A four months' reaction resulted in the formation of xonotlite, reyerite and gyrolite.

Samples with C/S=0.8

Hydrothermal reactions of CaO and silicic acid, which were carried out between 220° and 300° C., led always to the formation of xonotlite as main constituent. Above 250° C. reyerite is the minor component; below that temperature it is gyrolite.

Samples with C/S=1.0

Samples having this C/S molar ratio reacted above 180° C. to form pure xonotlite. Below this temperature tobermorite was the main component of long reactions. Short reaction times resulted in the formation of CSHI. A distinction of these phases was discussed earlier.

Reactions with synthetic reyerite (C/S=0.5)

A pure sample of reyerite was reacted in a Morey bomb in order to obtain some information concerning the upper stability limit of this material at relatively low pressures. The reactions are listed in Table 2. The results combined with previous experiments show that reyerite is transformed into xonotlite and α-cristobalite at saturated steam pressures above 300° C. The reaction is however quite sluggish. At 425° C. and 4000 psi wollastonite was also observed.

Discussion of Synthesis

The results of the hydrothermal reactions lead to several important conclusions concerning the mineralogical relationship between reyerite and gyrolite.

The experiments carried out at 300° and 320° C. show conclusively that reyerite cannot have a C/S ratio larger than 0.6. At higher ratio xonotlite appears in the products indicating the presence of excess lime. On the basis of hydrothermal runs, it is, however, impossible to pinpoint the lime/silica ratio of reyerite, which may vary between 0.5 and 0.6. Since no crystalline silica appeared in *x*-ray diffraction patterns of the 0.5 material, the lime/silica ratio of 0.5 was taken as the reyerite ratio. This ratio corresponds to the one found by Mackay and Taylor (1954).

Reactions at lower temperatures indicate that CSHI is the first phase which is formed in a short time. An increase in reaction time leads to the formation of gyrolite, which is converted to reyerite after prolonged hydrothermal treatment. The rate of this transformation is dependent upon temperature and time, though high pressure and low solid-to-liquid ratio are minor accelerators. It is possible to stop this conversion and the result will be a random mixed-layered material intermediate between reyerite and gyrolite. The transformation of gyrolite to reyerite takes about four months at 220° C. Gyrolite does not form below 145° C. The experiments further suggest that gyrolite is a metastable phase while reyerite is actually stable above 145° C. This is the reason why gyrolite rarely occurs as a pure phase in nature.

Since gyrolite is metastable and is often converted partially to reyerite it is impossible to determine its chemical composition by hydrothermal equilibrium studies. *X*-ray diffraction data may aid in a detection of mixed-layering, but only if interlayered phases are predominant. It has been observed that frequently gyrolite-reyerite mixed-layered phases contain only small amounts of one component, which does not alter the *x*-ray powder patterns appreciably. A good example is the natural mineral "truscottite" (reyerite) from Greenland which was investigated by single crystal *x*-ray diffraction methods. Non integral basal reflections were observed which clearly indicate that this reyerite contains a small amount of gyrolite in interlayered positions. It is suspected that synthetic gyrolite would show similar interlayering features, if single crystals of appropriate size could be grown.

It was observed that the rate of conversion of gyrolite to reyerite is mainly dependent on the temperature. This is the reason why "pure" gyrolite should appear close to its lower stability limit (at about 145° C). At this temperature, however, all reactions are very slow, so that the experimentation time has to be increased if a complete reaction of the raw materials is expected. Such an increase of reaction time will also enhance the formation of reyerite from metastable gyrolite, and therefore prevent the formation of pure gyrolite.

Another possibility to form gyrolite was briefly investigated. A sam

of synthetic reyerite was reacted at 200° C. (saturated steam pressures) for two weeks. It was assumed that reyerite would convert into gyrolite if gyrolite were a stable phase at that temperature, but no change in crystal structure was noted.

All these experiments demonstrate that it is impossible to determine the C/S ratio in synthetic gyrolite. The results further show that this molar ratio can vary between 0.5 and 0.67. At a ratio of 0.67 xonotlite appears together with gyrolite. Definite information can only be given for the reyerite ratio which is 0.5.

Discussion of the Gyrolite-Reyerite Relationship

X-ray and electron diffraction data

Hydrothermal experiments have shown that pure reyerite can easily be synthesized under saturated steam conditions. A synthesis of pure gyrolite was found to be impossible because this phase is metastable and converts to reyerite. This phase transformation passes through stages intermediate between the two end-members, which can be observed with great ease if the reaction is interrupted before reaching equilibrium. These intermediate phases are characterized by diffraction peaks which appear in non-integral positions along the (000l) diffraction nodes. Since selected area electron diffraction studies demonstrate that the intensity and sharpness of the (hki0) diffraction spots do not change in the course of this conversion, it has to be assumed that the phase transition consists of a contraction of the lattice. This observation is confirmed by the constant sharpness of the $(20\bar{2}0)$ and $(41\bar{5}0)$ peaks in x-ray powder patterns. The intermediate phases resulting from a partial shrinkage of the gyrolite lattice are, therefore, one-dimensional disorder structures. The fact that the (hki0) reflections of natural or synthetic gyrolite and reyerite have the same relative intensities and spacing (Fig. 4) leads to the conclusion that both mineral species are composed of layers which have exactly the same structure and composition. The same conclusion is reached if the intensities of the basal reflections are compared. Mackay and Taylor (1954) already noted that the basal reflections of gyrolite and reyerite appear strong and weak in identical bands at similar sin θ/λ values, although the indices of corresponding intensities do not coincide. Such an intensity distribution is obtained only if both minerals are composed of essentially the same basic structural layers and differ but in the manner of stacking of such layers. The reyerite lattice represents then the tightest stacking of these structural layers ($c = 18.7$ Å), while gyrolite is composed of the same structural units, which are loosely stacked ($c = 22.1$ Å). Since the variations in intensity of the basal reflections of

both gyrolite and reyerite, plotted against sin θ/λ values form a smooth curve, which is similar to the form-factor function curve for montmorillonite-organic liquid complexes (Bradley, 1953), it has to be assumed the interlayer space in gyrolite is filled with material of low scattering power such as water molecules.

Single crystal studies of reyerite, which were presented by Mackay and Taylor (1953) strongly suggested trigonal symmetry for this mineral. Other specimens investigated by the same authors seemed to be hexagonal. Our electron diffraction studies revealed that all specimens had hexagonal Laue symmetry. The conflicting evidence can be explained, if it is assumed that the basic layers, of which both minerals are composed, actually have trigonal symmetry. Perfect stacking of these structural layers leads to a trigonal arrangement (reyerite), which sometimes may appear hexagonal if one basic layer is rotated against the other. In the case of gyrolite the structural layers are separated from each other probably by a layer of water molecules and may be rotated against each other by 60°. This rotation produces a hexagonal Laue symmetry.

Intermediate phases which have been observed are also composed of such structural layers. In their case the stacking arrangement corresponds partially to reyerite, which means several layers are perfectly stacked, and partially to gyrolite where layers are loosely arranged and have a wider *c*-spacing. Due to the imperfect stacking of the gyrolite component these mixed-layer crystals appear to have hexagonal Laue symmetry, although their *c*-parameter may correspond nearly to reyerite.

Chemical composition of gyrolite and reyerite

Diffraction data have shown that both minerals are composed of the same basic structural layers, which must have the same chemical composition. Hydrothermal experimentation suggests that reyerite has a C/S ratio of 0.5. Dehydration studies reveal that only little water is lost below 600° C. (about 1%), which appears to be adsorbed molecular water. Between 600° and 800° C. a weight loss of about 4% is registered which corresponds to the expulsion of hydroxyl water. The chemical composition of reyerite is therefore $CaO \cdot 2SiO_2 \cdot \frac{1}{2}H_2O$, giving the formula $Ca_2[Si_4O_9(OH)_2]$. Six molecules are present in the unit cells. The calculated density of 2.46 compares favorably with the observed density of 2.4. This composition corresponds to that proposed by Mackay and Taylor (1954); it is, however, in disagreement with the formula suggested by Strunz and Micheelson (1958) who assume a C/S ratio of 0.75.

The chemical composition of gyrolite has undergone several revisions since the mineral was first described. Mackay and Taylor (1953) su

gested a C/S ratio of 0.67, while Strunz and Micheelson (1958) propose a ratio of 0.75. The present investigation demonstrates that the exact C/S ratio cannot be deduced from hydrothermal experimentation. It can only be shown that the ratio has to be lower than 0.67. Additional information as to the chemical composition can be obtained from *x*-ray diffraction and dehydration data. Diffraction data clearly indicate that gyrolite is composed of the same basic layers which also occur in reyerite. These structural units, which are tightly superposed to form the reyerite lattice, have a C/S ratio of 0.5. If gyrolite had a C/S ratio higher than 0.5, that is, higher than these layers, the additional calcium would have to be located in the interstices between two adjoining reyerite-type sheets. Dehydration data show that about two-thirds of the total water content of gyrolite is lost below 200° C. The water loss does not affect the crystal structure indicating that the water is loosely bound interlayer water. Therefore, calcium ions, which could be present between layers, must be in exchange positions similar to ions between montmorillonite layers. The ion-exchange capacity of gyrolite is, however, on the order of 0.1 meq. per 100 grams. This value is much too low to account for an appreciable calcium content between the reyerite-type sheets. Since reyerite shows only a small water loss below 200° C., it cannot contain loosely bound interlayer water. Infrared spectrographs of the two phases confirm the observation that gyrolite contains water molecules which are not found in reyerite. The hypothesis that calcium may appear as a calcium hydroxide sheet between the basic layers cannot be maintained in the face of adverse evidence. The reasoning presented leads to the conclusion that gyrolite must have the same C/S ratio as reyerite. Consequently the chemical composition of gyrolite is $CaO \cdot 2SiO_2 \cdot 2H_2O$. The calculated density based on the hexagonal unit cell ($c = 22.1$ Å) which contains 12 molecules, is 2.35. This value is somewhat lower than the observed density of 2.39. It has been shown that gyrolite easily converts to reyerite at high temperatures and moderate pressures.

The formula of gyrolite is therefore $Ca_2[Si_4O_9(OH)_2] \cdot 3H_2O$.

Dehydration of gyrolite and reyerite

The chemical formulae of gyrolite and reyerite clearly reflect the close relationship which exists between both phases. Actually they suggest that gyrolite could be a water expanded reyerite. The dehydration characteristics of the two minerals seem to support this view because they differ only in respect to their water loss at low temperatures (below 400° C.). A heat treatment of gyrolite up to about 400° C. will only remove interlayer water, which can be replaced by exposure of the material to the atmosphere. The gyrolite lattice, however, is not contracted

if the interlayer water is driven off. Yet both minerals show the same loss of hydroxyl water between 600° and 800° C., which indicates similarity of both structures. After heating to 825° C. gyrolite is converted to wollastonite (β-$CaSiO_3$) and amorphous silica. Reyerite is transformed to pseudowollastonite (α-$CaSiO_3$) and silica at 835° C. These observations on synthetic phases are in contradiction with the results obtained by using natural minerals (Mackay and Taylor, 1953).

The fact that gyrolite and reyerite are not converted to the same high temperature phases, although both minerals seem to have similar lattice and composition, has been used as argument in favor of a different chemical structure for the two minerals. It will be shown that such a conclusion is not necessarily warranted and that the interpretation of these differences which result from the thermal treatment will also explain other contradictory evidence.

It has been demonstrated that gyrolite and reyerite are composed of the same basic structural units. In reyerite these basic layers, which probably have trigonal symmetry, are stacked in such a way that interstices are at a minimum. The structure of this reyerite type layer arrangement corresponds closely to the structural building plan of pseudowollastonite (α-$CaSiO_3$). Jeffrey and Heller (1953) have pointed out that pseudowollastonite has a triclinic unit cell which departs only slightly from a hexagonal symmetry ($a = 6.85$ Å, $c = 19.65$ Å). During the transformation of reyerite to pseudowollastonite the c-axis remains the same while the (2130) direction of gyrolite (3.18 Å) coincides with the (11$\bar{2}$0) direction (3.40 Å) of pseudowollastonite. This similarity of their structures favors a transformation of reyerite to pseudowollastonite, although the latter phase is stable only above 1125° C. (Muan and Osborn, 1952). In gyrolite the structural layers are separated by molecular water and show distinct rotational disorder. The bonds between these basic units must be weakened due to this enlargement of the interstices. Hence at 800° C. the gyrolite structure gives way to an amorphous material, from which wollastonite crystallizes, because it is the stable phase at this temperature. This reasoning shows clearly that the presence of different high temperature phases, which appear after a heat treatment of synthetic gyrolite and reyerite, can be explained on the basis of stacking differences of the same layers.

Strunz and Micheelson (1958) suggested that gyrolite is a water-expanded reyerite. This hypothesis is indicated by chemical composition, x-ray and electron diffraction, infrared spectroscopy and in part by dehydration characteristics. It is only partially correct, however, because the heat treatment of gyrolite at 200° to 400° C., which removes the interlayer water, does not reduce the c-parameter to 18.7 Å. This s

nifies that gyrolite cannot be converted to reyerite by dehydration at atmospheric pressures. Therefore it has to be assumed that the interlayer water is not essential for the wider separation of the reyerite-type layers in gyrolite. It was suggested earlier that these structural layers may have trigonal symmetry. If successive layers are perfectly matched, the resulting crystal structure will be trigonal and will have a short c-parameter, (reyerite). An angular displacement of 60° of the successive layers will create hexagonal symmetry. Since this angular displacement is connected with a lattice expansion of about 3.4 Å it must be assumed that the basic layers are undulating. Therefore the misalignment is responsible for the expansion of the structure. The interstices resulting from this misfit of undulating sheets are filled with molecular water which can be easily removed without changing the basic structure.

The actual structure of this reyerite-type layer has not been determined. Mackay and Taylor (1953) already noted that the a-parameter is much too large for a kaolinite-type or mica-type structure. Mamedov and Belov (1958) suggest that reyerite is composed of a silicate network, which consists of octagonal and pentagonal rings, and a closely packed layer of calcium octahedra. The silica tetrahedra of the network, which represents a condensation of wollastonite chains, are pointing upwards and downwards. This alternating position of the tetrahedral vertices gives the sheet an undulating effect. The symmetry of such a layer arrangement is not trigonal, however. Strunz and Micheelson (1958) propose that zeophyllite is a $Ca(F, OH)_2$-expanded reyerite. Such an interpretation requires a C/S ratio of 0.75 for reyerite, which cannot be confirmed.

Conclusions

The present investigation has shown that hydrothermal experiments may be used to determine the chemical composition of hydrated calcium silicates. The reaction in the system $CaSiO_3$-SiO_2-H_2O revealed that reyerite has a CaO/SiO_2 ratio of 0.5. This composition agrees with the analytical results presented by Mackay and Taylor (1954), but differs from the formula given by Strunz and Micheelson (1958). At temperatures below 250° C. the reaction between lime and silica at saturated steam pressures as well as at supersaturated steam conditions is extremely sluggish, so that equilibrium is only attained after several months. Therefore it is nearly impossible to obtain pure low temperature phases (gyrolite, tobermorite). Several attempts to produce pure gyrolite were not successful, because gyrolite converted to reyerite before the raw materials were completely reacted. During the transformation of gyrolite to reyerite intermediate phases are detected, which are mixed-

layer minerals. Due to this conversion and due to the slow rate of reaction between lime and silica at low temperatures, it is impossible to determine the exact chemical composition of gyrolite on the basis of hydrothermal experimentation.

It had been demonstrated by Mackay and Taylor (1953) and by Strunz and Micheelson (1958) that gyrolite and reyerite are structurally related. Due to the fact that the basal reflections of both minerals follow the same form-factor function curve, it has to be assumed that the basic layers are the same for both mineral phases. The expansion of the lattice in gyrolite ($c = 22.1$ Å) compared to reyerite ($c = 18.7$ Å) may be due to interlayer water. Although gyrolite loses about two-thirds of its water below 200° C., the lattice does not contract to the reyerite spacing. During this dehydration the relative intensities of the basal reflections do not change. Selected area diffraction patterns of gyrolite and reyerite show that the (*hki*0) reflections have the same intensities in both minerals. These observations support the hypothesis that both minerals are composed of the same unit layers, that they have the same chemical composition in respect to lime and silica. The individual layers have probably trigonal symmetry. Reyerite represents a close stacking of these basic layers, so that the trigonal symmetry is maintained and a small c parameter is observed. If the basic layers are rotated 60°, a hexagonal symmetry of gyrolite is obtained. Due to the improper fit of the layers the lattice is irreversibly expanded and molecular water penetrates between the layers.

The idealized formula for reyerite therefore is $Ca_2[Si_4O_9(OH)_2]$. The structure is trigonal ($a = 9.7$ Å, $c = 18.7$ Å). Gyrolite has the same composition except for molecular water: $Ca_2[Si_4O_9(OH)_2] \cdot 3H_2O$. This structure is hexagonal having the same a-parameter.

The upper stability limit of reyerite at saturated steam pressures is about 300° C. At this temperature reyerite is slowly transformed into xonotlite and α-cristobalite according to the formula:

$$3\ Ca_2Si_4O_9(OH)_2 \xrightarrow{300^\circ\ C.} Ca_6Si_6O_{17}(OH)_2 + 6SiO_2 + 2H_2O$$

The appearance of wollastonite below 425° C. is in agreement with the findings of Buckner, Roy and Roy (1960).

Acknowledgments

The authors are indebted to Mr. R. H. Brailey for his help in interpreting the infrared spectra. We wish to thank Prof. H. F. W. Taylor, Dr. W. F. Bradley, Dr. R. I. Harker, and Margaret Schmachtenberger for a critical reading of the manuscript.

References

Assarsson, G. O. (1957) Hydrothermal reactions between calcium hydroxide and amorphous silica: the reactions between 180° and 220° C. *J. Phys. Chem.* **61,** 473–479.

Bradley, W. F. (1953) Analysis of mixed-layer clay mineral structures. *Anal. Chem.* **25,** 727–730.

Buckner, D. A., Roy, D. M., and Roy, R. (1960) Studies in the system CaO-Al_2O_3-SiO_2-H_2O, II. The system $CaSiO_3$-H_2O. *Am. Jour. Sci.* **258,** 132–148.

Flint, E. P., McMurdie, H. F., and Wells, L. S. (1938) Formation of hydrate calcium silicates at elevated temperatures and pressures. *J. Res. Nat'l. Bureau Standards* **21,** 617–638.

Gard, J. A. and Taylor, H. F. W. (1957) A further investigation of tobermorite from Loch Eynort, Scotland. *Miner. Mag.* **31,** 361–370.

Gard, J. A., Harrison, J. W., and Taylor (1958) Synthetic compounds related to tobermorite: An electron-microscope, *x*-ray and dehydration study. *Mag. Concrete Res.* **11,** 151–158.

Heller, L. and Taylor, H. F. W. (1951) Hydrated calcium silicates, II. Hydrothermal reactions: Lime/silica 1:1, *J. Chem. Soc.* (*London*), 2397–2401.

Heller, L. and Taylor, H. F. W. (1956) Crystallographic data for the calcium silicates. London, 79 p.

Jeffrey, J. W. and Heller, L. (1953) Preliminary *x*-ray investigation of pseudo-wollastonite. *Acta Cryst.* **6,** 807.

Kalousek, G. L. and Prebus, A. F. (1958) Crystal chemistry of hydrous calcium silicates. III. Morphology and other related properties of tobermorite and related phases. *J. Am. Ceram. Soc.* **41,** 124–132.

Kalousek, G. L. and Roy, R. (1957) Crystal chemistry of hydrous calcium silicates II. Characterization of interlayer water. *J. Am. Ceram. Soc.* **40,** 236–239.

Mackay, A. L. and Taylor, H. F. W. (1953) Gyrolite. *Miner. Mag.* **30,** 80–91.

Mackay, A. L. and Taylor, H. F. W. (1954) Truscottite. *Miner. Mag.* **30,** 450–457.

Mamedov, Kh. S. and Belov, N. V. (1958) Crystal structure of mica-like hydrous calcium silicates: Okenite, Nekoite, Truscottite and Gyrolite. New silicate radical (Si_6O_{15}). *Doklady Akademii Nauk SSSR* **121,** 720–723.

Nuan, A. and Osborn (1952) Fundamental investigation of steel plant refractory problems IV. *Industrial Heating* **19,** 1293–1298.

Peppler, R. B. (1955) The system lime, silica and water at 180° C. *J. Res. Nat'l Bureau Standards* **54,** 205–211.

Serratosa, J. M. and Bradley, W. F. (1958) Determination of the orientation of OH-bond axes in layer silicates by infrared absorption. *J. Phys. Chem.* **62,** 1164–1167.

Strunz, H. and Micheelson, H. (1958) Calcium phyllosilicates. *Naturwiss.* **45,** 515.

Tuttle, O. F. (1948) A new hydrothermal quenching apparatus. *Am. Jour. Sci.* **246,** 629–635.

Manuscript received September 6, 1960.

ARTIFICIAL AND NATURAL PHOTOELASTIC EFFECTS IN QUARTZ AND FELDSPARS

HANS RAMBERG, *Escola Nacional de Minas e Metallurgia, Ouro Preto, Brasil.**

ABSTRACT

Optical disturbances occur in quartz and feldspars around stress centers as caused by impact from carborundum grains during preparation of thin sections. This photoelastic phenomenon is described and compared with the optical disturbance observed around stress centers produced in various substances such as cellophane paper, photographic film, plexiglass and common glass. The interference figures observed with crossed nicols show that the stress fields have cylindrical or spherical symmetry, the stress decreasing rapidly with distance from the centers. Similar photoelastic effects are seen around inclusions in quartz and feldspars, showing that inclusions are sometimes surrounded by stress fields with maximum compressive stress parallel to the radius. Some piezo-optical properties of quartz and potash feldspar are measured qualitatively in order to interpret the character of the stress fields. For these minerals the deformation of the indicatrix under unidirected compressive stress is similar to the deformation of the strain ellipsoid in the sense that the indicatrix becomes elongated, relatively, in directions normal to the stress. Plexiglass behaves in an opposite manner, its indicatrix being relatively elongated parallel to the direction of compressive stress.

CENTERS OF PHOTOELASTIC DISTURBANCES IN QUARTZ AND FELDSPARS AS PRODUCED DURING PREPARATION OF THIN SECTIONS

Quartz grains cut quasi-normal to the optic axis often show a faint grating texture when observed with crossed nicols at moderate magnification. At the first glance the texture usually appears as a set of somewhat irregular extinction bands making about a 45° angle with the vibration directions of the nicols, crossed by a quasi-normal set of irregular bright bands. Being invisible when the quartz grain is in position of extinction, the grating texture shows up at only a few degrees deviation from this position and remains visible at any angular deviation from extinction of the quartz grain, provided that the optic axis is quasi parallel to the microscope axis. Rotation of the thin section makes the dark bands and the complementary bright ones alternate between the first–third and the second–fourth quadrants, bisecting symmetrically the vibration directions of the nicols.

This apparently common texture seems so far to have failed to arouse sufficient interest among petrographers and mineralogists to motivate publication. During thin section work on gneisses from Brazil the writer studied the feature in some detail and found that it represents an interesting example of photoelasticity in minerals, a phenomemon hardly di

* Present address: Department of Geophysical Sciences, University of Chicago.

cussed in geological literature. Although recognized as chiefly caused by stresses produced during preparation of the thin sections, the feature may serve as a model for the optical disturbances induced by stresses around inclusions and some lattice defects in minerals.

The feature appeared most distinctly at moderate magnification, *e.g.* between 50 and 200X, the dark and bright bands generally being too fine for less magnification, whereas higher power (say 500X) made the pattern very diffuse.

The appearance of the grating is produced by numerous little separate crosses consisting of two hourglass shaped bars, one dark, one bright, intersecting orthogonally and bisecting symmetrically the vibration direction of the nicols (Fig. 1).

FIG. 1. Microphotograph of interference crosses around stress centers in quartz cut quasi normal to *c*. The vibration direction ϵ' of the quartz is marked by ink. The extinct bars of the crosses strike NE, the bright bars NW. Crossed nicols parallel to the edges of the photo whose length is 0.4 mm.

The maximum length of the bars was about 0.03 mm., but most were less than one third that size. All the little crosses were parallel, the dark bars constituting one set of parallel features, the bright bars another parallel set. The crosses were mostly scattered randomly, but occasionally occurred in rows.

In all sections studied the crosses changed consistently as follows when rotating the sections clockwise starting with the extraordinary ray of the quartz vibrating in NS direction:

A few degree rotation produced simultaneously and rather suddenly an

appearance of numerous crosses with dark bars bisecting at about 45° the first–third quadrants, and bright bars or elongate regions bisecting the second–fourth quadrants, the vibration directions of the nicols being the reference coordinates. This pattern remained immobile, except for minor variations in the brightness and darkness of the bars, until ϵ the vibration direction of the extraordinary ray is lined up with the EW direction when the uniform extinction is interrupted only by hardly visible small areas of light in the regions where the largest crosses had been.

A few degree further rotation caused a sudden reappearance of the crosses, but in a reversed position *viz.* with the dark bars bisecting the second–fourth quadrants and the bright ones in the first–third quadrants. The crosses remained in this position during the next 90° rotation of the quartz, *i.e.* until uniform extinction when ϵ' became parallel to the NS direction after 180° rotation from the starting point.

Checks with $\frac{1}{4}\lambda$ quartz plate showed that, within the circular regions swept out by the bars of the little crosses, the intersection of the indicatrix with the plane of the thin section was deformed (or rotated) in the manner shown in Fig. 4.

The variation of the brightness and darkness of the bars indicated that in general the magnitude of indicatrix deformation increased toward the centers.

This indicates a photoelastic effect created by local concentric distribution of anisotropic stress in the quartz lattice, the intensity of the stress increasing toward the center.

Before discussing some tests made to check this assumption, we shall describe the optical disturbances around the few centers of exceptionally strong deformation inasmuch as these showed details not visible in the little crosses.

When the quartz grains were in the position of extinction, some interference light passed through a few scattered small regions. In these regions the extinction was complete only along the arms of an orthogonal cross parallel to the vibration directions of the nicols, leaving a sector of faint light in each quadrant.

Clockwise rotation from a position $\epsilon' \mid$ NS made the bars of the cross bend, the north end of the vertical bar and the east end of the horizontal bar bending into the first quadrant at the same time as the south end of the vertical bar and the west end of the horizontal bar bent into the third quadrant. The cross thus changed into a figure 8 pattern, the longest axis of which bisected symmetrically the first–third quadrants while the section was rotated until ϵ' became parallel to EW. During this rotation however, the long axis of the figure 8 "isogyre" changed, its length co

inuously decreasing during the first 45° rotation of the section and in-reasing again until ϵ' was parallel to EW, at which point the figure 8 pat-ern opened up to an orthogonal cross. Further clockwise rotation pro-uced a figure 8 pattern in the second–fourth quadrants. A similar inter-erence pattern occurs in glass, Fig. 2.

Insertion of a $\frac{1}{4}$ λ quartz plate with ϵ vibrating in the first quadrant ave additive interference color within the "eyes" of the figure 8 when it ell in the second–fourth quadrants, and subtractive color when the gure 8 fell in the first–third quadrants. Outside the figure 8 pattern, ut close to its center, additive interference color stronger than in the st of the quartz grain occurred when the figure 8 occupied the first–ird quadrants. In these same regions outside the figure 8, substractive

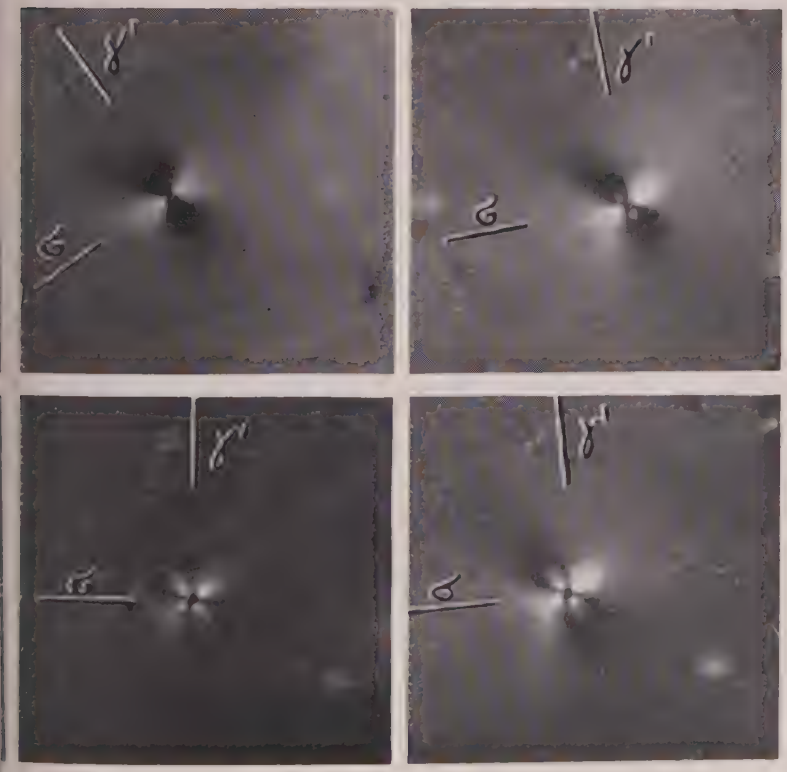

FIG. 2 Microphotograph of interference figures in stress fields caused by little grains carborundum pressed between cover glass and objective glass made double refracting application of compressive stress in direction σ. The vibration direction of the high ex ray is marked γ'. Crossed nicols parallel to edges of photos. Note how the central re 8 pattern changes with varying angle between γ' and the nicols. Length of photos mm.

interference color lower than the rest of the crystal occurred when th figure occupied the second–fourth quadrants.

When the bulk of the crystal was in the position of extinction such tha a dark cross with four small sectors of light occurred at points of excep tional strong optical disturbance, the $\frac{1}{4}\lambda$ quartz plate gave always add tive color for the light sectors in the second and fourth quadrants, an substractive color in the first and third quadrants.

These observations on the regions of strong disturbances verified th notion that the quartz indicatrix was significantly deformed within mor or less circular (spherical, cylindrical?) regions, the general pattern c deformation being as shown in Fig. 4.

The figure 8 extinction pattern may perhaps not seem an obvious cor sequence of such radial distribution of indicatrix deformation, but a close study will reveal that a pattern of this kind is exactly what should be ex pected if the indicatrix is deformed in a field of anisotropic stress wit spherical or cylindrical symmetry.

A grating texture similar to that described from the quartz was som time seen in plagioclase and potash feldspar. In the feldspars, howeve the pattern was rarely developed as clearly and as symmetrically as the quartz. The bright and dark elongate regions were rather diffus they were not always quasi-normal to one another but appeared som what controlled by the tricline structure of the feldspars, and often on set of linear regions showed up much better than the other.

In quartz as well as in feldspars the feature here described would b come less and less visible the more the optic axis deviated from t microscope axis. For large angular deviation of these axes the optical d turbances could only be seen when the crystals in bulk were close to t position of extinction.

Experimental Tests

It is generally true that transparent solids show photoelastic effects the sense that their indices of refraction vary with magnitude and geom try of the stresses applied, the piezo optical coefficient being the measu of the relationship between stress and indices of refraction. An excelle discussion of this phenomenon is found in Nye (1957). Unfortunate nothing seems to be known with reference to the piezo optical coefficie of quartz and feldspar.

As an interpretation of the described optical disturbances to the fi approximation does not require a quantitative knowledge of pie optical coefficient (the sense of the change of double refraction wi stress is sufficient) the experiments were limited to qualitative stress te on small polished samples of quartz and feldspars.

Rectangular plates some 2–4 mm. thick were cut and polished normal to the c-axis of quartz, and other plates of similar thickness were cut parallel to this axis. The plates were subjected to compressive stress in direction parallel and normal to the c-axis in the plane of the plates, and the variation of the double refraction noted in the microscope by help of compensating quartz wedges. It was found that in all cases the double refraction changed in such a fashion as to show that the indicatrix was deformed in a manner similar to the elastic strain ellipsoid, *i.e.* dimensions of the indicatrix which were parallel to the applied compressive stress decreased relative to dimensions normal to the stress.* When compressive stress was applied parallel to c on the plates cut parallel to this axis the double refraction $\Delta n = \epsilon' - \omega'$ decreased; when stress was applied normal to c on the same plates the double refraction increased. Stress applied normal to the trigonal axis on the plate cut normal to this axis made the plate distinctly double refracting with the smaller axis of the deformed indicatrix parallel to the stress. In the latter case the indicatrix became a biaxial ellipsoid.

The significance of these tests is to show that for quartz the photoelastic distortion (*i.e.* the deformation of the indicatrix under stress) is similar to the deformation of the elastic strain ellipsoid. This was necessary to check inasmuch as there exist solids whose indicatrix distortion under stress is opposite to the deformation of the strain ellipsoid. In other words the indicatrix becomes elongated (relatively) in the direction of the highest compressive stress. It is, however, possible that all axes of the indicatrix increased under uniaxial compression, but to different degree. Potassium chloride is an example of a crystalline solid with this character (Nye, 1957, p. 255); plexiglass, which was used in the model tests below, is an example on an amorphous substance with such photoelastic character.

Because of low symmetry the number of piezo optical coefficients necessary to describe fully the photoelastic character of feldspars is great—36 different coefficients for triclinic feldspars and 20 for monoclinic (Nye 1957, p. 250) as compared with 8 for low quartz. No attempt was made to determine fully the photoelastic character of feldspar, but a few tests were made on cleavage fragments parallel to (001) and parallel to (010) of potash feldspars (adularia and orthoclase of the type characteristic of charnockite rocks).

When the basal cleavage fragments were compressed in direction parallel to the a- and the b-axes respectively, and the change in double

* The experimental tests did not give information about the absolute variation of the indices of refraction; it may well be, for example, that all three indices increased with increasing uniaxial compressive stress.

refraction observed on basal cleavage flakes, it was found that the in dicatrix cross section was relatively compressed in direction of the stres

Cleavage flakes parallel to (010) showed a similar deformation of ir dicatrix cross section, *i.e.* the indicatrix was elongated normal to the com pressive stress when applied parallel to *a* as well as when applied norma to (001). It appeared, however, that the effect was sensibly less whe stress was applied normal to (001) than when applied parallel to *a*.

It appears then, at least for stress applied in the direction noted abov that adularia and orthoclase behave photoelastically similar to quart (but opposite to plexiglass) in the sense that the distortion of the ind catrix under stress is qualitatively similar to the distortion of the stra ellipsoid under the same stress.

In light of these tests of the photoelastic character of quartz and fel spars, it follows that the concentric optical disturbances as describe from thin sections are caused by a spherical or cylindrical stress field wi the highest principal stress parallel to the radius, a stress distribution be expected if caused by a nucleus of high pressure.

To obtain more detailed information about the photoelastic effe of a spherical or cylindrical stress field in an optically anisotropic mediu such fields were artifically produced in various transparent solids whi either possessed permanent double refraction (cellophane paper, phot graphic film, plexiglass), or were made double refracting by applicati of directed uniform stress (common glass), superimposed on the spheri or cylindrical stress field.

In sheet-shaped samples of these substances smaller or larger regio of quasi-concentrically distributed stress were developed by pressu from a pointed instrument (on cellophane paper, photographic fil plexiglass), by hitting the surface with a pointed metal tool (glass), or drilling tiny holes in which plugs of lead were stampted (plexiglass, filr The points of pressure or impact, and the plugs of lead acted as cent about which the concentric stress is distributed with the largest pr cipal stress parallel to the radius and decreasing rapidly with dista from the center as given by equations (1) to (3) below.

This stress pattern simulates the condition to be expected for exam around mineral inclusions with small compressibility enclosed in m compressible mineral if exposed to increasing external pressure. If an clusion is more compressible than its host, release of confining rock pr sure (*e.g.* elevation of a rock complex from depth due to surface erosi may result in the same kind of stress pattern around the inclusion. Va able temperature combined with unlike thermal expansion of inclus and host could also give stress distribution of this type. Similar stress

ibution may moreover result from an inclusion growing in a mineral, ie inclusion executing a certain "force of crystallization."

In some instances the stress pattern was reversed during the tests in ich a fashion that the largest principal compressive stress was made ormal to the radius. This was achieved by subjecting a circular sheet of lexiglass with a small open hole to planar compressive stress acting in idial direction around the circumference. In the vicinity of the hole, aximum principal compressive stress is then normal to the radius, and ecreases with increasing distance from the hole.

This situation would serve as a model for the stress distribution around n inclusion whose compressibility is greater than that of the host min- al provided the mineral is exposed to increasing rock pressure. If an clusion is less compressible than its host, release of rock pressure may use a stress distribution as here mentioned. Unmixing of alkali feldspar ould create a similar stress pattern around the albite lamellae inasmuch . the unit cell of albite is considerably less (about 10% by volume, ves, 1952, p. 551) than that of microcline.

All the thus prepared samples showed at crossed nicols under the icroscope interference pattern essentially similar to that around the scribed disturbances in quartz and feldspars. The pertinent feature mmon to the disturbed little regions in all samples was an area of ex- ction in each of two diametrically opposite quadrants of the crossed cols and areas of brightness in the two other quadrants. The fields of tinction and brightness would alternate among the quadrants upon ro- tion of the microscope stage. Indeed, in common glass, texture indis- guishable from that in quartz was produced simply by grinding a ce of glass as if it were a mineral section, applying canada balsam and ver glass. When this section was put under homogeneous plane stress, h as to give it a faint double refraction, and observed under crossed cols its grating structure of optical crosses looked identical to that of artz. During grinding, impacts of the carborundum grains on the sur- e of the quartz creates the same kind of stress centers as they do on e ground glass.

The most ideally symmetrically interference figures were developed und plugged holes in the plexiglass (Fig. 3). This substance was there- e best suited for a detailed study. One must note, however, that plexi- ss (at least the piece that was used in these experiments) has photo- stic properties of opposite character to quartz, feldspars and the other stances (glass, cellophane paper, film) tested. Independent stress cks on plexiglass showed that its indicatrix becomes relatively elon- ed in the direction of maximum compressive stress.

The deformation of the indicatrix is essentially determined by th difference between radial and tangential stresses around the stress cente and by the orientation of the stress ellipsoid relative to the origina indicatrix. The difference of radial and tangential stresses $\sigma_r - \sigma_\theta$, abou the cylindrical hole (pressure = 0) varies with distance r from the cente thus

$$\sigma_r - \sigma_\theta = \Delta\sigma_1 = \frac{2a^2b^2}{b^2 - a^2} \frac{P_c}{r^2} \tag{1}$$

where a is radius of the hole, b radius of the disk and P_c pressure on th circumference of the disk. As a and b are constant for a given test disk is seen that the stress difference decreases rapidly with distance fro center.

For a plugged hole in which pressure is P_h and pressure on the circur ference on the disk is zero, the stress difference at distance r from cent is

$$\sigma_r - \sigma_\theta = \Delta\sigma_2 = -\frac{2a^2b^2}{b^2 - a^2} \frac{P_h}{r^2}, \tag{2}$$

(see Jaeger 1956, p. 126). If the disk is large relative to the hole the equ tion reduces to

$$\Delta\sigma_1 = 2a^2 \frac{P_c}{r^2}; \qquad \Delta\sigma_2 = -2a^2 \frac{P_h}{r^2}. \tag{3}$$

Fig. 3 shows a sequence of microphotos of the interference figu around a plugged hole in plexiglass.

In analyzing the interference figure of the plexiglass let us for si plicity assume that the stress is distributed with cylindrical symmet around the plugged cylindrical hole whose axis is normal to the surfa of the sheet. The conditions that the radial compressive stress decrea with distance from the center, and that the relative elongation of t indicatrix increases with increasing intensity of stress difference, *i.e.* c ference between radial and tangential stresses, result in the following p tern of indicatrix deformation: Along the radial direction from the str center which is parallel to the long axis of the indicatrix in the unc turbed plexiglass, the elongation of the indicatrix simply increases as center is approached. Along the radial direction which is parallel to small axis of the undisturbed indicatrix, the elongation of the indicat decreases as one approaches the stress center until at a certain dista the indicatrix cross section becomes circular. At this distance the str is exactly sufficient to neutralize the optical anisotropy of the plexigla This happens at two diametrically opposite points about the str

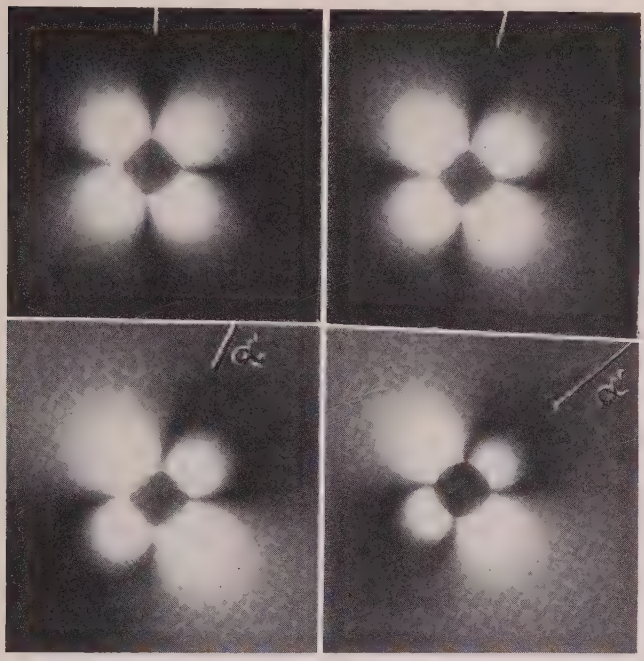

Fig. 3. Microphotographs of interference figures in stress field around plugged hole in plate of plexiglass. The lines in upper middle and upper right sides of the photos give the vibration direction of the low-index ray in the plexiglass, and indicate the angular deviation of the sample from the crossed nicols which are parallel to the edges of the photos. Diameters of photos 1.3 mm.

nter. These points are extinct at any angular position of the sheet lative to the nicol directions, and the figure 8-shaped "isogyre" must ways pass through these points.

In the region between the two "isotropic points" and the center of ress the indicatrix becomes increasingly elongated in direction parallel the radius as the center of stress is approached.

For quartz and orthoclase cut quasi-normal to the optic axis, for llophane paper and photographic films whose indicatrix respond to ress in a sense opposite to that of plexiglass, the indicatrix deformation ound a stress center is as indicated in Fig. 4. This figure is also valid for mmon glass made double refracting by application of an uniform anar directed stress superimposed on a stress center.

In the quadrants between the coordinate axes x and y the deformed dicatrix is rotated because the principal axes of stress are inclined to e original indicatrix. As we do not know accurately the piezo optical

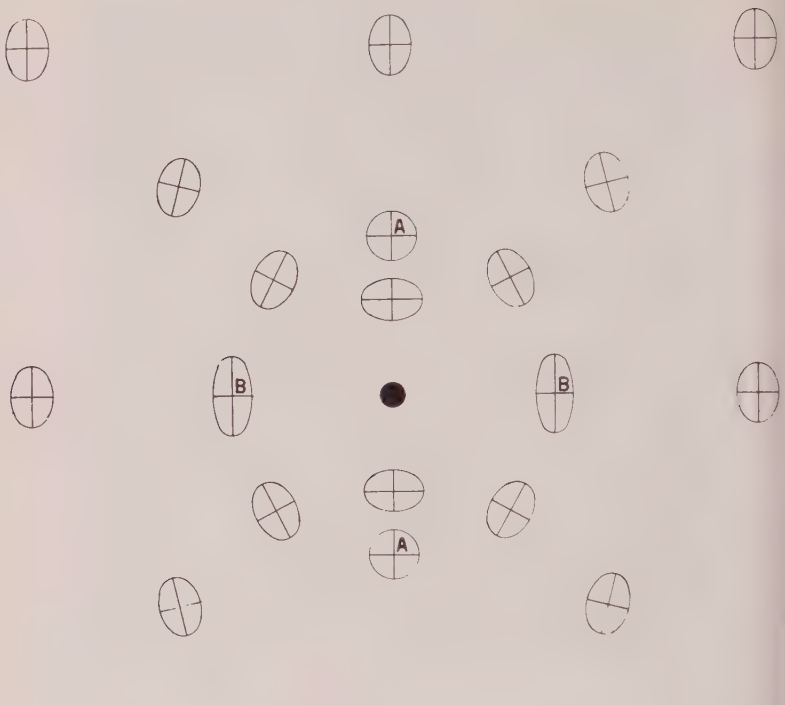

FIG. 4. Schematic map of indicatrix cross sections around a center of stress in plexigla or quartz cut quasi normal to the *c* axis. The ellipticity of the undisturbed indicatrix (al the edges of the figure) is considerably exaggerated. If the figure refers to quartz maxim compressive stress is parallel to the radius from the stress center; if referring to plexigl maximum compressive stress is normal to the radius.

coefficients of either plexiglass or quartz and feldspars, it is not possil to determine quantitatively the degree of strain and rotation of t indicatrix, but it is plain that the vibration direction of the light ra must follow a pattern similar to that shown in Fig. 5. This figure can thought of as representing plexiglass as well as quartz cut quasi norn to the *c* axis, containing a center around which the decreasing maximu compressive stress is either parallel to the radius or tangential to the c cumference. If the figure is to refer to plexiglass with a center of rad maximum compressive stress or to quartz with a center of tangent maximum compressive stress the lines indicate the vibration directions the low-index ray. If the figure is to refer to plexiglass with a center tangential maximum compressive stress, or to quartz with a cen

f radial maximum compressive stress the lines represent the vibration f the high-index ray.

When one of the crossed nicols vibrates parallel to the *y* axis, it is seen hat a peripherial field of the figure as well as an orthogonal cross through he center of stress will be extinct. If rotated clockwise until one nicol is arallel to line 2, a loop shaped area marked by heavy lines and the num-

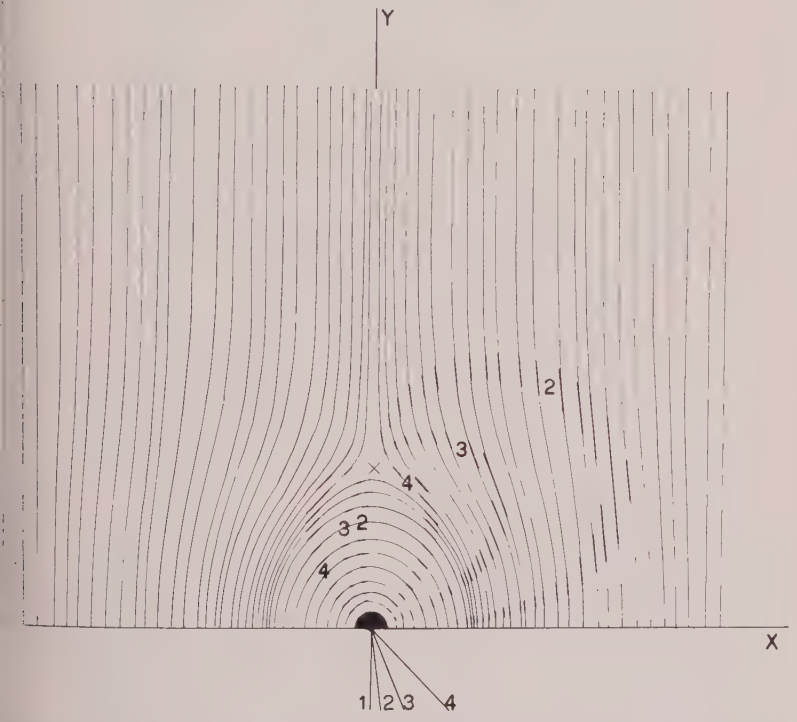

Fig. 5. Map of vibration direction of one of the two polarized rays around a stress nter in a double refracting solid. Only half of the stress field is shown, rotation of the ure 180° about the stress center produces the other half. The loops indicated by heavy es and marked 2, 3, and 4 represent regions of extinction when one of the crossed nicols rates parallel to the lines 2, 3 and 4 respectively. The cross slightly below the center of e figure represents one of the "isotropic" points of no double refraction.

r 2 will become dark. Further rotation makes the loop shrink con-nuously to the areas marked 3 and 4, respectively when one nicol is rallel to line 3 and 4. Stage 4 represent 45° rotation of the sample. The ader may convince himself that further rotation makes the loop of ex-ction (*i.e.* the locus for the points at which the vibration directions in e sample is parallel to the nicols) expand out in the region between the

positive y axis and the negative x axis. This continues until 90° rotation at which y is parallel to the horizontal nicol. Further rotation makes the loop of extinction redevelop in the region between the positive y- and x-axes (*i.e.* now in the 4th quadrant of the crossed nicols). One also realizes that the loop of extinction at all times is symmetrically situated in the quadrants of the vibration direction of the crossed nicols.

The explanation above is valid for cylindrical stress distribution around a center such as will essentially prevail if the stress center is linear and normal to the test plate, the stress in this direction being zero (or constant) throughout. In such a stress field the vibration directions remain fixed through the entire thickness of the plate along any given ray normal to the surface. Extinction is then limited to points where the vibration directions of the test plate coincide with those of the crossed nicols. (We note that the double refraction of both the stressed and unstressed parts of the tested materials —including the thin sections of quartz and feldspar —is too low to produce other than first order gray.)

At other stress distributions the conditions for extinction are less simple. Suppose for example that the stress is distributed with spherical symmetry about a center in a test plate sufficiently thick to leave the indicatrix undisturbed over the entire surface. None of the rays which have passed through the plate are therefore polarized normal to the analyzer (unless of course the whole sheet is in position of extinction) and extinction of the rays passing the internal field of stress must be caused by interference rather than parallelism with the nicols.

Without attempting to determine the extinction figure quantitatively which follows from an enclosed stress field of spherical symmetry, it may be of some interest to compare it qualitatively with the above considered cylindrical stress field. Consider two test plates with the same thickness and double refraction, one with a cylindrical stress field around a circular plug normal to the plate, the other with a spherical stress field around an inclusion, the stress of the latter not reaching out to the surface.

For simple comparison let us assume that the strength of the two stress fields, measured in terms of σ_r and σ_θ is the same for given radial distance from the centers. If these two fields are observed under the microscope in crossed nicols one finds that the extinction pattern is very similar, both showing the figure-8 pattern described above. This was verified with simple tests on plexiglass. However one essential difference is that the extinct figure 8 is always considerably smaller for the spherical field than for the cylindrical one of the same strength. This is a consequence of the fact that a light ray which passes the spherical stress field must cross thicker and thinner layers of optically undisturbed material above and below the

eld of stress. Moreover, through the field itself the indicatrix controlling he ray changes continuously. For the cylindrical stress field no such ffect is theoretically present, or in reality (because of imperfect cylinrical symmetry) the effect is much less than for the spherical field.

The photoelastic disturbances which were observed around inclusions n quartz and feldspars (see below) did not produce the distinct figure-8 attern shown by the plexiglass and some stress centers in ground quartz nd common glass. Around inclusions in quartz and orthoclase only ather small differences in extinction angle and intensity of interference ght appeared: diffuse region of excess darkness in the first–third quadants and complementary region of excess light in the second–fourthquadrants, or vice versa. Such effects seem a reasonable result of weak ress fields, everywhere too weak to reverse the elongation of the natural ndicatrix in the stressed medium. In such fields the two "isotropic" oints (Fig. 5) do not appear, and the whole central region of elliptical aces of the optical vibration direction as shown in the figure fails to de- elop. Only the outer diffuse pattern will appear under the microscope at rossed nicols, giving diffuse regions of extinction in one of the sets of iametrically opposite quadrants and regions of brightness in the other. his pattern was common around the stress centers caused by impact or oint pressure on cellophane paper and photographic film. The pattern as also produced around holes without plugs drilled part way through a heet of plexiglass, Fig. 6. The pressure from the drill at the bottom of

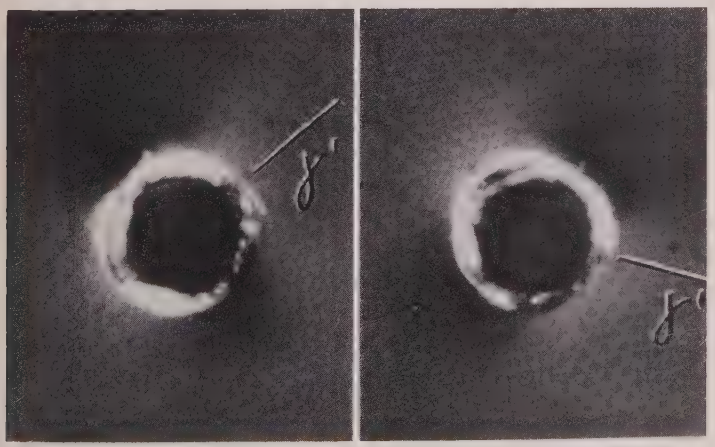

Fig. 6. Microphotographs of diffuse interference figures produced by a weak stress eld around a hole drilled 1 mm down in a 5 mm thick plate of plexiglass. The lines marked ′ indicate the vibration direction of the high-index ray. Crossed nicols parallel to the dges of the photos. Diameter of hole 0.4 mm.

the hole probably produced the weak elastic or plastic field necessary t produce the diffuse interference pattern.

Photoelastic Effect Around Inclusions in Quartz and Feldspars

In several of the thin sections examined from Brazilian gneisses, optic disturbances were seen around inclusions in quartz and feldspars. Muc of these features showed interference patterns of a kind to be expected the inclusions function as centers of stress.

Inclusions in quartz

In quartz visible photoelastic effect around inclusions was rather rar and when observed it was always faint, considerably less clearly deve oped than the best ones in orthoclase.

Inclusions surrounded by visible stress in quartz were zircon, apati and hornblende. The effect always appeared as diffuse regions of fai excess light in two diametrically opposite quadrants and shaded regio in the two other quadrants when referring to the vibration directions the nicols as the reference coordinates.

The interference disturbance usually appeared when the grains we within limited angular deviation from bulk extinction. Without exce tion ϵ' of the quartz proved to vibrate in the quadrants which contain the shaded regions, the shaded and bright regions consequently alte nating among the quadrants when the sections were rotated. This conc tion, in combination with the tested piezo optical character of quar (see above) shows that in all observed cases the inclusions functioned centers of relatively high pressure, or that the concentric stress field w formed as a result of increased pressure or anisotropic stress affecting t rock after the inclusions were emplaced. Since quartz is considerab more compressible than all common minerals reported for example Birch in Handbook of Physical Constants, 1942 (including zircon, apati and actinolitic hornblende, see Table I) increasing external pressure o quartz grain will create a field of intensified radial stress around inc sions of almost any kind of common mineral.

Inclusions in orthoclase

The optical disturbances around inclusions in orthoclase was mu more common and more intense than in quartz. (The orthoclase was the type characteristic of charnockite gneisses and granulite facies roc *i.e.* it did not show distinct twinnings, was usually microperthitic, a often showed a type of wavy extinction perhaps caused by submic scopic microcline-type twinning, see below.) Inclusions of apatite, zirc

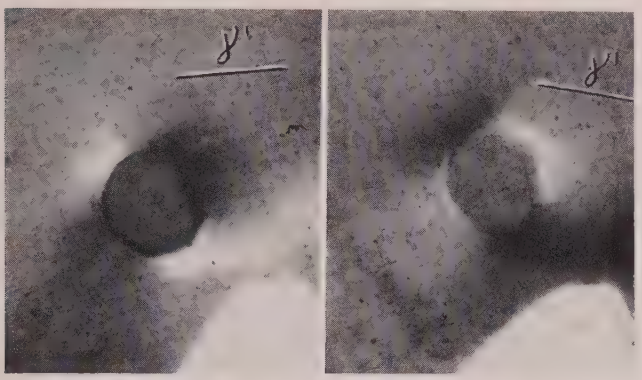

FIG. 7. Microphotographs of interference pattern in orthoclase around inclusion of quartz. The vibration direction γ' shown by ink lines. Crossed nicols parallel to edges of photos. Diameter of inclusion 0.009 mm. Section 65b–60.

ne minerals and plagioclase in orthoclase were more often than not surrounded by a region of disturbance of similar characters as described from quartz. Figs. 7 and 8 show examples of this feature. Also in orthoclase the lower index ray (α') was consistently found to vibrate in the right quadrants and the higher index ray (γ') in the shaded quadrants. This observation, combined with the piezo optical character of orthoclase indicates that the inclusions were surrounded by stress fields with maximum compressive stress in radial directions. According to Table I or-

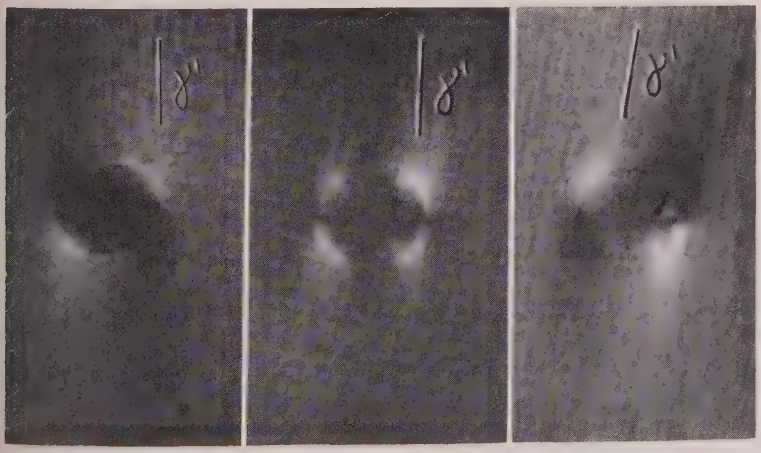

FIG. 8. Microphotographs of interference pattern in orthoclase around inclusion of apatite. Note the small angular deviation between γ' and the vertical nicol in A and C. In B, γ' is parallel to the vertical nicol. Crossed nicols parallel to the edges of photos. Longest diameter of inclusion 0.02 mm. Section 3–60.

thoclase has higher compressibility than oligoclase, labradorite, zircon oxide ore minerals and apatite. The observed photoelastic effects coul therefore be taken to indicate that the stress field around the inclusion was developed during a period of increased isotropic or anisotropic stres affecting the rock in bulk. This conclusion is not contrary to othe features in the studied rocks. Undulatory extinction of orthoclas plagioclase and quartz, so common in the granulite facies gneisses und study certainly shows that the rocks were subject to intense stress durin their later period of evolution.

In closing, let us point out that there are features of the optical di turbances around inclusions in orthoclase which perhaps indicate tha they do not represent a simple photoelastic phenomenon, but that su

TABLE I. VOLUME COMPRESSIBILITIES AFTER FORMULAE—$\Delta V/V_0 = aP - bP^2$ (Handbook of Physical Constants, 1942)

	$-\Delta V/V_0$		
	$10^7 a$	$10^{12} b$	Temp. ° C.
α-quartz	27.06	24.0	30
Fe_2O_3	6	—	0
$FeTiO_3$	5.6	—	0
Apatite	10.91	4.1	30
TiO_2	4.83	0.92	30
Zircon	8.6	—	0
Orthoclase	21.23	14.5	30
Labradorite	15.0	9.8	25
Actinolite	13.0	—	25

microscopic twinning may be involved, facilitated by the stress fie Firstly, it is surprising that the optical disturbances caused by inclusi is without comparison more abundant and intense in orthoclase than quartz, not to mention plagioclase in which the effect is all but lacki Yet the tests of the piezo optical properties of quartz and orthocl did not indicate orthoclase to be more sensitive to stress than quar Secondly, it was sometimes seen that the optically disturbed regi around inclusions in orthoclase were structurally controlled in sense that the light and dark regions tended to be limited by directi closely parallel or normal to (010) (see Fig. 8), *i.e.* directions parallel the cross-hatch twinnings in microcline. Thirdly, some tendency to mic clinization of the orthoclase, chiefly adjacent to fractures, albite lamel and inclusions, was evident in many thin sections. It is not unreasona that the stress fields around the inclusions have facilitated the transit

om orthoclase to microcline, giving rise to submicroscopic twinning or ntinuous variation in "triclinity" in regions were the stress field had a roper orientation for twinning production. That twinning in potash ldspars is produced by stress is not a new idea (see Alling 1921–24). owever, if the cases described above are examples on incipient micro- inization, it is interesting that they show an indicatrix reorientation of type to be expected on purely photoelastic grounds, *i.e.* without a phase ansition but rather continuously varying stress (and strain) in con- ntric stress field.

References

LING, H. L. (1921), The mineralography of the feldspars, I, *Jour. Geol.* **29,** 193–294.

—— (1924), The mineralography of the feldspars, I, *Jour. Geol.* **29,** 282–305 and 353–357.

RCH, F., SCHAIRER, J. F., SPICER, H. C. (1942), Handbook of Physical Constants, *Geol. Soc. Am. Special paper No.* **36.**

EGER, J. C. (1956), Elasticity, Fracture and Flow, Methuen et Co., Ltd., London.

VES, F. (1952), Phase relations of the alkalifeldspars, *Jour. Geol.*, **60,** 549–574.

YE, J. F. (1957), Physical Properties of Crystals, The Clarendon Press, Oxford.

THE AMERICAN MINERALOGIST, VOL. 46, JULY–AUGUST, 1961

SOME OBSERVATIONS ON THE MORPHOLOGY AND PHYSICAL CHARACTERISTICS OF SYNTHETIC DIAMOND

H. P. Bovenkerk, *Diamond Products Section, Metallurgical Products Department, General Electric Company*

Abstract

The growth of diamond in the laboratory has made possible investigations of th crystal habit, color and surface structure as related to variations in the growth proces Many of the variations found in natural diamond have been reproduced. The preferre growing faces are the octahedral planes, with the exception of the low temperature cul forms, which grow on the cube face.

Introduction

The morphology of diamond has been of great interest from the tin man first determined its composition and crystal habit. The early ge cutters were undoubtedly aware of the curious surface markings visib on many stones with the unaided eye. They also soon realized the dire tional properties of hardness and cleavage as related to the cryst orientation. Early observations on the occurrence of diamond were r corded by Fersmann and Goldschmidt (1911), Williams (1932), a others along with detailed speculation concerning the genesis and grow mechanism as related to the crystal variations observed. Later more d tailed studies of diamond surfaces have been undertaken by Tolansk (1955) and others. There is great interest in diamond crystal growth a its relation to surface features since a diamond crystal represents a rel tively simple atomic structure.

Now that diamond can be grown under controlled conditions, we ha the opportunity to study the many variations in diamond crystals a can attempt to relate them to variations in the growth process. Many the growth variations observed in natural diamond have been repr duced in the laboratory and the modifications of the process sufficient yield these variations have been determined.

The high pressure, high temperature apparatus used for studyi diamond growth characteristics was the taper piston device designed Hall (1960). The diamond growth systems used have been describ previously by Bovenkerk, *et al.* (1959).

One of the most interesting features of diamond growth is the appare sharp boundary condition between growth and dissolution at the hi temperatures at which the process takes place. Growth can be stopped will by changing the pressure or temperature or both and the diamo crystal can easily be converted to graphite if the pressure is not ma

tained at these high temperatures. This may mean that the diamonds found in nature have been subjected to solution following growth in many cases. Therefore, the appearance of a natural or synthetic diamond surface is not necessarily representative of the surface as it was when the growth process was completed.

Crystallography

Diamond always crystallizes in the cubic system. The crystal forms commonly observed in nature are the octahedron, cube and rhombic dodecahedron.

In the growth of diamond in the laboratory compared to what is found in nature, there are many similarities and some apparent differences. A striking example of an apparent difference is the regularity of the crystal forms of diamond produced in the laboratory. If conditions are such that inter-growth, aggregation or gross dissolution are not present, the synthetic diamond has a regular, easily recognized crystal form. In natural diamond, perfectly straight-edged regular crystals are rare; more commonly, rounded crystals or irregular pieces having no easily recognized faces are found. This may be interpreted as meaning that in nature diamond grows in restricted or confined environments where the crystal more or less conforms in contour to the surrounding rock masses. A restriction in carbon reaching the growing faces uniformly may also account for this. The rounded crystal form could be produced by abrasion or dissolution after the diamond is formed. The growth of diamond in the laboratory supports the latter theory. In our synthesis of diamond where the crystallization occurs through a relatively thin film of metal catalyst with adequate graphite present, uniform deposition over the entire crystal face can easily take place. This metal film need never exceed a couple of hundred microns in thickness.

As in nature, we have found that diamond tends to the octahedron as the most common crystal form. However, under certain conditions only the cube and rhombic dodecahedra will result. The factors that influence the crystal habit have been examined and are discussed in the third portion of this paper.

Crystal Surfaces

A study of the surface topography of diamond shows a variety of surface markings. In the growth of diamond in the laboratory, an attempt was made to correlate these surface markings with the variables of the growth process. In doing so, it was anticipated that some information might be uncovered that would be helpful in elucidating the detailed growth mechanism.

Our experiments indicate that diamond prefers to grow by the piling up of sheets of material parallel to the (111) face. The cleavage and "grain" of diamond is parallel to these faces. Steps indicating the edges of sheets and the so-called "growth trigons," formed by intersection of these edges, can be found on laboratory made diamond. Fig. 1 shows synthetic diamond with these surface markings, which are identical in all characteristics to natural diamond. Note the large step parallel to the crystal edge composed of several growth layers. This step probably was caused by a deficiency of catalyst over the lower portion of the crystal

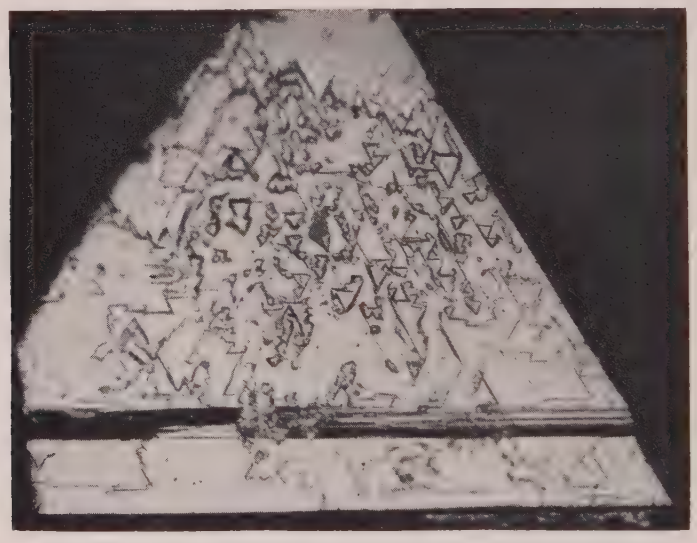

FIG. 1. Trigons and steps on octahedral face. Growth on seed. 300×.

face. There may be a wide range of trigon sizes. The trigon corners point toward the edges of the octahedral faces. The shallow depression represented by a trigon usually represents a difference in surface elevation of several hundred angstrom units. However, since trigons may exist too shallow to be resolved, the growth layers may be much thinner. Laboratory evidence indicates that these surface markings are found when the diamond was actually growing at the time it was removed from the selected conditions of temperature and pressure. The new growth appears to be added in plane waves advancing toward the octahedral edges, where trigons are observed.

These trigons or surface steps are not always found on synthetic diamond after its formation. When conditions are such that the growth is followed by holding the diamond at a temperature above the growth

temperature and a little outside the diamond stable region, etch pits are found on the (111) face (Fig. 2). The sides of the triangular pits are parallel to the octahedron edge. Etch pits have also been produced by slowly dissolving the surface of natural and synthetic diamond in fused potassium nitrate at 500 to 600° C. These etch pits probably mark imperfections of the atomic arrangement in the crystal lattice. The marking of imperfections or dislocations by etching is an established art in studying crystals in other materials. The etch pits are rather uniform in size as shown and the depth and diameter depends on the degree of etch. Fully developed pits have about an eight to one width to depth ratio.

FIG. 2. Etch pits on octahedral face as removed from high pressure cell. 300×.

It is considered that these etch pits are produced by a dissolution process. If at constant pressure the temperature is increased after the diamonds are formed until conditions exist where diamond is no longer stable the diamond is converted to graphite. This process has been demonstrated many times in diamond synthesis studies. If the increase in temperature is only enough to cause slight instability, dissolution is slow and etch pits are produced. Greatly increased temperatures under these conditions produce a more catastrophic attack of the diamond. Very rough surfaces may be produced on diamond in this manner. It has been observed that cube faces appear to etch more rapidly than the octahedral faces under these conditions.

Synthetic diamond may be etched at one atmosphere in the same manner as natural diamond. The octahedral and cube faces lightly

FIG. 3. Etch pits on octahedral face produced by etching in fused KNO_3. 200×.

etched at 900° C. in fused potassium nitrate are shown in Fig. 3 and 4. Fersmann and Goldschmidt probably were the first to study etch pits and propose the dissolution process.

Still another surface characteristic is found on the faces of cube diamond grown under conditions of minimum temperature and pressure for each catalyst. Under these conditions diamond appears to grow by the addition of layers to the cube face only. A cross section of the diamond clearly shows the layered structure. The stepped surfaces on these faces resulting from the edges of the layers is shown in Fig. 5. The use of the

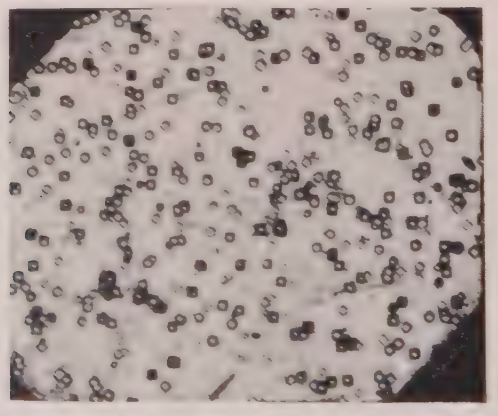

FIG. 4. Etch pits on cube face produced by etching in fused KNO_3. 100×.

FIG. 5. Cube face showing growth steps. 120×.

erference microscope shows the step height to average about 300 Å th the center of the face higher than the edges giving a slope of about to 300. In contrast, natural cube faces always have a rough pitted rface, the surfaces of which are (111) planes. The layered structure on e cube face is apparently a double growth spiral on a dislocation. One follow the edges to form closed loops. Although single growth spirals ve been observed, the double growth spiral is much more common. The diamond which grows almost exclusively on the cube face is al-ost always black, possibly due to graphite between the layers. *X*-ray alysis of these crystals shows a distorted crystal structure due to the

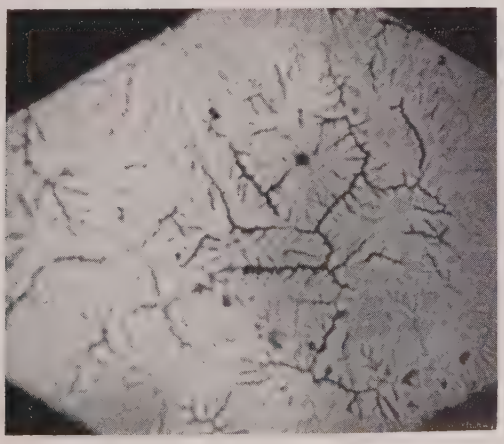

FIG. 6. Veined surface. Cube face. 120×.

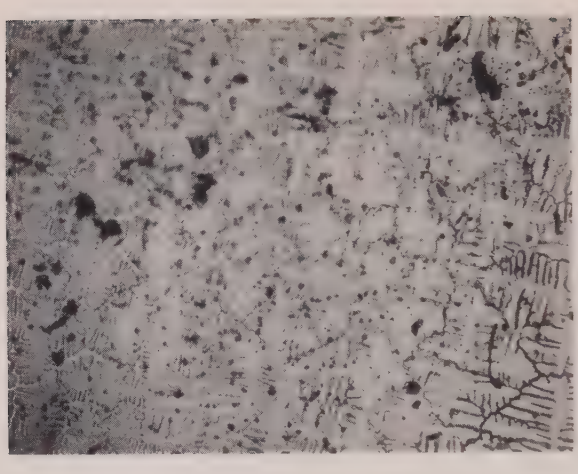

FIG. 7. Dendrite imprint on cube face. 120×.

inclusion of much foreign material. This results in a weak structure easi cleaved and crushed. This form of diamond has not been observed nature.

Another type of surface marking is commonly found on synthetic d mond. This surface detail resembles a network of veins or streams (F 6). In many cases, the detail looks more like dendrites. This pattern c be found on both octahedral faces and the cube faces (Fig. 7) of the d mond. This surface condition is considered to be a reflection (or) impri of the dendritic structure of the metal catalyst. If the catalyst film stripped off the crystal face after the diamond is removed from the gro ing media, and the metal film examined metallographically, the sa dendritic structure is seen in the catalyst film. During the last stages the growth of the diamond with this surface pattern, the catalyst is i semi-solid state with dendrites freezing in the metal and being mirro on the diamond surface. Carbon may still be migrating in the unfro portion of the catalyst building up or dissolving the diamond surfa The last stages of growth then occurred at a temperature near the carb metal eutectic. Trigons are found only when higher temperatures oc relative to the carbon-metal eutectic.

If diamonds, such as shown in Fig. 7, are etched in potassium nitr at 550 to 600° C., the dendritic pattern slowly disappears and the vei structure of Fig. 6 remains. Further etching brings out etch pits, angular on the octahedral and rectangular on the cube faces.

Another type of cube diamond can be grown that is different from black cube described previously. The diamond may start as an o hedron and grows to a symmetrical cubo-octahedral shape and finally

cube with very small (111) faces at the corners. Cubes grown in this manner are not necessarily black in color nor do they incorporate as much impurity in the crystal. The (111) faces grow faster, leaving the cube faces predominating. Under marginal growth conditions, it appears that the growth may be almost completely stopped on the cube faces. Higher temperatures appear to favor growth on the octahedral faces exclusively and the cubo or cubo-octahedral habit of crystal is not produced. The cube and octahedral faces produced may be very flat or slightly concave. Again, this crystal form is not observed in natural diamond.

The fact that the two different growth habits are dependent on the temperature at which the growth occurs can be demonstrated readily by growing under both conditions consecutively. The temperature is first maintained so as to grow a cubo-octahedron and then lowered about 0° C. to the cube face growing condition. The finished diamond in section shows the center clear cubo-octahedron surrounded by the black opaque layered cube growth in the same orientation as the center crystal.

Rhombic dodecahedra are rarely found in laboratory grown diamonds. When they are found, however, the entire yield will consist of dodecahedra. Since they are so rare and since the conditions where they are grown are those where dissolution is suspected, the rhombic dodecahedron is not considered to be a true growth form in the case of synthetic diamond. All the dodecahedra examined show rough faces with deep striations as shown in Fig. 8. Frequently, octahedra are produced with dodecahedral faces starting to form. Again, this takes place where etching or dissolution of the crystal is occurring and etch pits are found

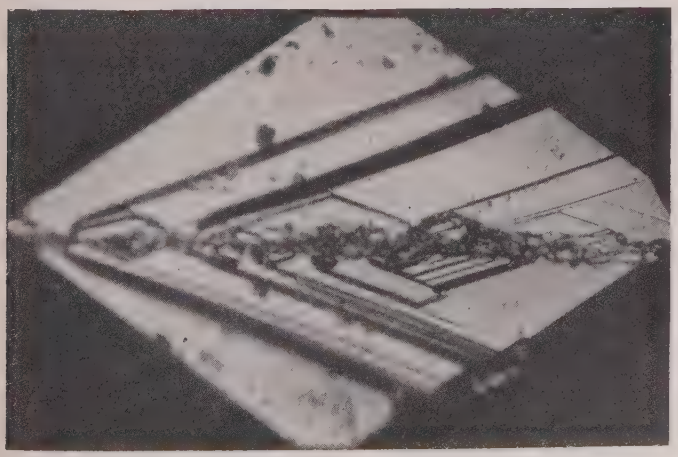

FIG. 8. Striations on dodecahedral face. 300×.

on the octahedral faces. Evidently preferred dissolving on the 110 fa must occur under certain conditions of physical and chemical enviro ment. These conditions must be common in nature since the rhomb dodecahedron is often found in natural diamond or else the natural c decahedron represents a type of growth we have not been able to repr duce.

If one looks at the crystal model of diamond and studies the oct hedral, cube and dodecahedral surfaces, the surface roughness var when observed on an atomic scale. This roughness is an indication of t relative ease with which atoms may be removed from the surface by solution process. The octahedral face presents the smoothest surface a the cube and dodecahedral faces, the most open or roughest surfac Near conditions of diamond growth, the octahedral face is less likely dissolve than the cube or dodecahedral faces. It appears that sligh different equilibrium conditions exist for the three different crystal fa and these differences in surface energy of the crystallographic plan partially account for the crystal forms of synthetic diamond descrit above. For example, a crystal can start as a cube or dodecahedron a grow with the crystal filling out to the octahedral form.

Crystal Habit Variations with Growth Rate

The growth rate of synthetic diamond is very high but has been var over a range of nearly two orders of magnitude with at least one-th millimeter per minute as the maximum. The rate is influenced prima by the pressure, temperature and temperature gradient so that farther into the diamond stable region, as we have determined it, and steeper the gradient, the higher the growth rate.

At high growth rates, it is difficult to prevent nucleation so that monds start growing simultaneously at many closely spaced intervals the catalyst-graphite interface. This leads to intergrowth and cluster of the crystals. The crystals grow into each other at random angles new crystals may nucleate and grow right on established growing face high growth rates. The edges of the octahedra may tend to grow fa with growth advancing toward the centers of the faces. This leads t hoppered surface and a skeletal structure. That is, the growth is initia at the edges of the faces and the initiation of growth layers is faster t the rate at which the growth proceeds across the crystal face. A typ intergrown diamond cluster showing hoppering and skeletal growt shown in Fig. 9.

A mosaic of many small oriented crystallites of diamond can be gro This structure may take many forms; an example of one form is show Fig. 10 which has been etched to bring out the oriented crystallites n ing up the large octahedral face. A structure, similar to natural ca

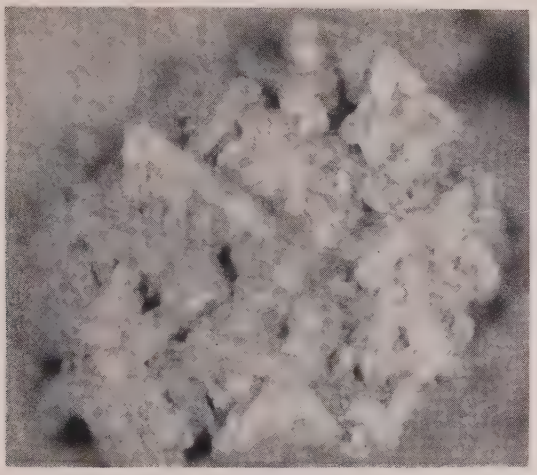

FIG. 9. Hoppered and skeletal growth. 50×.

nado diamond, can be grown with the crystallites joined to form a diamond to diamond bond by intergrowth. The structure may be porous with foreign material filling the voids. The carbonado is a polycrystalline diamond formed by small crystallites grown together. The carbonado is grown at the lowest temperatures of formation with spontaneous nucleation at closely spaced intervals giving a relatively small grain size.

The "ballas," a rare form of natural diamond with radial symmetry composed of apparently spherically grown layers, has not been synthesized to our knowledge.

In general, as the growth rate is slowed down, the crystals become better in quality. The crystals generally incorporate less impurity and the skeletal or hoppered structure may not be formed. This is only a general observation as the action of the catalysts vary; that is, some cata-

FIG. 10. Mosaic diamond. 300×.

lysts appear to promote skeletal and hoppered crystals even at lowe growth rates.

Color

Variations in temperature and pressure result in variations in color o the diamond produced. As the temperature is raised, the low temperatur black is usually replaced by shades of yellow and green until colorles diamond is formed at the higher temperatures. If the color is caused b strains in the crystal lattice due to the insertion of interstitial foreig atoms, this change of color may be simply due to the inclusion of fewe foreign atoms as the temperature of the reaction is raised. However, eve colorless diamonds may show *x*-ray patterns from the catalyst metal i the crystal. The color may be affected by the nature of the impurity i some cases and only by the amount of a given impurity in others. Se lected conditions permit a wide variety of shades such as black, degree of gray, amber, yellow, green, blue and colorless. The intensity of th color and the size of the crystal may make the diamond opaque or trans parent.

Twinning

Twinning is very common in diamond. The macle or spinel twin is th most common form in natural diamond. We observe true twinning an random intergrowth in synthetic diamond. However, the macle twin ca be grown in a range of thickness to length ratios. Interpenetrating cub at random angles are also commonly observed. Diamond is predispose toward twinning due to the relatively slight energy difference betwee the normal and twinned configuration.

Inclusions

It has not been possible so far to grow diamond without trace incl sions. This is true especially of the more rapidly grown diamond. In th more slowly grown crystals, the inclusions are frequently found to l oriented along the crystal axes and can be easily seen under the micr scope.

Foreign inclusions in diamond including diamond in diamond (grow on a seed) are a source of strain. The strain patterns originating at the i clusion can be seen in the polariscope and such diamonds are easi fractured.

Foreign materials may be introduced into the growing process i tentionally or otherwise and analysis of the diamond may show the pre ence of many of the light elements such as are found in natural diamon Since the inclusions may be magnetic, the resulting diamond may exhib weak magnetic properties. Garnet, which is found associated with a sometimes as an inclusion in natural diamond, is stable under some of t

conditions of our synthesis and garnet has been present as an intrusion in synthetic diamond. It does not act as a seeding agent, however.

Another mineral inclusion supposedly found in natural diamond is quartz. In attempts to introduce quartz into diamond, the quartz always changes to coesite. The quartz in all natural diamond so far examined is not totally enclosed by diamond but is found in cracks, fissures, or pockets. Under the quartz, one can often see (111) steps and trigons on the diamond surfaces. There is no evidence so far that natural diamond was grown at pressures and temperatures where quartz is stable.

Seed diamond can be used as a growth site for new diamond, which follows the same crystal orientation as the seed. However, the seed can always be seen if the new growth is transparent. Apparently, an interface of trapped impurity always makes the seed visible. This is also observed in natural diamond. There is little if any advantage in growing on seeds as opposed to not seeding as the conditions for good seed growth are the same as for new growth without seeds.

Conclusions

In synthetic diamond, we found a number of the forms and habit characteristics of natural diamond. Most of the growth variations in structure and habit have been duplicated with apparently some additional forms. The growing faces of a diamond crystal are usually, but not always, on the (111) crystallographic planes. Growth on the cube faces by a spiral growth mechanism sometimes occurs near minimal temperature conditions. Dendritic surface markings on synthetic diamond represent the imprint of the catalyst metal structure upon freezing.

The crystal habit is influenced by the physical conditions of formation and the growth rate. Dissolution apparently can take place to produce rhombdodecahedral planes. Therefore, this growth habit is considered to be not a true growth form in synthetic diamond. Polycrystalline diamond is obtained when nucleation occurs at closely spaced intervals with relatively high growth rates.

The color of diamond is affected by impurity type and concentration and can be changed by varying the temperature at which the growth takes place.

References

Bovenkerk, Bundy, Hall and Wentorf, (1959), Preparation of diamond: *Nature*, **184**, 1094.

Fersman, A. and Goldschmidt, V. (1911), Der Diamant. Winter, Heidelberg.

Hall, H. T., (1960), The belt: *Rev. Sci. Instr.*, **31**, 125.

Polansky, S., (1955), The Microstructure of Diamond Surfaces: N. A. G. Press, London.

Williams, A. F., (1932), The Genesis of the Diamond. Benn and Co., London.

Manuscript received July 24, 1960.

THE AMERICAN MINERALOGIST, VOL. 46, JULY-AUGUST, 1961

POLIANITE PSEUDOMORPHS

F. M. Nakhla, *National Research Centre, Cairo, Egypt*

Abstract

A study of the morphology, composition, *x*-ray data and optical properties of ra polianite pseudomorphs from Um Bogma mine, Egypt, shows that they are pseudomorph after an unknown orthorhombic mineral.

Introduction

The manganiferous iron ore deposits of Um Bogma district, wes central Sinai, Egypt, are believed to be a late Tertiary mineralizatio (Ball, 1916; Fenine, 1931; Attia, 1956; Gill and Ford, 1956; El-Shazl 1957). The ore is composed essentially of pyrolusite, manganite, psil melane, wad, goethite, and minor amounts of barite, siderite, and oth rare minerals.

Very small cystals about 2 to 4 mm. in length and 0.4 mm. in diamet occur rarely in cavities in some specimens. Morphological, microchemic *x*-ray, and optical examinations of the crystals was carried out by th writer (Nakhla, 1958). Additional information is included in this pap

Description

The rare crystals occur as single individuals or as parallel untwinn groups, and a few exhibit a fibrous radiating structure. The cryst shown in Fig. 1, are characterized by vertical and deeply striated prisn terminated by well developed, steep smooth pyramids, commonly wi a sharp pointed end. The mineral is dark steel gray in color, with metal lustre, and black streak. It is barely scratched by a steel needle. It p sesses a perfect cleavage parallel to (010), and has an even fractu Blowpipe tests are identical to those of polianite.

The morphological investigation shows that the system is orth rhombic, probably dibipyramidal. The calcuted ϕ and ρ values (Table correspond to an axial ratio $a:b:c=0.729:1:1.084$. Figures 2 and illustrate the habit of the crystals. Additional tiny faces too small to g signals were located approximately by direct reflections. These shown in Fig. 4.

A microanalysis carried out on 6.612 mg. of the dried material pro that the chemical composition of the mineral is essentially mangan dioxide (MnO_2).

An *x*-ray powder pattern was made using a 9.0 cm. diameter cam Cu Kα 30 Kv, and 10 M.A, with powder mounted on glass fiber suppo There is a close agreement with polianite (or pyrolusite). Furtherm Dr. Carapezza of Palermo University, Italy, kindly carried out an *x*-

TABLE I. PHI AND RHO VALUES FOR (*hk*0) FACES WHICH YIELDED SHARP REFLECTIONS OR BANDS

hkl	Calculated values		Measured values and range		Remarks
	ϕ	ρ	ϕ	ρ	
010	00°00′	90°00′	0°55′±30′	89°41′± 6′	Weak band
140	18°58′	90°00′	18°50′±10′	89°45′±12′	Strong band—no signals
130	24°34′	90°00′	24°56′±20′	89°50′± 2′	Strong band—no signals
250	28°45′	90°00′	28°49′± 4′	89°48′±30′	Strong band —no signals
120	34°26′	90°00′	34°40′±30′	89°44′±13′	Medium band
470	38° 6′	90°00′	38° 4′±30′	89°58′± 4′	Strong band
350	39°27′	90°00′	39°45′±30′	90°21′±15′	Strong band
230	42°27′	90°00′	42°18′±18′	89°48′±24′	Strong band and sharp signal
340	45°48′	90°00′	45°36′±48′	90°11′± 8′	Weak band
450	47°40′	90°00′	47°41′± 7′	89°37′±18′	Strong band and sharp signal
670	49°37′	90°00′	49°28′±16′	89°54′±12′	Strong band and sharp signal
110	53°54′	90°00′	53°31′±49′	89°58′± 5′	Medium band
430	61°20′	90°00′	61°10′±25′	89°32′±25′	Strong band
320	64° 4′	90°00′	64° 7′±58′	89°53′±23′	Strong band
530	66°22′	90°00′	66°29′±29′	90° 3′± 4′	Strong band
210	69°58′	90°00′	69°21′±28′	89°37′± 9′	Medium band
520	73°45′	90°00′	73°15′±10′	89°45′±20′	Very weak band
310	76°18′	90°00′	77°00′±50′	89°55′±15′	Weak band
100	90°00′	90°00′	90°18′±20′	89°55′±10′	Weak band
321	64° 5′	78°36′	64° 5′±12′	78°36′±16′	Very sharp signal

FIG. 1. Photographs of the polianite pseudomorphs. ×150.

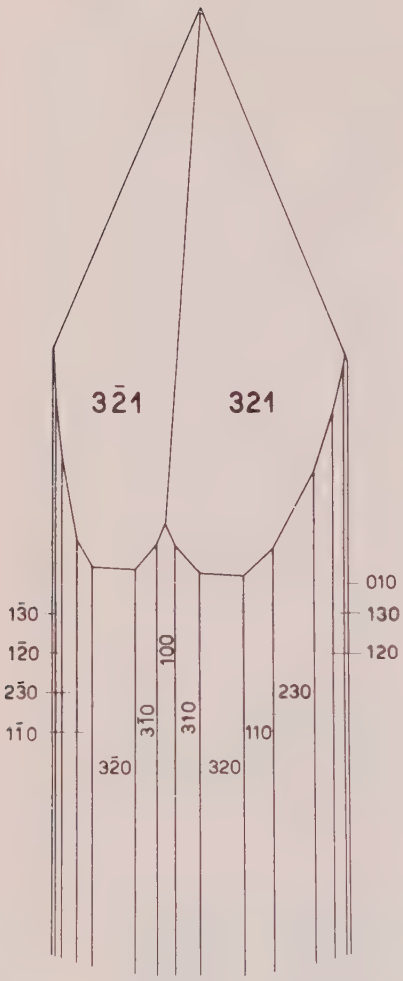

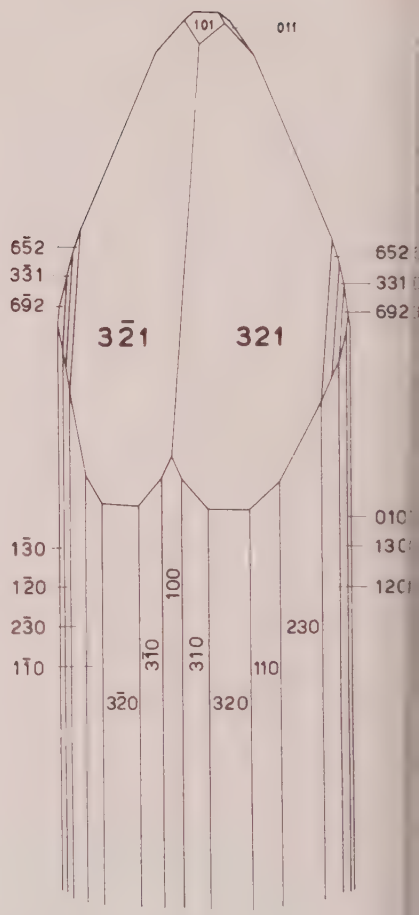

Fig. 2. (Left) Drawing showing the most common type.
Fig. 3. (Right) Habit rarely shown.

analysis on a rotating crystal, and after determining the unit-cell dimen sions he concluded that the actual structure is that of polianite.

Mineralographic examination of the mineral showed that the colo reflectivity, anisotropism, and etch reactions are identical with those o polianite as given in the standard texts.

It seems obvious that we are dealing with a pseudomorph of polianit after an unknown orthorhombic mineral. Köchlin (1888) describe similar pseudomorphs from Macskamezö in Hungary, which were repr

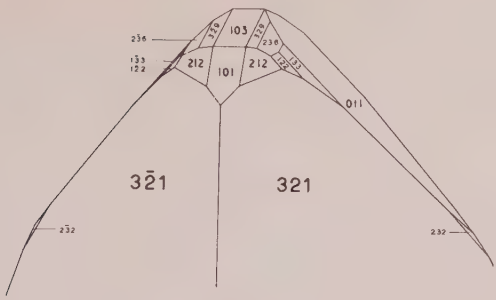

FIG. 4. Top of crystal showing the extremely small (*hkl*) faces observed by direct reflection.

sented as manganite. Similar examples were also reported by Kossmat (1905), Goldschmidt (1918) and Strunz (1943).

In the present case, however, the interfacial angles, the axial ratio, and the strange habit of these pseudomorphs do not fit those of manganite. Furthermore, the predominant and excellently developed (321) pyramidal faces which characterize these pseudomorphs, would yield very complicated symbols when referred to the manganite axial ratio. Neither does the polianite seem to be pseudomorphous after huebnerite, lepidocrocite or kentrolite.

There is an apparent close relation between the crystallographic data here given and that for the mineral lautite (CuAsS), although this seems improbable because of their chemical compositions. If the indices assigned to these pseudomorphs have the last figure doubled, there is fairly close agreement of phi and rho values with those of lautite, as seen in Table II. The corresponding axial ratios are 0.729:1:1.084 and 0.691:1:2.090. However, lautite crystals are elongated parallel to [100], rather than [001].

It would seem preferable to state that these "crystals" with the composition and stucture of polianite are pseudomorphs after an unknown

TABLE II. PHI AND RHO VALUES FOR POLIANITE AND LAUTITE

Polianite (Nakhla)			Lautite (Palache, *et al.*)		
hkl	θ	ρ	*hkl*	ϕ	ρ
321	64°05′	78°36′	322	65°15′	78°40′
101	90°00′	56°05′	102	90°00′	56°31′
232	42°28′	65°35′	234	43°58′	65°20′
122	34°27′	52°45′	124	35°53′	52°13′

mineral that could be determined only if fresh crystals of the original mineral are found. However, this seems to be a remote possibility, as diagenetic processes have concealed the original characteristics of the ore, and have produced pseudomorphism throughout the manganese deposits of Um Bogma mine.

References

Attia, M. I. (1956), Manganese deposits of Egypt: *Int. Geol. Congress, 20th., Mexico, Symposium sobre Yacimientos de Manganeso*, **2,** *Africa*, 143–171.

Ball, J. (1916), The geography and geology of west-central Sinai: *Survey Dept., Cairo.*

El Shazly, E. M. (1957), Classification of Egyptian mineral deposits: *Egyptian Jour. of Geol.*, **I,** 1–20.

Fenine, M. A. (1931), La formation geologique des gisements de mineralis de manganese du Sinai: *Bull. Inst. Egypte*, **13,** 15–26.

Gill, D., and Ford, S. (1956), Manganiferous iron ore deposits of the Um Bogma district, Sinai, Egypt: *Int. Geol. Congress, 20th., Mexico, Symposium sobre Yacimientos de Manganeso*, **2,** *Africa*, 173–177.

Goldschmidt, V. (1918), Atlas der Krystallformen, **5,** (tables), 196, tables 121 (fig. 48), and 122 (fig. 49); **5** (text), 128.

Köchlin, R. (1888), *Tschermak's Min. Petr. Mitt.*, **5,** 38–39.

Kossmat, J. (1905), Geologie der mangan Mineralien: *Zs. pr. Geol.*, **13,** 305.

Nakhla, F. M. (1958), Polianite pseudomorphs from Um Bogma, Egypt: *Egyptian Journal of Geology*, **2,** 89–101.

Palache, C. , *et al.* (1944), Dana's system of mineralogy: John Wiley & Sons, London, I 327, 564, 613.

Short, M. N. (1940), Microscopic determination of the ore minerals: *Bull. U. S., Geol Surv.*, no. 914, 168.

Strunz, H. (1943), Beitrag zum pyrolusit problem: Naturwiss, **31,** 89.

Uytenbogaardt, W. (1951), Tables for the determination of the ore minerals: Princeton University Press, Princeton, New Jersey, 176.

THE AMERICAN MINERALOGIST, VOL. 46, JULY-AUGUST, 1961

SHEARED ILMENITE IN VEIN QUARTZ

P. S. Chakravarty, *Department of Geological Sciences, Jadavpur University, Calcutta, India*

Abstract

Sheared ilmenites with megascopic slip planes, embedded in vein quartz from Rautara (22°49′ N; 86°39′ E) Bankura Dt., West Bengal, India, have been studied. Major slip along one or more important directions has resulted in subsidiary slips along available cleavage, twinning and other oblique surfaces. Interesting textural features comprising translation gliding, twin gliding, and intersecting translation units are described.

A specimen polished on several faces was examined to study the orientation of slip-planes. The composite polar diagram of all available planes was superimposed on a complete stereogram of ilmenite from published interfacial angles. From complete matching of the poles it has been concluded that prominent translation planes are 0001, (t=[10$\bar{1}$0]) and 10$\bar{1}$0. Minor slip planes include $\bar{5}$054, $\bar{2}$021, 1$\bar{1}$22, 55$\bar{1}$03 and 21$\bar{1}$2.

Localization of the blebs and spindles of exsolved hematite along twin-planes in ilmenite from sheared portions of the vein indicates the prominent role of deformative stress in bringing about the exsolution.

Occurrence of ilmenite-bearing quartz veins has been discovered by the author near Rautara (22° 49′ N; 86° 39′ E), Bankura Dt., West Bengal, India. The associated garnet-staurolite-sillimanite-muscovite-schists dip N.E. at high angles of 45°–60°. The veins run parallel to the foliation strike of the country rock. The quartz veins have been locally sheared with development of close-spaced jointing. The ilmenite from the highly sheared portions of the veins has developed numerous conjugate slip-planes, some of which can be recognized megascopically. The shear planes developed in a quartz vein marked by lensoid grains of quartz at an angle with the megascopic slip-planes in the ilmenite, owing to difference in competency of the two minerals (Fig. 1). In less deformed parts of the vein, jointing is wide-spaced and slip planes in ilmenite are absent.

The study of polished specimens in reflected light shows strong development of twin-lamellae in ilmenite in the deformed part of the vein. In extreme cases, the twin-lamellae have been bent, fractured and displaced (Fig. 2). Beautiful translation units are common in these deformed ilmenites. The translation units can be seen as broad lamellae by partial crossing of the nicols or by reflection pleochroism alone. Commonly the translation units form parallel bands within ilmenite crystals. The trace of the translation plane is at an angle with that of the twinning composition plane in the main mass of ilmenite.

Each translation unit shows either one or two sets of twins, diagonal to the length of the unit; when only one set is present, its orientation is rotated to almost 90° with respect to the lamellae in the adjacent undis-

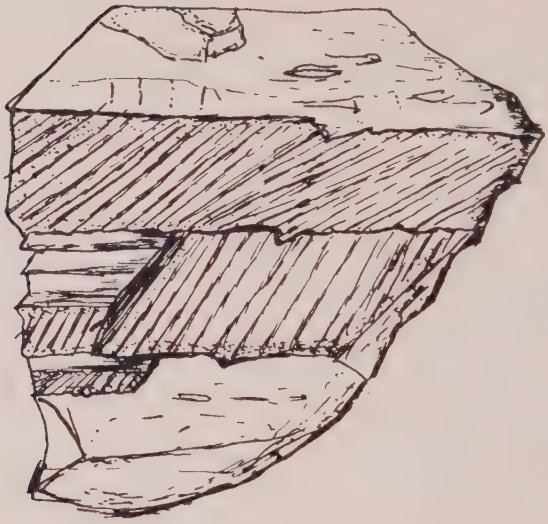

FIG. 1. Megascopic slip-planes in ilmenite embedded in quartz. Shear planes develop in vein quartz marked by lensoid grains are at angle with the megasopic slip planes ilmenite. Natural size.

turbed parts. In the undisturbed part, on either side of a translation un the twin-lamellae are continuous in trend. Within some translati units there are fine lamellae resembling polysynthetic twins, parallel the trace of the translation plane. Such fine lamellae are also visible in t undisturbed crystal along the border of the translation units (Figs. and 4). The fine twin-lamellae within translation units which are paral

FIG. 2. Bent, fractured and displaced twin lamellae in ilmenite. ×140.

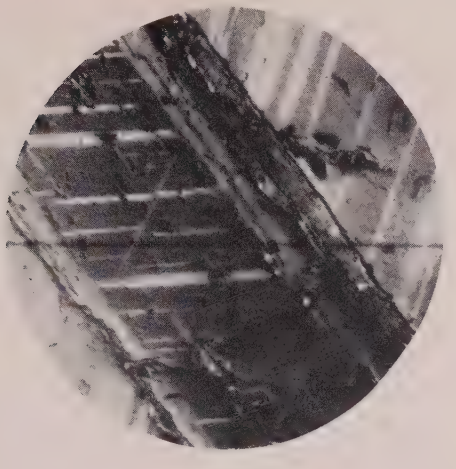

FIG. 3. A translation unit in ilmenite. Twining lamellae in undisturbed part of ilmenite continuous in trend. Three sets of twins are visible within the translation unit, some of which exhibit minor slips. ×140.

the trace of the translation plane, indicate twin gliding. Disturbances along translation planes have influenced the development of fine twins in the undisturbed part of the ilmenite adjacent to the translation units.

Locally two or three sets of translation units may be seen intersecting at a point (Fig. 5); some of the units may taper like leaf-laminae, where the traces of the translation surfaces meet, suggesting bend gliding. Numerous planes are seen extending from the tapering edge, most of

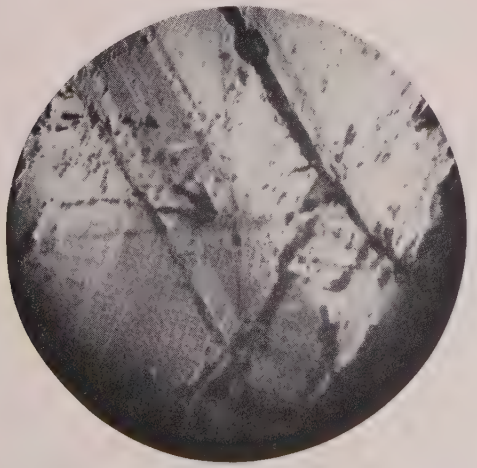

FIG. 4. Fine twin lamellae parallel to the trace of the translation plane within and outside the translation unit. ×140.

which are parallel or sub-parallel to the visible traces of the twinning co position planes. These have formed consequent to the impact of t tapering edge of the translation unit.

In most cases the bent translation units are seen to be composi planes, having resulted from a number of slips along sub-parallel planes step-like arrangement. These transverse planes in the steps are som times planes of visible slips possibly slightly post-dating the main slip.

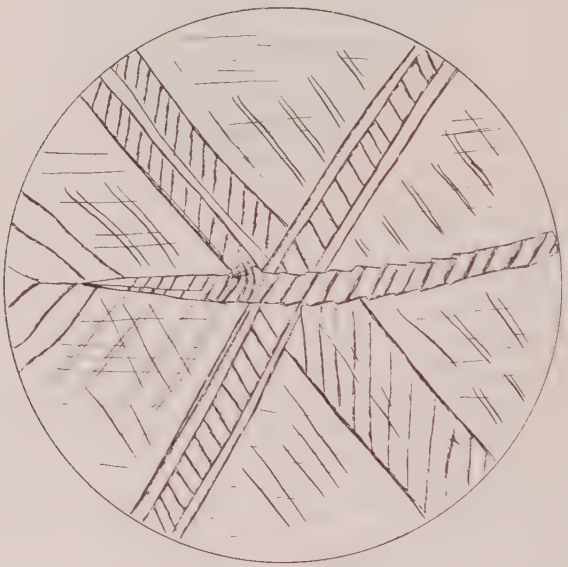

FIG. 5. Three intersecting translation units in ilmenite. One of them is bent and tapers like a leaf. ×100.

Another interesting feature is local thinning of bands showing str reflection pleochroism along planes parallel to translation units (Fig. This thinning appears to have resulted from slip along the diago planes within the translation units in a direction oblique to the plane polished surface, or by twist gliding* along axes parallel or sub-parallel the twin-lamellae or normal to the diagonal plane.

To study the orientation of the slip planes, a specimen was polished four faces and was examined in incident light on UTR_2 stage (Ehrenb Stage). All the available planes on each of the four polished surfaces w oriented horizontally and separate stereographic diagrams were prepa for each face. All the plottings were then transferred to one face by ro

* Synonymous with "tortional translation-gliding," Fairbairn, Structural Petrolog Deformed Rocks, 1942, p. 83.

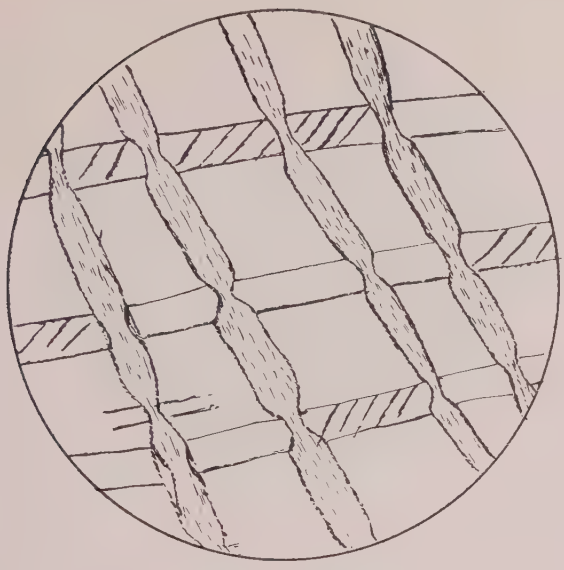

FIG. 6. Local thinning of certain bands along the translation units. ×150.

ion. As there was no optical or crystallographic control in orientation he composite polar diagram of all the available planes was superimposed n a complete stereogram of ilmenite from the published interfacial ngles. The position at which there was complete matching was used for dentifying the planes.

The results of the study are given in the following table:

Prominent translation planes (Megascopically visible)	Minor slip planes	Slip direction
0001 (Ramdohr, 1950)		[10$\bar{1}$0]
10$\bar{1}$0		Cannot be determined
	$\bar{5}$0·4	
	$\bar{2}$0·1	
	1$\bar{1}$·2	Cannot be determined
	55·3	
	2$\bar{1}$·2	

The translation occurred along multiple slip-planes and major slip long one or more important planes resulted in subsidiary slips along vailable cleavage, twinning or other planes.

Another interesting observation is that ilmenite from the sheared por- on of the veins exhibits blebs and spindles of hematite arranged parallel the visible twin planes (Figs. 7 and 8); whereas the specimens from

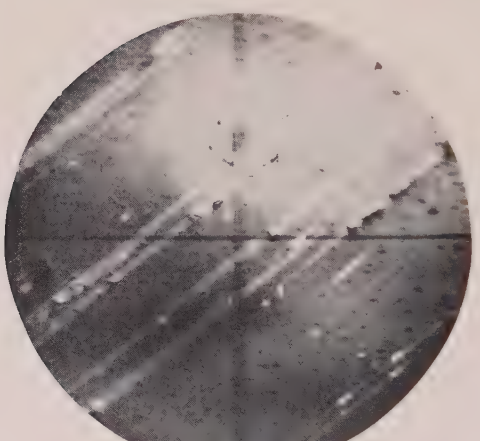

FIG. 7. Exsolution blebs of hematite in ilmenite arranged in two planes. ×360.

relatively massive part of the vein are rarely twinned and are free fr these exsolution blebs.

Hematite in thin tabular grains parallel to (0001) is a feature of man ilmenites; but exsolution of hematite along rhombohedral twin planes ilmenite has only been rarely reported (Ramdohr 1926, cited by Grun 1929). Perhaps the exsolution of hematite along the twin-planes ilmenite is facilitated in an environment of shearing stress. Sen (in pres has indicated that formation of antiperthite is also favored by stress.

The two minerals ilmenite and hematite form a continuous solid soluti somewhat above 600° C. (Ramdohr, 1926; Edwards, 1938); wi

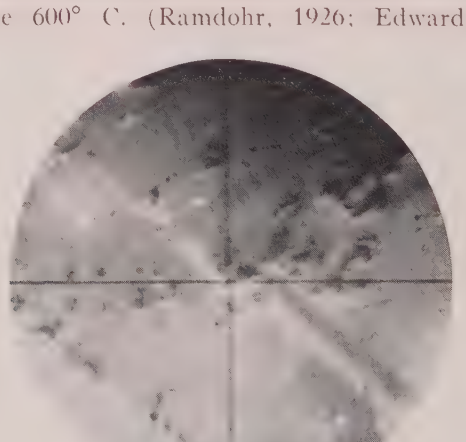

FIG. 8. Exsolution blebs of hematite arranged parallel to the visible twins in ilmenite. ×3

moderately slow cooling, it unmixes into two solid solutions. The ilmenite-bearing veins in the present area are associated with high grade schists of the amphibolite facies. (Chakravarty, 1955). The occassional appearance of granular pleonaste (R.I. 1.71) in the associated garnet-sillimanite-schists indicates that the temperature of metamorphism reached that of the highest part of the amphibolite facies, if it did not surpass it. Ramberg (1952, p. 137) estimates temperature for the amphibolite facies as between 350°–550° C. Rosenqvist (1952, p. 101) suggests a temperature range of 400°–750° C. at depths less than eight miles.

If the veins have been subjected to metamorphism similar to that of the associated pelitic schists (which is still to be established) the temperature of metamorphism was high enough to permit unmixing of ilmenite and hematite at a lower temperature. But the localization of the oriented hematite blebs in ilmenite in sheared parts of the veins points out that deformative stress rather than rise of temperature controlled the unmixing in this particular case.

Acknowledgments

The author tenders his grateful acknowledgments to Dr. S. N. Sen, University of Calcutta, for his guidance throughout the work; his sincere thanks are also due to Dr. S. Deb, Jadavpur University and Prof. S. Ray, Presidency College, Calcutta, for their help, warm sympathy and encouragement.

References

CHAKRAVARTY, P. S. (1955) Study of Metamorphic rocks around Ranibandh and Rautara, Bankura Dt., West Bengal, M.Sc. thesis, Calcutta University. Synopsis published in *Bhu-Vidya, Journal of the Geological Institute, Presidency College, Calcutta,* **17,** (1955) p. 81.

——, (in press) Zonal metamorphism near the Trijunction of Bankura, Midnapore and Purulia Districts. *Quart. Jour. Geol. Min. Meta. Society of India.*

EDWARDS, A. B. (1938) Some ilmenite microstructures and their interpretation. *Aust. Inst. Min. Meta. Proc. N. S.* **110,** 38–58.

——, (1947) *Texture of the ore minerals and their significance.* Melbourne.

GRUNER, J. W. (1932) Structural reasons for orientated intergrowths in some minerals. *Am. Mineral.*, **14,** 227–237.

RAMBERG, HANS (1952) *The origin of metamorphic and metasomatic rocks.* Chicago Univ. Press, p. 137.

RAMDOHR, P. (1926) Beobachtungen an Magnetit, Ilmenit, Eisenglanz und überlengungen über das system FeO-Fe_2O_3-TiO. *Neues Jahrb. Min. Geol. Pal.* **54,** *Beil. Bd. Abt. A,* 320–379.

—— (1950) *Die Erzmineralien und ihre Verwachsungen.* Akademie-Verlag GmbH., Berlin.

ROSENQVIST, I. T. (1952) The metamorphic facies and feldspar minerals. *Univ. Bergen Arbok,* p. 10.

SEN, S. (in press) Potash content of natural plagioclases and the origin of antiperthite. *Journal of Geology.*

NOTES AND NEWS

THE FORMATION OF COESITE AND KYANITE FROM PYROPHYLLITE AT VERY HIGH PRESSURES AND HIGH TEMPERATURES

A. A. Giardini, J. A. Kohn, D. W. Eckart, and J. E. Tydings
U. S. Army Signal Research and Development Laboratory, Fort Monmouth, New Jersey

In the course of studies carried out during the past two years on vari ous chemical systems at elevated pressures and temperatures, the altera tion of pyrophyllite specimen capsules was investigated. The pyrophy lite was found to decompose to coesite and kyanite, the present not being a preliminary report on this finding. Additional, more detailed studies will be presented as a portion of a more comprehensive paper at a future date.

A few words are in order concerning pyrophyllite-like materials a components in high-pressure equipment. The use of catlinite as a com pressible, solid, pressure transmitting material was first recognized b Bridgman (1938). More recently, massive pyrophyllite (commercially Tennessee Grade A Lava Stone or Wonderstone) has received wide a ceptance both as a solid, pressure-transmitting medium, and as an ele trical and thermal insulator in equipment capable of generating su tained very high pressures and high temperatures (Birch and Robertso 1957; Hall, 1958; Giardini, Tydings and Levin, 1960). Both materials a very fine-grained, relatively homogeneous, hydrous aluminum silicat that are readily machinable. Compositionally, pyrophyllite is relative pure and can be described by the chemical formula $H_2Al_2Si_4O_{12}$, whereas catlinite may contain up to 8 or 9% Fe_2O_3 and occasional trac of quartz. In practice, catlinite generally performs in a manner superi to pyrophyllite because of the high coefficient of static surface friction imparted by the presence of Fe_2O_3, which tends to restrict flowage unde pressure. With respect to availability, however, catlinite is difficult to o tain, whereas pyrophyllite can be purchased in commercial quantities relatively uniform quality. Consequently, the latter is in general use t day in static high-pressure high-temperature devices.

Figure 1 shows a sectioned specimen capsule (graphite charge) befo being subjected to elevated pressures and temperatures. A detailed de scription of the entire pressure apparatus has already been given (Gia dini, Tydings and Levin, 1960).

Figure 2 depicts a polished section of a specimen capsule that w stressed at 85 kilobars (1,250,000 psi) and heated to approximat 1600° C. in the vicinity of the charge. The latter in this case was graph (A, Figure 2), placed between two solid nickel cylinders (B). Note t

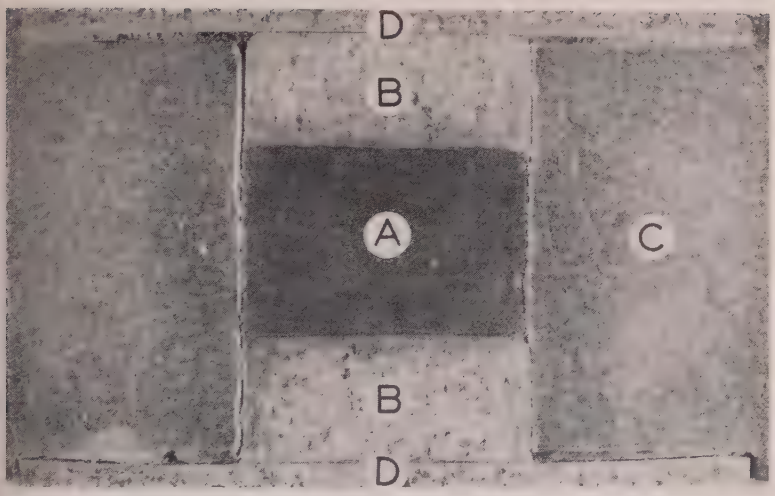

FIG. 1. Axial section of an assembled specimen chamber before stressing: A, graphite charge; B, solid nickel cylinders; C, pyrophyllite ring; D, nickel contact caps. 7.3×.

one of alteration (C) surrounding the charge. Similarly altered zones have been observed when the charge consisted of other materials, *e.g.*, barium titanate, contained within platinum or tantalum electrical resistance heating tubes. In area D, beyond the alteration zone, pyrophyllite was found to be unchanged. It is interesting to note the forma-

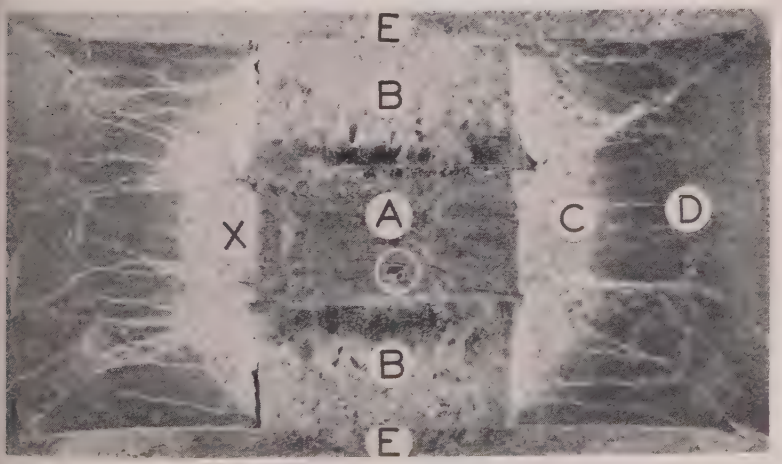

FIG. 2. Axial section of a specimen chamber stressed at 85 kilobars and heated to approximately 1600° C.: A, graphite charge (note circled diamond crystal); B, solid nickel cylinders (note recrystallization); C, altered pyrophyllite; D, unaltered pyrophyllite; E, nickel contact caps. 7.3×.

tion of small amounts of $NiAl_2O_4$ (spinel-type) at the interface between the nickel plug and the graphite charge. The aluminate was more abundant at higher temperatures. The graphite charge often showed intrusion by thin coesite veins (Fig. 3), demonstrating a surprising mobility for the silica phase at these pressures.

Polished sections and thin sections (both of these along capsule axis) were examined with a petrographic microscope; a few samples were further studied by electron microscopy. Positive identification of phases

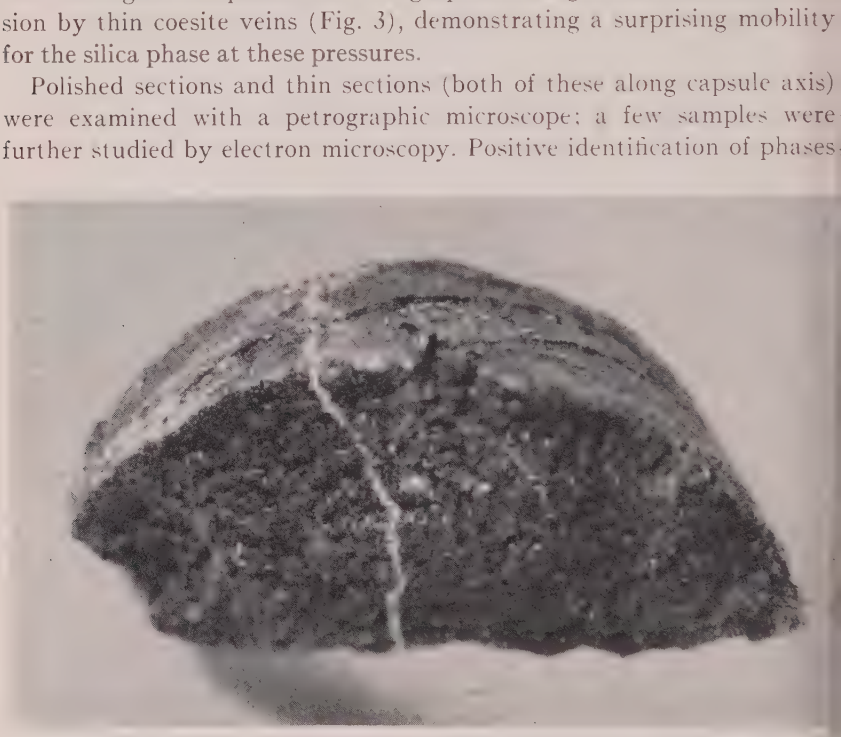

FIG. 3. Graphite charge showing intrusion by thin vein of coesite (30×).

was made by powder *x*-ray diffraction of small specimens removed fro polished sections. Coesite reference standards were prepared by subjec ing quartz, mixtures of quartz and sodium silicate, and sodium silicat alone, all sealed within platinum capsules, to 51 kilobars at 1500° C.

Table I lists the phases found in zone C (point X) of Fig. 2 at variou combinations of temperature and pressure; the charge in this series wa barium titanate within a platinum heating tube. Pressures were dete mined by extrapolation from the first two pressure-induced bismut electrical resistance discontinuities; the accuracy is approximately ±5% Temperatures were obtained by linear extrapolation of input pow versus platinum melting point at the particular pressure employed; th accuracy is approximately ±50° at 500° C. and ±100° at 2000° C Coesite and kyanite were invariably the major decomposition products a the more extreme P-T conditions. The tabulated data show the kyanit

TABLE I. PYROPHYLLITE REACTION PRODUCTS

Pressure (kilobars)	Temperature (° C.)	Reaction Products (principle)	(secondary)	(trace)
10^{-3}	500	pyrophyllite		
10^{-3}	1000	modified pyrophyllite		
10^{-3}	1500	mullite	SiO_2 glass	α-Al_2O_3
13.5	500	pyrophyllite		
13.5	1000	pyrophyllite		
13.5	1770	α-Al_2O_3	quartz	
27.0	25	pyrophyllite		
27.0	500	pyrophyllite		
27.0	1000	pyrophyllite		
27.0	1500	kyanite	coesite	α-A_2O_3
27.0	1900	kyanite	coesite	α-Al_2Ol_3
40.5	1500	coesite	kyanite	
40.5	2070	coesite	kyanite	
47.25	2100	coesite	kyanite	
54.0	25	pyrophyllite		
54.0	500	pyrophyllite		
54.0	1000	pyrophyllite		
54.0	1500	coesite	kyanite	α-Al_2O_3
54.0	1950	coesite	kyanite	α-Al_2O_3
54.0	2000	coesite	kyanite	α-Al_2O_3
67.5	25	pyrophyllite		
67.5	500	pyrophyllite		
67.5	1000	pyrophyllite		
67.5	1500	coesite	kyanite	α-Al_2O_3
67.5	2000	coesite	kyanite	α-Al_2O_3
81.0	25	pyrophyllite		
81.0	1000	pyrophyllite		
81.0	2000	coesite	kyanite	α-Al_2O_3

oesite onset at a temperature between 1000° and 1500° C. and a pressure etween 13.5 and 27 kilobars. Kyanite is slightly more predominant than oesite up to a pressure between 27 and 40.5 kilobars, above which oesite is the principal phase. The "modified pyrophyllite" obtained at tandard pressure and 1000° C. is essentially a dehydrated phase, the *x*-ay diffraction pattern of which is only slightly changed from that of the riginal pyrophyllite. This is probably the same phase as that noted by arte (1955).

Petrographic examination of the alteration zone material obtained at 7.5 kilobars and 2000° C. showed essentially two phases (Fig. 4): a very ne-grained, markedly birefringent, rod-like material (kyanite), and a mewhat more coarsely grained, flaky phase of lower birefringence

(coesite). The kyanite appeared more uniform in crystallite size, averaging approximately $1\times5\mu$. Coesite, on the other hand, showed fragments as small as 1μ and large flakes up to $40\times85\mu$.

Since the original synthesis of coesite (Coes, 1953), interest in this material has grown steadily, the pace having been quickened by its recent discovery at Meteor Crater, Arizona (Chao, Shoemaker and Madsen 1960). This positive identification of a natural occurrence firmly estab

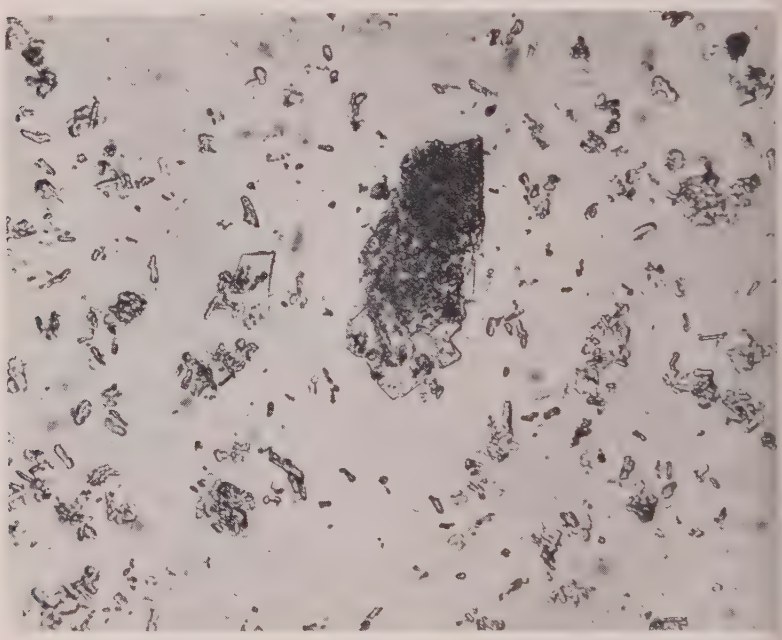

FIG. 4. Photomicrograph showing kyanite (fine-grained, rod-like) and coesite (lar flakes) from alteration zone material obtained at 67.5 kilobars and 2000° C.; transmitt light, 1.54 immersion oil (390×).

lishes the mineralogical name coesite, as opposed, for example, to th term "silica-C" (Sosman, 1954). The general crystallography of coesi (Ramsdell, 1955) and its crystal structure (Zoltai and Buerger, 195 have been described, along with further accounts of its synthesis ar characteristics (Khitarev, Slutskiy and Arsen'yeva, 1957). In additio several studies have been made of quartz-coesite relationships (Ma Donald 1956; Dachille and Roy, 1959; Boyd and England, 1960).

As of 1954, the synthesis of kyanite had not yet been achieved, th difficulty having been ascribed to the required octahedral coordinati for Al^{3+} (Roy and Osborn, 1954). More recent investigations, howeve

have resulted in successful laboratory preparations of kyanite (e.g., Kennedy, 1955; Clark, Robertson and Birch, 1959).

The Meteor Crater occurrence of coesite has suggested "that the presence of coesite may afford a criterion for the recognition of other impact craters on the earth and perhaps ultimately on the moon and other planets" (Chao, Shoemaker and Madsen, 1960). This possibility has been further discussed in light of a second natural occurrence of coesite at Rieskessel caldera in Bavaria, Germany (Pecora, 1960).

The synthesis of coesite from a complex silicate under laboratory conditions of relatively static pressures and temperatures, as described in this communication, implies that the occurrence of coesite in nature need not be restricted to environments of impact stress upon quartz-rich materials. Relatively long-duration stresses (shear, compressive, or combinations thereof) also will induce coesite formation from silica or from simple or complex silicates, providing that sufficiently high temperatures occur sometime during the period of elevated pressure. Consequently, coesite might be expected to occur in silicate compositions, not only at depths sufficient to provide necessary compressive stress, but also at near-surface localities that have undergone severe metamorphism.

The occurrence of kyanite in nature is almost invariably associated with relatively intense metamorphic activity. The present co-synthesis of kyanite and coesite shows that conditions of stable formation for the two are compatible, at least within the limits covered here. It might be inferred, then, that coesite and kyanite are potentially co-existent natural phases. Should this prove to be the case, once the overall chemistry of a locality is established, the relative abundance of coesite and kyanite could be used to provide information on the pressure-temperature environment. Thus coesite—originally a laboratory curiosity may prove to be a significant index mineral not only to pinpoint specific natural phenomena, *e.g.*, impact craters, but also to establish the severity of a local geophysical environment.

References

Birch, F., and Robertson, E. C. (1957), Properties of materials at high pressures and temperatures: *Harvard University, ONR Final Report, Contract N5ori-07644.*

Boyd, F. R., and England, J. L. (1960), The quartz-coesite transition: *J. Geophys. Research* **65,** 749–756.

Bridgman, P. W. (1938), The resistance of nineteen metals to 30,000 kg/cm²: *Proc. Am. Acad. Arts Sci.* **72,** 157–205.

Carte, A. E. (1955), Thermal constants of pyrophyllite and their change on heating: *Brit. J. Appl. Phys.* **6,** 326–328.

Chao, E. C. T., Shoemaker, E. M., and Madsen, B. M. (1960), The first natural occurrence of coesite: *Science* **132,** 220.

Clark, S. P., Jr., Robertson, E. C., and Birch, F. (1957), Experimental determination

of kyanite-sillimanite equilibrium at high temperatures and pressures: *Am. J. Sci.*, **255,** 628–640.

Coes, L., Jr. (1953), A new dense crystalline silica: *Science* **118,** 131–132.

Dachille, F., and Roy, R. (1959), High pressure region of the silica isotypes: *Z. Krist.* **111,** 451–461.

Giardini, A. A., Tydings, J. E., and Levin, S. B. (1960), A very high pressure-high temperature research apparatus and the synthesis of diamond: *Am. Mineral.* **45,** 217–221.

Hall, H. T. (1958), Some high-pressure, high-temperature apparatus design considerations; equipment for use at 100,000 atmospheres and 3000° C : *Rev. Sci. Instr.* **29,** 267–275.

Kennedy, G. C. (1955), Pyrophyllite-sillimanite-mullite equilibrium relations to 20,000 bars and 800° C.; *Geol. Soc. Am. Bull.* (abstract) **66,** 1584.

Khitarov, N. N., Slutskiy, A. B., and Arsen'yeva, R. V. (1957), Synthesis and characteristics of coesite: Geokhimiya **8,** 666–672 (in Russian).

MacDonald, G. J. F. (1956), Quartz-coesite stability relations at high temperatures and pressures: *Am. J. Sci.* **254,** 713–721.

Pecora, W. T. (1960), Coesite craters and space geology: *Geotimes* **5,** 16–19.

Ramsdell, L. S. (1955), The crystallography of "coesite": *Am. Mineral.* **40,** 975–982.

Roy, R., and Osborn, E. F. (1954), The system Al_2O_3-SiO_2-H_2O: *Am. Mineral.* **39,** 853–885.

Sosman, R. B. (1954), New high-pressure phases of silica: *Science* **119,** 738–739.

Zoltai, T., and Buerger, M. J. (1959), The crystal structure of coesite, the dense, high pressure form of silica: *Z. Krist.* **111,** 129–141.

Note added in proof: A third natural occurrence of coesite has been found. Chao, Fahey and Littler (1961), Coesite from Wabar Crater, near Al Hadida, Arabia: *Science* **133,** 882–3.

THE AMERICAN MINERALOGIST, VOL. 46, JULY–AUGUST, 1961

LATTICE CONSTANTS OF SYNTHETIC LAWSONITE

Carl W. F. T. Pistorius, *National Physical Research Laboratory, Council for Scientific and Industrial Research, Pretoria, Union of South Africa*

Natural lawsonite, $CaO \cdot Al_2O_3 \cdot 2SiO_2 \cdot 2H_2O$, is orthorhombic, space group $C222_1$ (Pabst 1959), with lattice constants ranging between $a_0 = 8.82$ 8.90 kX, $b_0 = 5.76$ 5.87 kX, $c_0 = 13.19$ 13.33 kX (Gossner and Mussgnug 1931, Wickman 1947, Rumanova and Skipetrova 1959). The remarkable fact that the molar volume of lawsonite, despite its two molecules of water, approximates that of anorthite, $CaO \cdot Al_2O_3 \cdot 2SiO_2$, is an indication that lawsonite might only be stable at high water vapour pressures. The stability of lawsonite should be scarcely affected by load pressure though very strongly influenced by water pressure. Fyfe and Turner (1958) pointed out that this makes lawsonite an excellent indicator of high water pressures.

Pure synthetic lawsonite has, in fact, up to the present moment only been synthesized under conditions of very high water pressure (Coes 1955; Pistorius, Kennedy and Sourirajan, in press). The latter author

reproducibly synthesized lawsonite in the presence of a large excess of quartz or coesite at H_2O pressures above 23 kilobars at 400–600° C. and 20 kilobars at 850° C. Since their starting material was natural Iceland scolecite, their lawsonite might have been slightly impure. Furthermore, the presence of excess silica influenced the stability field of lawsonite, since the lawsonite was formed by the phase reaction zoisite+pyrophyllite+water$\rightleftharpoons$4 lawsonite+2 coesite.

In the present experiments lawsonite was prepared from a hydroxide mixture of its own composition. Analytic grade chemicals were used throughout. The finely ground samples were subjected to suitable conditions of H_2O pressure and temperature in the simple squeezer high-pressure apparatus (Griggs and Kennedy 1956).

In the absence of excess silica it was found that lawsonite starts to form at H_2O pressures at least as low as 19 kilobars, and possibly even lower. The temperatures used ranged from 500° to 650° C. This means that the field of stability of lawsonite is extended towards lower H_2O pressures by at least as much as 4 kilobars if no excess amount of silica is present. Experiments of longer duration might increase this figure slightly. At pressures of 14–19 kilobars, a mixture of zoisite, pyrophyllite and corundum was obtained at these temperatures.

Some runs were also made using a hydroxide mixture of zoisite composition as starting material. In this case lawsonite did not appear until 27 kilobars H_2O pressure at 650° C.

The best yield of lawsonite was obtained in a run made at 28.5 kilobars and 650° C. from hydroxide starting material of its own composition. The duration of the run was one hour. This lawsonite was subsequently used for the determination of the lattice constants from the powder pattern.

The x-ray powder diffraction pattern of the finely ground synthetic lawsonite at 25° C. was obtained in a Philips high angle recording diffractometer, using filtered Co Kα radiation ($\lambda = 1.7889$ Å). The resulting powder data are given in Table I.

A least-squares treatment of the observed reflections yielded the following lattice constants:

$$a_0 = 8.787 \pm .005 \text{ Å}$$
$$b_0 = 5.836 \pm .005 \text{ Å}$$
$$c_0 = 13.123 \pm .008 \text{ Å}$$

The systematic absences correspond to the space group $Ccmm$. However, Pabst (1959) has shown that false symmetry, the Templeton effect (Templeton 1956), arises in lawsonite due to special values of the y parameters of all atoms in general positions. Consequently, though the space group is actually $C222_1$, the systematic absences correspond to $Ccmm$.

TABLE I. POWDER DATA FOR SYNTHETIC LAWSONITE

(CoKα radiation)

hkl	d_{obs} in Å	d_{calcd} in Å	I	
002	6.557	6.562	30	
110	4.862	4.861	40	
111	4.565	4.559	15	
201	4.167	4.166	50	
202	3.650	3.651	60	
020	2.918	2.918	25	
114	2.720	2.719	100	
022	2.666	2.666	40	
204	2.631	2.629	50	
310	2.618	2.618	70	
220, 312	2.432	2.431, 2.431	40	
221	2.391	2.390	5	
115	2.313	2.310	40	
222	2.279	2.279	20	
205	2.253	2.253	20	
313	2.247	2.246	5	
006	2.189	2.187	20	
024	2.180	2.180	10	
401	2.166	2.167	5	
223	2.125	2.125	70	
402	2.084	2.083	5	
403	1.964	1.965	20	
206	1.958	1.958	5	
130	1.898	1.899	2	
131	1.880	1.880	20	
026, 117	1.752	1.750, 1.749	15	poorly
133	1.747	1.747	15	resolved
207	1.724	1.724	15	
405, 510	1.684	1.685, 1.683	2	
511	1.668	1.669	10	
008, 134	1.642	1.640, 1.644	5	
512, 423	1.630	1.630, 1.629	40	
226	1.625	1.626	5	
330	1.620	1.620	5	
406, 424	1.549	1.550, 1.548	30	
040, 425	1.459	1.459, 1.459	5	

The calculated density of synthetic lawsonite is 3.100 g/cm^3 taking 4 formula weights in the unit cell. This is in good agreement with th pycno-metric value for natural lawsonite, viz. 3.084–3.091 g/cm^3.

REFERENCES

COES, L., JR. (1955), High-pressure minerals: *J. Am. Cer. Soc.* **38,** 298.

FYFE, W. S., AND TURNER, F. J. (1958), Correlation of metamorphic facies with expe

mental data, in Fyfe, W. S., Turner, F. J., and Verhoogen, J., ed., Metamorphic reactions and metamorphic facies: *Geol. Soc. Amer. Memoir* **73,** 149–185.

Gossner, B., and Mussgnug, F. (1931), Röntgenographische Untersuchungen an Prehnit und Lawsonit: *Centralblatt Min.* 419–423.

Griggs, D. T., and Kennedy, G. C. (1956), A simple apparatus for high pressures and temperatures: *Am. Jour. Sci.* **254,** 722–735.

Pabst, A. (1959), False symmetry, the Templeton effect, in lawsonite: *Z. Krist.* **112,** 53–59.

Pistorius, C. W. F. T., Kennedy, G. C., and Sourirajan, S. (1961), Some relations between the phases anorthite, zoisite and lawsonite at high temperatures and pressures, *in press.*

Rumanova, I. M., and Skipetrova, T. I., (1959), Crystal structure of lawsonite: *Doklady Akad. Nauk S.S.S.R.* **124,** 324–327.

Templeton, D. H. (1956), Systematic absences corresponding to false symmetry: *Acta Cryst.* **9** 199.

Wickman, F. E. (1947), The crystal structure of lawsonite, $CaAl_2(Si_2O_7)(OH)_2 \cdot H_2O$: *Arkiv Kemi, Min. Geol.* **25A,** no. 2, 1–7.

THE AMERICAN MINERALOGIST, VOL. 46, JULY–AUGUST, 1961

ALLANITE FROM WADI EL GEMAL AREA, EASTERN DESERT OF EGYPT, AND ITS RADIOACTIVITY

Amin R. Gindy, *Department of Geology, Alexandria University, Alexandria, Egypt, U.A.R.*

Introduction

The Geological Survey of Egypt recently reported small pegmatite dikes and veins carrying sporadic large crystals of allanite in the Precambrian basement complex rocks of Wadi El Gemal area, near the Red Sea coast, Eastern Desert of Egypt. Sadek (1953) indicated the localities of these occurrences and gave a brief report of other mineral deposits there. The allanite-bearing pegmatites are particularly frequent in the rectangle limited by longitudes 34° 40′–34° 50′ and latitudes 24° 30′ · 24° 40′ where they seem to be closely associated with a complex of xenolithic and gneissic tonalites, granodiorites and diorites. These pegmatite dikes and veins are of rather simple mineralogy and are mainly made up of unzoned acid oligoclase with smaller amounts of quartz and potash-rich feldspars. Allanite is almost the only colored constituent present; other accessories being either absent or in rare tiny grains. These include opaque ores, apatite, sphene and late hydrothermal clinozoisite, epidote and muscovite. The allanite-pegmatites show signs of late stage hydrothermal alterations; plagioclase being variably sericitized or kaolinized and allanite is also affected as described below.

Allanite

Allanite occurs erratically in the pegmatite bodies, sometimes in large euhedral to subhedral crystals measuring up to 3 inches in length (presumably parallel to *b*) and have a cross section of about $1\frac{1}{2}$ square inches. Usually it occurs in stubby subhedral crystals about a square inch in cross section. Much smaller crystals are also present in the feldspar-quartz matrix.

The mineral is opaque with a brownish black color and resinous luster on fresh broken surfaces. Along major fractures or along its contact with the matrix of the rock, the mineral has a somewhat rusty surface. Thin splinters of the mineral are translucent in dark or smoky amber colors. The powdered mineral has a dark buff grayish color and a greasy luster. Surface striations and cleavages parallel to *b*, the length of the crystal, are sometimes developed in the large crystals. Specific gravity ranges from 3.32 to 3.75. Hardness 5.5. The mineral in small fragments or powder readily swells and intumesces when heated in a platinum loop. The magnetism of the dark brown fused mass is variable, probably indicating different contents of iron. A borax bead gives a test for iron. Boiling HCl briskly decomposes the mineral, leaving a white but not gelatinous precipitate (cf. Hutton, 1950, p. 244–7).

The mineral apparently varies widely in composition in the different samples studied. In individual large crystals, however, zonal growths of different or contrasting compositions are generally slight or entirely lacking. When present, they are indicated by slight and patchy differences in color or birefringence. These differences in composition within a large crystal are revealed better when the mineral is altered. Fresh, birefringent crystals are pleochroic with $Z \sim Y$ olive green and X pale yellowish green or straw yellow. The darker fresh varieties are more pleochroic and also richer in iron and radioelements than fresh allanites of paler pleochroic colors. In the fresh allanites, n varies between 1.74 and 1.70. 2V is negative and ranges from 77° to 84°.

In thin section, the large cyrstals appear to have crystallized early. Sometimes their outer borders show mild sinuous embayments as if they had been partly resorbed at a late stage in their history. The resorbed margins were later framed by a fringe of complicated fine granular aggregates of clinozoisite, epidote, red or orange allanite, magnetite or hematite, some quartz or even albite (Fig. 1). Near their outer borders, fresh large subhedral allanite plates may show some signs of irregularity in original composition and patches of colorless clinozoisite appear. Relatively late hydrothermal clinozoisite commonly traverses the broad allanite plates in tiny veinlets along pre-existing fractures. These veinlets do not usually extend beyond the allanite plate into the quartz-feldspa

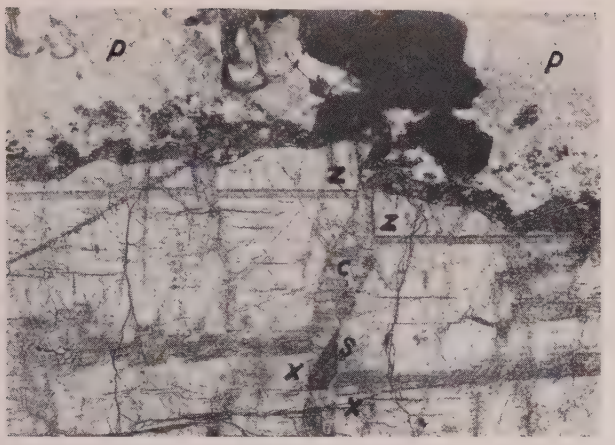

FIG. 1. Photomicrograph of part of the outer border of a large allanite crystal showing a resorbed sinuous border outlined by a dark fine-granular intergrowth of yellow to red allanite, clinozoisite and opaque grains. A clinozoisite vein (*c*) with a sphene crystal (*s*) traverses the allanite plate along a micro-fault indicated by the displacement of two subparallel lightly altered zones (*z* and *x*) within the allanite plate. This particular allanite plate is fairly fresh and anisotropic. It is also the least radioactive variety encountered. Matrix of altered acid oligoclase (*p*) with opaque grains. Ordinary light, ×22.

matrix, but at the outer boundaries of allanite they merge with the late peripheral clinozoisite growths. The clinozoisite veinlets may also contain rare crystals of sphene, also apatite and quartz.

Alteration of Allanite

All allanites from Wadi El Gemal show replacement by a bright yellowish, orange, red or brown variety around their borders and along some internal cleavages and fractures; rarely in certain internal zones that seem to be of a slightly different composition more susceptible to alteration. In a more advanced stage of alteration, clouds of tiny hematite-like lamellae are formed. In the iron-rich allanites, these lamellae become concentrated into tiny brown to black opaque irregular clots spangling the altered mineral. The small crystals of allanite in the quartz-feldspar matrix of the pegmatites are always entirely replaced by this deeply colored allanite. In the larger crystals of originally weak radioactivity or in isotropized ones of higher radioactivity some internal parts of the plates remain clear, and retain the original pale olive green color.

The apparently fresh and homogeneous islands remaining in the relatively iron-rich strongly altered allanite crystals, while fairly clear and retaining their original olive green color, become almost non-pleochroic and non-birefringent. Under crossed nicols, this isotropism is not perfect

or homogeneous but is rather mottled throughout by slightly birefringent small patches which, however, give no interference figures. Further alteration of this clear isotropic allanite gives very complex and intimate fine granular intergrowths of the reddish birefringent allanite and a low birefrigent white or gray mineral (clinozoisite?) accompanied by a release of hematite-like lamellae, or, in intensified alterations, by the dark brown, almost opaque (amorphous?) ferruginous clots and veinlets. Several granules of this secondary reddish allanite may retain a common optical continuity over some patches of this complex intergrowth. In other parts, pleochroic greenish epidote and colorless clinozoisite are among the alteration products. Indeed some of the relatively wider and better defined clinozoisite veinlets traversing the allanite may taper near their narrowing ends deep inside the host into epidote-veinlets or epidote clinozoisite veinlets that soon merge and lose their identity among the fine granular alteration products of the host. Elsewhere in such allanite crystals, relatively large epidote and clinozoisite patches in the altered parts seem to be of a straightforward replacement origin. No isotropized allanite was observed in the transitional stages of alteration of the originally weakly radioactive and usually iron-poor allanite specimens. Also no definite green epidote is found among their alteration products.

As the clear relatively more radioactive and iron-rich allanites are isotropized and are also much more strongly altered and replaced by the deeply colored allanite-hematite-clinozoisite-epidote aggregates than the least radioactive and iron-poor allanites which are never isotropized but undergo a milder alteration to the reddish allanite-hematite or red allanite-clinozoisite-aggregates, it seems convenient to distinguish between two somewhat independent lines of changes; (*a*) isotropization and (*b*) replacement by the deeply colored allanite-hematite-clinozoisite aggregates. Isotropization may be tentatively ascribed to metamictization by radiation with hydrothermal alterations taking a doubtful part. Hydrothermal alteration is, however, directly responsible for the deep red allanite-hematite-clinozoisite aggregates irrespective of the degree of radioactivity of the original allanite. Nevertheless, the original composition of the allanite seemed to present an important measure of its susceptibility to the hydrothermal alterations, the more ferruginous and more radioactive allanites being much more affected. Damage and breakdown of ionic bondages brought about by radiation would certainly help the hydrothermal alteration. Completely oxidized and hydrolysed outer parts of the originally strongly radioactive crystals are transformed into deep brown opaque pseudomorphs that are perhaps amorphous. In the Elberton granites of Georgia, Silver and Grunenfelder (1957) have considered the principal alteration of accessory allanite to have resulted no

rom simple metamictization but rather from reactive deuteric or later olutions.

Radioactivity of Allanite

Radioactivity of allanite was studied from polished specimens and uncovered thin sections previously stored in a dry container for at least two months in order to restore original radioactive equilibrium. Ilford Nuclear Research plates, emulsion types G.5. and C.2. were used. An exposure of two to three weeks of specimens in close contact with G.5. plates was sufficient to give good megascopic autoradiographs (Fig. 2, B). Similar autoradiographs were also obtained on medical double-coated -ray sheets. For quantitative work on alpha tracks, Ilford C.2. plates were used at varying exposures from 5 to 20 days and special precautions were taken to guard against fading of latent images in the humid atmosphere of Alexandria.

The total surface radioactivity of the large clear allanite crystals udied in the pegmatite specimens ranged from 0.087 to 0.672 α/cm.^{2} sec. (eU_3O_8 content of about 0.066 to 0.51%) but large clear individual rystals in the same specimen do not usually differ widely in their adioactivity. The most frequent range of activity for fresh crystals is etween 0.35 and 0.5 α/cm.^{2}/sec. Clear crystals of weaker radioactivity with a surface activity perhaps up to about 0.4 α/cm.^{2}/sec.) were mostly irefringent and looked fairly homogeneous in thin section as well as in he spatial distribution of alpha tracks in their corresponding autoradiographs. Crystals of higher radioactivity generally showed a marked lteration and a corresponding irregular pattern in their autoradiographs (Fig. 2, A and B). The highest values of radioactivity are measred from the relatively clear isotropized and least affected relict areas ithin the altered crystals. In such areas, radioactivity is still much ore evenly distributed than in the surrounding altered areas. In the ltered parts of the allanite crystals a clear decrease in radioactivity indicates leaching away of part of the radioelements together with iron and robably other cations. Radioactivity of the pleochroic yellowish or ddish alteration variety of allanite is very variable but may equal that the parent mineral. In the altered parts, however, some highly radioctive spots are occasionally present. These are not produced by highly tive mineral inclusions but are probably remains from old radiocolloid ggregates as mentioned later.

The total surface area of the thin section of allanite shown in Fig. 2, (excluding areas occupied by the large clinozoisite veinlets) has a total tivity of 0.4 α/cm.^{2}/sec. In the clear isotropized core, the activity is 59 while in many altered parts it is down to 0.23. The clear clinozoisite

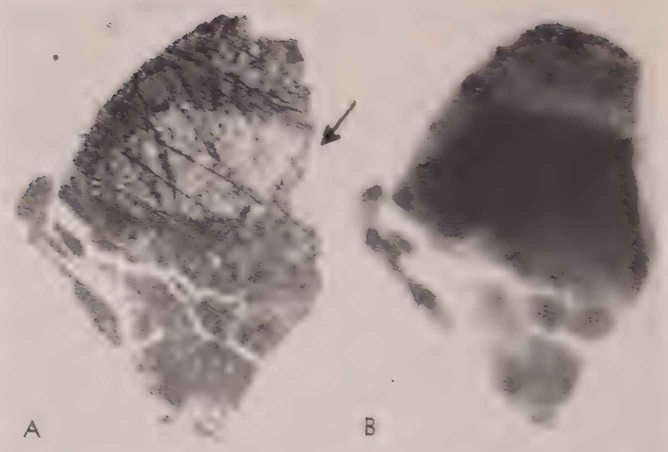

FIG. 2. (A) Thin section of part of a large altered crystal showing a rather clear [illegible] altered [illegible] island surrounded by a darker much altered area with [illegible] veinlets × about 2). Arrow points to a narrow alteration channel in the less altered more radioactive island. (B) Autoradiograph of the same specimen in (A) on Ilford C.5 plate. Note the higher radioactivity of the less altered island compared with the altered part and non-radioactivity of the [illegible] veinlets. The autoradiograph was originally made from the polished surface of a thick slice of allanite which was later mounted on a slide and thinned from the other surface to standard thickness. A part of the upper edge of specimen in (A) was lost in the process.

veinlets are found to be almost completely non-radioactive (Fig. 2. The few alpha tracks emitted from them were actually traced to ferru nous dark brown particles and films that had been leached from the ad cent much altered parts of the host. The photograph in Fig. 2 may g the impression of an originally zoned allanite crystal with an inter core of a different composition and a higher radioactivity than the ou now turbid and altered zone. This is disproved by the irregular distri tion of radioactivity in the entire crystal and by the fact that nar zones of alteration identical to those of the outer zones lie across at ran directions into the clear core, producing narrow zones of reduced activ These narrow zones do not show well in the sliced fragment under small magnification used. Fragments from another part of the sa allanite crystal, part of which is shown in Fig. 2, A, were powdered part of the powder was boiled in dilute HCl (1:5). The powder and white pulverulent material resulting from the acid leaching had spe activities of 0.44 and 0.0025 α/cm.^{2}/sec. respectively.

In order to estimate roughly the ThO_2 and U_3O_8 contents, meas ment of lengths of individual alpha tracks was attempted on autora graphs of two clear allanites giving a fairly uniform pattern of al

[illegible] preparation. The two allanite slices had specific activities of 0.25 and 0.15 and the corresponding Th/U ratios were found to be 2.04 and 1.748 respectively. This would indicate roughly a content of about 0.125% UO_2 and 0.110% UO_2 for the first slice, and of 0.257% ThO_2 and 0.147% ThO_2 for the second slice. If the average Th/U ratio of 1.9 is considered as fairly constant for all the fresh or clear allanites, then the highest uranium to thorium contents of the examined specimens corresponding to an activity of 0.672 would be about 0.478 and 0.504%, respectively. A. I. Gorzhan (personal communication, 1958) determined the Th/U ratio for the large allanite slices from Wadi El Gemal area by the same technique and gave the following values 1.765, 1.685 and 1.485. He further checked the last two values by the second technique available in such studies, viz. by counting the relative frequency of the various alpha tracks produced by the successive disintegration of the short-lived decay products (Bremner, 1951). He obtained Th/U ratios of 1.767 and 1.815 respectively. If all the preceding Th/U values were correct, then the present fresh allanites would be rather unusual in containing a much greater amount of uranium relative to thorium than is usually given in the literature on allanite. It is not quite certain at present whether the five allanite slices on which Th/U ratios were determined all come from the same pegmatite dike or from different pegmatite bodies. Th/U ratios and rare-element contents of the altered allanites were not studied in detail. There are indications of the well known higher release and mobility of uranium relative to thorium during hydrothermal alterations and weathering of allanite. It is therefore advisable, when Th/U ratios for allanites are given to mention the degree of alteration of the minerals.

Colloid aggregates and zones of higher radioactivity in altered allanites

Many highly radioactive spots in autoradiographs of allanite were strongly traced to the strongly altered and leached parts (Fig. 5) and were emitted by areas of either the fresh anisotropic allanite or the clear recrystallized allanite. It may be recalled that it is in such highly altered parts that the radioactivity is strongly reduced. Fig. 5, A, shows the most radioactive spot so far observed in the altered allanite. Judging from the boundary line enclosing all vertical and nearly vertical alpha tracks of this spray in the autoradiographs, the source must have been no larger than 14 square microns with an activity of over 6000 α cm^{-2} sec^{-1}. The active spray was traced to a spot in an opaque dark brown (amorphous?) ferruginous veinlet leached in a channel within the altered allanite. In one odd example of a strongly altered outer border of an allanite crystal, these active spots occurred at a frequency of about 340 spots per square centimeter of the surface area of the altered mineral. Usually they are much fewer. Slight repolishing of the allanite surface

causes earlier sprays to disappear but new ones may appear elsewhere in the corresponding autoradiographs. Investigation of the lengths of alpha tracks emitted by such sprays in autoradiographs of suitable periods o exposure indicated that these tracks do not exceed in length those emitted by RaC′, the longest tracks of the uranium family. Such sprays are thu most probably produced by segregation, during leaching of the altered allanite, of daughter products of the uranium series, and may represen radiocolloid aggregates (cf. Yagoda, 1946).

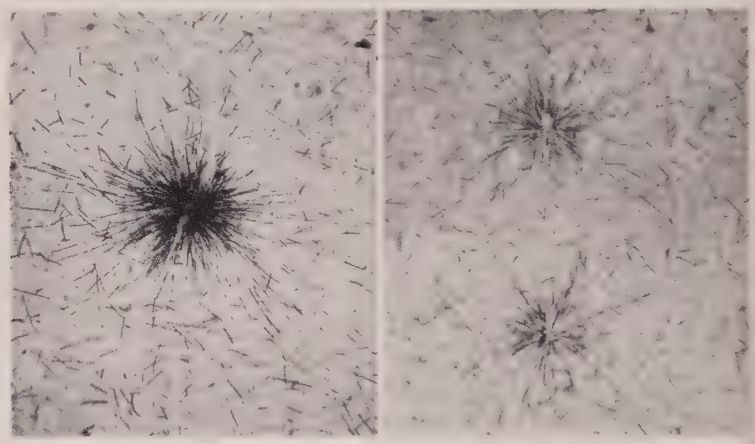

FIG. 3. (A) (left) Photomicrograph of an alpha autoradiograph of an altered allani showing a strong spray of alpha tracks emitted by a center probably suggesting an origi radiocolloid aggregate, ×200. (B) (right) Two weaker sprays from the same autorad graph of (A), probably representing older segregates than the one shown in A, ×200.

Beside these highly active sprays, the autoradiographs also show a fe very narrow ribbon-like, oval or ill defined small zones where alph tracks show some marked concentration. These zones were also located the altered parts of allanite, particularly at the strongly altered allani margins opposite the veinlets of clinozoisite, clinozoisite-quartz or clin zoisite-epidote-quartz. These zones are mostly traced to areas occupi by the dark brown, almost strongly altered variety of allanite or opaque pseudomorphs and alteration products

The radioactivity of all such narrow zones was not observed to exce $3\alpha/\text{cm.}^2/\text{sec.}$ and may be about seven times higher than the radioactivi of the remaining fresh parts of the corresponding allanite and more th ten times higher than the average radioactivity of the ordinary alter parts. It may be tempting to consider them as relics after old incipie stages in radiocolloid development. Long ThC′ tracks are present in th but these can be accounted for by the background radiation of thorium

he altered allanite. They may be also due to concentration of the radio-lements in some of the new red-brown varieties of allanite after the breakdown of the original allanite to red brown allanite, clinozoisite and pidote. Compared with clinozoisite, green epidote granules occasionally ound in the clinozoisite veinlets are slightly more radioactive.

ACKNOWLEDGMENTS

Thanks are due to Dr. E. M. El Shazly of the International Atomic Energy Agency, Vienna and the Egyptian Geological Survey for kindly providing the writer in 1956 with several allanite specimens from Wadi El Gemal, and to Mr. A. I. Ghozlan, now at the Laboratory of Mass-pectrography, Amsterdam, for making available his Th/U estimates on Wadi El Gemal allanites.

REFERENCES

REMNER, J. W. (1951), A method for determining uranium and thorium in rocks by the nuclear photographic plate: *Proc. Phys. Soc. London*, **64A,** 25–31.

UTTON, C. O. (1951), Allanite from Yosemite National Park, Tuolumne Co., California: *Am. Mineral.*, **36,** 233–248.

ADEK, M. (1953), Summary of prospecting in Wadi El Gemal area, Eastern Desert, 1948, and 1951: Egypt. Mines & Quarries Dept., *Government Press*, Cairo.

ILVER, L. T. AND GRUNENFELDER, M. (1957), Alteration of accessory allanite of the Elberton area, Georgia (abs.): *Geol. Soc. Am. Bull.*, **68,** 1796.

AGODA, H. (1946), Radiocolloid aggregates in uranium minerals: *Am. Mineral.*, **31,** 462–470.

THE AMERICAN MINERALOGIST, VOL. 46, JULY–AUGUST, 1961

A DIFFRACTOMETER MOUNT FOR SMALL SAMPLES*

A. J. GUDE, 3rd AND JOHN C. HATHAWAY,
U. S. Geological Survey, Denver 25, Colorado

Buerger and Kennedy (1958) discuss the problem of scattered x-radiation from a diffractometer sample holder and describe improved results using a BT-cut quartz oscillator plate. They point out that when a small amount of sample is supported in the x-ray path, background noise from various mounting media yields random deflections that may be indistinguishable from low-intensity peaks of the diffraction pattern. Specimens large enough to be packed, pelleted, or slabbed are quasi-infinite in thickness and thus mask the background contributed by the holder or support. However, where samples are very small, any contribution from the substrate may add significantly to the background scattering.

* Publication authorized by the Director, U. S. Geological Survey.

We have borrowed a technique from electron microscopy (Fig. 1) t solve the scattering problem in a manner that compares favorably wit the use of a quartz plate. The powdered specimen is supported on, unde or between membrane substrates made from any of several plastic These materials are transparent to x-rays when fashioned into very thi

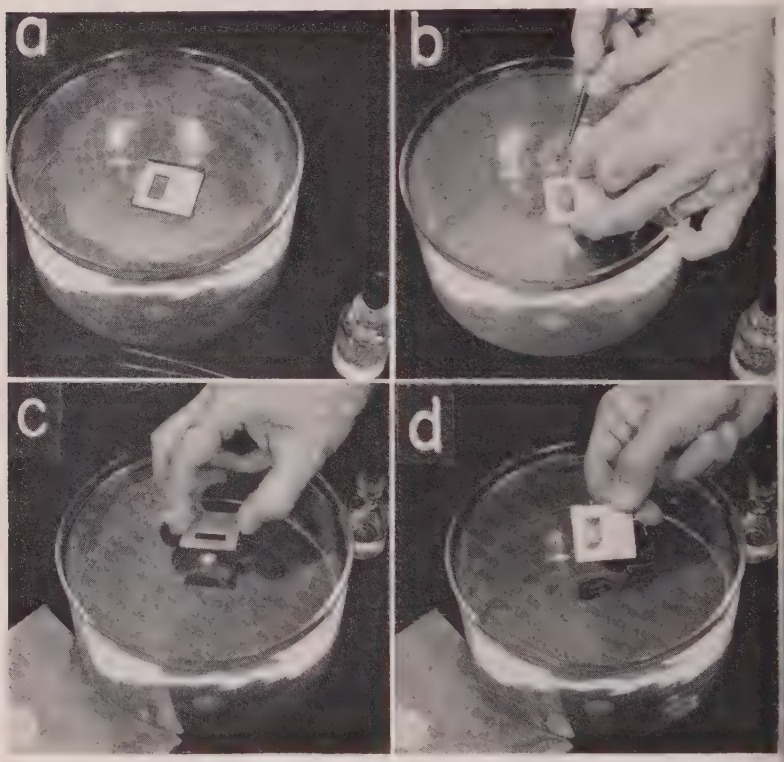

FIG. 1. Photographs of materials and method for preparing membranes used as san substrates for diffractometer.

a. A diffractometer sample mount placed on floating membrane.
b. Removal of excess membrane.
c. Powdered sample placed on second membrane.
d. Completed mount with sample between first and second membranes.

films. A flat aluminum sample holder with a rectangular opening, si as those regularly supplied with diffractometer equipment, can be u as a supporting frame for the membrane. A special holder, however, w an oversized opening gives superior results. The special holder ha narrow rim which lies almost entirely outside the primary x-ray be particularly at low 2θ angles.

Membranes are quickly and easily made from plastics such as collodion issolved in a lyophobic solvent. Accordingly, water-miscible alcohols nd the like are not suitable. The following list of plastics has been tried, nd all have been found equally adaptable:

Plastic	*Solvent*	*Setting time (on water)*
Ethyl cellulose	Toluene	2 to 4 minutes
Ethyl cellulose	Toluene and ether (1:1)	30 to 60 seconds
Collodion	Ether	5 to 10 seconds
Collodion	Amyl acetate	1 to 2 minutes
Parlodion	Amyl acetate	1 to 2 minutes

The mixtures of plastic and solvent must be thin enough for a drop to ow freely from an ordinary dropping pipette (medicine dropper). mpirical factors which can be readily adjusted by the user govern the mounts of plastic and solvent to be mixed. Similarly, the size of drops eeded for a membrane is quickly determined by a few minutes of experi- entation.

One or more drops of the plastic mixture dropped in quick succession nto a water surface will spread out into a thin film. This film will "set" o form a membrane as the solvent vaporizes—the elapsed time de- ending on the volatility of the solvent, the temperature of the room, nd temperature of the water. One can determine when the membrane s set and estimate its thickness, from the appearance of the inter- erence colors produced by the film. Some membranes may crinkle ightly; but usually this does not affect the mount, since the membranes ill stretch taut in the holder as they dry. If the wrinkles remain and are ronounced, it will be necessary to repeat the mounting procedure.

Gently place a sample holder, top surface down, against the membrane s as to cover the opening (Fig. 1-*a*). For best results this operation should e performed when the film is still slightly tacky, although the inter- rface cohesion may make a good bond even when the membrane has t. Trim or tear away the surrounding floating membrane while it is ill on the water (Fig. 1-*b*) so as to avoid flipping the excess onto the ount. Slip the holder out of the water sideways with a minimum of ownward pressure on the stretched membrane. Shake the water off ntly and dry the mount. Heat from a steam bath or from an infra-red mp will hasten drying though excessive heating may rupture the film.

The sample may be placed on the membrane in several ways. The mple may be dusted or sprinkled on top. A water suspension may be ried on top of the membrane. The latter procedure, however, may cause e substrate to rupture. The sample may be spread on the membrane rior to attaching the membrane to the sample holders. This yields a mple suspended under the film.

A preferred technique is to sandwich the sample between two film The thick under-membrane is prepared and mounted on a holder. Ne a thin membrane is spread on the water and the sample placed on th surface (Fig. 1-*c*). The holder with the relatively thicker substrate positioned over the sample and then the sample and second membra are picked up as described above. The sample is thus held securely the correct geometric position with respect to the top of the flat hold surface (Fig. 1-*d*).

From the preceding, it can be seen that no special equipment, and n more dexterity nor skill are required than one needs for the usu methods of sample preparation. Although the membrane is fragile wh compared with other mounts, it has sufficient strength to support a stat load of well over one gram. This is adequate for the purpose when o considers that the 10 by 20 mm. cavity in the regular holders can packed to hold from 0.3 to 0.5 gm. of powder. Samples sprinkled dusted on or under the substrate can be readily recovered by gen brushing. "Sandwiched" samples can be easily salvaged, by dissolvi and rinsing away the plastic with acetone.

BT-cut quartz plates were not available for testing, but AT-cut plat were obtained and tried as a substitute. Reflections from the $(10\bar{1}0)$ a $(10\bar{1}1)$ planes are present as small broad peaks in one orientation. Wh the plate is turned 90° in the plane of its surface, very strong reflectio from these planes are produced.

In Fig. 2 are shown comparisons between diffractometer patterns cording the background scatter at constant machine settings from vari substrates. The first four sets of patterns (Fig. 2*a* to *d*) are a relat series of records of background scatter only. Three traces are on e diagram: the "instrumental background, *x*-rays off" is the lowest tr present in each figure. The other two traces compare the signific results of the investigation. It should be noted that the hump at low angles (Fig. 2-*b*, *c*) is contributed by white radiation scattered from portions of the aluminum holder that are in the *x*-ray path. This

FIG. 2. Diffractometer patterns of the background scattering from various sa substrates (a, b, c, d) and the patterns of a mixed sample on a glass slide and on a m brane (e).

a. Glass slide and AT-cut quartz plate.
b. AT-cut quartz plate and membrane in standard Al holder.
c. Membrane in standard holder and empty holder.
d. Membrane in oversize holder and air scatter (no holder).
e. 1:1 (by vol.) quartz:montmorillonite on glass slide and on membrane in stand holder.

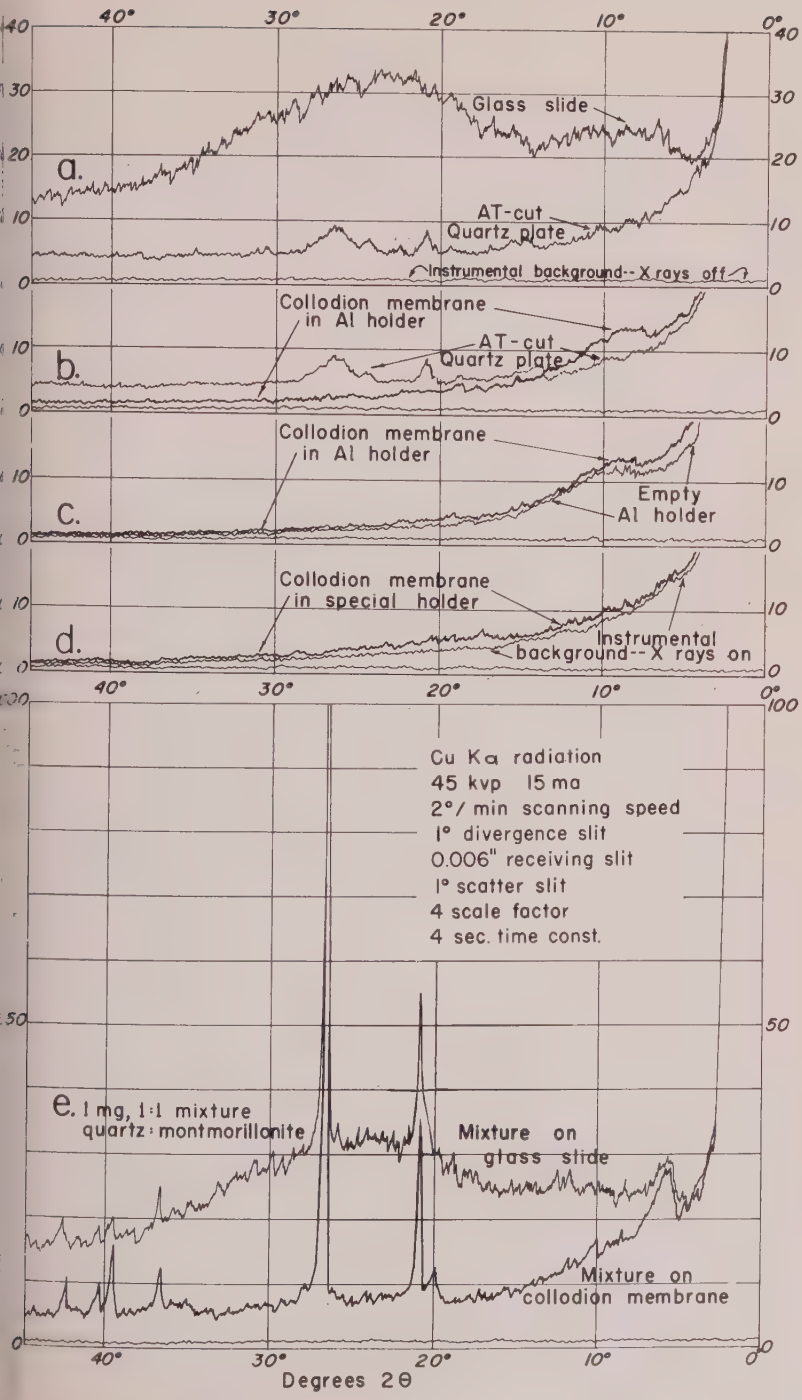
40°
30°
20°
10°
0°
a.
Glass slide
AT-cut
Quartz plate
Instrumental background--X rays off
b.
Collodion membrane
in Al holder
AT-cut
Quartz plate
c.
Collodion membrane
in Al holder
Empty
Al holder
d.
Collodion membrane
in special holder
Instrumental
background--X rays on
Cu Kα radiation
45 kvp 15 ma
2°/ min scanning speed
1° divergence slit
0.006" receiving slit
1° scatter slit
4 scale factor
4 sec. time const.
e. 1 mg, 1:1 mixture
quartz : montmorillonite
Mixture on
glass slide
Mixture on
collodion membrane
Degrees 2θ

eliminated in Fig. 2-*d* by the use of a holder with a larger opening an with very little metal bathed by the primary *x*-ray beam.

The final display (Fig. 2-*e*) is a comparison of the record from a milli gram of a 1:1 mixture by volume of quartz and montmorillonite. Thi amount of material is about half the amount of powder shown bein mounted in Figure 1-*c*, *d*. The excessive "hash" in the glass-slide recor masks the (02) montmorillonite band at 20° 2θ and yields many randor deflections that might be erroneously interpreted as true diffractio maxima.

Appendix

Materials required for this method:

1. Collodion or similar plastic dissolved in a lyophobic solvent.
2. Dropper bottle.
3. Petri dish or similar container filled with water.
4. Tweezers, toothpick, or any other instrument for trimming away excess membran
5. Standard diffractometer sample holders.

Reference

Buerger, M. J. and Kennedy, G. C. (1958), An improved specimen holder for the focu ing-type *X*-ray spectrometer: *Am. Mineral.*, **43,** 756–757.

THE AMERICAN MINERALOGIST, VOL. 46, JULY-AUGUST, 1961

THE MORPHOLOGY OF ESKOLAITE, Cr_2O_3

Christel Tennyson, *Technische Universität, Berlin, Germany*

Kouvo & Vuorelainen* described in 1958 the new mineral eskolaite, na ural Cr_2O_3 isotypic with Al_2O_3 and Fe_2O_3, forming idiomorphic crysta up to about 5 mm. in size, from Outokumpu, Finland. The authors me tion that the prismatic or platy crystals show the forms: $\{11\bar{2}0\}$, $\{0001$ and $\{1123\}$, but the rhombohedrons $\{0112\}$ and $\{10\bar{1}4\}$ which shou be dominant, were not observed.

The Institute of Mineralogy of the Technical University of Berlin g some well developed eskolaite crystals from the type locality, with length up to 12 mm. (Fig. 1). They have, in addition to the report forms, also the rhombohedron r $\{10\bar{1}1\}$ in the combinations of Fig. Our indices are derived from the morphological axial ratio $c/a = 1{,}37$ as used for Al_2O_3 and Fe_2O_3 in Dana (System of Mineralogy 1944) a in Strunz (Mineralogische Tabellen 1957).

* Kouvo, O. and Vuorelainen, Y. (1958), Eskolaite, a new chromium mineral. *A Mineral.*, **43,** 1098–1106.

Eskolaite from Outokumpu, Finland
$c/a=1.3715$, $\alpha=85°22'$, $p_0:r_0=1.5837:1$

Hexagonal	Rhombohedral	ϕ	ρ	A_1	A_2
c 0001	111	—	0°00′	90°00′	90°00′
a $11\bar{2}0$	$10\bar{1}$	0°00′	90°00′	60°00′	60°00′
r $10\bar{1}1$	100	30°00′	57°44′	42°55′	90°00′
n $22\bar{4}3$	$31\bar{1}$	0°00′	61°20′	63°59′	63°59′

With cell dimensions $a_0=4.958$ Å, $c_0=13.60$ Å and $c_0:a_0=2.743$* the ndices would be $c\{0001\}$, $a\ \{11\bar{2}0\}$, $r\ \{10\bar{1}2\}$, $n\ \{11\bar{2}3\}$. $a_{rh}=5.361$ Å, $=55°05'$.

Fig. 1. Eskolaite crystals in chalcopyrite and pyrrhotite. Natural length 12 mm.

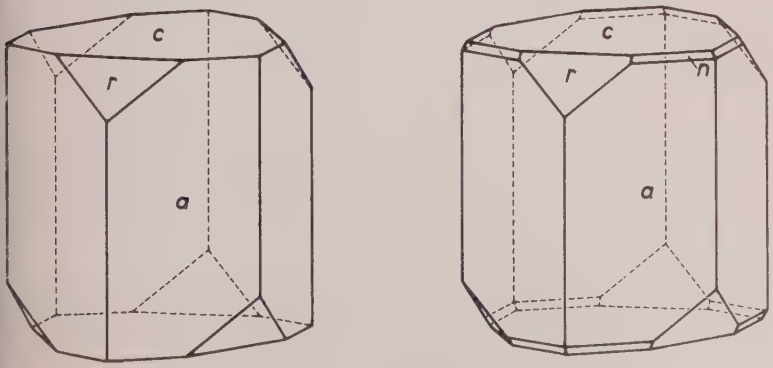

Fig. 2. Eskolaite. The two observed combinations.

PITTSBURGH DIFFRACTION CONFERENCE

The annual Pittsburgh Diffraction Conference will be held Novembe 1–3, 1961, at Mellon Institute, Pittsburgh, Pennsylvania. Sessions wi be devoted to metals and alloys, instrumentation, structures, polymer and fibers, refractories, and electron probe, including special sessions o electron diffraction and X-ray diffraction microscopy. The evening mee ing will be addressed by Dr. Peter J. W. Debye, emeritus professor chemistry, Cornell University. Further information can be obtaine from T. B. Massalski, Mellon Institute, 4400 Fifth Avenue, Pittsburg 13, Pennsylvania.

Cap. John Sinkankas, recently retired from the U. S. Navy, has been appointed edit of the *Lapidary Journal*, effective Sept 1, 1961.

ERRATUM

Tom. F. W. Barth

Those who have read my speech of acceptance of the Roebling Medal (*Am. Mineral.* 509–10, 1961) may have wondered what Dr. H. S. Washington said to me at the Geoph ical Laboratory in 1930, when he taught me the art of making chemical analyses of roc His consoling words were: "In order to do research it is *not* necessary to have a particula brilliant mind, or a very high intelligence. To be able to do good research is a state of min

On page 510, 8th line from the bottom, the little word *not* is missing in the above que tion.

BOOK REVIEWS

EOLOGIE UND BODENSCHÄTZE AFRIKAS, by Erich Krenkel. 2nd ed., Akad. Verlagsgesellschaft Geest & Portig K.-G., Leipzig, 1957, xvi+597., 158 illustrations, DM. 61.00.

Dr. Krenkel, who is Professor Emeritus of Geology at the University of Leipzig, has mpletely reworked his authoritative work on the geology of Africa. The first edition, hich appeared in 1939 in three volumes, contained 1900 pages of text and over 450 illus- ations and tables. It was part of the famous series "Geologie der Erde" published by ebrüder Borntraeger, Berlin. The second edition, which, of course, has been greatly ortened, has many parts that were completely reworked and also contains new chapters aling, e.g., with such features as orogenies, guiding lineaments, and magmatic periods. the compilation the author brings an abundance of personal experiences and investiga- ns: in Morocco, Algeria, Tunis; in Egypt, Eritrea, Uganda, Kenya, and Tanganyika; d in South Africa and the Congos.

The book is divided into two parts: I, The Geology of Africa, and II, The Ore Deposits Africa. The geology is described in terms of the following general regions: The Atlas, hara, Red Sea Graben, Syrabia, Abyssomalia, East Africa, Madagascar, South Africa, Congo Basin, Guinea-Sudan, and the Atlantic Islands. Most of these sections are fur- r subdivided on an areal basis, as, for example, in the section on South Africa: 1. The stern stem—the Rhodesian shield, the Transvaal, the Lebombo zone, the Karroo basin, Cape, the coastal sedimentary strip, and the Kalahari region; 2. The western stem— Nama Massif, the Samara Massif, and the Namib. This part, which consumes 486 ges of the book, concludes with a general summary—Africa in retrospect.

Part II is split into a section on "ores"; i.e., deposits yielding metals, thus including xite; and one on non-metallic deposits. A noteworthy omission is the absence of infor- tion on the Rand uranium, which is mentioned but briefly under Gold but not at all der Uranium.

Each part is followed by its own index—not a particularly convenient arrangement. e book concludes with two bibliographies, one for each part. The older literature of 2400 ries, listed in the first edition, is not repeated in the second, in which only selected newer rences are cited.

It is unfortunate that the second edition could not be published in the detail and style he first; nevertheless it is a most welcome modernized and succinct account of the geol- of an entire continent. The illustrations, especially the numerous maps and sections, are erally excellent, but the half-tone reproductions are poor owing to the quality of the er. The book clearly belongs in the library of anyone interested in the geology of Africa.

E. Wm. Heinrich
University of Michigan

EMENTS OF CRYSTALLOGRAPHY AND MINERALOGY, by F. Alton Wade and Richard B. Mattox. xiv+332 pages. Harper & Brothers, New York, 1960. Price $7.50.

According to the editor's introduction to this new member of Harper's Geoscience ies, the book lies "in the middle ground between the orthodox and the novel" in the arch for new ways of handling beginning mineralogy." The book contains 10 chapters: ntroduction; 2. A Review of the Concept of Matter; 3. The Crystalline State; 4. The ssification of Crystals; 5. Crystal Chemistry; 6. Physical Properties; 7. Chemical Proper- ; 8. Descriptive Mineralogy; 9. Economic Mineralogy; 10. Genetic Mineralogy; Mineral

Associations. An appendix is devoted to the construction of the stereographic projectio and there are mineral and subject indexes. Of the approximately 450 names in the mine index over 200 are described in detail. Tables for the determination of minerals are n included.

After brief histories of mineralogy and crystallography are given in the introductio the constitution of crystalline matter is introduced. Beginning with atoms the writers d velop the ideas of atomic bonding, lattices, crystal symmetry, and finally crystals. T presentation of crystal form names which cut across systems is especially effective with t accompanying drawings. No attention is paid to goniometry and mathematical relatio ships. All 32 symmetry classes are presented in tables along with Hermann-Mauguin sy bols, symmetry elements, and mineral examples. However, only the more common class in the mineral kingdom are discussed in detail. For each of these there are excellent li drawings showing the symmetry elements, forms, combinations of forms, and a stereogra Unfortunately the crystallographic axes are not indicated on the stereograms, an omissi which might lead to some confusion, especially in Fig. 4.181, where the monoclinic *b* axis in the center of the projection. In a separate section twinning is discussed and illustrat by good line drawings for each of the systems. Terms used for crystalline aggregate str tures are defined and photographs illustrate many of these terms. The writers do not in date if cerussite is the mineral which illustrates the reticulated habit in the photograph Fig. 4.241. Crystal chemistry, the last topic considered in crystallography, includes ato and ionic packing, along with the concepts of radius ratio and coordination number. T section probably would have fit in better where atomic bonding and the crystalline st are discussed earlier. Other things considered here are chemical formulas, isomorphis polymorphism, pseudomorphism, and mineral classification. The classification of nons cates is covered briefly in less than a page, while ten pages are devoted to the silicate m erals.

The usual physical properties of minerals are summarized, followed by a list of prop ties not generally used in routine analyses, e.g., electrical conductivity, piezoelectrici heat of inversion, specific heat, etc. Standard blowpipe reactions are outlined for 46 ments. Other analytical techniques briefly touched upon are spectrochemical analysis ray diffraction, spot test methods, and differential thermal analysis. These topics no do illustrate that "the reader is constantly reminded of the highly specialized and diffi phases of the subject at the very time he is handling concepts and materials which . . . can readily comprehend," a statement made in the editor's introduction.

In the descriptive section the minerals are arranged according to Dana's *Syste Mineralogy*, 7th edition. Although the descriptions are quite complete and accurate section could be improved in several ways. A discussion of mineral groups is almost wh lacking in the systematic presentation. For example one finds no mention of the sp group, the rutile group, the calcite group, the aragonite group, as well as many others. S of the silicate groups are mentioned, but, except of the garnet group, only briefly in general discussion of the classification of the silicates. Although the silicates are classi on a structural basis, the writers have retained the older classification names based on hypothetical silicic acids. No figures appear in the descriptive section except for thos lustrating silicate structures, and illustrations identical to these appeared earlier in Cha 5. In the preface the authors explain that figures are absent because the student is expe to have mineral specimens available while using the book. There are a number of min name misspellings, e.g., cerussite (pp. 211, 212, 280), triphylite (pp. 222, 223), laz (pp. 222, 227).

In the economic section 28 elements are listed in alphabetical order, and their ores, u

l chief producing areas are discussed. This is followed by nonmetallic minerals used for asives, gems, fertilizers, etc.

The chapter on genetic mineralogy and mineral associations is especially good. The nation of minerals from melts (magma), sublimation, water solutions (hydrothermal, poration, ground water), metamorphism, etc. is treated. Chemical reactions including nerous equations are given, as well as lists of minerals which occur in each mode of for-tion.

R. S. MITCHELL
Department of Geology
University of Virginia
Charlottesville, Virginia

STEINS- UND LAGERSTÄTTENBILDUNG IM WANDEL DER WISSEN-SCHAFTLICHEN ANSCHAUUNG (The formation of rocks and ores scientifically considered), by WALTHER FISCHER, 592 pages, 12 plates, 12 figures, 36 tables in the text and on 4 inserts. E. Schweizerbart'sche Verlagsbuchhandlung, Stuttgart. 88 marks ($22.00).

This is an elaborate compendium of the historical development of the sciences of petrol- and mineral deposits, with reference to the work of some 2400 authors. The index of e 3000 entries includes reference to localities and to minerals, rocks, geological struc-s, and concepts and theories. In short, the student will find information, historical and ository, on almost any topic in these fields of science. The twelve plates comprise several en excellent portraits of famous petrologists.

There is no equivalent work in the English language, and it will be found most useful key to the older literature.

CHARLES MILTON
Petrological Services and Research
Branch of Experimental Geochemistry
and Mineralogy

NEW MINERAL NAMES

Lueshite

A. SAFIANNIKOFF. Un nouveau mineral de niobium. *Acad. royale sci. d'outre-mer, Bu* **5,** 1251–1255 (1959).

The mineral occurs as black cubes up to 1.5 cm. on an edge, but mostly 0.5–1 cm. T cube faces are lightly striated. Cleavage (001) imperfect, but easy. Color black, str gray. Biaxial, anisotropic, sign not given, n (Na) (in S-Se melts) 2.30 ± 0.03. G. 4.44, H.

Analysis by Haine and Copette, Centre recherches miniere de Bukavu, gave Nb 79.74, Ta_2O_5 traces, Na_2O 12.23, K_2O traces, CaO 0.76, MgO 0.62, $R_2O_3+SiO_2$ 5.62, on ignition 0.49, sum 99.46% (given as 100.46%. M.F.). A separate analysis by the Ka ituga Laboratory gave Fe_2O_3 1.27, TiO_2 3.62, leaving 0.73% for SiO_2. This correspo nearly to $NaNbO_3$. (The analysis calculates to $(Na_{1.32}\ Ca_{0.05})\ (Nb_{2.00}\ Ti_{0.15})O_6$ indicatin deficiency in the A position. Possibly the loss on ignition should be calculated as hydro M. F.). Before the blowpipe, gives a sodium flame. No data are given on solubility.

Indexed x-ray powder data agree well with A.S.T.M. data on synthetic $NaNbO_3$. T strongest lines are 3.91 (I = 100) (110), 2.77 (69) (200, 020, 114), 1.955 (43) (221, 215), (34) (220), and 1.596 (30) (314). The mineral is orthorhombic, perovskite-type, space gr $P\ 222_1$, with a 5.51 ± 0.006, b 5.53 ± 0.01, c 1.550 ± 0.12 Å. (The value for c is evident misprint for 15.50. M. F.), Z = 8.

The mineral occurs at Lueshe, 150 km. north of Goma, Belgian Congo, as incrustat on a compact yellow mica; the latter contains MgO 19.27, CaO 8.08, Na_2O 0.20% and haves like vermiculite when heated. The mica occurs at the contact of cancrinite sye with carbonatite containing pyrochlore.

The name is for the locality.

Discussion.—The name igdloite was given to a mineral, apparently $NaNbO_3$, Sørensen and Danø (see *Am. Mineral.*, **44,** 1327, 1959). This is stated, according to a priv communication from Sørensen to Soffiannikoff to contain appreciable SiO_2. It seems p ably, however, that these represent the same mineral. The description of igdloite was adequate, yet it would have been better not to give a new name to lueshite. E. M. B shtedt-Kupletskaya in an abstract in *Zapiski Vses. Mineral. Obshch.*, **90,** 95 (1961) ac cates dropping the name igdloite in favor of lueshite because the latter is better descril I agree with some reluctance.

Michael Fleische

Unnamed rare-earth calcium phosphate-silicate

I. V. Bel'kov and M. I. Volkova. Rare-earth calcium phosphate-silicate. *Izvest. Ki i Kolsk Filial, Akad. Nauk S.S.S.R.*, 1958, No. 2, 90–93; from an abstract by E. Bonshtedt-Kupletskaya in *Zapiski Vses. Mineral. Obshch.* **90,** 108–109 (1961).

The mineral occurs as fine prismatic crystals with acute terminations and hexago cross-section. Color reddish-brown, streak light-yellow. No cleavage. H. about 6, G. 4 isotropic, n 1.756. Amorphous to x-rays; after being heated gives an x-ray pattern clos that of the apatite group (a_0 9.40, c_0 6.96 kX); and becomes uniaxial, n 1.81.

Analysis gave SiO_2 17.88, P_2O_5 2.56, $Al\ O_3$ (+BeO) 0.49, Nb_2O_5 0.41, TiO_2 and ZrO_2 found, MgO 0.11, MnO 0.62, CaO 12.64, SrO 0.07, Ce_2O_3 19.04, ΣLa_2O_3 18.04, ΣY_2O_3 19 ThO_2 0.32, CO_2 2.34, F 2.38, H_2O 0.83, loss on ignition 4.03, sum 101. 12—$(O = F_2)$ = 100.12%.

Discussion.—This is very close to britholite.

M. F

Ward's 35mm Color Slides for Geolo

PLUS BLACK-AND-WHITE SLIDES ON ASTRONOMY, GLACIE

Ward's Color Slides for Geology. The finest suite of color slides available for teaching general geology. The set is the work of many photographers and illustrates topics in both physical and historical geology. Can be effectively used with any geology course or textbook.

LW 105—Complete set of 485 slides **$360.00**

LW 105-A—Special set of 50 selected slides **35.00**

LW 105-B—Supplementary set of 50 slides **35.00**

LW 105-C—Second supplementary set of 50 slides **35.00**

Ward's offers many other 35mm slides for teaching, study, reference, or recreational use on interesting and significant geological topics (numbers in parentheses are the number of slides in each set):

Folded rocks; anticline with lateral eros down dip. From LW 105

Color Slides:

LW 106—The Geology of Europe (151) $1
LW 26—Ward's Color Slides for Mineralogy (157) 1
LW 21—Gem Minerals from the Harvard Collection (26) .....
LW 22—Fine Minerals from the Harvard Collection (79) .....
LW 115—Color Photographs of Crystal Structure Models (25) .....
LW 74—Thin Rock Sections (37) .....
LW 25—Interference Figures Under Polarized Light (41) .....
LW 109—Structures and Features of Hawaiian Volcanoes (54) .....
LW 31—Meteorology: Cloud Formation (30) .....
LW 35—Invertebrate Fossils in Kodachrome (131) .....

Black-and-White Slides:

LX 30—Astronomy Slides (25) .....
LX 80—The Glaciers of Alaska (30) .....

Send color slide orders to:

WARD'S OF CALIFORNIA
P.O. Box 1749—Monterey, California

Send catalog requests to:

WARD'S NATURAL SCIENCE ESTABLISHMENT, INC.
P.O. Box 1712—Rochester 3, New York

GEORGE BANTA COMPANY, INC., MENASHA, WISCONSIN